STANDARD MEASUREMENTS OF THE PHYSICAL PROPERTIES OF SHORT WAVELENGTH X RAYS

A Thesis

submitted to the

University of London

for the degree of Ph.D. in Physics

by

J.H. Martin, B.Sc.

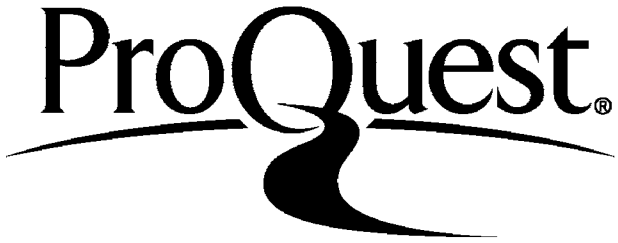

TABLE OF CONTENTS

Table of Contents (cont.) Page

INTRODUCTION - THE PRODUCTION OF SHORT WAVELENGTH X RAYS

Recent developments have made available to physicists and other workers a variety of sources of short wavelength electromagnetic radiation. Included among such sources are electrostatic generators of the Van de Graaff type[1,2], where a high voltage is obtained by conveying charges to an insulated terminal by a rapidly moving belt, this voltage then being applied across an X-ray tube in the conventional way. The voltage obtainable is limited only by the insulation which can be provided for the high voltage terminal. Generators of this type have been developed to give voltages up to about ten million. By enclosing the entire generator under pressure in a bell the dimensions of these units have been greatly reduced, a very compact two million volt source being, in fact, in production.

The betatron[3-10] is a high energy generator utilising magnetic induction to accelerate electrons. The acceleration is carried out in an evacuated toroid, usually called a donut, which is placed between the poles of a large A.C. electromagnet. Electrons are provided by an electron gun mounted in the donut. The gun is pulsed to fire the electrons in when the magnetic field is just beginning to increase above zero, in the first quarter cycle of the current sine wave. The increasing magnetic

field then accelerates the particles. The shape of the magnet pole face is designed such that the magnetic field not only accelerates the electrons but also curves their path. When the condition $\phi_o = 2\pi r_o^2 . H_o$ is satisfied where ϕ_o = flux within the orbit at radius r_o

H_o = magnetic field at r_o

the electrons settle into a stable orbit at a fixed radius and are accelerated during the first quarter cycle as both ϕ_o and H_o increase. Near the point of maximum current the electrons are made to spiral in or out to hit a target on the inside or outside face of the donut. Generators of this type have been developed to give energies up to 100 MeV.

The synchrotron[11,12,13] is a development of the betatron. Here the initial acceleration only is by betatron action, up to an energy where the electrons approach the speed of light. Thereafter the magnetic field merely holds the electrons in their orbit while additional energy is given to them by a time varying electric field provided from a quarter wave radio-frequency oscillator mounted in the donut. Since changes of energy are now reflected in a change in mass rather than velocity, it is possible to arrange for the circulating electrons to be synchronised with the variations of this electric field and to receive additional energy from it at each revolution. The frequency of the electric field required is of the

order of 500 megacycles per second and since the electrons make of the order of a million revolutions in the donut a small field will suffice to add an appreciable total increment of energy.

This type of generator enables a saving to be made on the size of magnet required as compared with a betatron designed for the same energy.

Machines of this type have operated up to 70 MeV. and a few are being built designed to operate at 300 - 400 MeV.

Also being developed as sources of high energy radiations are linear accelerators. Originally used by Sloan and Lawrence,[14] these have been rapidly developed following the advent of radar techniques where high peak powers and short wavelengths can be obtained.[15-18] The electrons are accelerated by the field due to a travelling radio-frequency wave. They are fired into a wave guide, at a suitable point in the cycle, carried down the guide and accelerated by the wave travelling in the guide. Such a generator has been operated up to 4 MeV. in a length of 6 feet and designs are in hand for a 20 MeV. model.

Also available as sources are a range of artificial radioactive materials produced, principally, in atomic piles.

The experimental work here reported has been

carried out with a 15 MeV. synchrotron,[11] a 4 MeV. linear accelerator[15-18] and up to 24 MeV. on a 30 MeV. synchrotron[12] during development at the Atomic Energy Research Establishment (A.E.R.E.), Gt. Malvern, a 20 MeV. betatron[6,7] in the Physics Department, University of Illinois, Urbana, Illinois, a 10.9 MeV. betatron[19,20] and a 70 MeV. synchrotron[13] at the General Electric Research Laboratories, Schenectady, New York, a 3 MeV. Van de Graaff at Massachusetts Institute of Technology (M.I.T.), Cambridge, Massachusetts, as well as with radioactive cobalt 60 and iodine 131 sources in the Physics Department, Royal Cancer Hospital, London.

APPARATUS AND ITS CALIBRATION

Most of the early measurements at the Telecommunications Research Establishment (T.R.E.), Gt. Malvern, were made using a direct-reading ionisation system embodying an F.P.54 electrometer valve in a Du Bridge-Brown circuit[21], with a set of ionisation chambers of fixed volume connected to the measuring system via an evacuated lead to avoid stray ionisation. The chambers, whose internal volume was cylindrical 2·000 cms. long by 2·000 cms. diameter, were those used by Mayneord and Roberts[22] some years ago in measurements in rontgens of the gamma rays from radium. They were carefully machined from pure materials and were available in carbon, graphited

paraffin wax, magnesium, copper and lead. Use was also made of air wall condenser chambers designed and constructed at the Royal Cancer Hospital.[23] Chambers of different designs gave maximum dose measurements up to 0.03, 0.25 and 2.50 r respectively when used on a valve electrometer system of a type developed by Newbery[24] at the Royal Cancer Hospital (Fig. 1). A simple portable direct-reading protection meter rendered valuable service. This consisted of a large ionisation chamber with variable type of end, from open work graphited gauze to various thicknesses of approximately "air-wall" materials, connected through a simple amplifier to an ordinary 50 μ-amp. meter.

For the visit to America, in the light of experience gained at Malvern special apparatus was designed and constructed at the Royal Cancer Hospital. This apparatus consisted of both direct-reading dosage-rate meters and condenser meters. The dosage-rate meters were of the "probe" type[25] having a balanced pair of miniature valves used inverted and embedded in ceresin inside a small duralumin tube. Three ranges of sensitivity were available, namely, full scale deflection of 50 μ-amps. for 5, 50 and 500 r/min. These units were designed for use with the sets of ionisation chambers mentioned above.

For the measurements at high energies the range of wall thicknesses available was extended to 6 cms. in

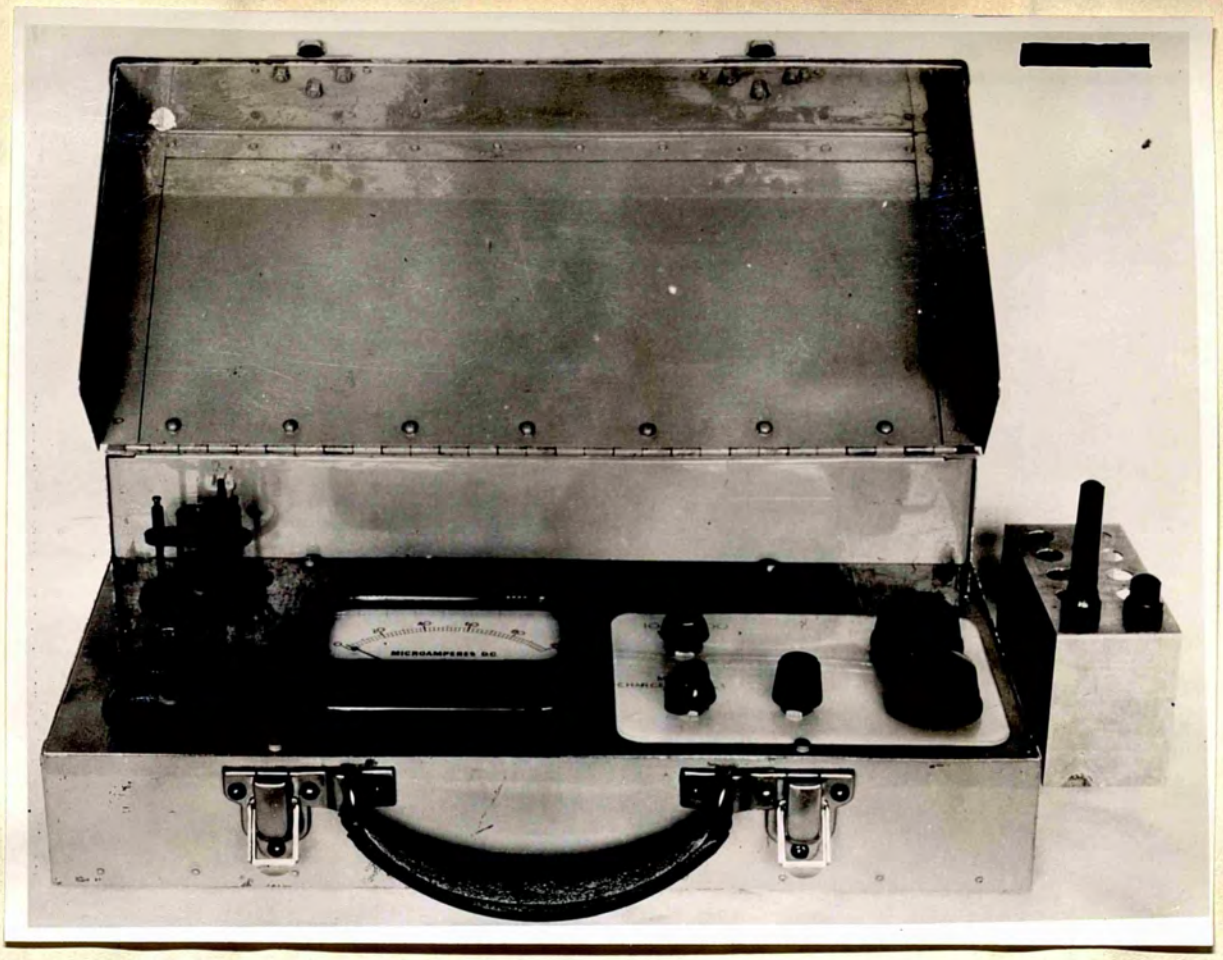

Fig. 1

Fig. 2

Fig. 3

Fig. 4

magnesium and 8 cms. in carbon by means of shells which slipped over the existing chambers. Carbon, magnesium, copper, lead and graphited paraffin wax chambers (the latter for neutron measurements) were constructed and taken to the United States. A graphited "Perspex" chamber of larger volume (384 cc.) (Fig. 2) was used on the probe system for "protection" measurements and also adapted as a standardisation chamber. Part of the end of this chamber could be removed and replaced by a similar wall to which was attached a radioactive cobalt disc. The resulting ionisation in the chamber corresponded to a dosage-rate of 0.110 r/min. and the disc was used to intervals between measurements to check the constancy of the apparatus. By means of a carbon adapter the smaller condenser chambers could be made to fit the series of chambers used with the probe unit, thereby providing a reserve system of instruments and checks. The whole apparatus was carefully fitted and packed in a duralumin case and constituted a small travelling "laboratory" which could be carried by one person and easily handled by two. The instruments are illustrated in Figs. 2, 3 and 4.

The carbon chambers on the probes were carefully calibrated against a standard victoreen condenser dosemeter kept for some years as standard in the Physics Department of the Royal Cancer Hospital. Immediately prior to these

calibrations the victoreen was checked by the National Physical Laboratory over a range of X-ray qualities from a half value layer of 0.05 to 2.1 mm. copper. The probe units were calibrated against this victoreen using the 2 mm. carbon wall chamber at a half value layer of 1.5 mm. copper. On return a further check of probe units against the victoreen was made. The only change recorded was one of 8% in one of the probes, the others having remained constant to within ± 1%. On examining the complete series of check measurements made with the radioactive cobalt disc on both sides of the Atlantic and at sea and making the necessary corrections for temperature and pressure, it was found that the change had occurred between leaving this country and arrival in Schenectady, after which the apparatus remained very constant.

The condenser ionisation chambers were calibrated using a standard 69.7 mgm. radium gamma-ray source also kept in the Physics Department of the Hospital. They were calibrated by mounting them at a known distance from the radium source, both source and chambers being arranged to be some metres from any possible scattering material, giving them a known time of exposure and calculating the dose received in rontgens. This could be obtained from the known relationship that at 1 cm. from 1 mgm. of radium filtered by 0.5 mm. platinum the dosage-rate is 8.3 r/hour.

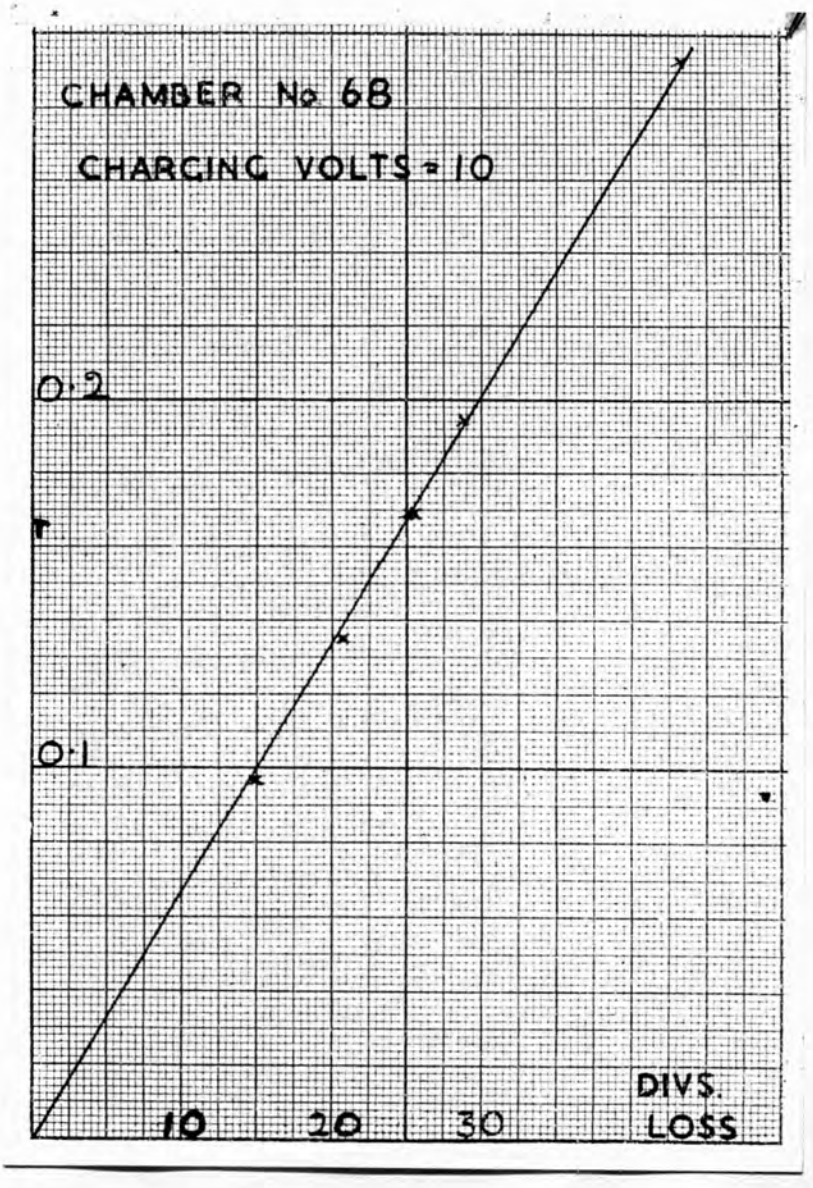

Fig. 5

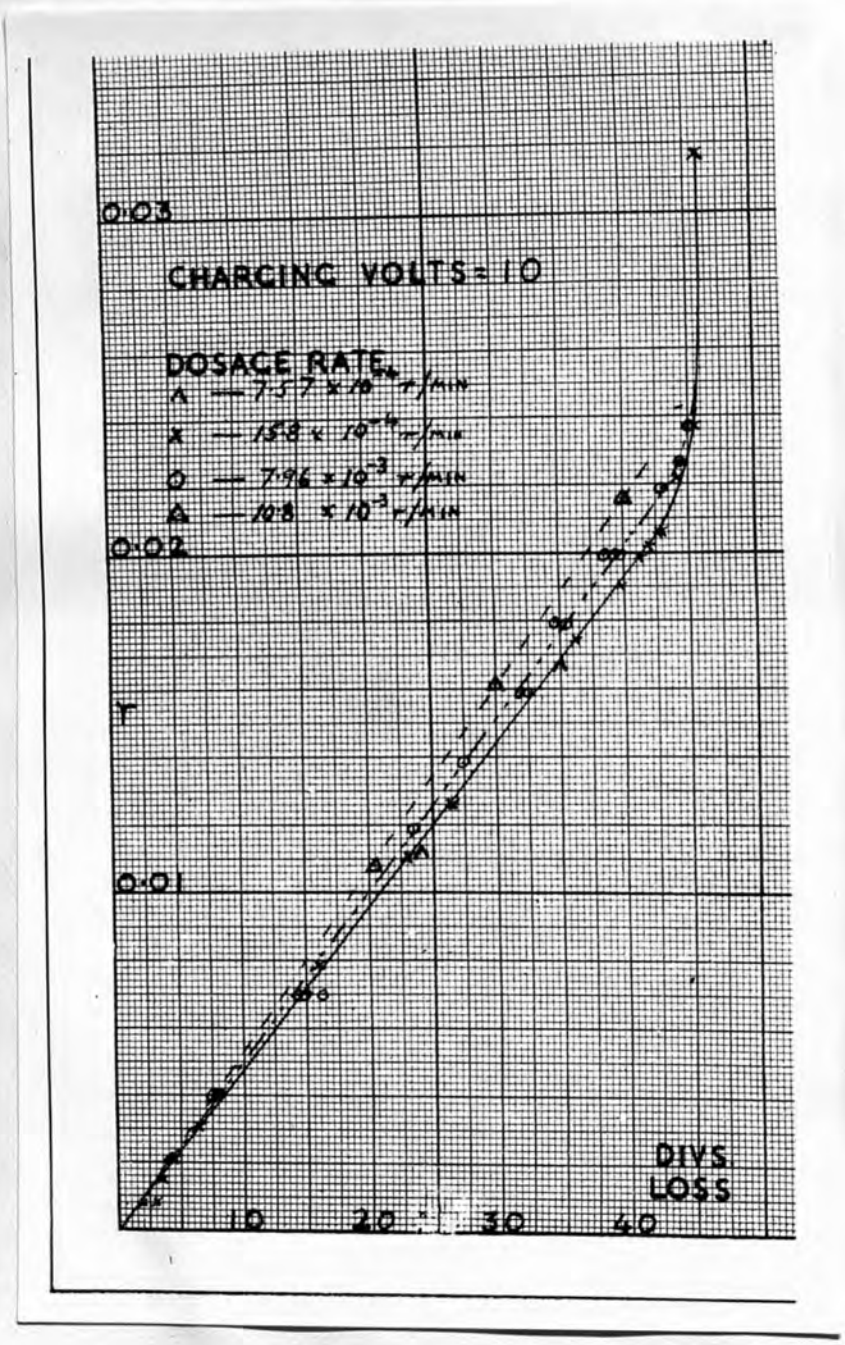
0·03
CHARGING VOLTS = 10
DOSAGE RATE
A — 7·57 × 10⁻⁴ r/min
X — 15·8 × 10⁻⁴ r/min
O — 7·96 × 10⁻³ r/min
Δ — 10·8 × 10⁻³ r/min
0·02
T
0·01
10
20
30
40
DIVS
LOSS

Fig. 6

A typical calibration curve is shown in Fig. 5. The longer chambers, which were designed to measure a maximum dose of 0.03r, were charged to 10 volts and since the inner and outer electrodes were some 3 mm. apart as compared with about 1 mm. in the smaller chambers some doubt was felt as to whether they would be working under saturation conditions. The original model was therefore carefully tested at various dosage-rates, varying from 1.58×10^{-3} r/min. to 7.6×10^{-4} r/min. with the results shown in Fig. 6. The full scale deflection of the measuring instrument was 45 divisions and it can be seen that although there are slight changes in the slope of the curve with dosage-rate the variation of deflection with dose remains linear down to a point at which the field in the chamber is extremely low. Over a range of dosage-rates up to approximately 20 tolerance dosage rate(T.D.R. = 10^{-6} r/sec.) the readings will not, however, be in error to greater than $\pm$ 5%. For ease of construction the design of the chambers was slightly modified and the maximum which could then be measured rose to 0.03r.

As originally constructed these condenser chambers utilised an amber ring to hold the central electrode and insulate it from the outer shell of the chamber. Amber, however, became unobtainable and two series of chambers were constructed and tested, one with insulators

of alkathene and the other using distrene insulators. The chambers were thoroughly tested over a wide range of dosage-rates and for natural leak. It was found when these insulators were pressed out and not machined that no spurious conducting effects appeared in the insulators when irradiated and that the natural leak of the chambers over a day was negligible. Pressing the insulators proved a great saving of time and trouble and it was found, since the entire chamber was now pressed out, that the calibration of all chambers was the same. Distrene was finally chosen as the standard insulator as the spongy nature of alkathene allowed the central electrode to work loose.

The direct-reading "protection meter" was also calibrated using the 69.7 mgm. radium standard. The calibration curve was linear and full scale deflection of 50 μ-amps. corresponded to a dosage-rate of 5×10^{-5} r/sec.

RADIATIONS FROM HIGH ENERGY GENERATORS

When a charge moves non-uniformly, i.e. is accelerated, it generates an electromagnetic field which propagates itself with the velocity of light.

The first hypothesis of this kind concerning the nature of X rays was given by Stokes[27] who supposed that X rays consisted of irregular electromagnetic pulses

due to the irregular accelerations of the electrons as they are stopped by the atoms of the target. Calculations, carried out by Thomson[28] and by Sommerfeld[29] using a simplified form of the above hypothesis, in that the accelerations were presumed to be opposite to the direction of motion of the particles, were confirmed, at least, in part by experimental results.

This simple treatment of the problem by the classical electron theory is for many purposes adequate but a number of phenomena associated with X rays such as the production of characteristic radiation, the occurrence of modified and unmodified scatter X rays are often better, and sometimes only explicable using quantum mechanics. It was, in fact, in the theory of radiation that the breakdown of classical concepts first became evident and led to the introduction, by Planck in 1900, of the quantum of action h.

In the quantum theory the particle or particles occupy discrete states characterised by their energy, momentum, spin, etc. and the transition from one state to another is accomplished by the emission or absorption of radiation in bundles of a definite size known as quanta. The energy (E) of a quantum is related to the frequency (n) of the radiation by the relation

$$E = h.n.$$

Quantum mechanics further requires the association of a

wave with a beam of electrons. The velocity (v) of the electrons is associated with a wavelength, λ, given by

$$\lambda = \frac{h}{mv} = \frac{h}{p}$$

Thus we have a connection between the particle properties of a beam of electrons (velocity v and energy $E = \frac{1}{2} mv^2$) and its wave properties:-

Wavelength: $\lambda = \frac{h}{mv}$

Frequency: $n = \frac{1}{h} \cdot \frac{1}{2} \cdot mv^2 = \frac{E}{h}$

The reconciliation of the wave and particle views leads to the principle of uncertainty, it being found that sharp values cannot be attached to every physical quantity. Certain of the quantities associated say with the electron are sharp according to the nature of the experiment. For example the velocity of the particle may be measured and hence a sharp value assigned to its velocity, energy and momentum, but its position will be unsharp and only probability values can be given for the latter.

Using quantum mechanics to obtain a theory of the production of X radiation by the impact of electrons on a target, a certain probability exists that a light quantum of momentum k is emitted while the electron makes a transition from the initial state (energy E_o, momentum p_o) to another state (energy E, momentum p) where

$$E + k = E_o$$

Bethe and Heitler[30] have obtained, in this way, an expression for the probability that a quantum of radiation is emitted in a direction forming a given angle with the direction of the primary electron.

From this basic theory it is known that the intensity of the X rays produced is a function of the electron energy, atomic number of the target and the angle between the direction of observation and that of the incident electron beam. The angular spread of the high energy X-ray beam due to the radiation process alone is of the order of $\frac{mc^2}{E}$ where E is the energy of the incident electron. By integrating the Bethe-Heitler formula Sommerfeld[31] has obtained an expression for the distribution of radiation produced by fast electrons in a thin target. These calculations are not applicable to the thicker targets normally used in betatrons and synchrotrons which are usually of the order of 1 to 3 mm. thickness. Schiff[32] has, accordingly, used Williams[33] distribution of electrons after penetrating a thickness t of a target and, since the electrons are radiating at all values of t, has integrated Williams' formula over the thickness t and combined this electron distribution with Sommerfeld's radiation distribution formula. He shows that for a given target thickness and given fraction of the intensity at $\theta = 0$ the product $E.\theta. = \text{constant}$. His results are valid

provided the target thickness is not sufficient to cause excessive straggling of the electrons. This thickness for tungsten is approximately 0.05 cm. At high energies an appreciable fraction of the incident electron energy is converted to X rays. The conversion in a tungsten target varies from about 8% at 3 MeV. to about 65% at 20 MeV., both figures showing sharp contrast with the corresponding figures of fractions of 1% in the region below say 200 kV.

With high energy generators the radiations emitted afford some interesting results. From generators of the betatron and synchrotron type, where the electrons being accelerated have to be held in a stable orbit by the magnetic field, it is found that in addition to the beam of high energy radiation emitted from the target in the same direction as that in which the impinging electrons were travelling there is a background of high speed electrons. Some of these undoubtedly escape by a "catherine-wheel" action all round the donut. Also one of the problems, not yet solved, in the operation of the these generators is how the electrons, fired by the gun tangential to the orbit, escape hitting the gun during the early revolutions since the rate of contraction of the orbit is slow. Undoubtedly a number do hit the gun and provide a further source of scattered radiation.

A large proportion of the electrons radiated

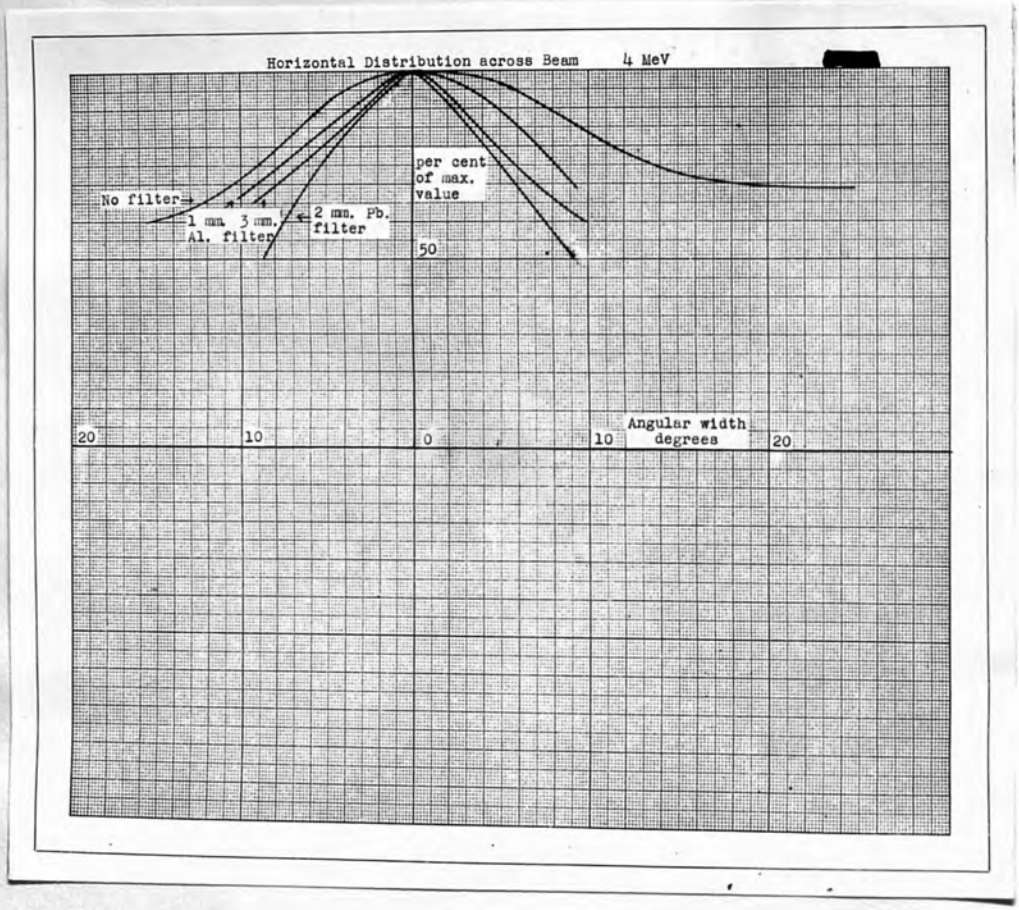
Horizontal Distribution across Beam 4 MeV
No filter
1 mm. Al. filter
3 mm.
2 mm. Pb. filter
per cent of max. value
50
20
10
0
10
20
Angular width degrees

Fig. 7

result from deflections at the target. Many of the electrons not completely stopped in the target get deflected and are curled by the fringing magnetic field and are recorded in any measuring apparatus set up in front of the generator.

Angular distributions of the radiation from the 15 MeV. Malvern synchrotron were measured by setting up a row of the small condenser ionisation chambers perpendicular to the expected direction of the beam. This, in fact, was the first experiment performed on the machine at each visit as it was the method used to determine the direction of the beam. This direction could easily be, and was, altered by a rotation of the donut relative to the magnet in the horizontal plane. This occurred each time the machine was stripped to fit and test various components. The results of the measurement of the ionisation in these individual chambers after an exposure at 4 MeV. were then plotted with the results shown in Fig. 7. The background of high speed electrons whose presence has been explained above is clearly demonstrated. Their removal by filtration left the narrow beam of high energy gamma radiation as shown.

Some experiments were undertaken to trace the source of these soft radiations. It was at first thought that some parts of the donut, for example, were being struck by electrons and giving rise to soft X radiation providing thus, several sources of radiation. A lead marker was set

up on the edge of the magnet coils and in the beam of radiation. Two photographic films were placed, one 30 cms. and the other 50 cms. from the marker, at right angles to the direction of the main beam. An exposure was made and resulted in a uniform blackening of both films with no trace of the shadow of the marker. The experiment was then repeated with a 5 mm. lead filter in the beam when sharp shadows of the marker appeared. A line through the edge of these and the edge of the marker passed as well as could be judged through the target. This was a clear demonstration that the softer radiations, which were removed by the filter in the second experiment, were coming from several directions and producing shadows of the marker edge so diffuse as to be undetectable.

A further test that the main beam was in fact coming from the intended target was made using a pinhole camera. This had a lead front 3 mm. thick and two pinholes of 1 mm. and 2 mm. diameter. As expected the lead front proved rather thin for the penetrating radiation, but against a background of "fog," due to the radiation penetrating the lead front, could be detected images of the target spot. The geometry of the experiment showed that these were in fact images of the correct target. The size of a betatron or synchrotron target is extremely small, the linear dimensions being of the order of 0.1 mm. so that a

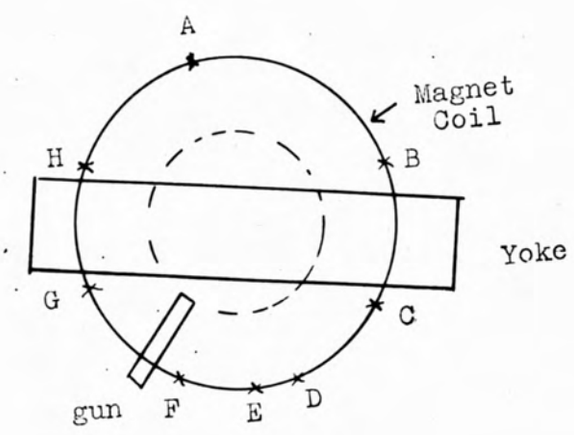

A - 100%
B - 60%
C - <1%
D - 5%
E - 1%
F - 4%
G - 3%
H - 65%

Fig. 8

measure of its size could not be obtained with "pinholes" of the size required in the above experiment to transmit sufficient radiation.

Finally it was suspected that the soft radiations were, in fact, electrons and it was thought that these were perhaps being sprayed out by a "catherine-wheel" action all round the donut as mentioned above. Accordingly a number of condenser ionisation chambers were set up round the periphery of the coils at positions shown in Fig. 8. After exposure the readings shown were recorded. The wide angular spread of the unfiltered beam is confirmed while between 1 and 5% of the primary beam intensity is detected behind the instrument. The slightly higher value obtained near the gun corroborates the belief that some of the electrons collide with the back of the gun during the initial stages of acceleration. That this radiation is, in fact, electrons becomes more apparent as a result of stray radiation surveys made around two of these generators. These will be described later.

There have been few experimental determinations made of such high energy distributions and in such diverse conditions that any exact comparison of theoretical and experimental distributions and of different experimental results is impracticable. It is interesting, however, to survey the experimental work which does exist.

A distribution of radiation from the same machine has been measured by Appelyard and Allen-Williams[34] at 14 MeV. They obtained their distribution using as threshold detectors copper foils to obtain the reaction Cu^{63}_{29} (γn) Cu^{62}_{29} which has a threshold of 10.9 ± 0.3 MeV. By fixing one foil in a definite position as a monitor and making a number of measurements with another foil in different positions a relative distribution of the number of photons between 11-14 MeV. was obtained.

In both these measurements with the Malvern machine a slight asymetry of the distribution is noticeable and the beam angular distribution is narrower than that predicted by Schiff for a tungsten target 0.05 cms. thick.

The target of the Malvern synchrotron was known to be a metal foil bent into a short V-shaped channel and fixed to a wire support with the angle of the V vertical and nearest the electron orbit. The dimensions were not known.

Westendorp and Charlton[35] show distributions measured with the 100 MeV. betatron. Their target was a vertical piece of wire 0.25 cms. diameter. Their distributions show the asymetry similar to that previously mentioned. Again considering the thickness of the target the distributions are too narrow as compared with Schiff's theory. Later measurements by Charlton and Breed[36] on the same plant do not show the asymetry previously observed,

though they give no details of changed experimental conditions which could account for this. The distributions are again narrower than the target thickness, given in this case as 0.38 cms., would lead one to expect.

As already stated the diverse circumstances prevent any rigorous comparison of the measured values and of the measured and theoretical values. It is, however, worthy of notice that the rate of collapse or expansion of the electron orbit on to the target is slow, the difference in successive orbits as the electrons spiral in or out being of the order of 10^{-4} cms. There is therefore a distinct possibility, since the targets have had curved surfaces, that thin target radiation is being obtained. Two possibilities also exist and may be superimposed. Deflection in the target may result in electrons being deflected such that a greater target thickness is traversed and this may explain the asymetrical distributions. Depending upon the magnetic field conditions electrons scattered in the target may be re-focussed and pass through the target again. Such repeated traversals may mean that a reasonable total output is being obtained from a thin target. Further doubt, however, is cast on the theoretical values of the angular distributions by some experiments made by Buechner and his colleagues[37] with a 3 MeV. Van de Graaff generator. They used targets thick enough to stop

the electrons completely and despite the effects of the various scattering processes their angular distribution for a tungsten target is narrower than predicted by theory.

The bremstrahlung theory of Bethe and Heitler is worked out for one collision but the expression given can be integrated over the whole range of the electrons in the target to obtain an approximate expression for the total quantity of X rays produced. Such a calculation has been performed by Chien-Shiung Wu[38] and she finds that the total energy radiated will vary almost linearly with atomic number. She herself concludes that the variation is linear with the square of the atomic number, but her results clearly show an approximately linear variation. Buechner[37] and his colleagues have found a similar linear variation of total output, obtained by integrating over the solid angle surrounding their target, with atomic number.

These results and similar work by Ivanov et al[39] may be taken as substantiating the Bethe-Heitler theory of the process. It should, however, be noted that in the energy region in which these experiments were carried out the inelastic collision losses, only, need be considered in calculating the range as compared with higher energies where the radiation losses become significant.

It therefore appears that the discrepancy between theoretical and experimental angular distributions arises

in the deductions made as to the electron scatter in the target. The scatter must be considerably less than predicted by theory. The theories of electron scatter are sufficiently at variance to make their conclusions doubtful and it should also be noted that, as demonstrated later, the stopping power for fast electrons in high atomic number materials increases considerably as compared with lower energies.

This means that the electron range in the material is considerably reduced with, consequently, less scattering.

Much more experimental work is, however, required before rigorous comparisons with theory can be made. Targets of various thicknesses and atomic numbers will have to be tested and it is recommended that the targets be flat sheets of material placed such that the electrons will impinge perpendicular to their surface thereby avoiding the complications introduced by the oblique incidence in Buechner's work and the curvature of the surfaces of the targets in the other experiments.

For some purpose an even field of irradiation will be desirable and this can be obtained by using a differential filter of cigar shape placed in the beam with the long axis parallel to the beam. Such a filter will reduce the dosage-rate at the centre of the field and

if properly designed will provide a flat field of irradiation. A filter of this type has been designed and used by Kerst[40] and his colleagues. Despite the apparent deviations from Schiff's theory it was thought worth while to use his values to indicate the order of size of flat field which would be available at various energies. The calculated values are shown in Table I, the edge being taken as the place at which the intensity falls to a given fraction of the central maximum.

TABLE I

0.5 mm. Tungsten Target.

Fraction of max. defined as edge.	Diameter of circle in cms. at 100 cms. focal distance.		
MeV.	0.50	0.20	0.10
10	35.3	81.6	119.7
20	17.5	39.2	55.2
30	11.6	26.0	36.3
50	7.0	15.5	21.6
100	3.5	7.7	10.8

It is clear that even up to 100 MeV. flat fields of reasonable size may be obtained, the possibilities depending on the output, which determines the amount of radiation which may be wasted in a filter.

ABSORPTION OF X RADIATION

When penetrating radiation passes through an absorbing medium the absorption of the radiation takes place by three processes. The energy of the radiation may be transferred to the electrons in the medium by either or both of two processes. When the whole quantum energy is transferred to the electron the process of photoelectric absorption takes place and a secondary electron results. The quantum-electron encounter may also occur according to the Compton[41] scattering process when a quantum of lower energy (i.e. longer associated wavelength) and a secondary electron results. Thirdly the quantum may interact with the nuclei in the medium and create pairs of particles, comprising positive and negative electrons. It is also possible for pair formation to occur in the field of the electrons in the medium but the effect is small and the theories so far given for the effect do not agree.

The theories for the photoelectric absorption and Compton effect have been developed and tested by a number of physicists and the predictions are well known. Where values of the coefficients of photoelectric absorption (τ) and the Compton effect cross-section (σ) have been required in the work to be described they have been calculated from the theories due to Fowler, Hulme et al[42] and Klein-Nishina[43] respectively.

Pair production is a process which, since it involves the creation of two particles each of mass equal to that of the electron (but of opposite charge), cannot begin at energies less than 1.02 MeV. (i.e. $\leq 2\ mc.^2$). The present theory of pair production is based on Dirac's[44] wave equation. His "hole theory" postulates that, in the absence of an external field, all the negative energy states of a free electron are filled. An energetic quanta of radiation or a particle of sufficient kinetic energy can cause the removal of an electron from one of the negative energy states. The "hole" thus left has a positive charge, positive energy and momentum opposite to that corresponding to a negative energy state. It therefore behaves as a positron. As mentioned before, since two particles of mass m have to be "created" the minimum energy required to create a pair is $2\ mc.^2$ Also in order that energy and momentum conservation is possible a third particle (e.g. a nucleus) must be present. A provisional estimate of the probability of the process was first given by Oppenheimer and Plesset[45] and a formula for the effect deduced by Bethe and Heitler.[30] The latters' values for the cross-section for the creation of pairs will be used in the subsequent calculations. Direct experimental proof of the creation of such pairs has been obtained in Wilson cloud chamber experiments by Curie and Joliot[46], Chadwick [47] and others. Further, when the

pairs so created are annihilated, which occurs, usually, once they have spent all their kinetic energy, the process gives rise to annihilation radiation of energy 2 mc.^{2} This appears as excess scattering of the incident radiation. The cross-section for this process is theoretically proportional to Z^2 and it has been found experimentally[48] that this excess scattering is proportional to Z^2, a further indication of the validity of the theory. Further, indirect check on the theory of the process may be obtained by measurement of the absorption coefficients of high energy radiations.

From the above theories the values of the absorption coefficients in any given material may be calculated. The total absorption coefficient is given by

$$\mu = \tau + \sigma + \pi$$

where τ is the photoelectric absorption coefficient[42], σ the cross-section for the Compton scatter process[43], and π the cross-section for pair formation.[30] The values of the absorption coefficient per electron have been calculated for a range of atomic numbers up to an energy of 300 MeV. and are shown in Fig. 9. As previously stated the absorption due to pair formation in the field of the electrons has been neglected since the effect is small and agreement on its value not yet obtained.[49-51] Since further, the theories for the cross-section for pair formation

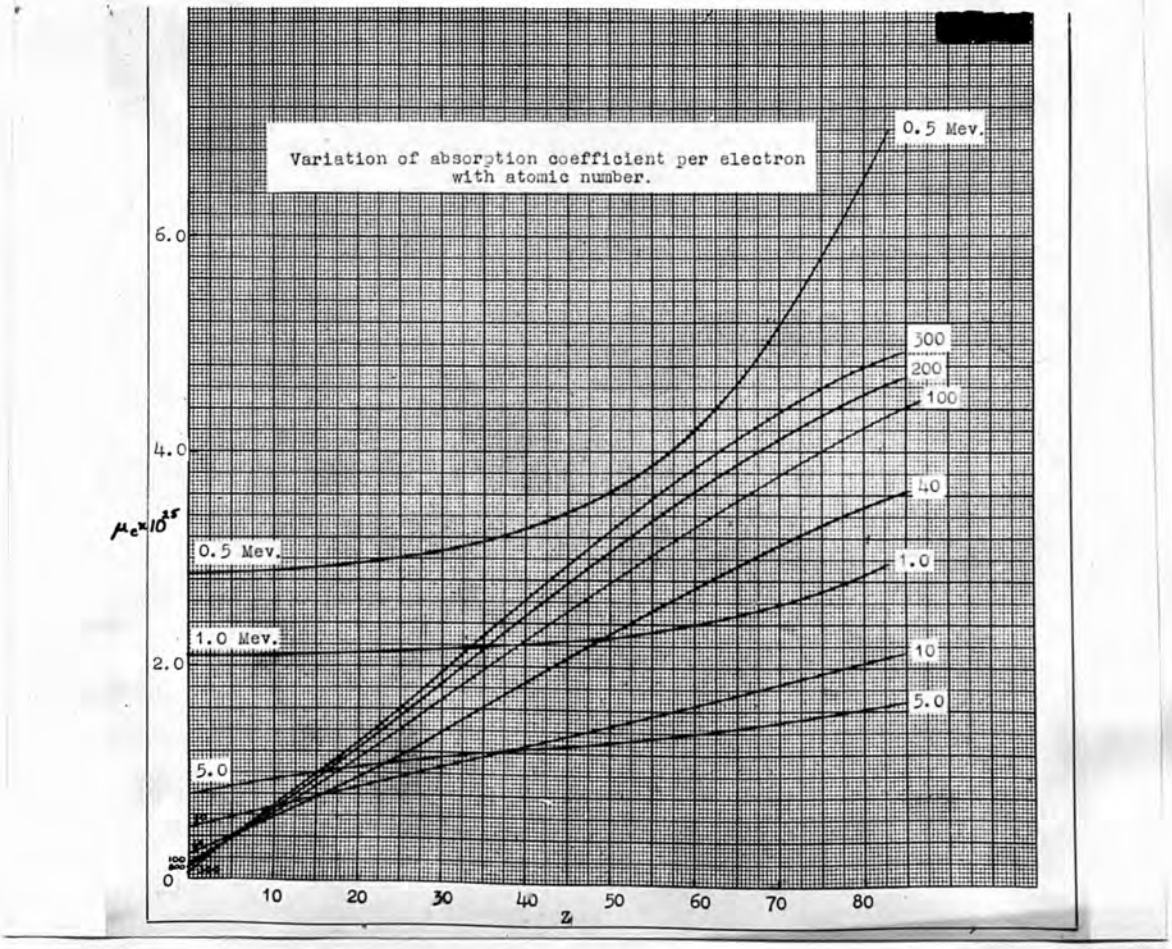
Variation of absorption coefficient per electron with atomic number.
0.5 Mev.
300
200
100
40
1.0
10
5.0
0.5 Mev.
1.0 Mev.
5.0
6.0
4.0
2.0
0
$\mu_e \times 10^{25}$
10
20
30
40
50
60
70
80
Z

Fig. 9

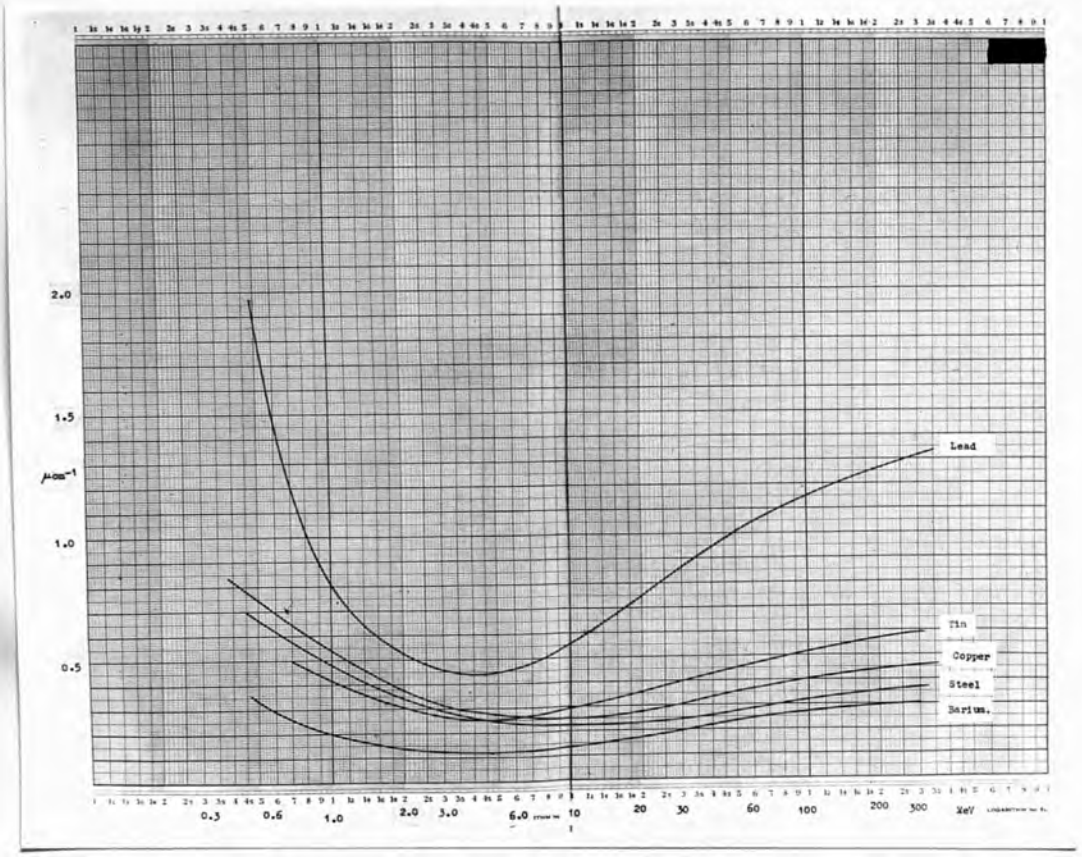
2.0
1.5
μcm⁻¹
1.0
0.5
Lead
Tin
Copper
Steel
Barium.
0.3
0.6
1.0
2.0
3.0
6.0
10
20
30
60
100
200
300
MeV

Fig. 10

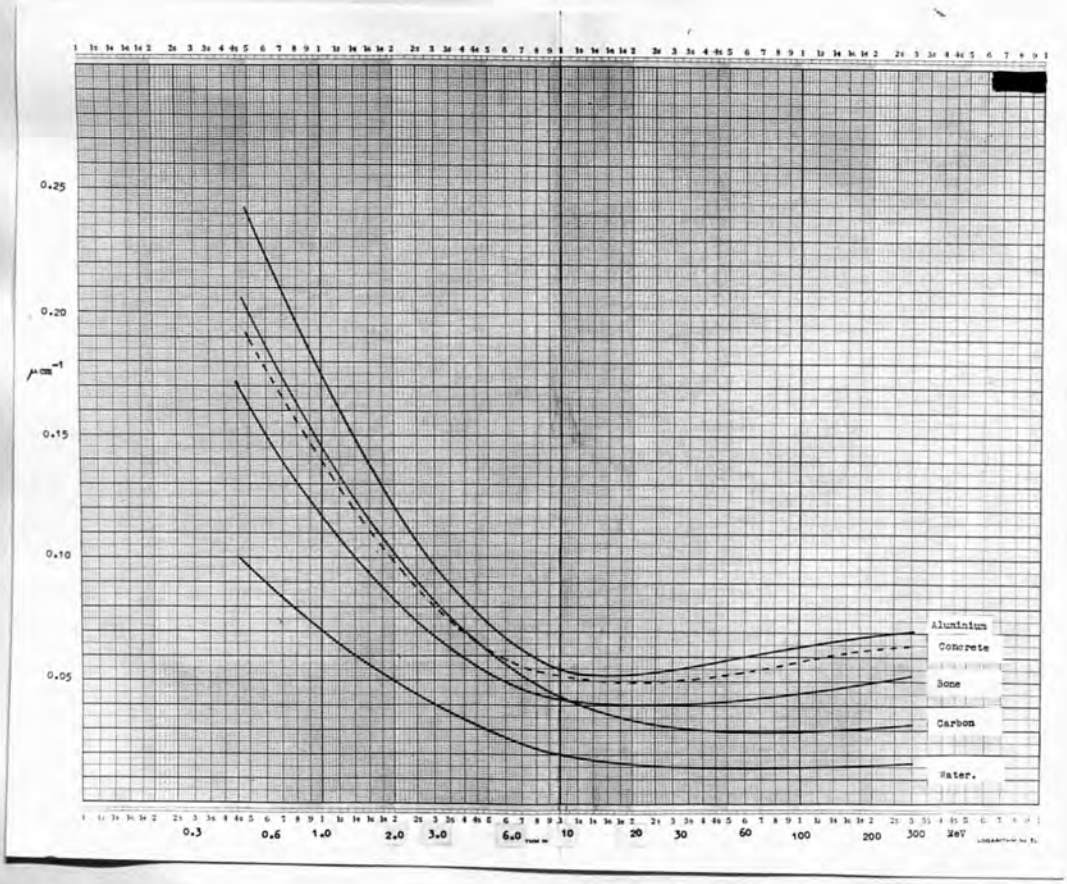
0.25
0.20
μcm⁻¹
0.15
0.10
0.05
Aluminium
Concrete
Bone
Carbon
Water.
0.3
0.6
1.0
2.0
3.0
6.0
10
20
30
60
100
200
300
MeV

Fig. 11

have been calculated using the Fermi-Thomas model of the atom and the Born approximation, the latter being doubtful for heavy elements and the former for light elements, precise values are not to be expected. It is doubtful if the theory is much guide above 100 MeV., although the values have been calculated up to 300 MeV.

The photoelectric cross-section, except for elements of high atomic number, rapidly becomes negligible as the energy increases. It is roughly proportional to $\lambda^3 Z^3$ per electron. It is appreciable in lead up to 2 MeV. but in aluminium only up to 50 KeV. Compton effect then becomes most important until above 1 MeV. when pair formation (proportional to Z per electron) commences. At about 5 MeV. in lead and 15 MeV. in aluminium Compton and pair formation effects are equal and thereafter pair formation becomes increasingly important. The effects of these various factors can be seen in Fig. 9 in the changing slopes of the curves. The coefficient is surprisingly constant in the region 1 - 2 MeV. while, as could be expected at higher energies, it varies roughly linearly with Z.

Linear absorption coefficients have also been calculated for a number of materials up to the same energy and are shown in Figs. 10 and 11. The values for bone were calculated for calcium phosphate by calculating, as also in the case of water, the fractional absorption due to the

constituent elements. For concrete the calculations were made for silica. In each case the appropriate density was used. Here we see clearly the effect of pair formation on the linear absorption coefficients of the various materials, the initial decreasing values with increase in energy are due to decrease in the values of τ and σ and the subsequent rise at higher energies, always exceeding 1.02 MeV., is clearly due to the advent of absorption by pair formation. It is interesting also to see how the position of minimum absorption coefficient moves with atomic number. Reference to the importance of this point will be made later.

Experimental Work

If the primary intensity of a beam of radiation be I_o and the intensity after passing through a thickness d of material be I, then the absorption coefficient μ for any wavelength present will be given by the exponential expression

$$I = I_o e^{-\mu d}$$

It is clear that the result obtained will depend on whether or not any radiation deflected from the original direction of the beam can enter the measuring system and therefore to minimise the deflected radiation measured a beam of small cross-section is usually employed along with as small a measuring system as possible. The latter is also removed

as far as possible from the absorber and other material which may scatter radiation into it.

Using the X-ray beam from the 15 MeV. synchrotron, filtered with a 5 mm. lead filter, absorption coefficients were measured in aluminium, copper, steel, tin and lead, at 4, 8, 11 and 14 MeV. Some preliminary absorption experiments were undertaken during the early part of the work at Malvern to investigate the quality of the unfiltered radiation. These were carried out with aluminium absorbers, this being the only material then to hand. The results are shown in Fig. 12 and clearly demonstrate the large amount of soft radiation emitted from the generator. A few millimetres of aluminium is sufficient to cut out the bulk of this radiation. The strange relative positions of the 4 and 8 MeV. curves are undoubtedly due to the conditions of operation. At 4 MeV. the machine was operating as a betatron while at 8 MeV. as a synchrotron. The resonator does not always succeed in collecting and accelerating all the electrons set in motion by betatron action and many of these are probably thrown out, making the 8 MeV. beam, initially, appear softer than the 4 MeV. The slopes of the curves after the removal of the electrons show the expected difference.

The filters used in the later tests were held and inserted in the beam, at a focal distance of 105 cms.,

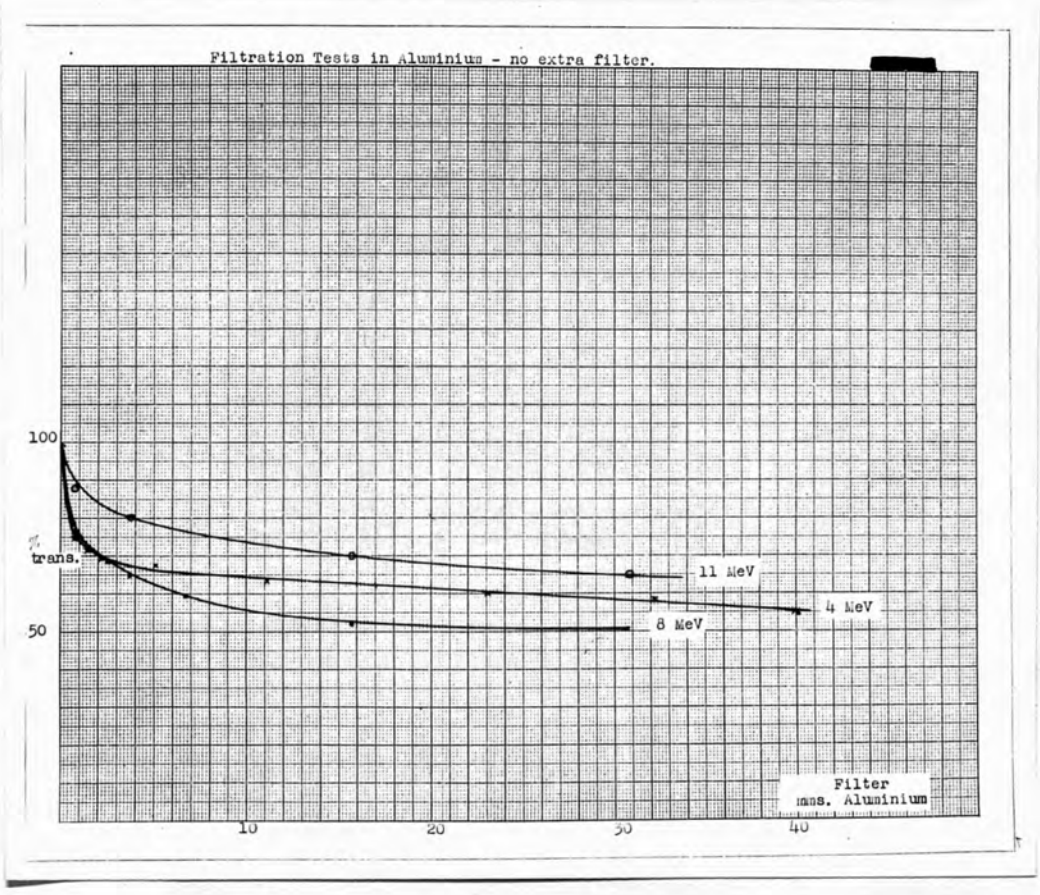
Filtration Tests in Aluminium - no extra filter.
100
% trans.
50
11 MeV
4 MeV
8 MeV
Filter
mms. Aluminium
10
20
30
40

Fig. 12

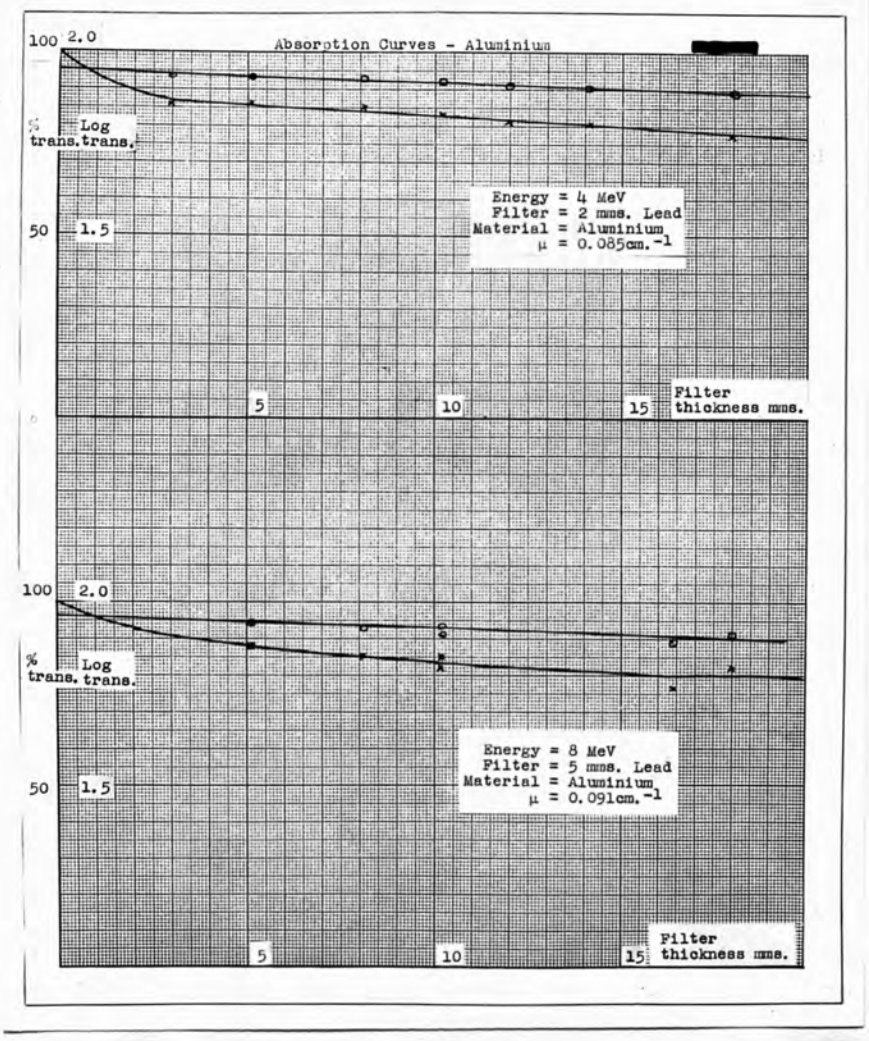
Absorption Curves - Aluminium
100
2.0
% trans.
Log trans.
50
1.5
Energy = 4 MeV
Filter = 2 mms. Lead
Material = Aluminium
μ = 0.085cm.-1
5
10
15
Filter thickness mms.
100
2.0
% trans.
Log trans.
50
1.5
Energy = 8 MeV
Filter = 5 mms. Lead
Material = Aluminium
μ = 0.091cm.-1
5
10
15
Filter thickness mms.

Fig. 13

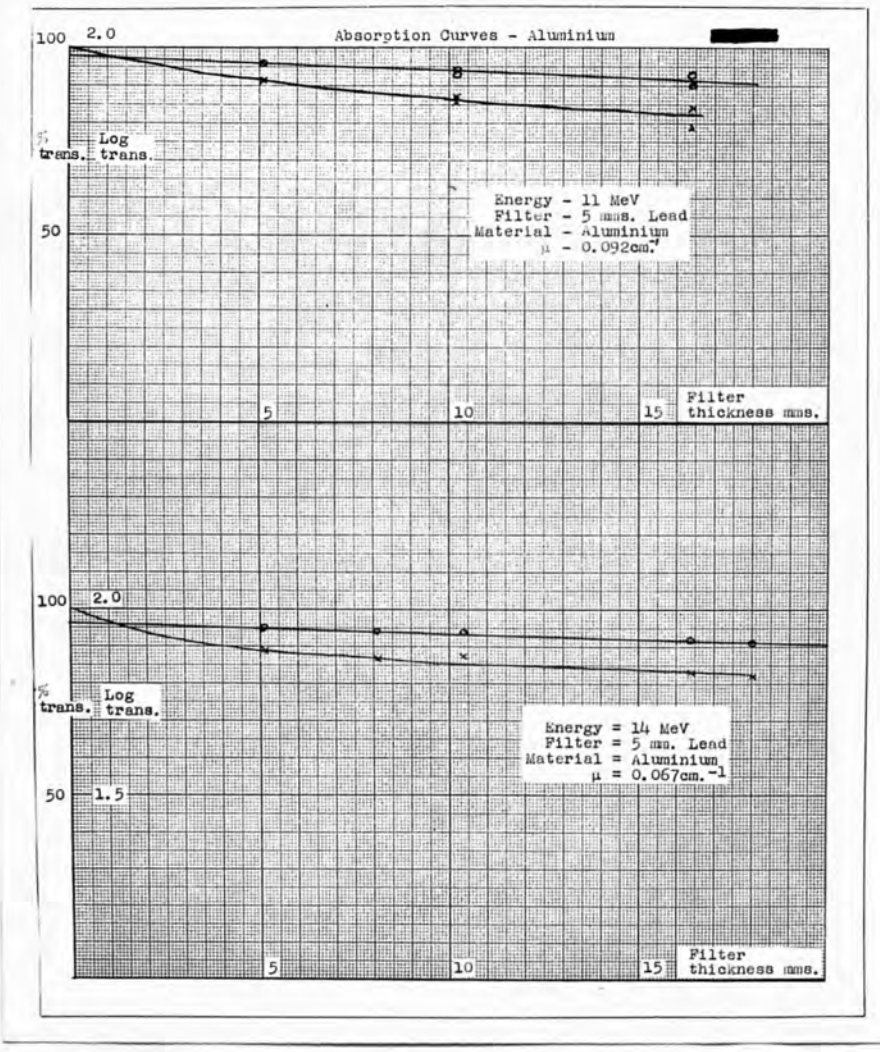
Absorption Curves - Aluminium
100
2.0
% trans.
Log trans.
50
Energy - 11 MeV
Filter - 5 mms. Lead
Material - Aluminium
μ - 0.092cm.-1
5
10
15
Filter thickness mms.
100
2.0
% trans.
Log trans.
50
1.5
Energy = 14 MeV
Filter = 5 mm. Lead
Material = Aluminium
μ = 0.067cm.-1
5
10
15
Filter thickness mms.

Fig. 14

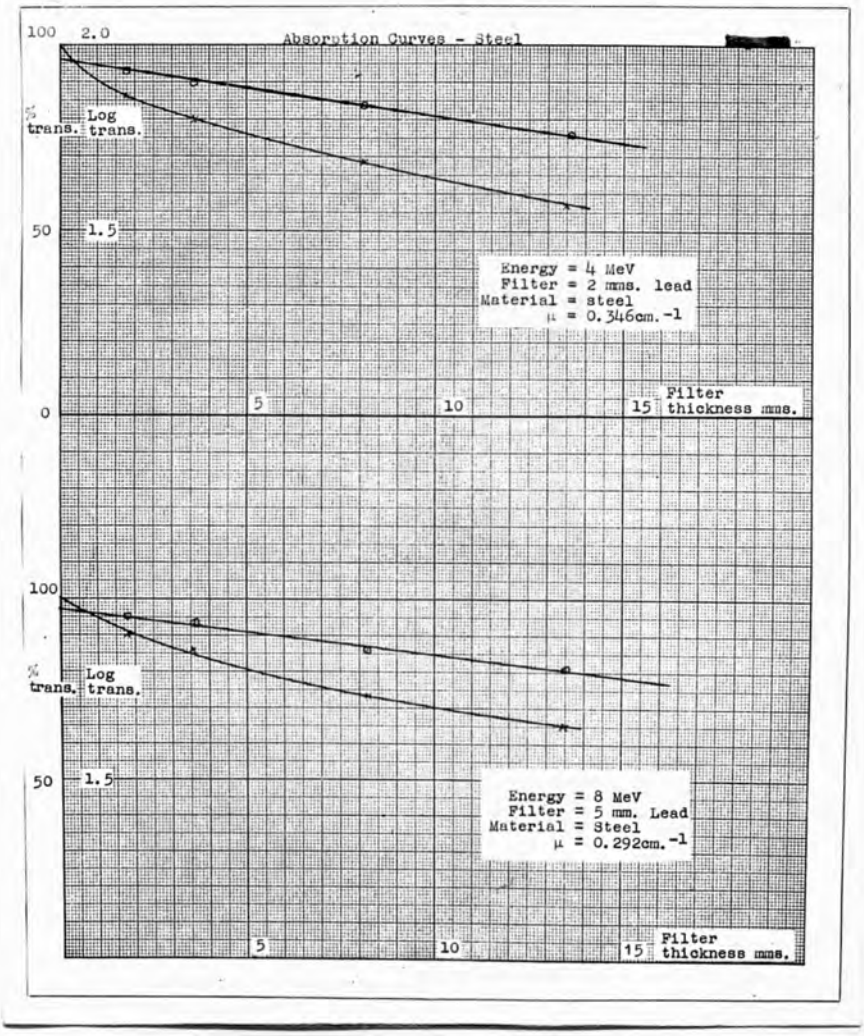
Absorption Curves - Steel
100
2.0
% trans.
Log trans.
50
1.5
0
Energy = 4 MeV
Filter = 2 mms. lead
Material = steel
μ = 0.346cm.-1
5
10
15
Filter thickness mms.
100
% trans.
Log trans.
50
1.5
Energy = 8 MeV
Filter = 5 mm. Lead
Material = Steel
μ = 0.292cm.-1
5
10
15
Filter thickness mms.

Fig.15

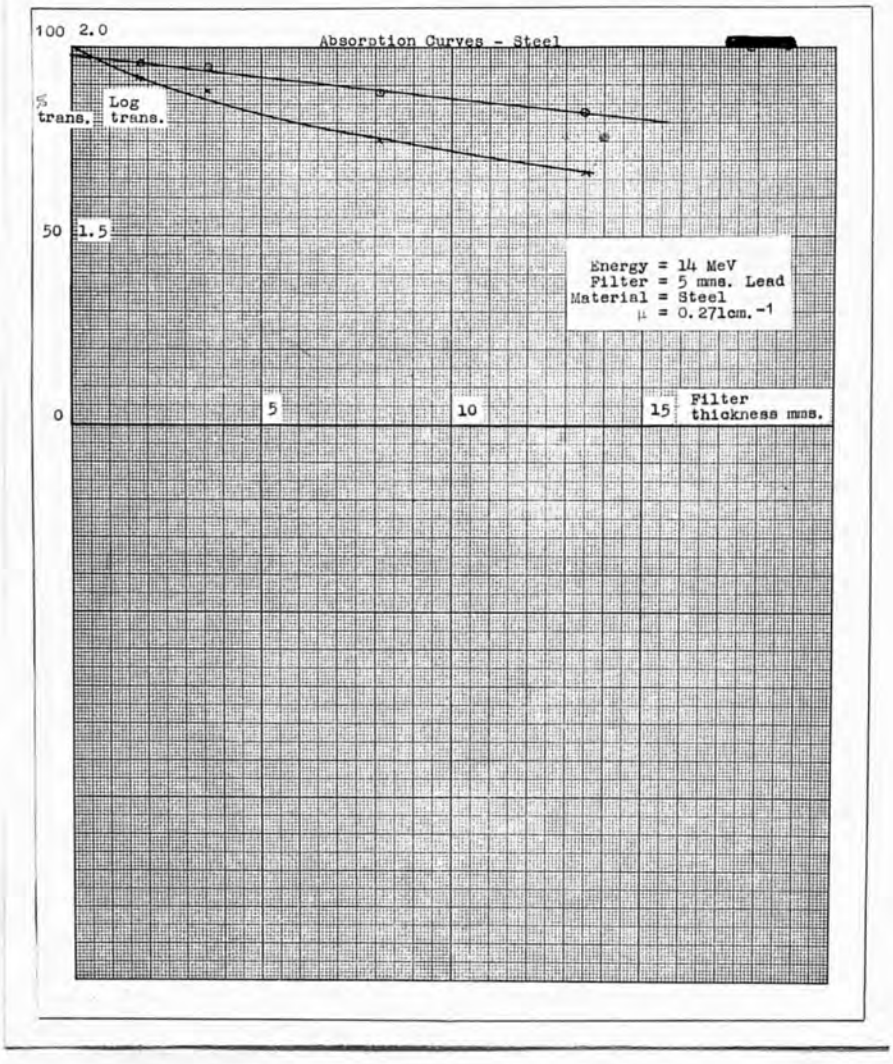
Absorption Curves - Steel
100
2.0
% trans.
Log trans.
50
1.5
0
5
10
15
Filter thickness mms.
Energy = 14 MeV
Filter = 5 mms. Lead
Material = Steel
μ = 0.271cm.-1

Fig. 16

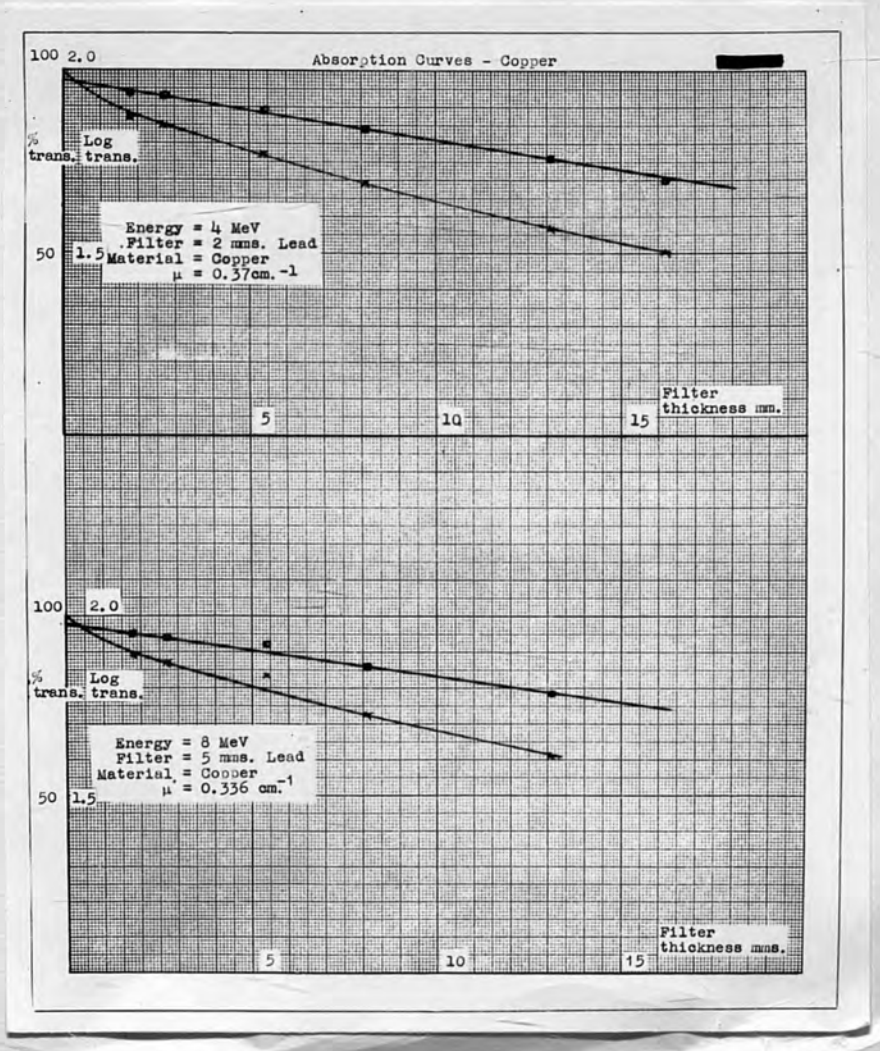
Absorption Curves - Copper
100
2.0
% trans.
Log trans.
Energy = 4 MeV
Filter = 2 mms. Lead
Material = Copper
μ = 0.37cm.-1
50
1.5
5
10
15
Filter thickness mm.
100
2.0
% trans.
Log trans.
Energy = 8 MeV
Filter = 5 mms. Lead
Material = Copper
μ = 0.336 cm.-1
50
1.5
5
10
15
Filter thickness mms.

Fig. 17

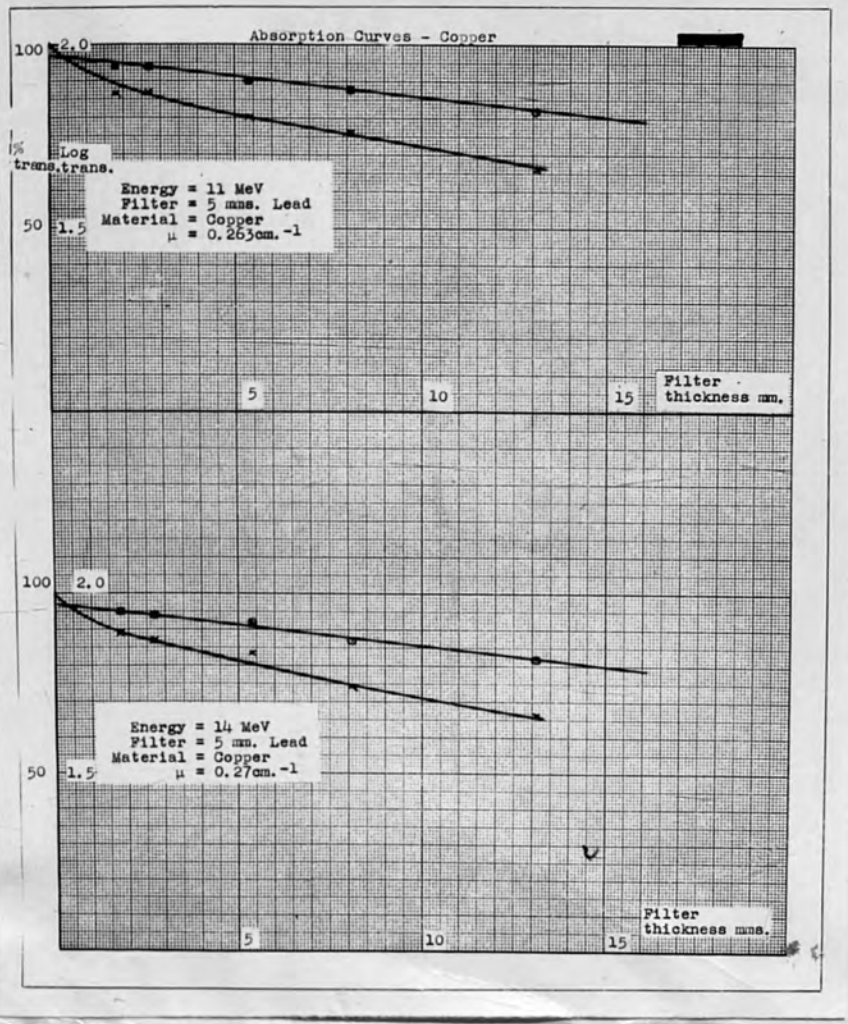
Absorption Curves - Copper
100
2.0
% trans.
Log trans.
Energy = 11 MeV
Filter = 5 mms. Lead
Material = Copper
μ = 0.263cm.-1
50
1.5
5
10
15
Filter thickness mm.
100
2.0
Energy = 14 MeV
Filter = 5 mm. Lead
Material = Copper
μ = 0.27cm.-1
50
1.5
5
10
15
Filter thickness mms.

Fig. 18

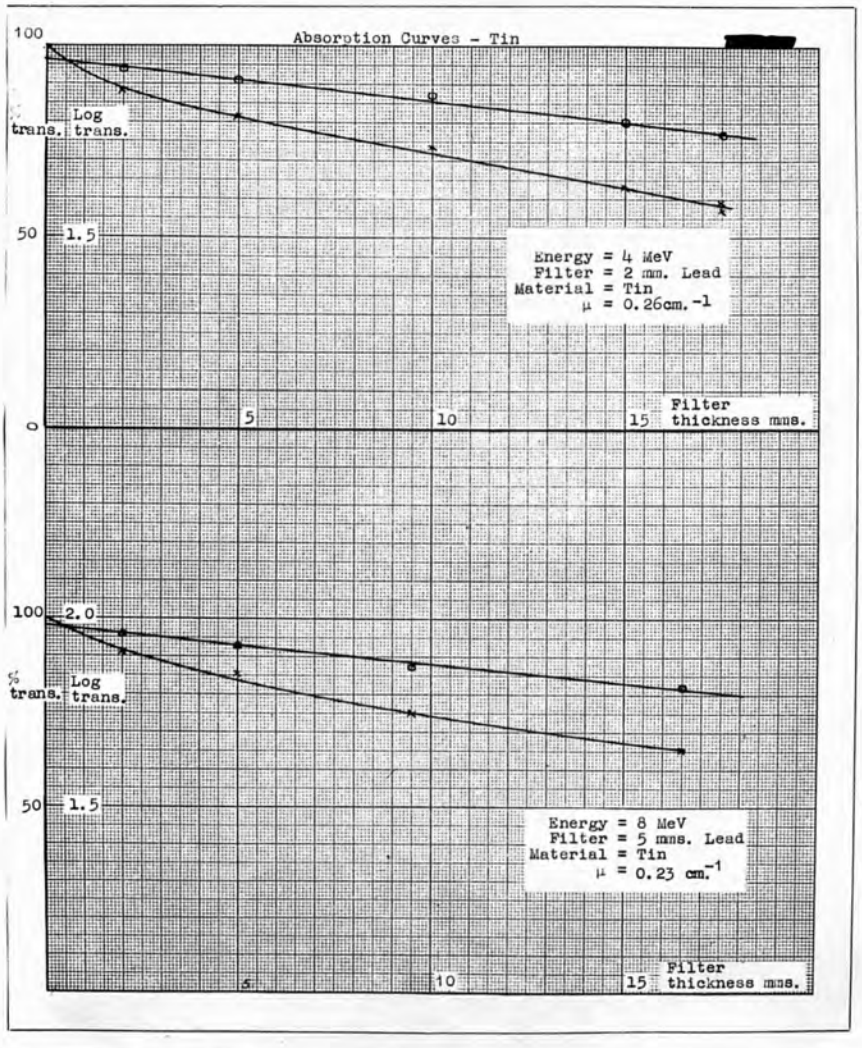
Absorption Curves - Tin
100
% trans.
Log trans.
50
1.5
0
5
10
15
Filter thickness mms.
Energy = 4 MeV
Filter = 2 mm. Lead
Material = Tin
μ = 0.26cm.-1
100
2.0
% trans.
Log trans.
50
1.5
Energy = 8 MeV
Filter = 5 mms. Lead
Material = Tin
μ = 0.23 cm.-1
5
10
15
Filter thickness mms.

Fig. 19

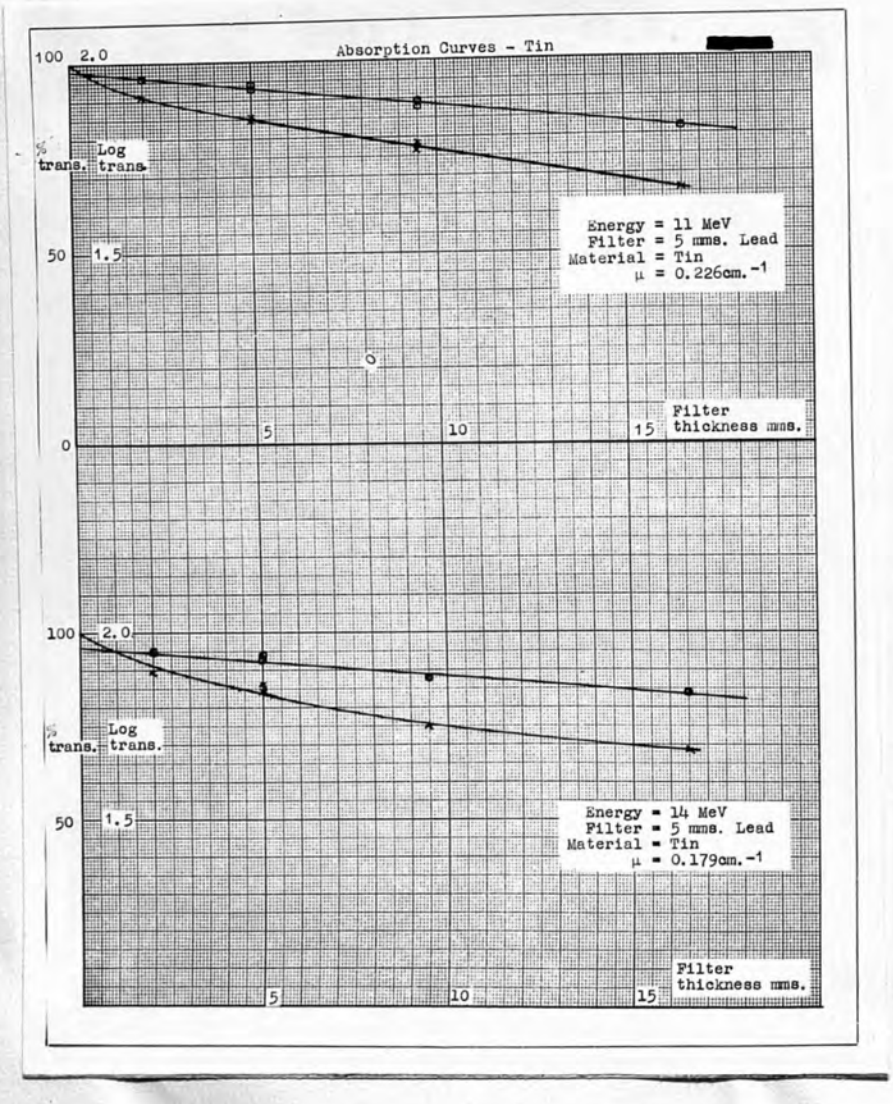
Absorption Curves - Tin
100
2.0
% trans.
Log trans.
50
1.5
0
5
10
15
Filter thickness mms.
Energy = 11 MeV
Filter = 5 mms. Lead
Material = Tin
μ = 0.226cm.-1
100
2.0
% trans.
Log trans.
50
1.5
5
10
15
Filter thickness mms.
Energy = 14 MeV
Filter = 5 mms. Lead
Material = Tin
μ = 0.179cm.-1

Fig. 20

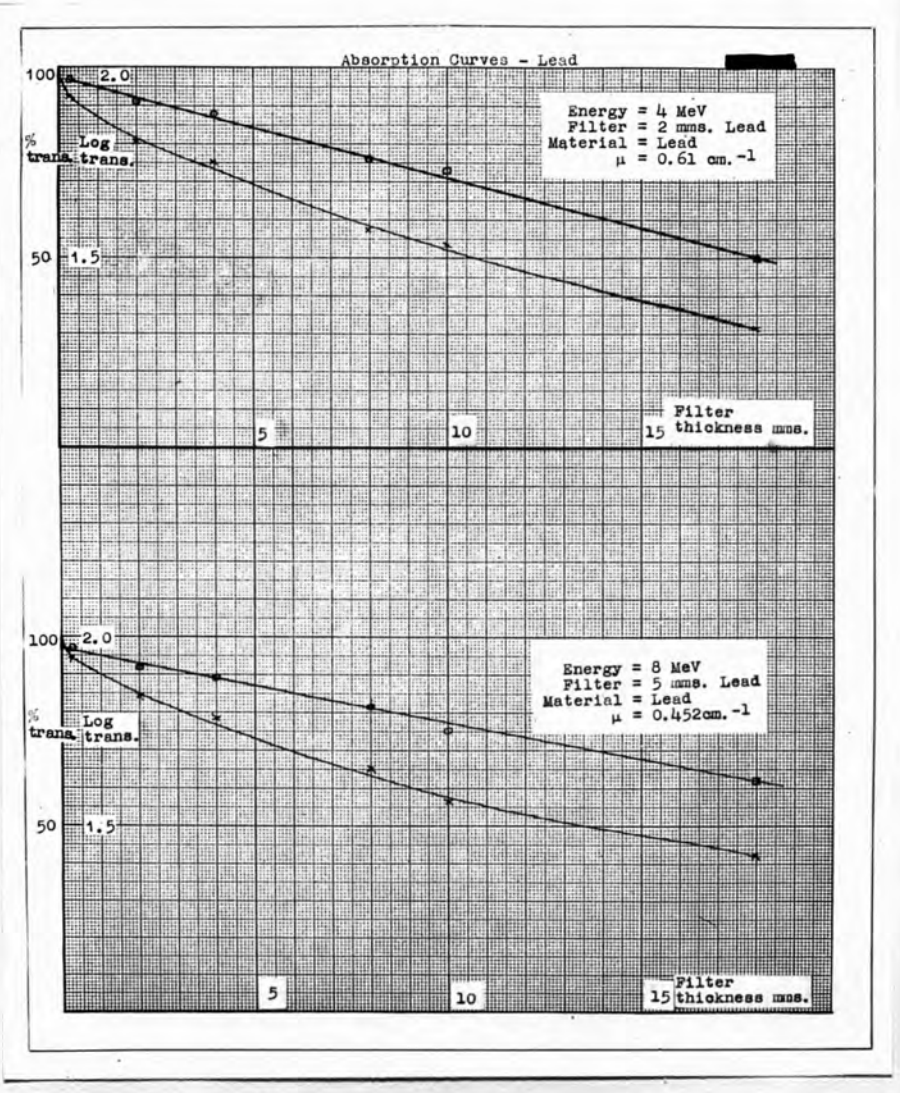
Absorption Curves - Lead
100
2.0
% trans.
Log trans.
50
1.5
Energy = 4 MeV
Filter = 2 mms. Lead
Material = Lead
μ = 0.61 cm.-1
5
10
15
Filter thickness mms.
100
2.0
% trans.
Log trans.
50
1.5
Energy = 8 MeV
Filter = 5 mms. Lead
Material = Lead
μ = 0.452cm.-1
5
10
15
Filter thickness mms.

Fig. 21

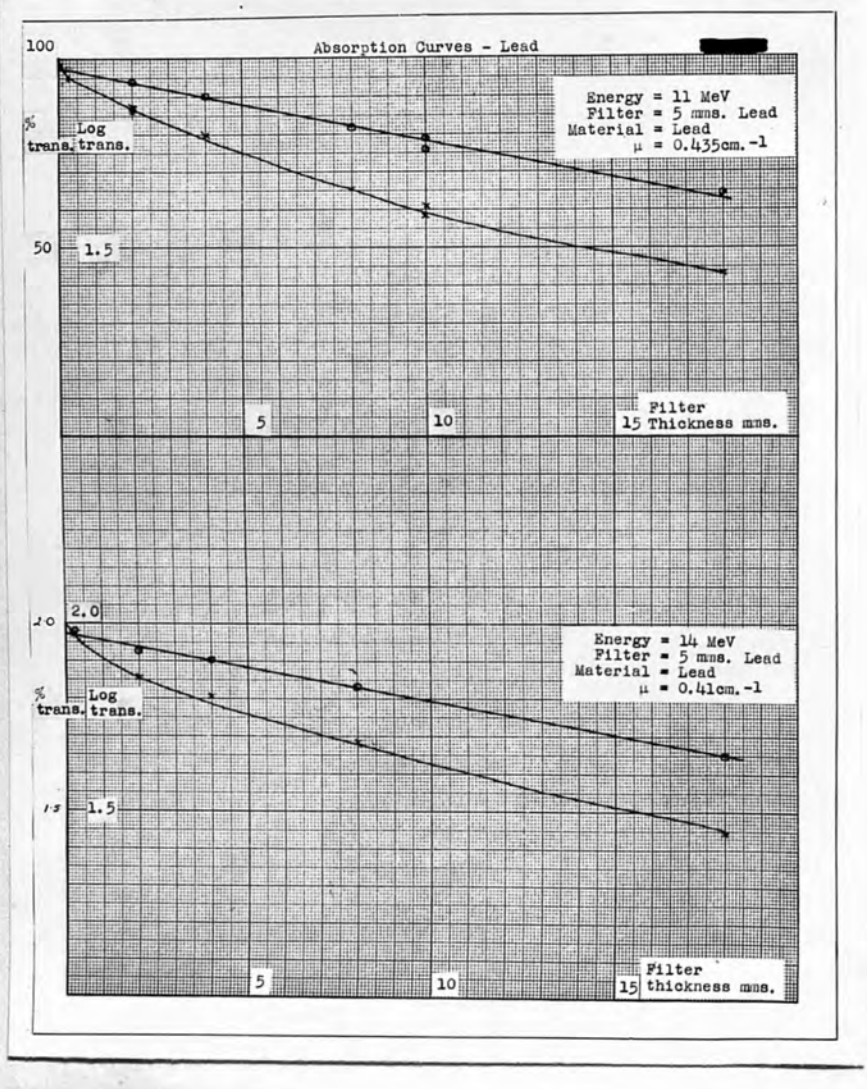
Absorption Curves - Lead
100
% trans.
Log trans.
50
1.5
Energy = 11 MeV
Filter = 5 mms. Lead
Material = Lead
μ = 0.435cm.-1
5
10
15
Filter Thickness mms.
2.0
1.0
% trans.
Log trans.
1.5
Energy = 14 MeV
Filter = 5 mms. Lead
Material = Lead
μ = 0.41cm.-1
5
10
15
Filter thickness mms.

Fig. 22

by a remotely controlled rotating wooden wheel. Twelve holes 5 cms. square, which just admitted the filters to be used, were cut on the wheel. Alternate holes contained filters, the other holes being left blank and affording a check on the unfiltered intensity before and after each measurement with a filter in the beam. The filters, which were 5 cms. square, just covered the measuring chamber, a carbon chamber of 1.0 cm. wall thickness, set up 24 cms. from the wheel. The wheel, which was faced with lead 1 mm. thick to prevent soft scattered radiation reaching the measuring system, was rotated by a motor operated from the control room of the synchrotron and a simple signalling system indicated when an aperture was in the beam. The system was satisfactory and speedy in operation but suffered the disadvantage that the beam was not well canalised. The measuring system was the F.P.54 system previously mentioned. The results of the experiments are shown in Figs. 13 to 22, where it will be seen that the log transmission curves yielded straight lines from which the absorption coefficient was calculated. That these lines did not pass through the origin probably showed that the soft radiation previously found in the beam had not been completely removed. The values of absorption coefficient obtained are shown plotted in Figs. 23, 24 and 25. The dotted curves are the theoretical values calculated as above. The measured values

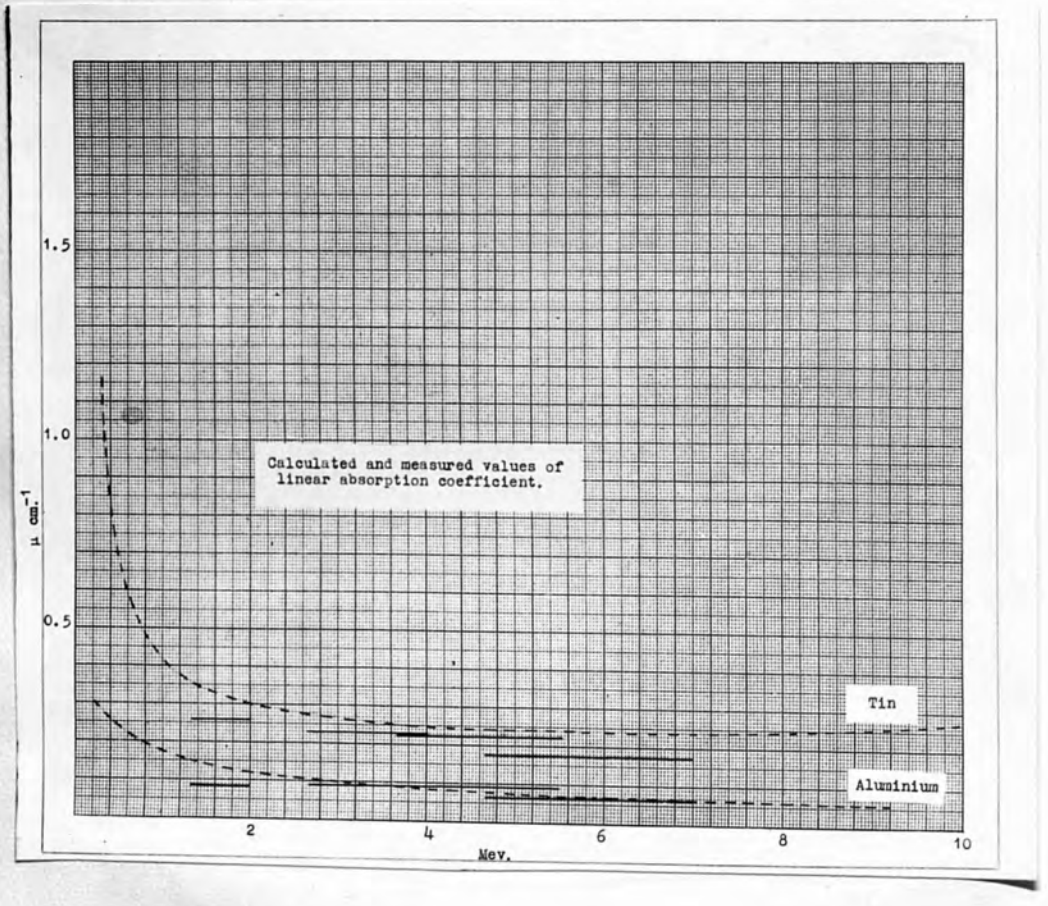
Calculated and measured values of linear absorption coefficient.
μ cm.⁻¹
1.5
1.0
0.5
2
4
6
8
10
Mev.
Tin
Aluminium

Fig. 23

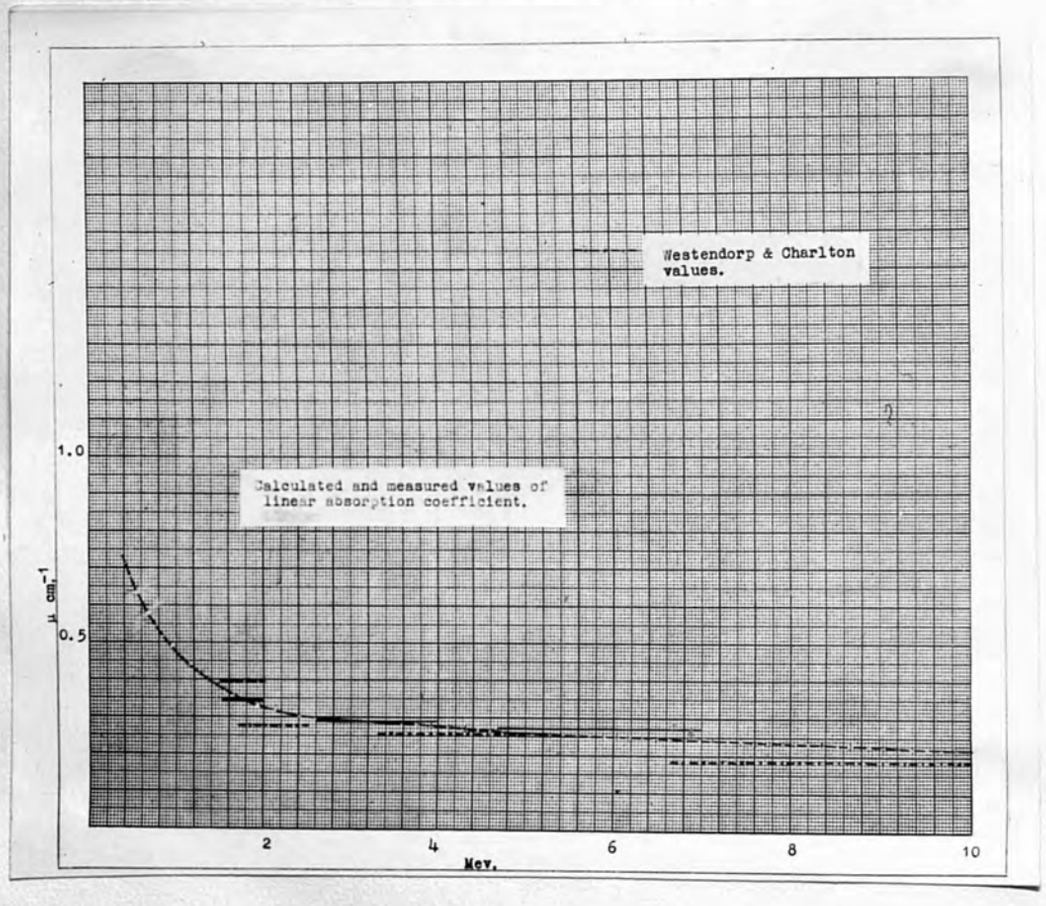
Westendorp & Charlton values.
Calculated and measured values of linear absorption coefficient.
1.0
0.5
μ cm⁻¹
2
4
6
8
10
Mev.

Fig. 24

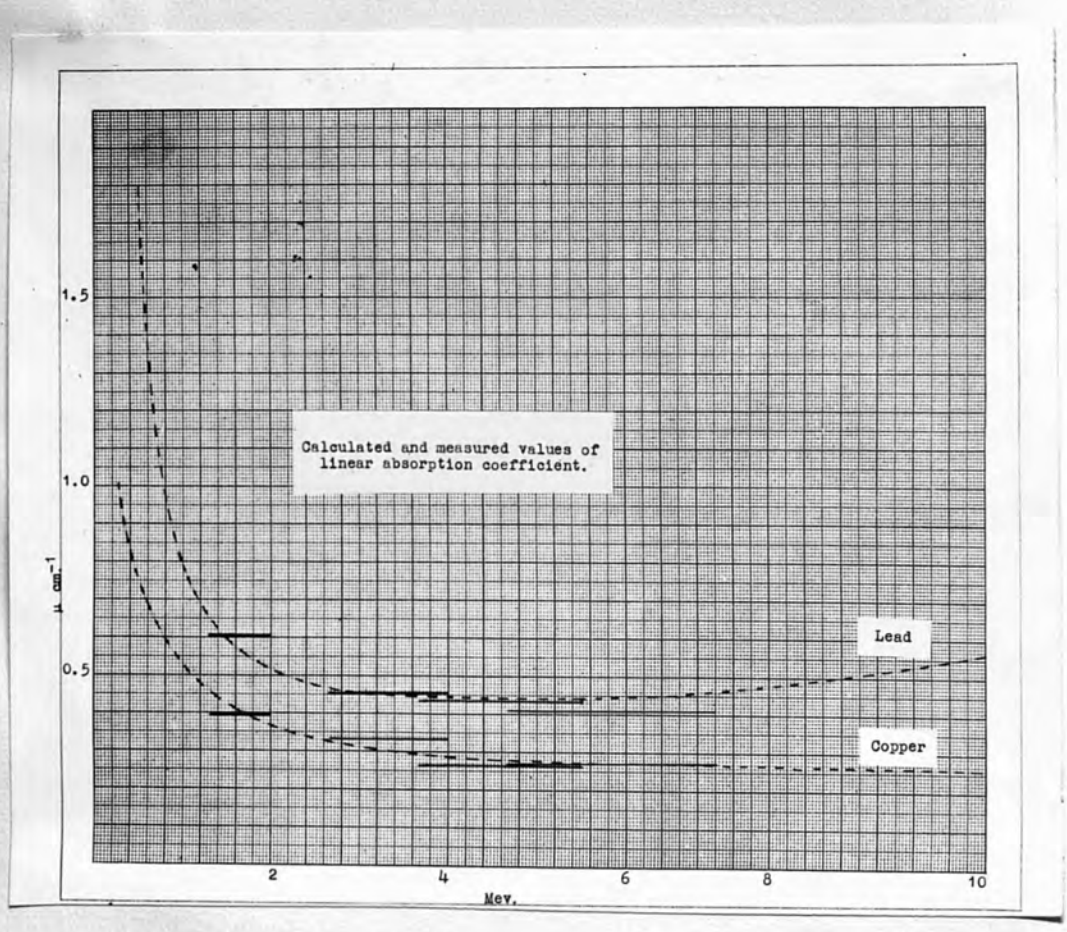
Calculated and measured values of linear absorption coefficient.
1.5
1.0
0.5
μ cm.⁻¹
Lead
Copper
2
4
6
8
10
Mev.

Fig. 25

are plotted as short horizontal lines extending from one half to one third of the peak excitation energy, since, owing to the heterogeneity of the original beams it is difficult to assign a unique "equivalent mean energy." No measurements of the spectral distribution of radiation from high energy generators are available and the theoretical values given by Heitler[52] have been used. Some verification of the correctness of the shape of these curves has been obtained by Lawson[53] who has observed the ratio of the intensity in adjacent energy bands and found agreement with theory and we can therefore assume the distributions correct without introducing appreciable errors. The factors one half and one third correspond to the mean values of the shapes of these spectral distribution curves which can be assumed roughly triangular or rectangular.

It will be seen that, except at the highest energy for the two elements of highest atomic number, tin and lead, the measured values are in fair agreement with theory, and in the case of steel with s ome early measurements by Westendorp and Charlton.[35]

Calculations using Tarrant's theory[54] show that this discrepancy is not due to scatter. Part of the discrepancy is undoubtedly due to the fact that the high energy quanta produce pairs and recoil electrons which in turn, particularly in a heavy element, will produce a continuous X-ray spectrum. The result will be a decrease

in "mean" quality of the beam which, if the primary energy of the quantum is higher than the energy of minimum absorption coefficient of the material, will result in the material appearing more transparent. For lead and tin this would be possible at the maximum energy of 14 MeV. at which these measurements are made. It has not been possible to repeat these experiments under more exacting conditions to determine more exactly the cause of the discrepancy.

In addition to these measurements, while at Malvern a measurement of the absorption coefficient of water was made at 12 MeV. Using a trough made of thin "Perspex" the transmissions through thicknesses of water of 10, 25 and 50 cms. were measured. A measurement was also made to enable a correction to be applied for absorption by the "Perspex" ends of the trough. The value of the coefficient obtained for water at 12 MeV. was 0.0342 $cm.^{-1}$, in fair agreement with theory.

At Urbana similar measurements were made with carbon absorbers ($\rho = 2.3$). The values of absorption coefficients obtained were, at 15 MeV., 0.43 $cm.^{-1}$ and, at 20 MeV., 0.405 $cm.^{-1}$, in reasonable agreement with theory.

A variety of other experimental data appears in the literature on measurement of absorption coefficients in various materials and using a number of different techniques. Most of the work is at energies between 1 and 3 MeV. but a few values at higher energies have been

obtained by some workers using as sources either induced radioactive transformations or high energy generators.

A particularly fine series of investigations at 88 MeV. has been carried out by Lawson[53] using the 100 MeV. betatron at Schenectady. Using a gold radiator to produce pairs he was able to restrict the spectral energy range in which he was measuring to between 82 and 100 MeV. and assuming this section of the spectral distribution as given by Heitler for 100 MeV. he finds his mean energy to be 88 MeV. Lawson has also checked the shape of the spectral distribution curve given by Heitler by comparing the intensities in adjacent energy channels and is satisfied that the theory and experiment are in good agreement. By using a narrow band of energies near the top of the spectrum he minimises the effect of scattered radiation on the radiation transmitted. This scattered radiation is of lower energy and therefore more penetrating since the absorption coefficient is rising with energy in this region. Any scattered radiation, if the energy band be narrow enough, will be so degraded as to be undetected. By means of a spectrum analyser, using a carefully designed arrangement of Geiger Muller counters, the relative intensity of the radiation with and without absorbers in the beam is obtained from measurements of the pairs formed in the gold radiator. His absorption coefficients, measured in beryllium,

aluminium, copper, tin, lead and uranium, compare well with theory but discrepancies exist, particularly in the heavier elements. Lawson attributes the discrepancies to the Born approximation used in the calculation of pair formation cross-sections. The ratio of theoretical value to experimental would, he points out, be expected to be proportional to $(Z/137)^2$ and a plot of the ratio as obtained by him against Z^2 shows a straight line, the values for beryllium, however, showing an inexplicable deviation. He thus obtains a clear indication that the disagreement arises from the approximations used in the theory.

By bombarding with X rays targets of different materials designed to be of such a thickness as to give the same theoretical scattering, the ratios of 88 MeV. pairs ejected was measured for equal X-ray bombardment.

Now if u' and u'' are total absorption coefficients in the materials, π' and π'' are the pair formation coefficients and σ' and σ'' the Compton coefficients, we have

$$\frac{\mu'}{\mu''} = \frac{\pi'\left(1+\frac{\sigma'}{\pi'}\right)}{\pi''\left(1+\frac{\sigma''}{\pi''}\right)} = \frac{\pi'\left(1+\alpha'\right)}{\pi''\left(1+\alpha''\right)}$$

Now μ'/μ'' can be measured as above and π'/π'' obtained from the ratio of the pairs from the pair forming targets. If also, say element II, is of high atomic number and the energy being used is high, as it is in this case, the value of α'' is very small and can almost be neglected and certainly

is so small that variations in theoretical predictions will have little effect on the value of α' as calculated from the equation. Thus knowing μ' by measurement and α', a value of π' can be deduced and, of course, a value of σ'. Lawson finds that, using several elements in this experiment, the values of σ are within 15% of the values given by Klein-Nishina formula, a very satisfactory result.

Appelyard and Allen-Williams[34] and also Adams[55] have made some measurements using an activation technique. By this method also it is possible to limit the energy band width in which the measurements are made. A material which has an activation threshold about the energy which is to be measured is used. For example, Appelyard and Allen-Williams have used the copper reaction Cu^{63}_{29} (γn) Cu^{62}_{29} which has a threshold at 10.9 ± 0.3 MeV. By operating the generator at 14 MeV. they restricted the measurements to the 11 - 14 MeV. region. One foil of copper was placed in front of the material whose absorption coefficient was to be measured and the other at the back. After an exposure the relative activities were compared and the absorption coefficient calculated from this ratio for several absorber thicknesses. The Appelyard-Allen-Williams value of 0.62 ± 0.02 cm.$^{-1}$ for lead at 11 - 14 MeV. is in good agreement with theory. Adams used the same technique using the copper reaction for measurements at 11 MeV., the

Fe^{54}_{26} (γn) Fe^{53}_{26} reaction with a threshold at 13.9 ± 0.3 MeV. and the C^{12}_{6} (γn) C^{11}_{6} reaction with a threshold at 18.7 ± 0.1 MeV. for values at approximately 14 and 19 MeV. Adams has also assessed the mean energy of the spectral band he has used by weighting the relative number of quanta at each energy level, with an estimated cross-section. Adams found that some of the secondary Compton quanta are sufficiently energetic to activate the detectors and he has made a correction for this effect. Unfortunately in publishing his results Adams has applied this correction to his theoretical values and it is difficult, since he does not state the method and values of the correction, to compare his results with other published values, but his values appear in fair agreement with theory. In his calculation of the theoretical values Adams has used, in place of Z^2 in the Bethe-Heitler formula for pair formation, the value $Z(Z + 1)$ to allow for pair formation in the field of the electrons. This correction, which as stated before is small and not included in the calculations of Figs. 10 and 11, is based on Watson's calculations.[50]

Cowen[56] has also measured values of the absorption coefficients in carbon, aluminium, copper, tin and lead. His measurements, made up to 2.3 MeV., have been carried out using the more conventional technique of measuring the total electromagnetic radiation before and after filtration by the material in question. He has, however, used monochromatic radiations using as sources the isotopes

Cs 137 (0.65 MeV.), Sb 114 (1.72 MeV.), Zn 65 (1.11 MeV.) and Na 24 (2.30 MeV. after filtration), and has taken elaborate precautions to avoid scattered radiation by mounting his absorbers, which were small, his source and geiger counter tube used for the measurement on slings out of doors and at long distances from any likely scattering sources. His results are in excellent agreement with his theoretical calculations. These latter values differ slightly from those given in Figs. 10 and 11 and it is not clear from Cowen's work on which theory he bases his values of the photoelectric absorption coefficients. Variations of the order of 10% can be found here owing to the empirical nature of some of the factors in the formula for the photoelectric absorption coefficient. A survey showing a variation of this order is given by Jones.[57]

Cork and Pidd[58] using carefully collimated sources of radioactive substances, Zn 65 (1.11 MeV.), Co 60 (1.30 MeV.) and Na 24 (1.38 and 2.76 MeV.) have made absorption coefficient measurements in copper and lead. Their values for the 1.11 MeV. and 1.3 MeV. radiations are in good agreement with theory, but their measurement for the high energy line of Na 24 is lower than theory and in particular for lead is lower than the minimum theoretical value of the absorption coefficient of lead. The source of this error appears to lie in their method of correcting for the presence

of the 1.38 MeV. line. They have measured the transmission through various thicknesses of absorber for the two lines together. Then using the calculated transmission curve for the 1.38 MeV. line the values so obtained have been subtracted from the total values. Since the mean quality of the radiation as the absorber thickness varies in the first case will change this subtraction is not valid. Further a change in sensitivity of the ionisation chamber is to be expected between 1.38 and 2.76 MeV. for which no allowance has been made. No details of the chamber used are given, but by assuming a reasonable wall thickness and atomic number for this chamber and then making a rough correction for the change of sensitivity it is found that the absorption coefficient measured by them can be brought into better agreement with theory. The value should, of course, be related to an energy of 2.76 MeV. and not 2.85 MeV. as given by them for the Na24 line. A similar method but using as detector a Geiger counter for measurement was used by Alburger[59] again using a Na24 source. His values are in good agreement with theory as also are values measured for the 2.76 MeV. line by Groetzinger and Smith.[60]

A later series of measurements by Cork[61] using stronger sources of Zn 65 and Co 60 shows divergences from theory. No information is given which would enable an explanation to be made. In later measurements with Co 60

Mayneord and Cipriani[62] have obtained excellent agreement between measured and theoretical values of the absorption coefficients in a range of materials and it therefore appears that the experimental technique used by Cork is at fault.

Mayneord and Cipriani have also shown that for the elements of low atomic number which they have used, where photoelectric absorption is negligible, the absorption coefficient per electron is constant and equal to 1.90 x 10^{-25} cm.^{2} per electron. This value is in excellent agreement with the value of scattering absorption coefficient as calculated from the Klein-Nishina formula.

Pair formation being negligible for Co 60 radiation these workers have, further, shown that the values of photoelectric absorption coefficients per electron obtained by subtracting the above value for the scattering coefficient from their measured total absorption coefficients are in good agreement with the Fowler-Hulme theoretical values.

An interesting determination made by them of the absorption of the radiation in water and heavy water showed, as expected, that the linear absorption coefficient (but not, of course, the mass absorption coefficient μ/ρ) was the same in both cases.

Using as source the heterogeneous but heavily filtered radiations from a Van de Graaff generator Petrauskas,

Van Atta and Myers[63] have made transmission measurements in water, carbon, aluminium, tin, copper and lead and these are again in reasonable agreement with theory. Some early measurements by Westendorp and Charlton[35] using the 100 MeV. betatron give reasonable values for steel except at the higher energies where the values are rather low. Their values for lead particularly at the higher energies are far too low. No details are given of their experimental arrangements but the shape of their transmission curves for lead, lead one to suspect that the measuring chamber has been too close to the absorber resulting in spurious effects due to scatter. Further, at the higher energies it is not considered that measurement of the transmission in this way will give correct absorption coefficients owing to the effect, now present, that the scattered radiation may be more penetrating than the primary radiation. It should, however, be stated that a measurement of the values of total transmitted radiation is of interest, for example, in protection problems. Other values of absorption coefficients by the transmission method have been made using the 6 MeV. gamma rays from fluorine bombarded by protons[64,65] and give good agreement with theory.

Several other workers have used the method of counting pairs created by radiation bombarding a target before and after an absorber has been inserted in the beam. A number of measurements have been made using the 17 MeV. gamma

radiation from bombardment of fluorine. In the earlier work[66,67,68] the measurements were made using a cloud chamber. A strong magnetic field was used to separate the two particles and their energy could be then measured from their radius of curvature in this known magnetic field while the number of pairs as well as the number of recoil electrons could be determined. Thus a measure of the absorption coefficient in the particular material and also the ratio of Compton coefficient (σ) to pair formation coefficient (π) could be obtained.

Satisfactory agreement with theory was obtained for measurements in aluminium and lead although the ratio of σ/π is difficult to measure accurately owing to difficulty in determining the origin of some of the tracks seen in the cloud chamber photos.

Finally a similar measurement for the 17 MeV. gamma-ray line from the lithium bombardment was obtained in lead and aluminium by McDaniel, Von Dardel and Walker[69] using this time a coincidence counter method, the two particles being bent through 180° by a magnetic field and recorded by two counters appropriately located. Their values are again in good agreement with theory.

It appears, therefore, that the Klein-Nishina formula for the Compton effect is accurate certainly to within 15% up to the highest energy of measurement (88 MeV.) and apart from deviations due to the known approximations

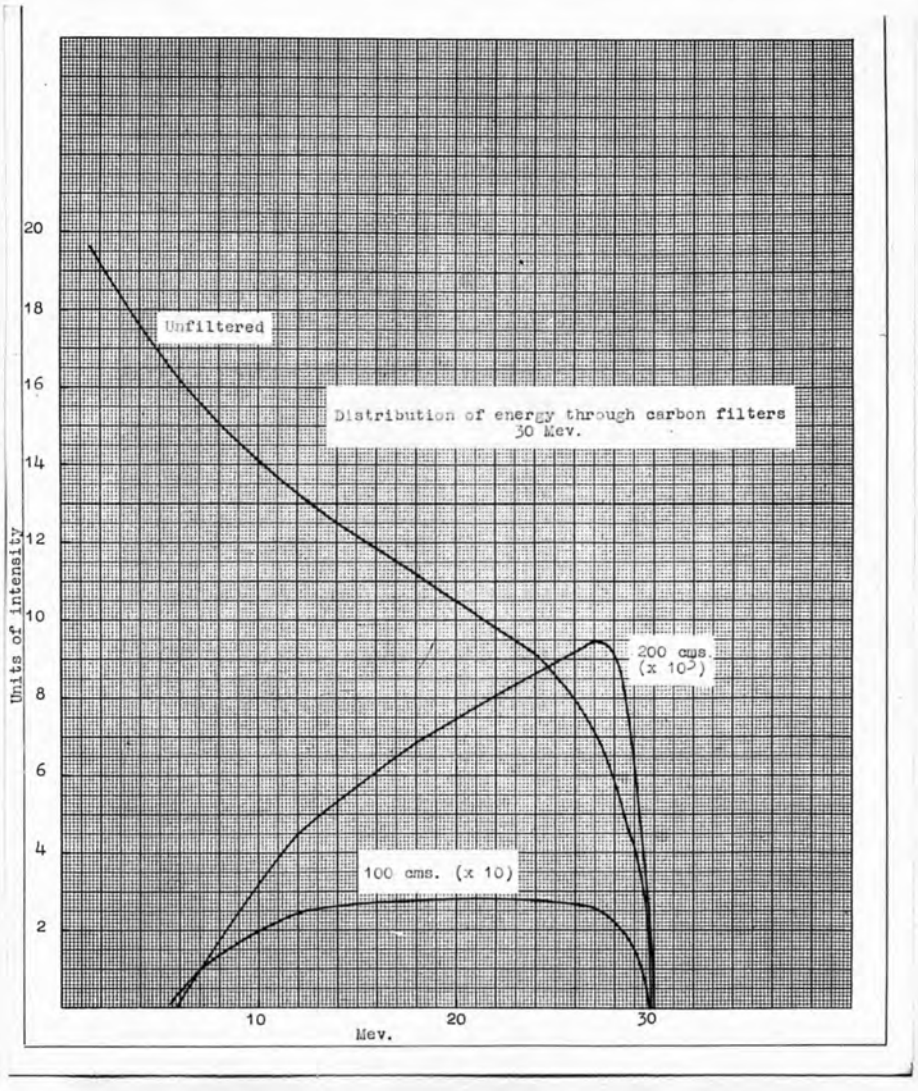
Distribution of energy through carbon filters
30 Mev.
Unfiltered
200 cms. (x 10)
100 cms. (x 10)
Units of intensity
Mev.
2
4
6
8
10
12
14
16
18
20
10
20
30

Fig. 26

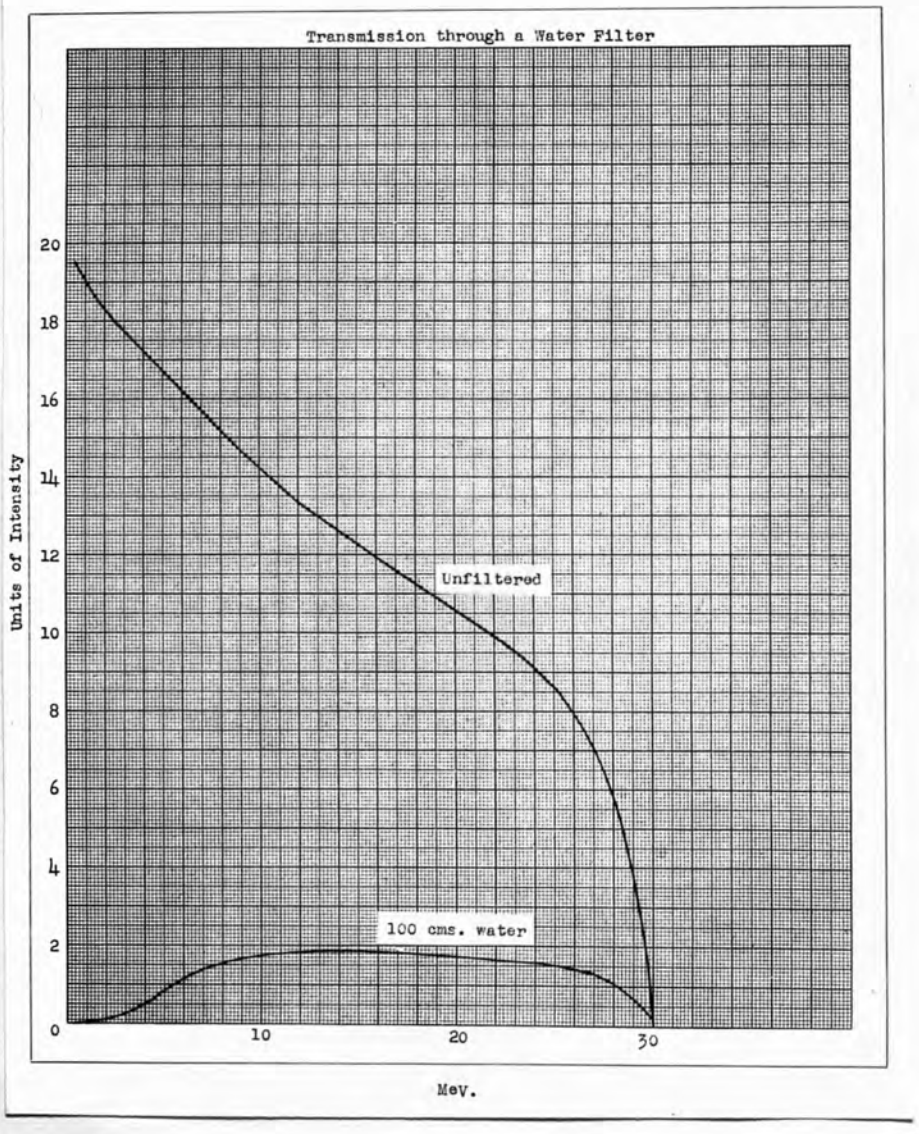
Transmission through a Water Filter
Units of Intensity
0
2
4
6
8
10
12
14
16
18
20
Unfiltered
100 cms. water
10
20
30
Mev.

Fig. 27

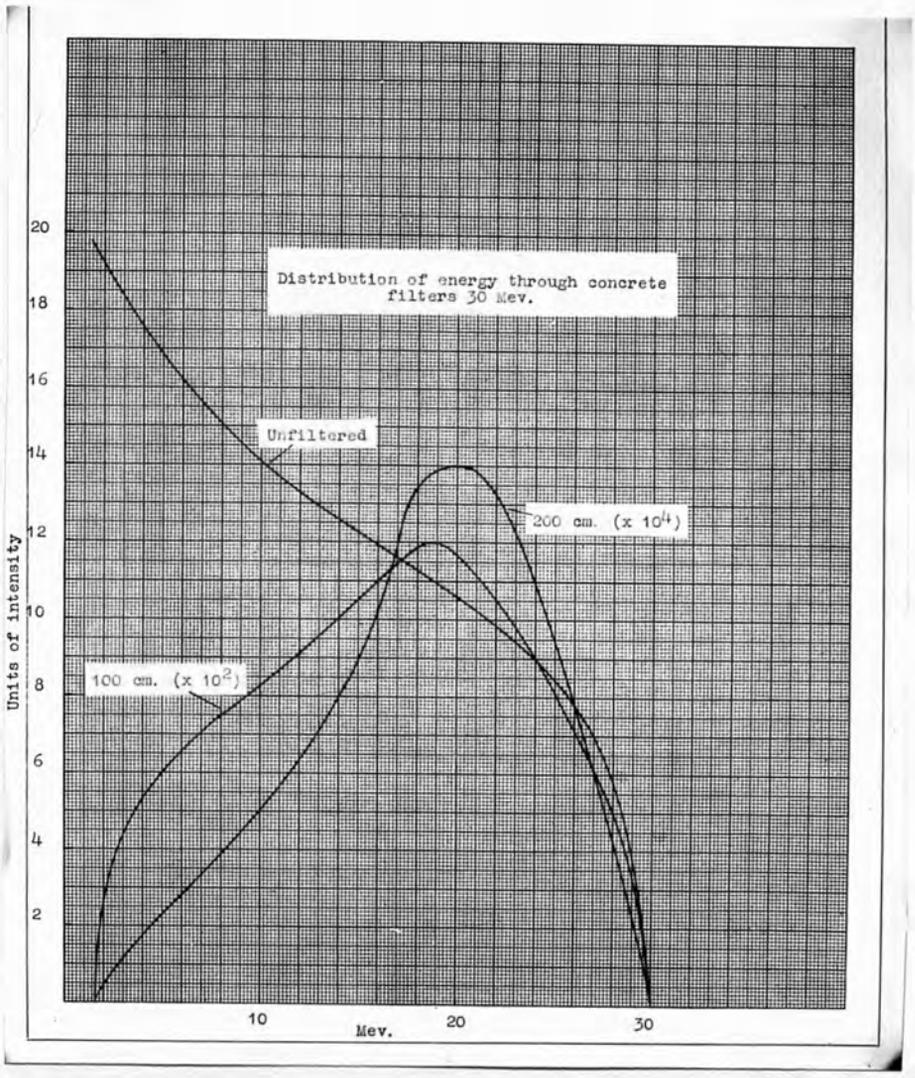
Distribution of energy through concrete filters 30 Mev.
Unfiltered
200 cm. (x 10⁴)
100 cm. (x 10²)
Units of intensity
2
4
6
8
10
12
14
16
18
20
10
20
30
Mev.

Fig. 28

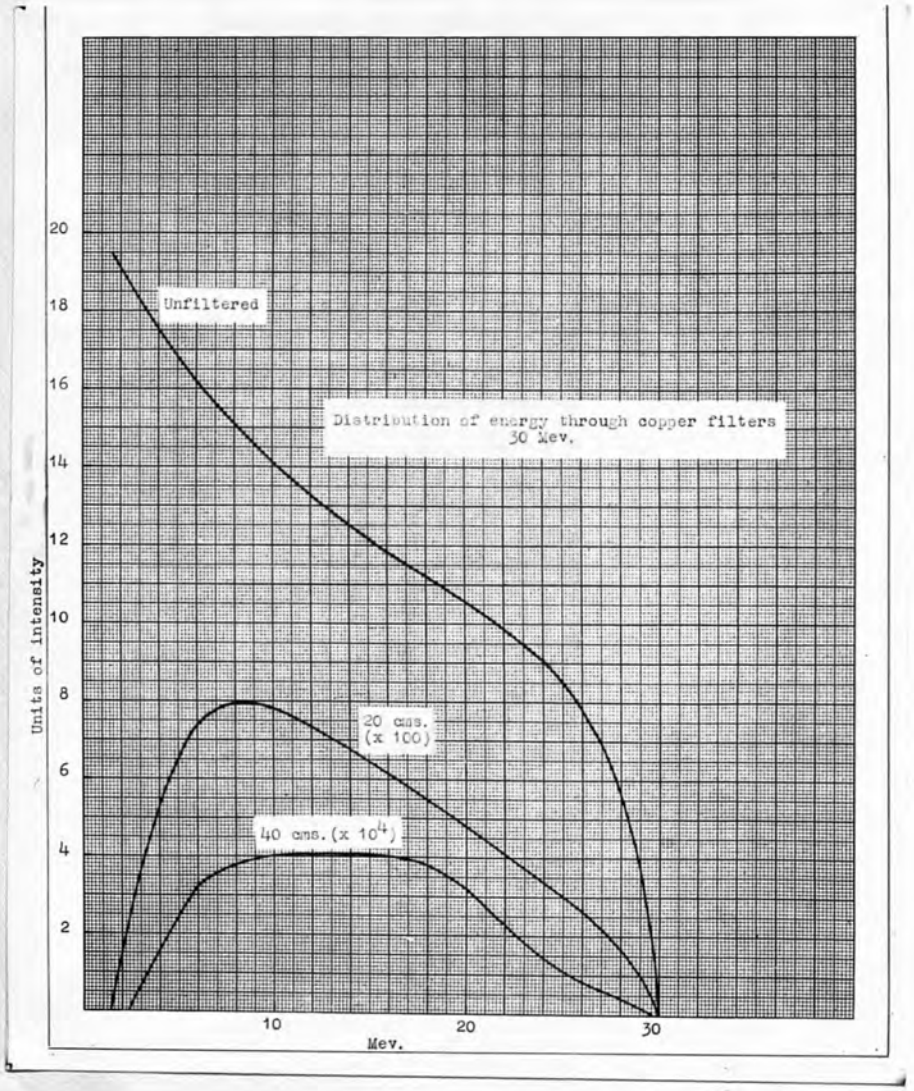
Distribution of energy through copper filters
30 Mev.
Unfiltered
20 cms.
(x 100)
40 cms. (x 10^4)
Units of Intensity
2
4
6
8
10
12
14
16
18
20
10
20
30
Mev.

Fig. 29

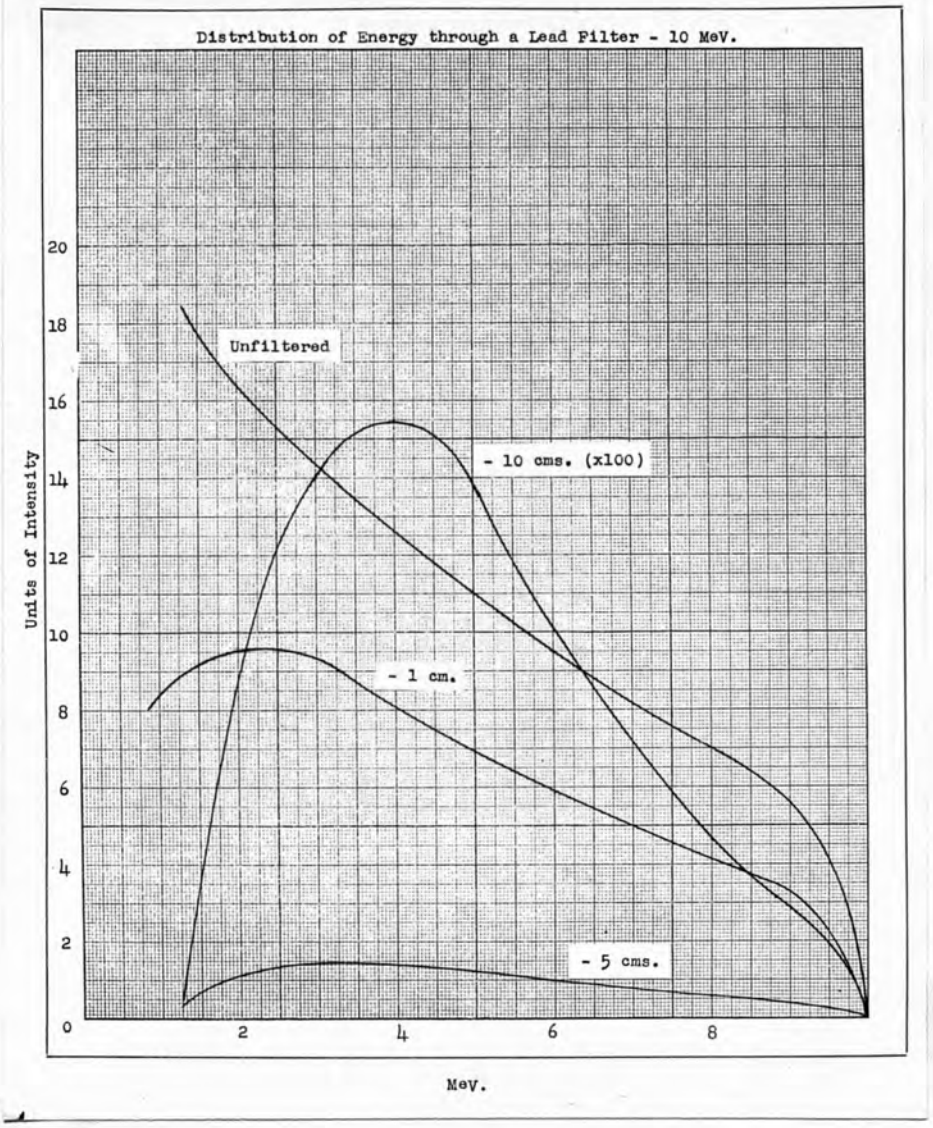
Distribution of Energy through a Lead Filter - 10 MeV.
Unfiltered
- 10 cms. (x100)
- 1 cm.
- 5 cms.
Units of Intensity
0
2
4
6
8
10
12
14
16
18
20
2
4
6
8
MeV.

Fig. 30

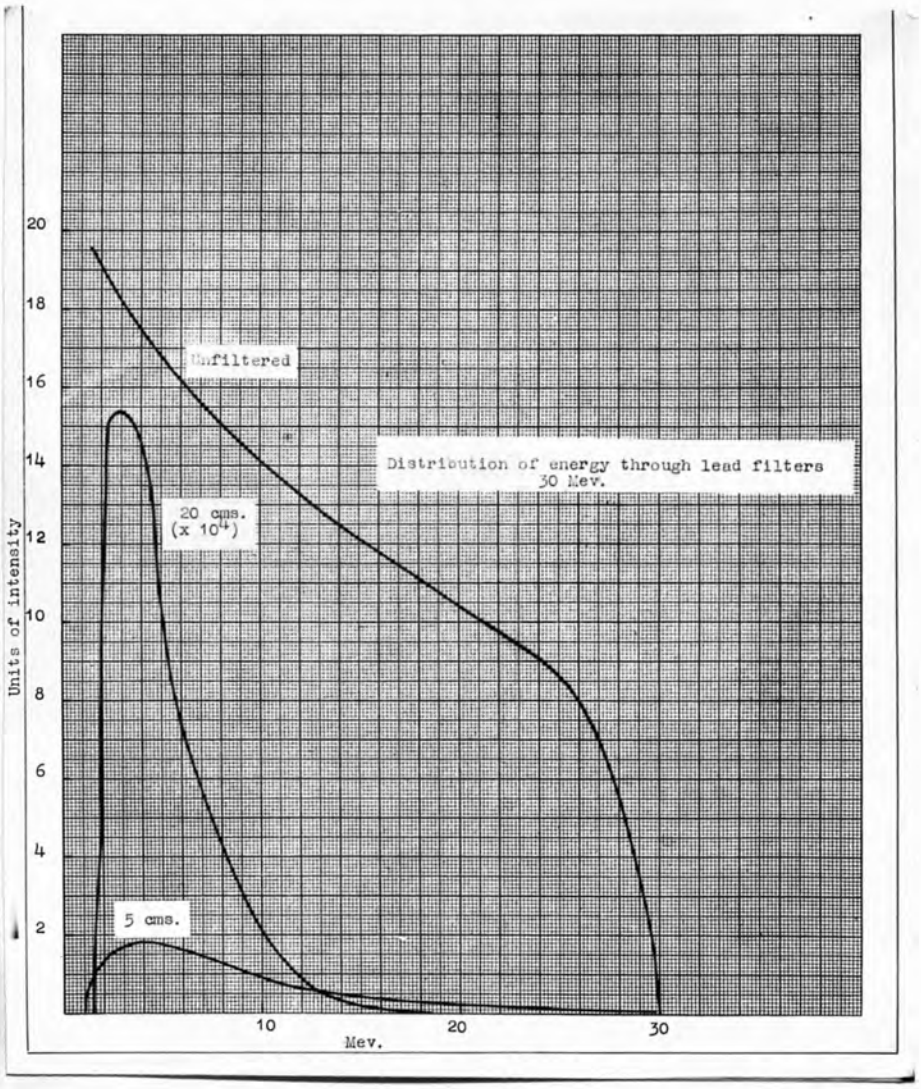
Distribution of energy through lead filters
30 Mev.
Unfiltered
20 cms.
(x 10⁴)
5 cms.
Units of intensity
Mev.
2
4
6
8
10
12
14
16
18
20
10
20
30

Fig. 31

made in the theoretical calculations of the pair formation effect this coefficient is also calculable to reasonable accuracy.

Using the calculated values of absorption coefficients some interesting results may be obtained by considering the effect of filtering a high energy X-ray beam with thick filters of various materials. From the Heitler spectral distributions and the absorption coefficients of Figs. 10 and 11 the distribution after passing through thicknesses of carbon, water, concrete, copper and lead filters have been calculated and are shown in Figs. 26 to 31. The distribution through a lead filter shows how the radiation of energies above and below the 3 - 4 MeV. region are heavily absorbed and an almost monochromatic radiation results. Lead would obviously be a bad filter for radiations from generators of energies above 4 MeV. In contrast to the practice at lower energies where a filter of high atomic number is used to filter the radiation produced, the appropriate filter for the higher energies is one of low atomic number. For example a carbon filter with a minimum absorption coefficient at approximately 70 MeV. would be a good choice. The effect of a carbon filter on the quality of the radiation will be demonstrated experimentally later. Since pair formation and photoelectric coefficients both depend on powers of Z greater than one the selective effect

is more marked in elements of high atomic number. Low atomic number materials give a fairly flat transmitted spectrum as can be seen in the cases of water and carbon.

DISCUSSION OF THE PROBLEM OF MEASUREMENT OF X RADIATION.

The measurement of a beam of X rays is an old problem and the answer not an easy one. We must first decide what we wish to measure. Do we wish to measure the electromagnetic radiation at a point or do we wish to measure the effective parameter, biologically, chemically or otherwise, at a point?

The physicist would, of course, desire to measure the energy flux in say ergs/cm.^{2}sec., but this quantity is often of little interest and the fraction of that flux left behind (i.e. absorbed) in say ergs/gm. is a more interesting quantity. Since the fraction of energy absorbed is small and varies with the penetration of the radiation a knowledge of the energy flux does not give much assistance.

Attempts, notably by Stahel[70] and Murdoch and Stahel[71], have been made to measure the energy absorbed from a beam of X radiation directly, but the results, while valuable, are difficult to assess as to accuracy. This approach to the problem is difficult as the energies involved are so small. For example, if all the gamma-ray energy from 1 mgm. of radium could be absorbed in 1 cc. of, say, water

and the heat retained the temperature rise in 1 hour would be approximately 0.01°C.

It is now almost universally agreed that the best method of measuring a beam of X radiation is to make use of the ionisation of a gas produced by it under standard conditions, e.g. saturation conditions in a given mass of dry air.

The ionisation observed in a given mass of air subjected to a beam of X or gamma rays depends on several factors such as the nature, extent and shape of the material surrounding the air. The unit of dose, however, should be related to the c.g.s. system and not arbitrarily dependent on one experimental set up and the ideal method of stating quantity or dose should enable us to express the energy absorbed per unit volume at any point throughout an irradiated mass.

Over a period of many years now the rontgen has established itself as a unit of the greatest value for the measurement of X-ray and gamma-ray dose. It was first defined in 1928 and later, in 1937, redefined in the following way: "The rontgen shall be that quantity of X or gamma radiation such that the associated corpuscular emission per 0.001293 gm. of air produces, in air, ions carrying 1 e.s.u. of quantity of electricity of either sign." The definition was revised principally to cover the measurement of gamma rays from radium in rontgens and the fundamental idea that

we take all the electrons set free in a given mass of air, utilize as much as possible of their energy in producing ionisation in air and measure the number of electrostatic units of charge thus liberated appears more clearly in the new definition.

In order that the measurement of a tertiary effect, such as the ionisation produced in air, may serve as the measurement of the primary X rays it is necessary that a clear correlation exists between the effect measured at a certain point and the flow of primary X rays at the same point, a "point" meaning a region of space sufficiently large so that the fluctuation arising from the atomic properties of radiation or matter may average out and still be sufficiently small so that the average distribution of radiation and matter throughout it does not show a systematic lack of uniformity.

Since the range of the electrons set in motion is not negligible above say 50 kV. it is essential that the measurements be carried out under conditions of equilibrium between the primary X rays and their secondary electrons. That is, conditions in which the total ionisation due to all electrons set free in the element of air in question is exactly equal to the ionisation produced in that air by electrons coming into it from outside. We must have, in fact, "electronic equilibrium."

Measurements in rontgens have been carried out

in great detail in the "free air" or parallel plate chamber notably by Behnken[72,73], Duane[74], Taylor[75], Kaye and Binks[76], Failla[77] and Mayneord and Roberts[78] and in an international comparison in 1931 of the apparatus at the National Physical Laboratory, the Bureau of Standards, the Reichanstalt and the French Standardising Laboratory agreement was reached to 0.5% up to 200 kV.

However, considerable difficulty was encountered[78,79] in measuring the gamma rays from radium in rontgens in a parallel plate chamber. This was due to the long range, some 3 to 4 metres, of the fastest recoil electrons involved. The dimensions of the parallel plate chambers used meant that the electrons reached the plates before they had expended all their useful energy in ionisation and also that equilibrium had not been reached in the distance between the collimating system and the measuring volume. The plate separation required, for example, would be of the order of 150 cms. A chamber of suitable dimensions was built at the National Physical Laboratory by Kaye and Binks[80] and successful results obtained. Obviously this difficulty caused by the range of the recoil electrons in air becomes even greater at energies rising to, say, 100 MeV. where the range of the electrons in air will be of the order of hundreds of metres.

Let us therefore consider the more convenient

"thimble" ionisation chamber which has been largely used in X-ray measurements and whose principles were first elaborated by Bragg[81] and later and independently by Fricke and Glasser[82], Gray[83] and Bruzau.[84] These workers showed that the introduction of a cavity in an irradiated homogeneous medium does not disturb the "electronic atmosphere," the number, speed and direction of the electrons crossing the cavity being unaltered by its presence. The introduction of air into the cavity makes little difference unless an appreciable fraction of the energy of beta rays is used up in crossing the cavity. This means the cavity should be small or the pressure low. The electrons are produced in the walls of the chamber and the work of Bragg and Gray[85] shows that the ionisation is a measure of the energy absorbed in the material surrounding the chamber provided the walls are too thick to be penetrated by the beta rays of highest energy.

For dosage measurements in rontgens the cavity should be surrounded by material having the same effective atomic number as air and of extent sufficient to allow of building up of the electronic equilibrium in it. In these circumstances the ionisation in the cavity is a measure of the energy absorbed per unit mass of air from the radiation and therefore a measure of the electromagnetic radiation itself. This implies, of course, that the current measured when the conditions of wall thickness and atomic number are

correct should be equal to that produced in a column of free air, i.e. in a parallel plate chamber. This conclusion has been tested[86,87] and found to be true to a fair degree of accuracy for moderate voltage X rays. Fortunately the energy lost by an electron in producing an ion pair in air is independent of the speed of the electron and is found[88,89] to be 32.5 e.v. and we can, therefore, easily convert a measurement in rontgens to a measurement of energy absorbed in unit mass of air. In a limited range of X-ray energy up to say 2 MeV. it is possible, therefore, for such a unit of dose to characterise both the primary radiation incident at a point and at the same time the physical quantity underlying any changes in the medium which take place at the point under consideration. This is not, however, the case at higher energies. The condition of electronic equilibrium is only simply related to the energy flux if the primary radiation is of constant quality and quantity throughout a region of extent equal to the range of the secondary particles produced in the medium, which, to measure in rontgens, must have an atomic number equal to that of air. Up to about 2 MeV., since the range of the electrons is relatively short, little variation of the primary radiation occurs but in the 10 to 100 MeV. energy band the range of the recoil electrons becomes comparable with the mean penetration of the X rays which set them in motion. Also

the absorption coefficient of the radiations ceases to decrease with increasing energy and then increases again so that the scattered X rays may become more penetrating than the primary ones. These, combined with the fact that secondary electrons are now produced also by pair formation, whose cross-section, in opposition to effects like the Compton effect, increases with energy, mean that the conditions underlying the establishment of equilibrium are poorly fulfilled. Also since the range of the secondary electrons is now of the order of centimetres the thickness of the wall of the ionisation chamber required becomes excessive, particularly if a measurement in true rontgens inside a medium is required.

Now the principle of X-ray dosage in rontgens may be said to be in two parts, (1) conversion of a portion of the X-ray energy into energy of secondary corpuscular radiation under defined conditions, and (2) measurement of the ionisation produced by the corpuscular radiation. In the high energy range it is the first step which causes the immediate difficulties and in fact the endeavour to characterise the quantity governing the changes which take place in a medium by a measurement of the X rays themselves ceases to have a meaning when the secondary corpuscles spread a relatively great distance from the "point" where the X rays deliver their energy.

A new system of dosimetry is at present under review which will avoid the now cumbersome task of attempting to measure the X rays themselves, but will attempt to obtain a measurement which will characterise the corpuscular radiation traversing the medium at the point under consideration since this will be a measure of the physical quantity underlying any changes which take place in the medium at that point.

The unit, suggested by the British Committee for Radiological Units,[90] is based on the measurement of the number of ion pairs produced in one gramme of air in an ideally small cavity in the medium of interest. The walls of the cavity will not now require to be air wall but of wall equivalent to the surrounding material and no conditions as to thickness need be imposed. The next point to be considered is the number of ion pairs per gramme of air which will constitute a unit. The Committee call the unit the J unit and suggest that "One J unit has been received at any point in a medium when the ionisation which would have been observed in an infinitesimal cavity containing the point is 1.58×10^{12} ion pairs per gramme of air enclosed in the cavity."

This number of ion pairs per gramme of air corresponds to the absorption of 93 ergs/gm. This value has been selected as 1 rontgen of electromagnetic radiation delivered to 1 gm. of water corresponds to an absorption

of energy of 93 ergs.

Since the unit will be used largely in clinical practice it was considered preferable to choose the energy absorption in water (i.e. approximately soft tissue) rather than the similar value (84 ergs/gm.) for air. The Committee have preferred the measured quantity (number of ion pairs per gramme) to the significant quantity (93 ergs/gm.) for the unit and since the conversion from one to the other is straightforward it seems preferable to express the unit in this way.

The reasons for avoiding the adoption of ergs/gm. as a unit, which from the purely physical point of view is the most acceptable unit, lie, no doubt, in the desire to have a unit such that for all ionising radiations the exposure of unit dose implies approximately the same absorption of energy per unit mass of tissue as an exposure to one rontgen of X or gamma radiation. In addition by maintaining a system of dosimetry based on the specific effect of the radiation there is the advantage that equal flows of the same charged particles constitutes the same "dose" no matter in what material the flow takes place. If a system of dosimetry based on a unit of energy absorption were adopted then the ratio of the ionisation produced in air by an equal flow of primary particles to the energy absorbed is a characteristic of the material.

Finally the unit suggested assists the correlation

of the effects of various types of particles and radiations causing ionisation such as neutrons, alpha particles and X or gamma rays.

EXPERIMENTAL MEASUREMENTS OF SHORT WAVELENGTH X RAYS.

The current in an ionisation chamber due to a beam of electromagnetic radiation being a function of size, wall thickness and material of the chamber a study of two of these factors has been undertaken. As at high energies the range of the secondary particles in air at atmospheric pressure is large compared to the dimensions of the usual chamber, Bragg's condition is fulfilled and the ionisation is accurately proportional to volume. The effects of wall thickness and material were therefore studied using the series of chambers described.

(1) Effect of chamber wall thickness on ionisation current.

Results of the experiments on the variation of wall thickness are shown in Figs. 32 to 52 in a range up to approximately 50 MeV.

The first results were obtained with the Malvern synchrotron up to 14 MeV. and more recently, with the 30 MeV. synchrotron being developed there, at 24 MeV. (Figs. 32 to 40). At Urbana the measurements were made on the 20 MeV. betatron, (Figs. 41 to 43), while at Schenectady a relatively small number of measurements were made at 11,

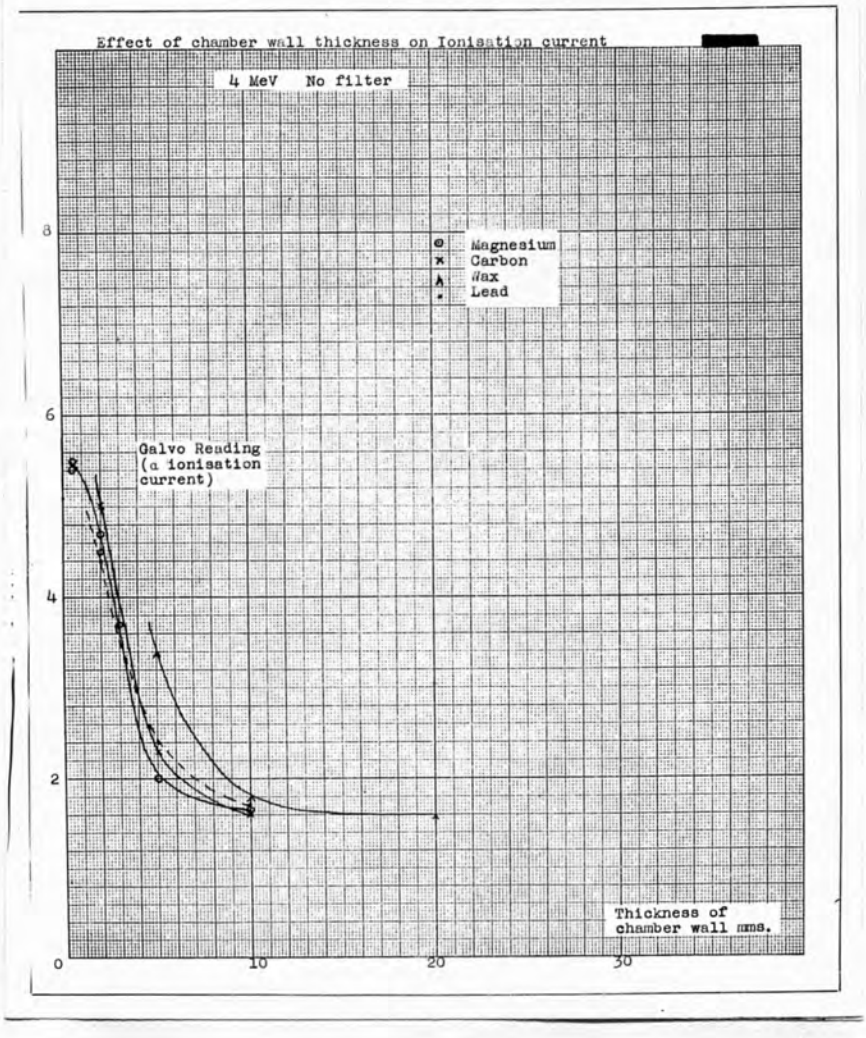
Effect of chamber wall thickness on Ionisation current
4 MeV No filter
Magnesium
Carbon
Wax
Lead
Galvo Reading
(a ionisation
current)
8
6
4
2
0
10
20
30
Thickness of
chamber wall mms.

Fig. 32

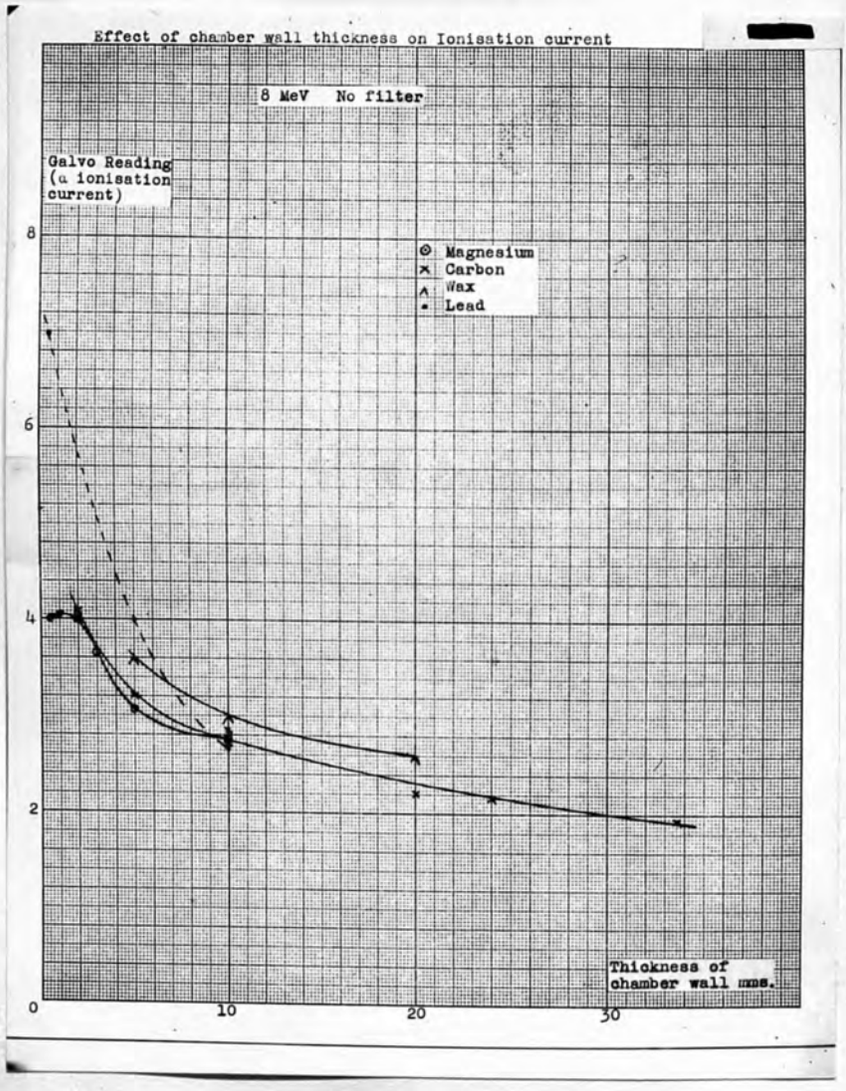
Effect of chamber wall thickness on Ionisation current
8 MeV No filter
Galvo Reading (a ionisation current)
Magnesium
Carbon
Wax
Lead
8
6
4
2
0
10
20
30
Thickness of chamber wall mms.

Fig. 33

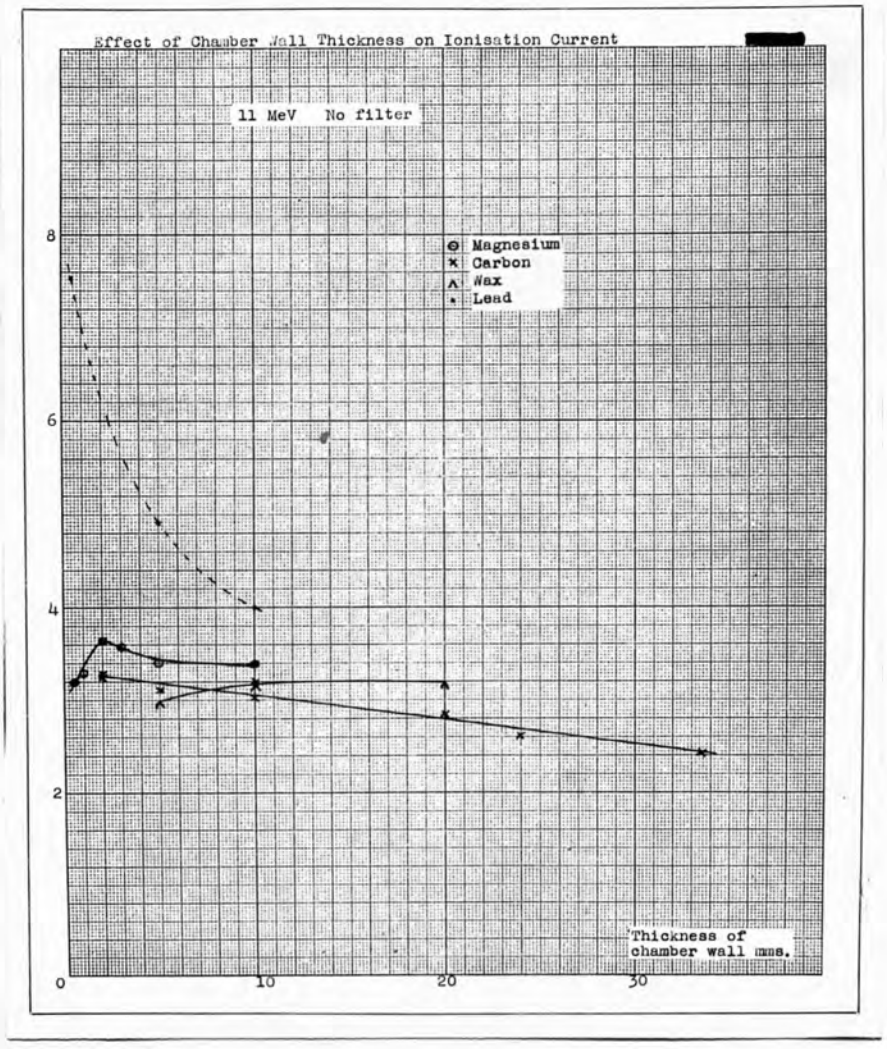
Effect of Chamber Wall Thickness on Ionisation Current
11 MeV No filter
Magnesium
Carbon
Wax
Lead
8
6
4
2
0
10
20
30
Thickness of chamber wall mms.

Fig. 34

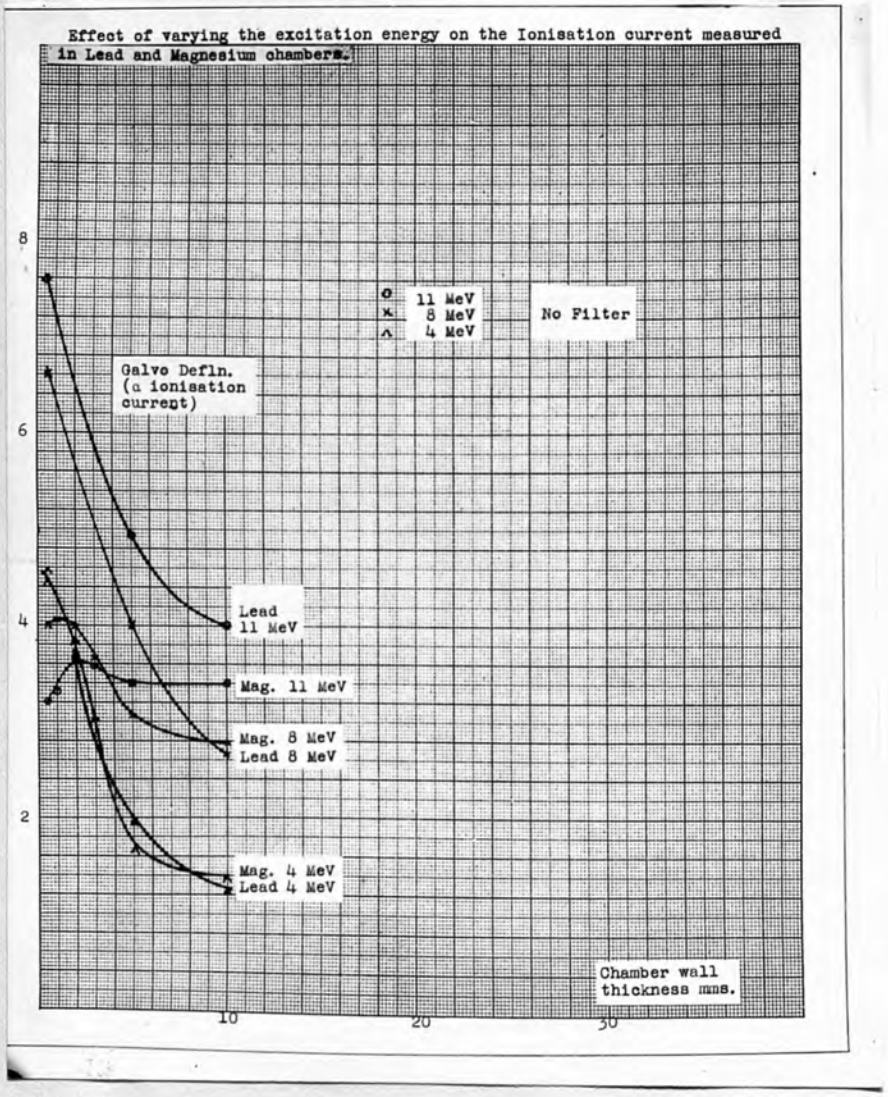
Effect of varying the excitation energy on the Ionisation current measured in Lead and Magnesium chambers.
11 MeV
8 MeV
4 MeV
No Filter
Galvo Defln. (a ionisation current)
Lead 11 MeV
Mag. 11 MeV
Mag. 8 MeV
Lead 8 MeV
Mag. 4 MeV
Lead 4 MeV
Chamber wall thickness mms.
8
6
4
2
10
20
30

Fig. 35

47 to 52 MeV. (Figs. 44 to 49). The number of measurements obtained here was cut severely by the incidence of technical troubles with the generators. Finally, a number of measurements were obtained with the 3 MeV. Van de Graaff generator at M.I.T., Cambridge, Massachusetts (Figs. 50 to 52).

In all cases the measuring apparatus was set up at a convenient distance from the target, this distance being a compromise, particularly where output was low, between obtaining a dosage-rate of sufficient magnitude for measurement and a beam of sufficient width to ensure uniform irradiation of the chamber. The output of the particular machine in use was monitored during the course of all experiments by a separate dosage-rate meter.

The first results shown in Figs. 32, 33 and 34 are those obtained at T.R.E. before the nature of the radiation had been fully realised. They serve to illustrate the presence of large quantities of electrons, the main result of increasing wall thickness being to decrease the ionisation current measured. Evidence of the expected "build-up" resulting from the establishment of electronic equilibrium can just be detected in magnesium chambers at the higher energies, Figs. 33 and 34. These curves represent an absorption curve (of the beta rays) superimposed on a build-up curve (for the X rays) of the usual type. In Fig. 35 an interesting result emerges from plotting the curves at various energies on one diagram. It will be seen

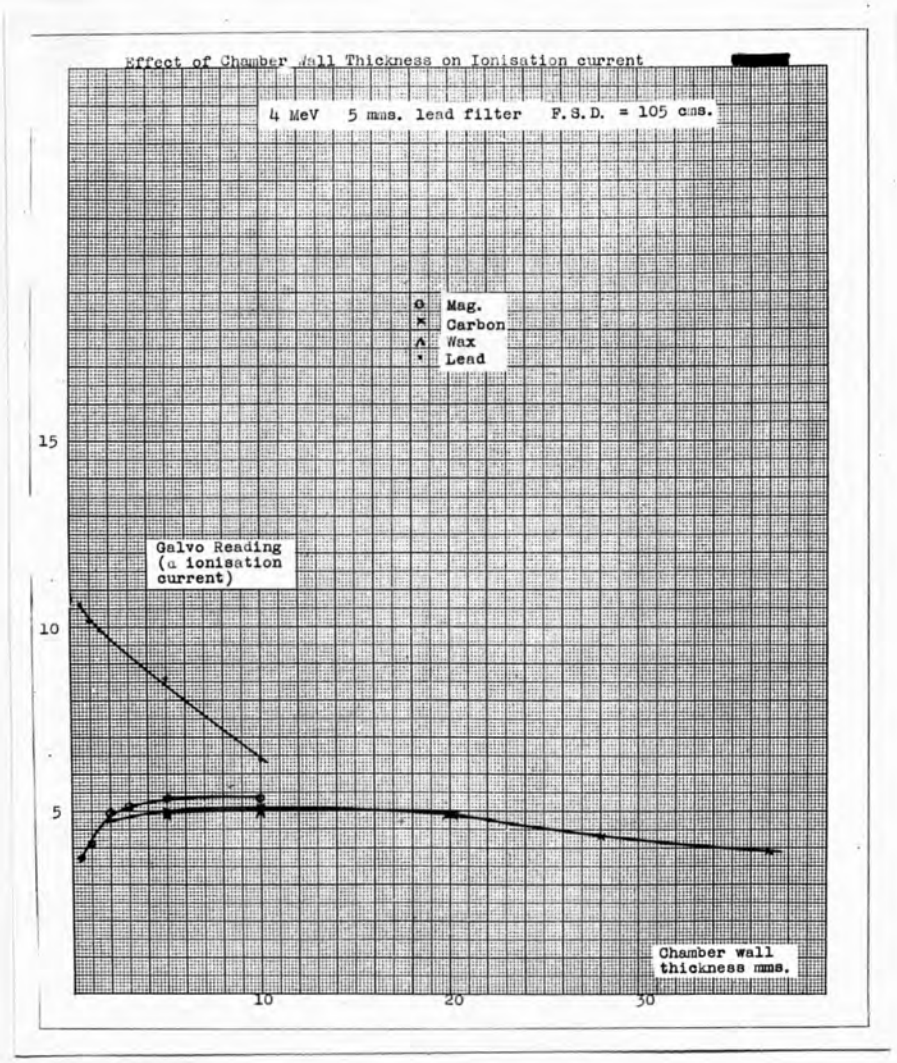
Effect of Chamber Wall Thickness on Ionisation current
4 MeV 5 mms. lead filter F.S.D. = 105 cms.
Mag.
Carbon
Wax
Lead
Galvo Reading (a ionisation current)
15
10
5
10
20
30
Chamber wall thickness mms.

Fig. 36

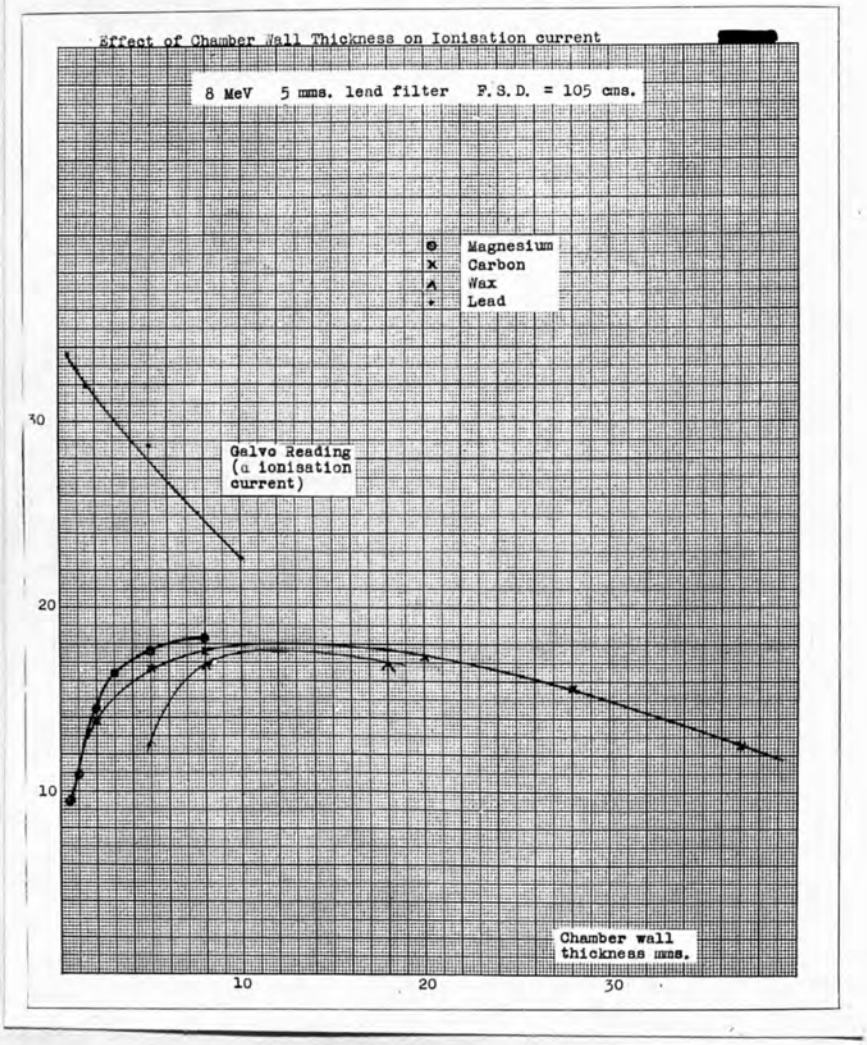
Effect of Chamber Wall Thickness on Ionisation current
8 MeV 5 mms. lead filter F.S.D. = 105 cms.
Magnesium
Carbon
Wax
Lead
Galvo Reading (a ionisation current)
30
20
10
Chamber wall thickness mms.
10
20
30

Fig. 37

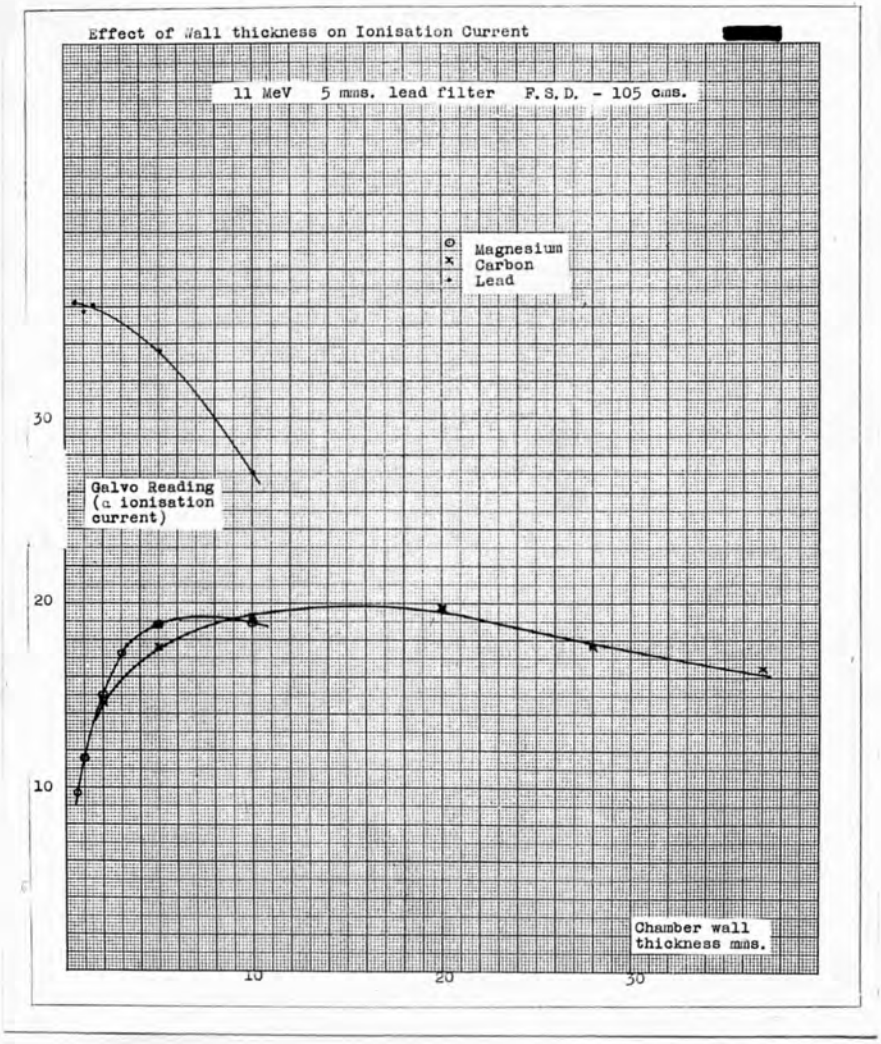
Effect of Wall thickness on Ionisation Current
11 MeV 5 mms. lead filter F.S.D. - 105 cms.
Magnesium
Carbon
Lead
Galvo Reading
(a ionisation
current)
30
20
10
10
20
30
Chamber wall
thickness mms.

Fig. 38

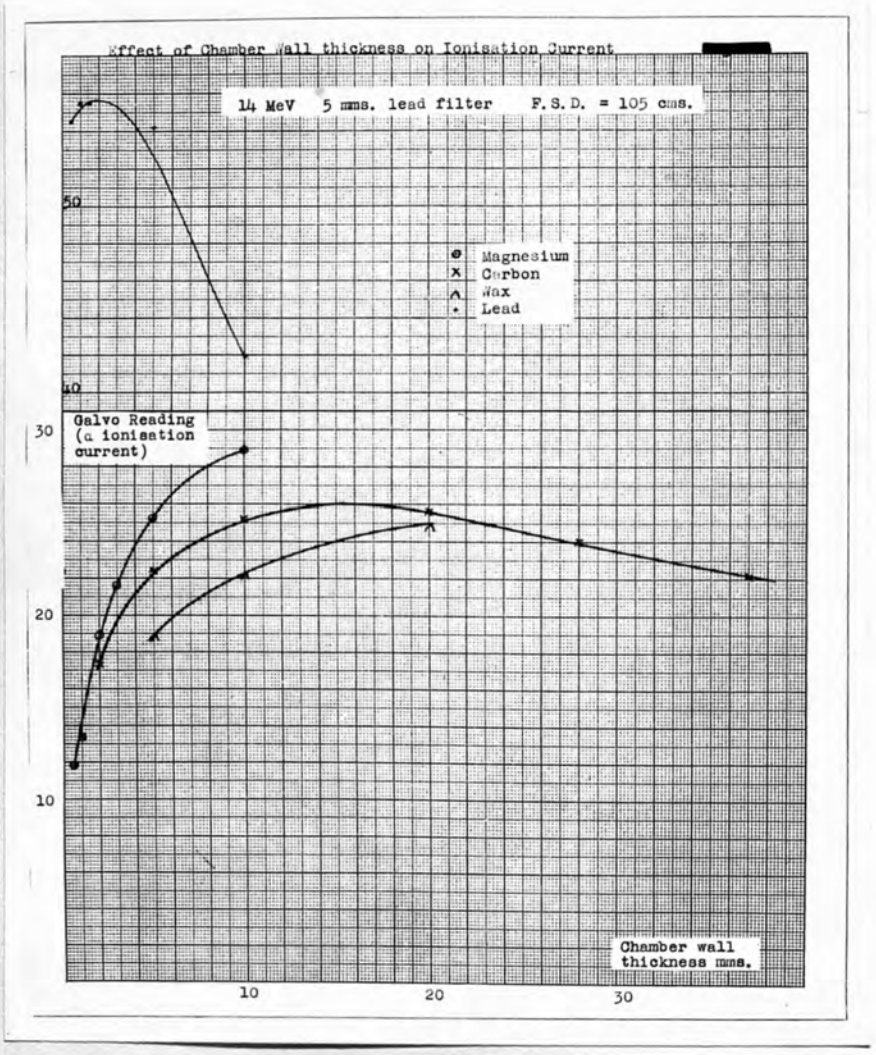
Effect of Chamber Wall thickness on Ionisation Current
14 MeV 5 mms. lead filter F.S.D. = 105 cms.
Magnesium
Carbon
Wax
Lead
Galvo Reading (a ionisation current)
50
40
30
20
10
Chamber wall thickness mms.
10
20
30

Fig. 39

that in a magnesium chamber it is possible to demonstrate that the intensity of radiation increases, decreases or stays stationary with change of excitation potential according to the chamber wall thickness selected! It is worth pointing out that, for just this reason, prior to these experiments some confusion had existed as to the output of this plant as a result of measurements made by different workers.

The experiments were repeated with a 5 mm. lead filter in the beam. It has been shown earlier that this was not the best filter to have used but lead was the only material readily available at the time. This set of results is shown in Figs. 36 to 39.

The "build-up" of the ionisation current with increasing wall thickness is now marked. The depth of the maximum build-up is due to the long range, at these energies, of the electrons set in motion by the incident X rays. At 14 MeV. evidence of the build-up even in lead is apparent.

More recently the 30 MeV. synchrotron being developed at Malvern became available and preliminary results were obtained at 24 MeV. and are shown in Fig. 40.

The results obtained at Malvern at 11 MeV. can be compared with some obtained at Schenectady at 10.9 MeV., the latter being shown in Figs. 44, 45 and 46. The large amount of soft radiation found in the beam of the 15 MeV.

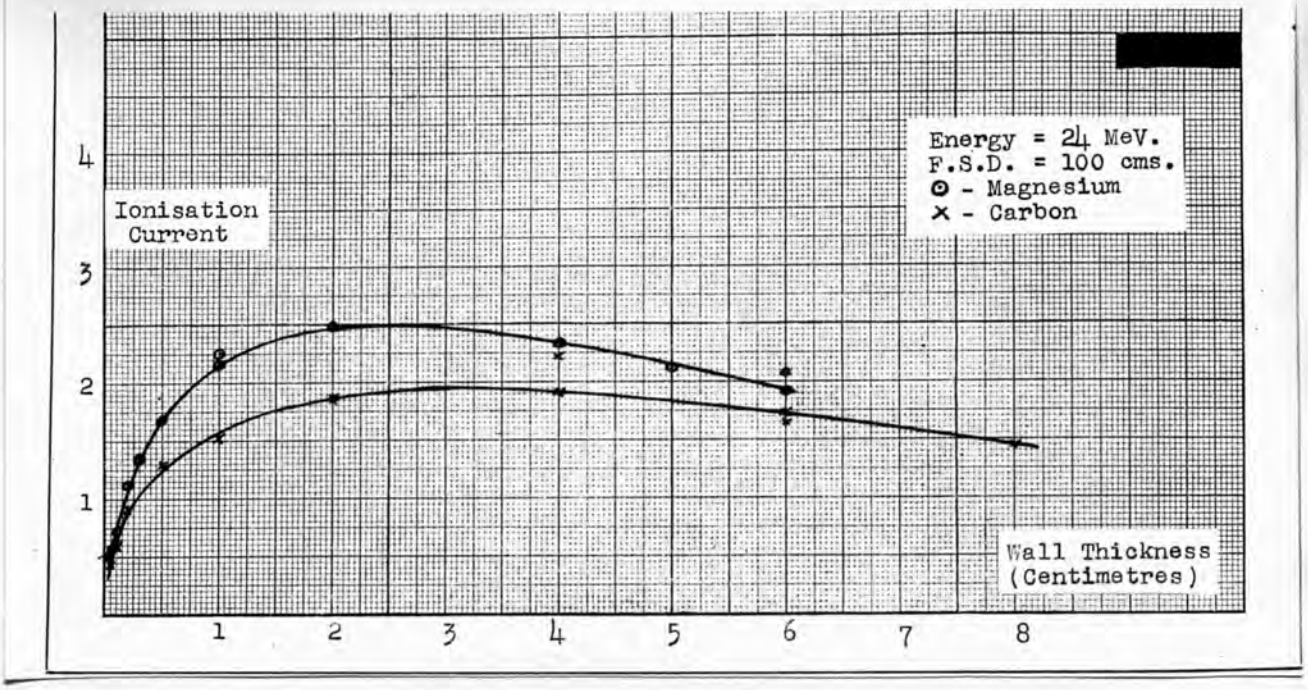
Energy = 24 MeV.
F.S.D. = 100 cms.
⊙ - Magnesium
× - Carbon
Ionisation Current
Wall Thickness (Centimetres)
1
2
3
4
5
6
7
8

Fig. 40

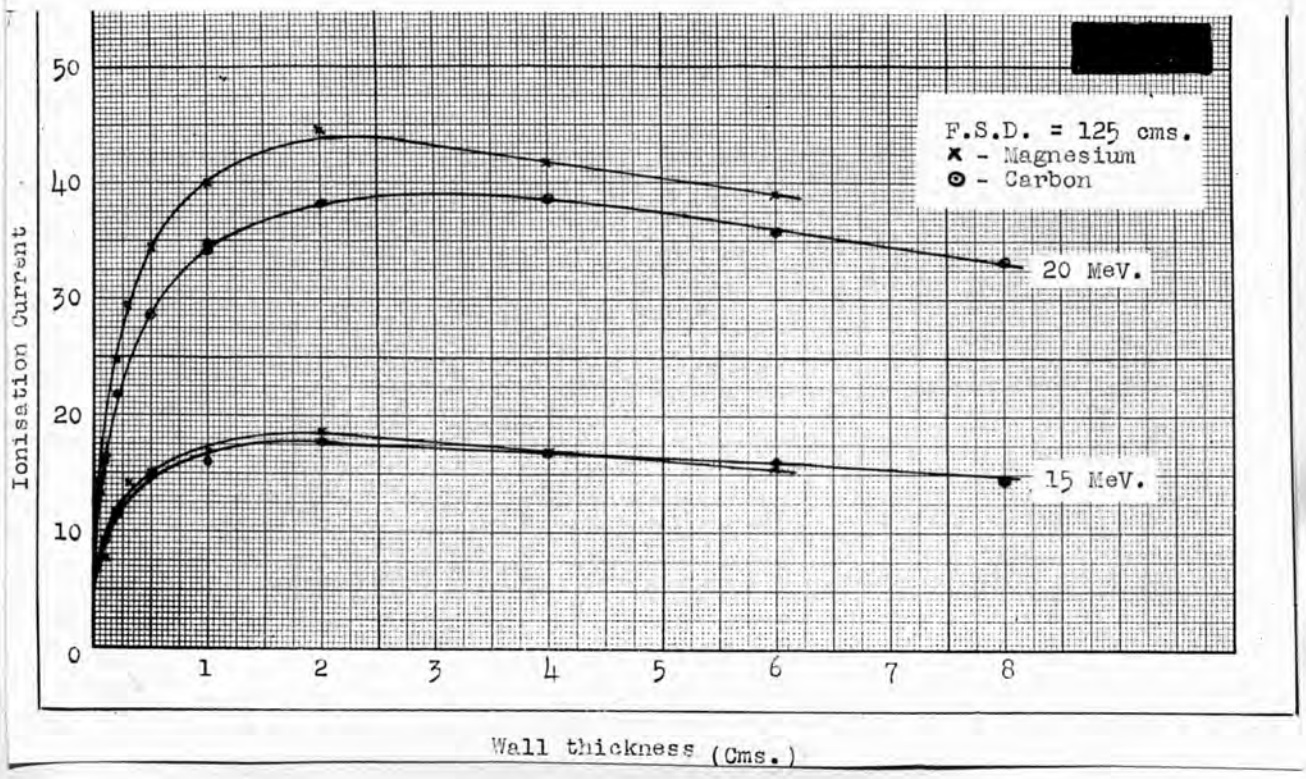
F.S.D. = 125 cms.
× - Magnesium
⊙ - Carbon
20 MeV.
15 MeV.
Ionisation Current
0
10
20
30
40
50
1
2
3
4
5
6
7
8
Wall thickness (Cms.)

Fig. 41

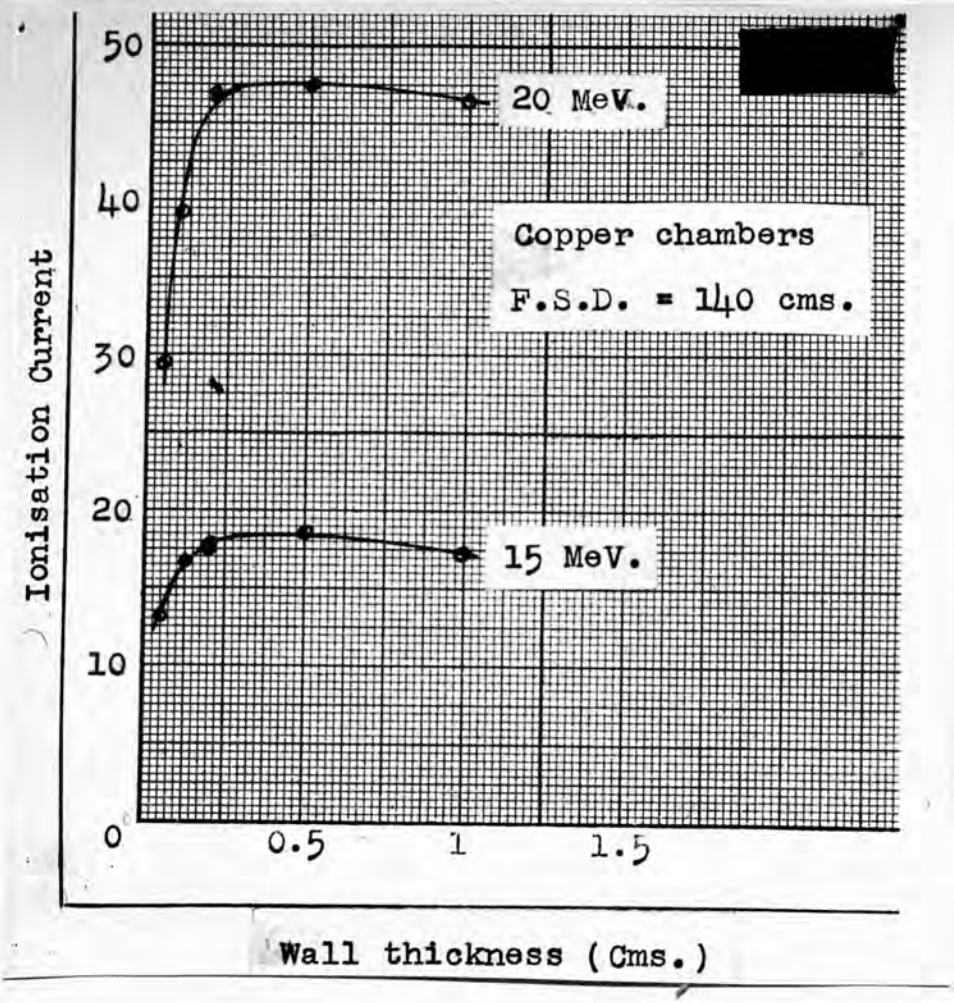
50
40
30
20
10
0
0.5
1
1.5
20 MeV.
15 MeV.
Copper chambers
F.S.D. = 140 cms.
Ionisation Current
Wall thickness (Cms.)

Fig. 42

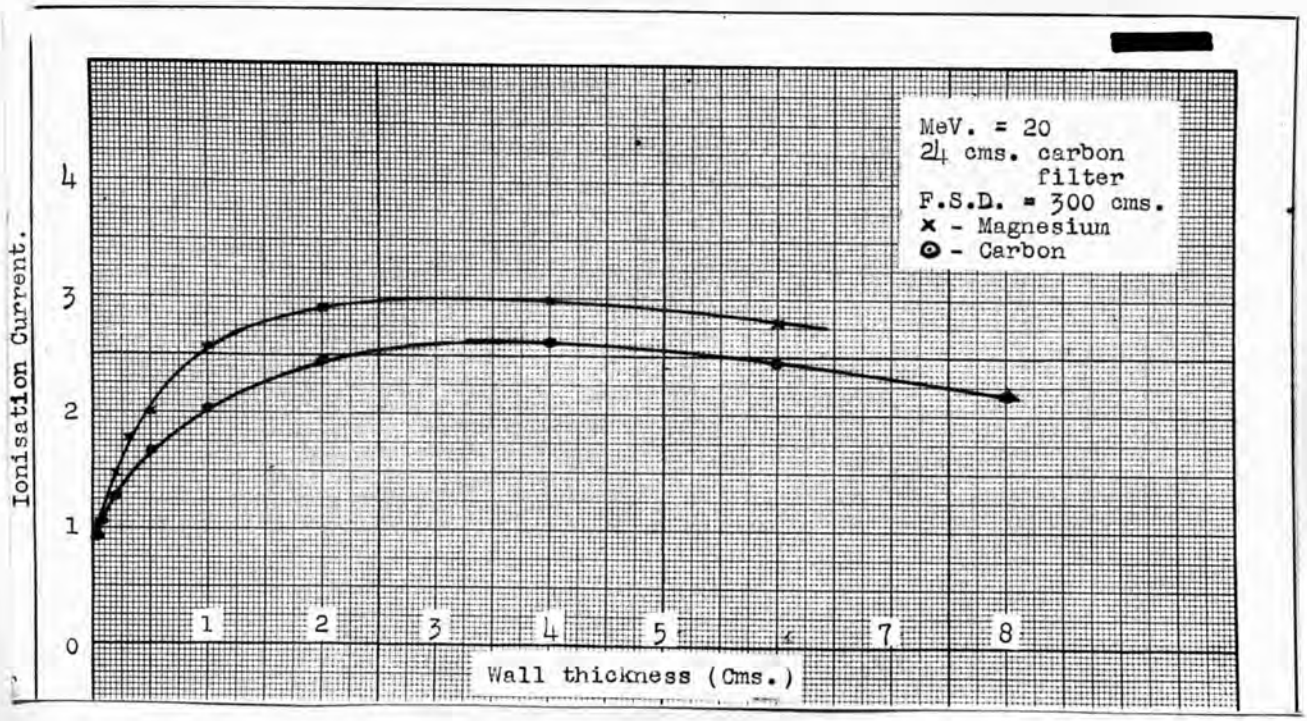
MeV. = 20
24 cms. carbon filter
F.S.D. = 300 cms.
× - Magnesium
⊙ - Carbon
Ionisation Current.
4
3
2
1
0
1
2
3
4
5
7
8
Wall thickness (Cms.)

Fig. 43

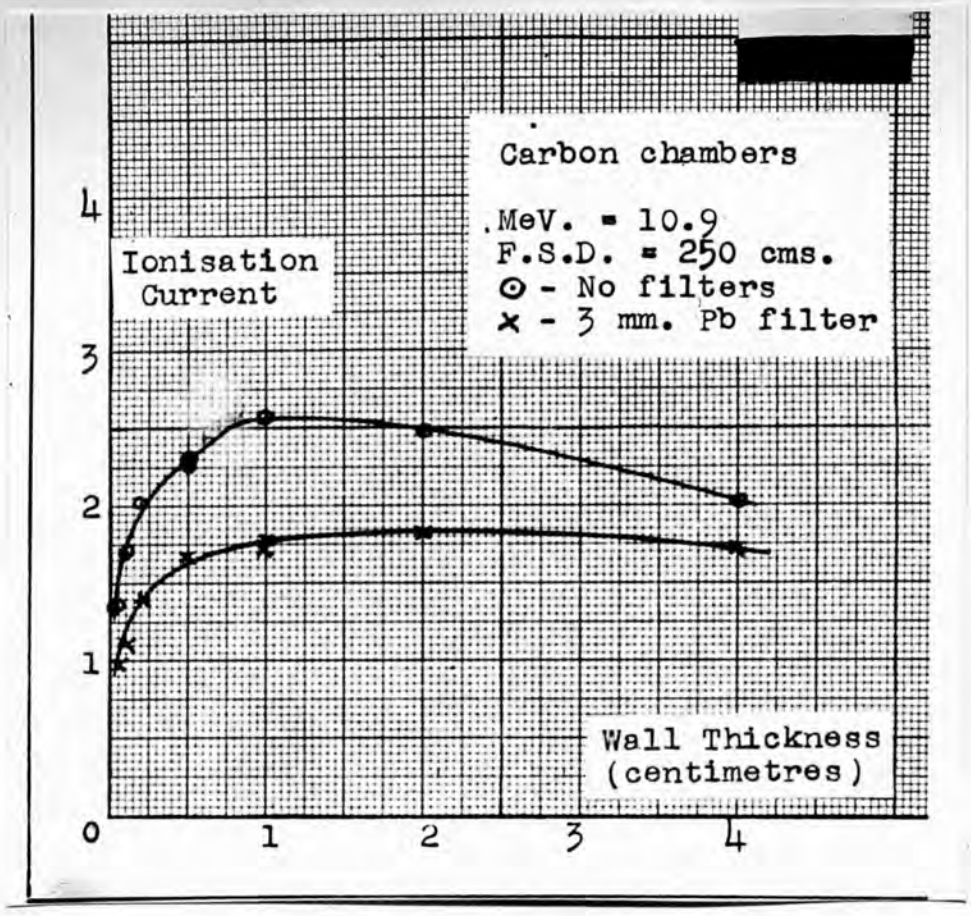
Carbon chambers
MeV. = 10.9
F.S.D. = 250 cms.
⊙ - No filters
× - 3 mm. Pb filter
Ionisation Current
Wall Thickness (centimetres)
0
1
2
3
4

Fig. 44

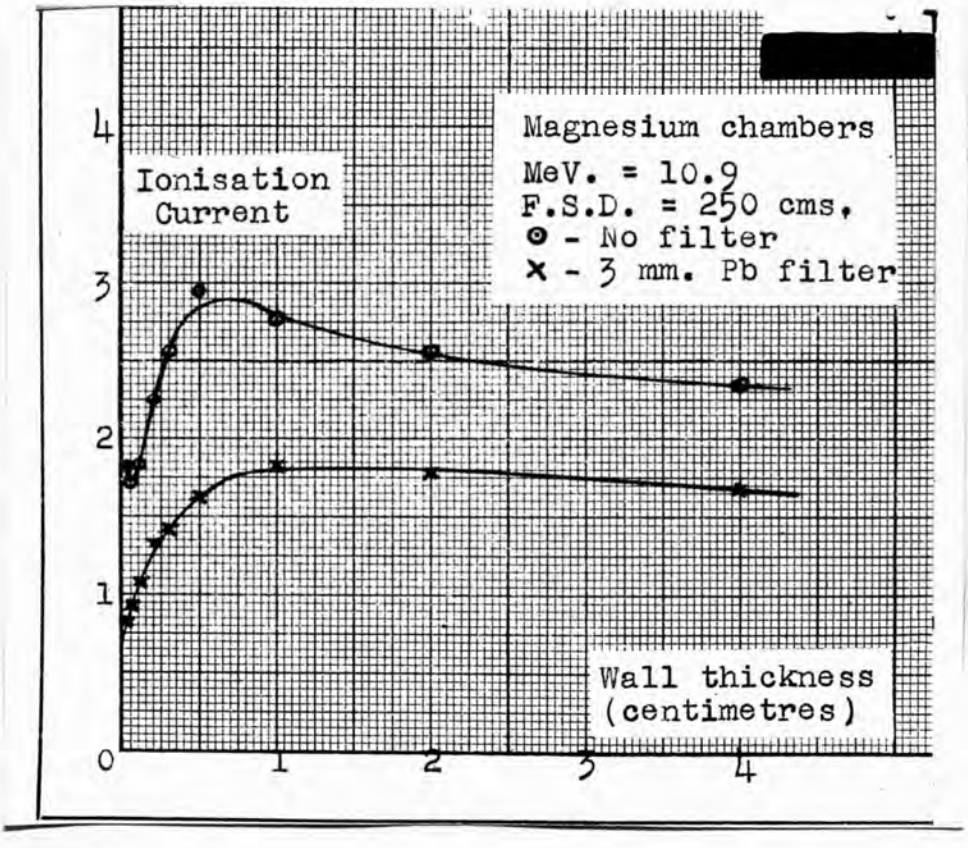
Magnesium chambers
MeV. = 10.9
F.S.D. = 250 cms.
⊙ - No filter
× - 3 mm. Pb filter
Ionisation Current
Wall thickness (centimetres)
0
1
2
3
4

Fig. 45

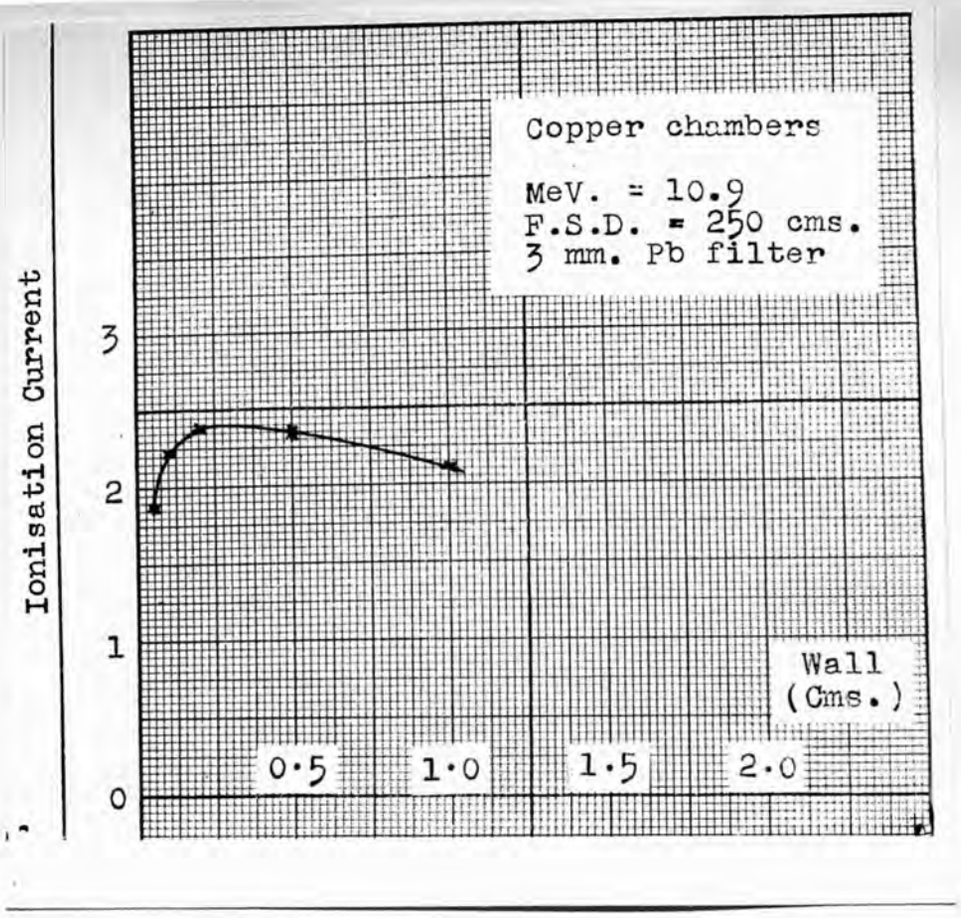
Copper chambers
MeV. = 10.9
F.S.D. = 250 cms.
3 mm. Pb filter
Ionisation Current
0
1
2
3
0·5
1·0
1·5
2·0
Wall
(Cms.)

Fig. 46

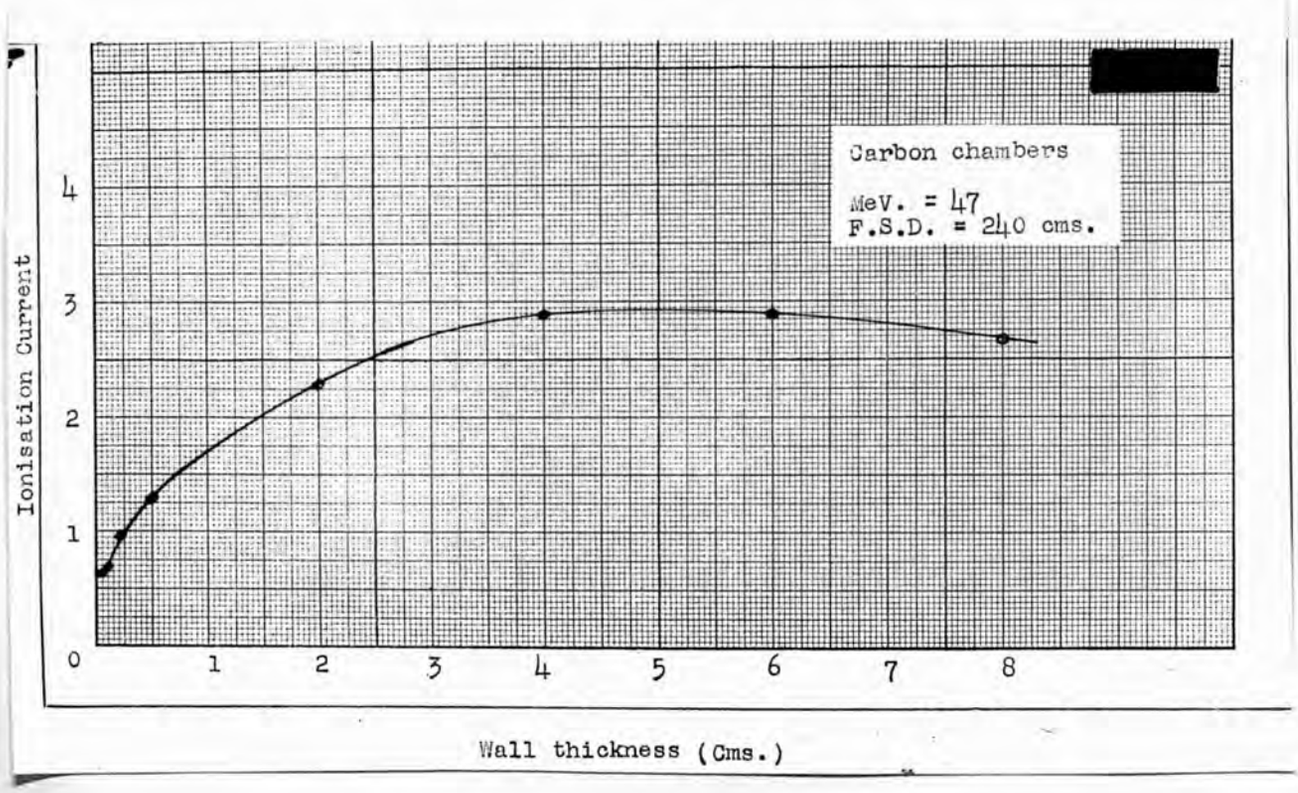
Carbon chambers
MeV. = 47
F.S.D. = 240 cms.
Ionisation Current
0
1
2
3
4
1
2
3
4
5
6
7
8
Wall thickness (Cms.)

Fig. 47

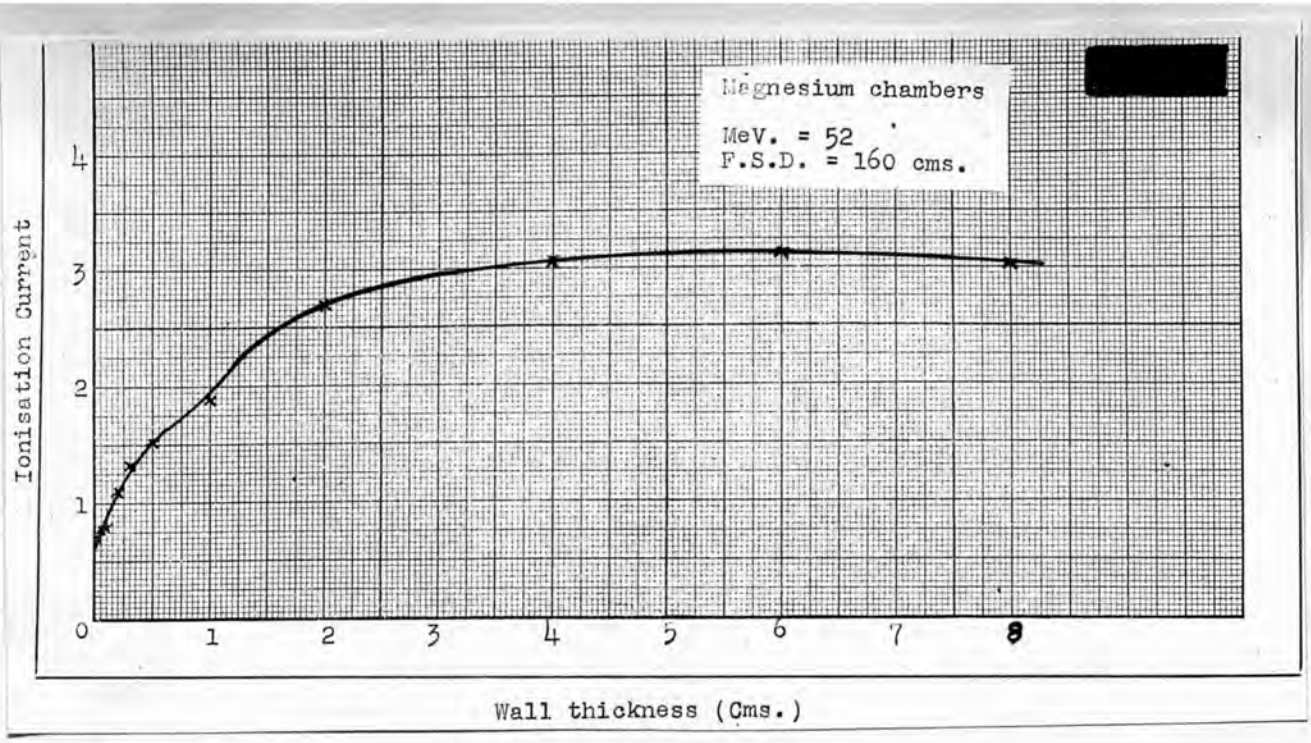
Magnesium chambers
MeV. = 52
F.S.D. = 160 cms.
Ionisation Current
0
1
2
3
4
1
2
3
4
5
6
7
8
Wall thickness (Cms.)

Fig. 48

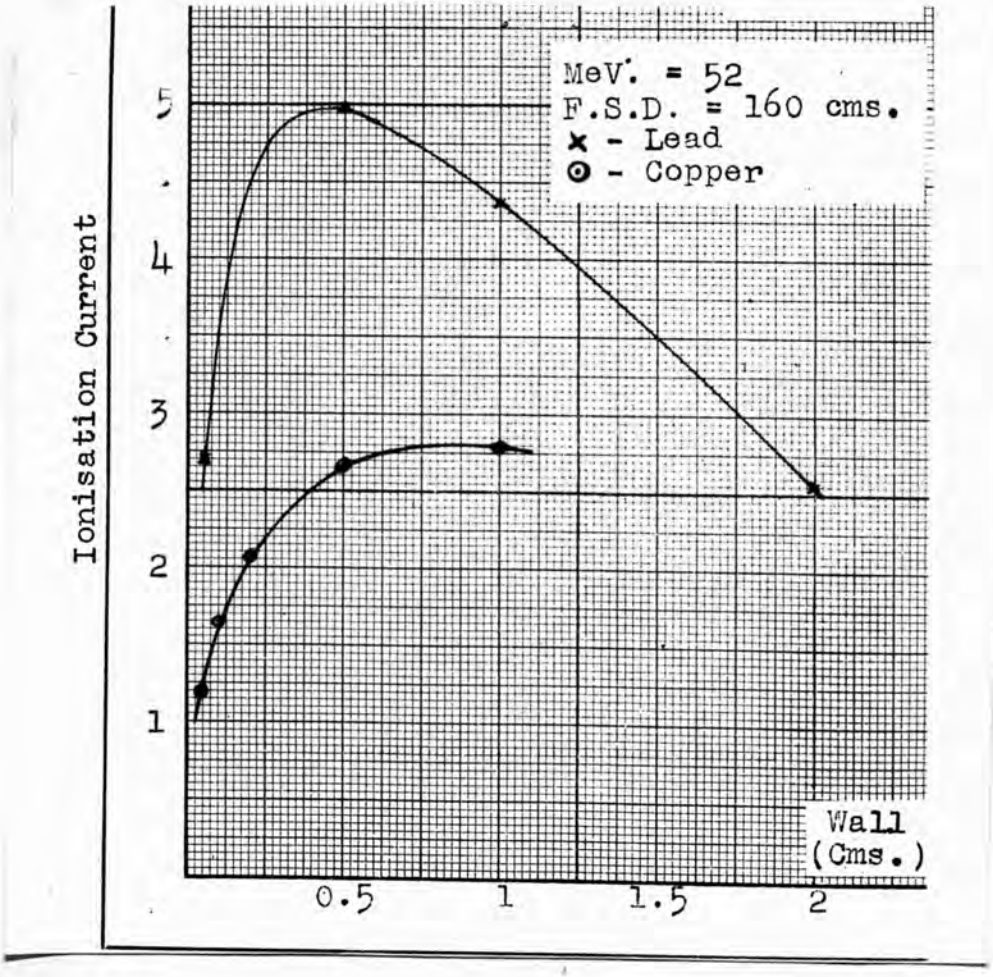
MeV. = 52
F.S.D. = 160 cms.
× - Lead
⊙ - Copper
Ionisation Current
1
2
3
4
5
0.5
1
1.5
2
Wall
(Cms.)

Fig. 49

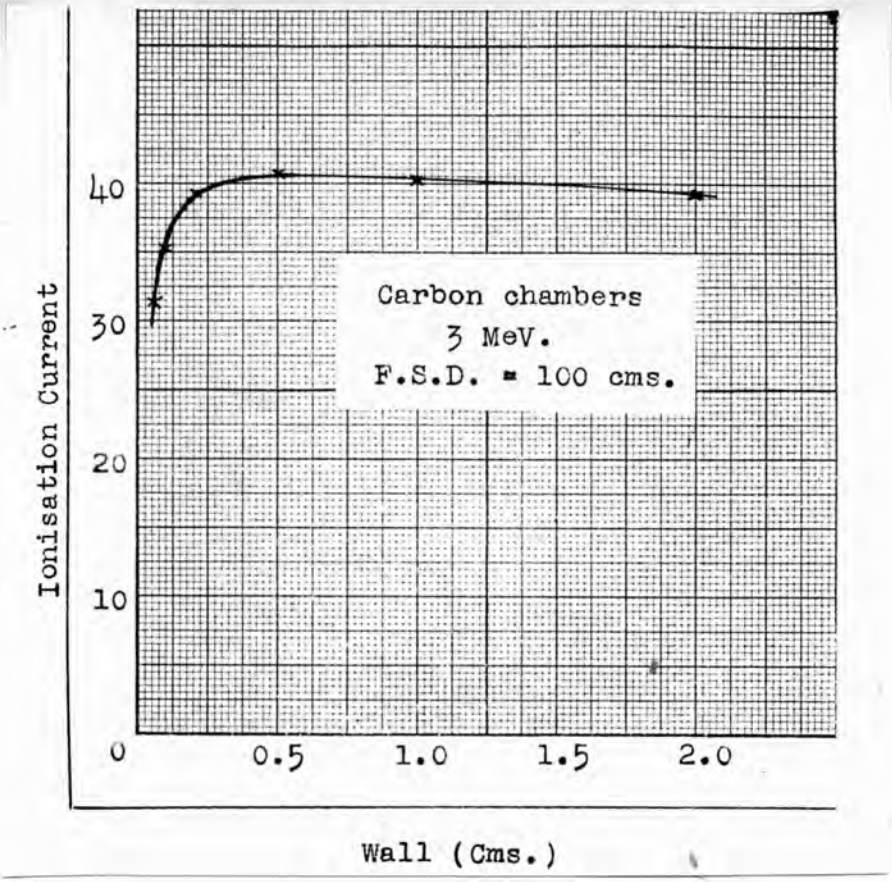
Ionisation Current
40
30
20
10
0
0.5
1.0
1.5
2.0
Carbon chambers
3 MeV.
F.S.D. = 100 cms.
Wall (Cms.)

Fig. 50

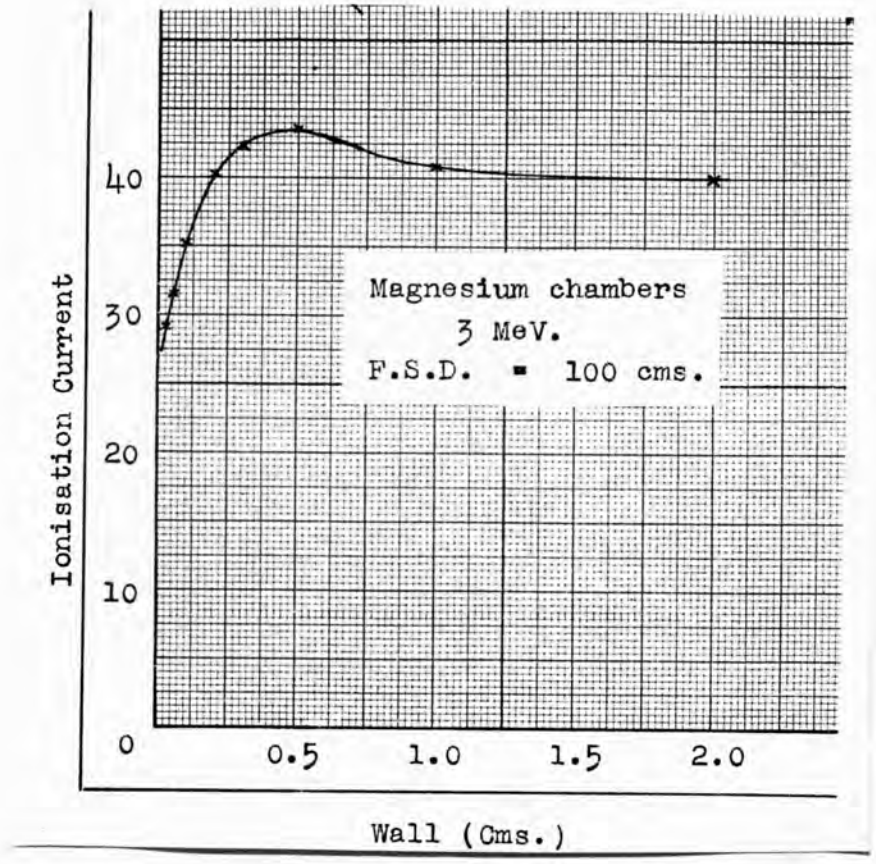
Ionisation Current
40
30
20
10
0
0.5
1.0
1.5
2.0
Magnesium chambers
3 MeV.
F.S.D. = 100 cms.
Wall (Cms.)

Fig. 51

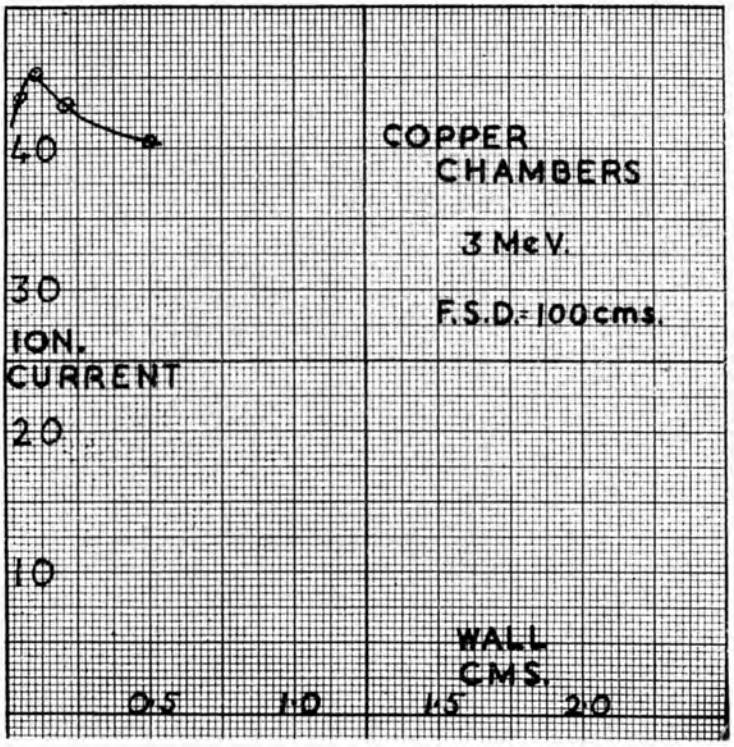
40
30
ION.
CURRENT
20
10
0.5
1.0
1.5
2.0
COPPER
CHAMBERS
3 MeV.
F.S.D.- 100 cms.
WALL
CMS.

Fig. 52

synchrotron was not found with the American machine, but evidence of the presence of electrons in the unfiltered beam is seen in the upward turn of the curve (Fig. 45) for small wall thickness in magnesium (in which metal the thinnest chamber, one of 0.25 mm. wall, was available). There also appear signs of subsidiary maxima which are very possibly due to electrons. The results for a filtered beam compare well with those obtained at Malvern.

The build-up in a carbon wall at 47 MeV. obtained with the 50 MeV. betatron at Schenectady is shown in Fig. 47 and the results of similar measurements at 52 MeV. with the 70 MeV. synchrotron also at Schenectady in Figs. 48 and 49. The technical trouble referred to prevented the completion of these experiments.

Probably the most reliable set of data was obtained at Urbana with the 20 MeV. betatron. The success of Kerst's[40] technique for removing stray electrons from the beam is indicated by the large ratio of maximum ionisation to that observed with very thin wall chambers, as well as the very smooth shapes of the curves (Fig. 41). The ratio of maximum to surface value may be as high as eight to one.

It is also interesting to see the result of using a 24 cms. carbon filter in the beam of the 20 MeV. betatron (Fig. 43). The choice of this material as filter is

explained earlier and we note here the greater thickness of wall giving maximum ionisation current in the filtered beam due to the fact that carbon is more "transparent" to the higher energy components of the beam emitted by the generator.

The precise shapes of the ionisation curves are evidently dependent on experimental conditions and an endeavour to provide a theory of the "build-up" for comparison with experiments is difficult since different assumptions as to absorption, scattering, etc. of the electrons in the wall of the chamber lead to quite different shapes. As would be expected, however, for thin walls, where complications are fewer, the current increases linearly with wall thickness. It is, however, interesting to collect with the above results the positions of maxima obtained at various potentials by other workers.[36,40,91,92] The positions are ill-defined and cannot be accurately determined. The position at any particular energy depends upon both focal distance and density of medium used for the measurements. A number of the measurements have been made with measuring systems completely surrounded by scattering material, but since backscatter at these energies is small (a value of about 3% has been measured) the effect on such measurements as compared to those made with chambers whose front and side walls only had been

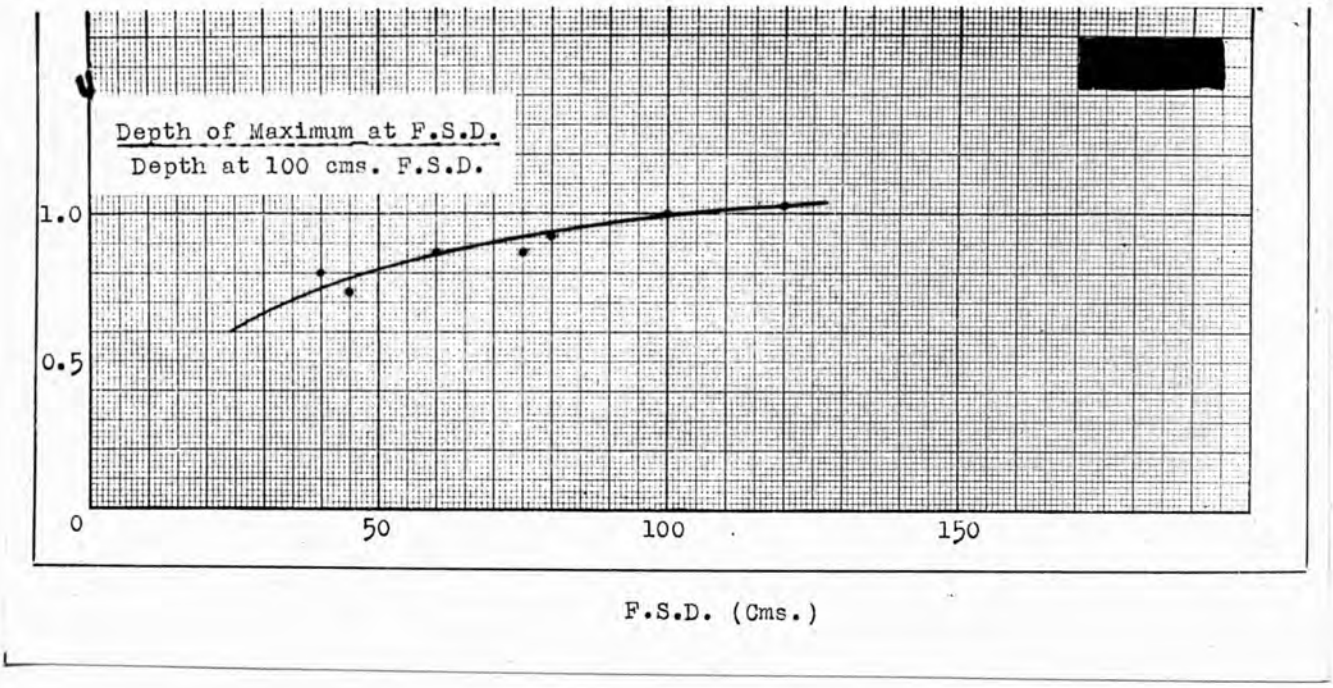
Depth of Maximum at F.S.D.
Depth at 100 cms. F.S.D.
1.0
0.5
0
50
100
150
F.S.D. (Cms.)

Fig. 53

increased is negligible. The values published have been corrected to a value for a medium of unit density taking the densities published by the various workers for their materials. Correction for focal distance is more difficult as a direct application of the inverse square law is not valid. However, Kerst as well as Charlton and Breed have published data of positions of maxima with varying focal distance and using these observations correction factors have been deduced to estimate the position of the maxima at 100 cms. focal distance (Fig. 53). The final corrected data are shown in Fig. 54 and it is interesting to see how well the values obtained with carbon chambers on changing wall thickness and reported above agree with observations made in "phantoms."

The values obtained by Failla and his colleagues and by Charlton and Breed with the 100 MeV. betatron in the lower potential range are evidently anomalous. Some of the results with this machine were obtained using a photographic method[36] and examination of the published photographs indicate that these discrepancies are due to the effects of stray electrons as already emphasised. It will be seen that the variation of depth of maxima with energy is approximately linear up to about 30 MeV. (roughly 5 MeV. per cm. depth) and sufficient data has been obtained up to about this energy to enable the curve to be used with confidence to estimate the position of the maximum for

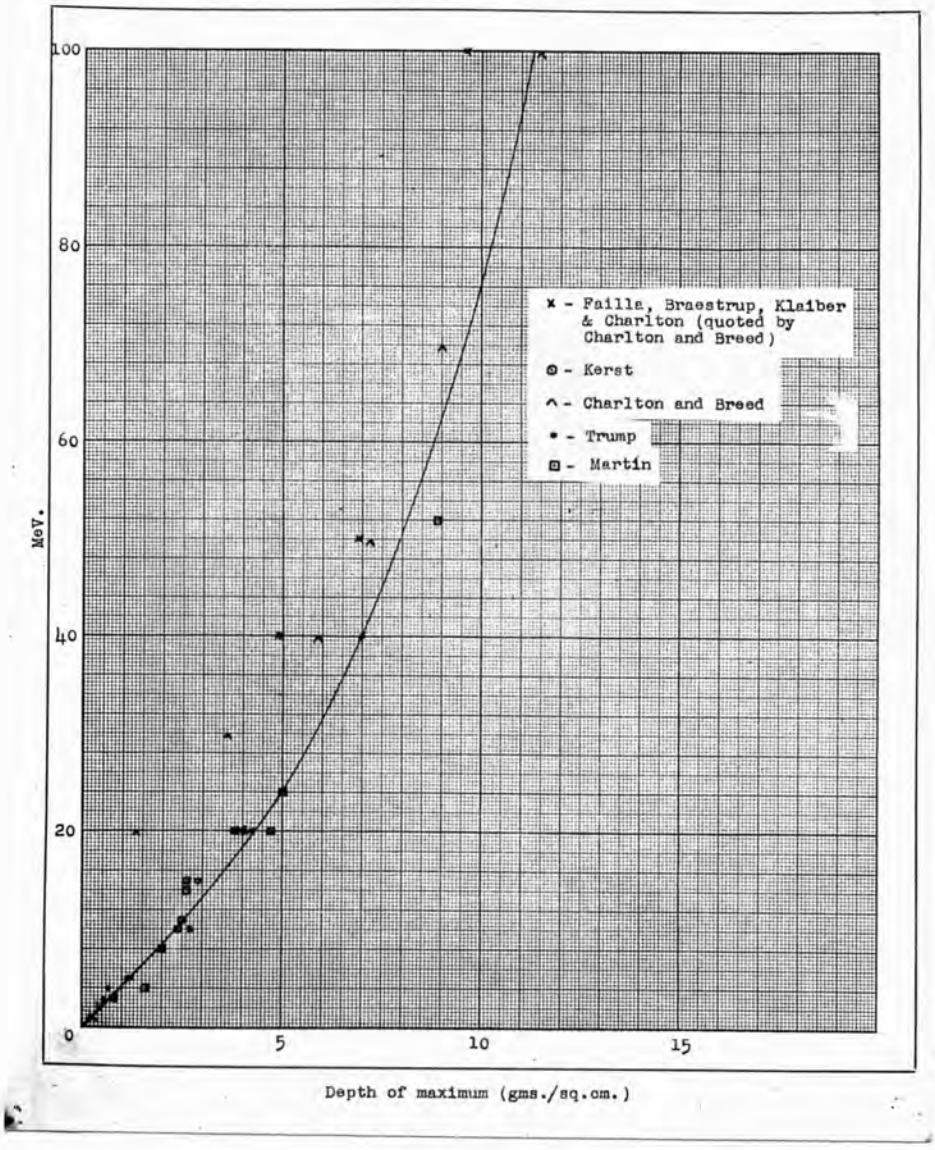
100
80
60
40
20
0
MeV.
5
10
15
Depth of maximum (gms./sq.cm.)
x - Failla, Braestrup, Klaiber & Charlton (quoted by Charlton and Breed)
⊙ - Kerst
^ - Charlton and Breed
• - Trump
⊡ - Martin

Fig. 54

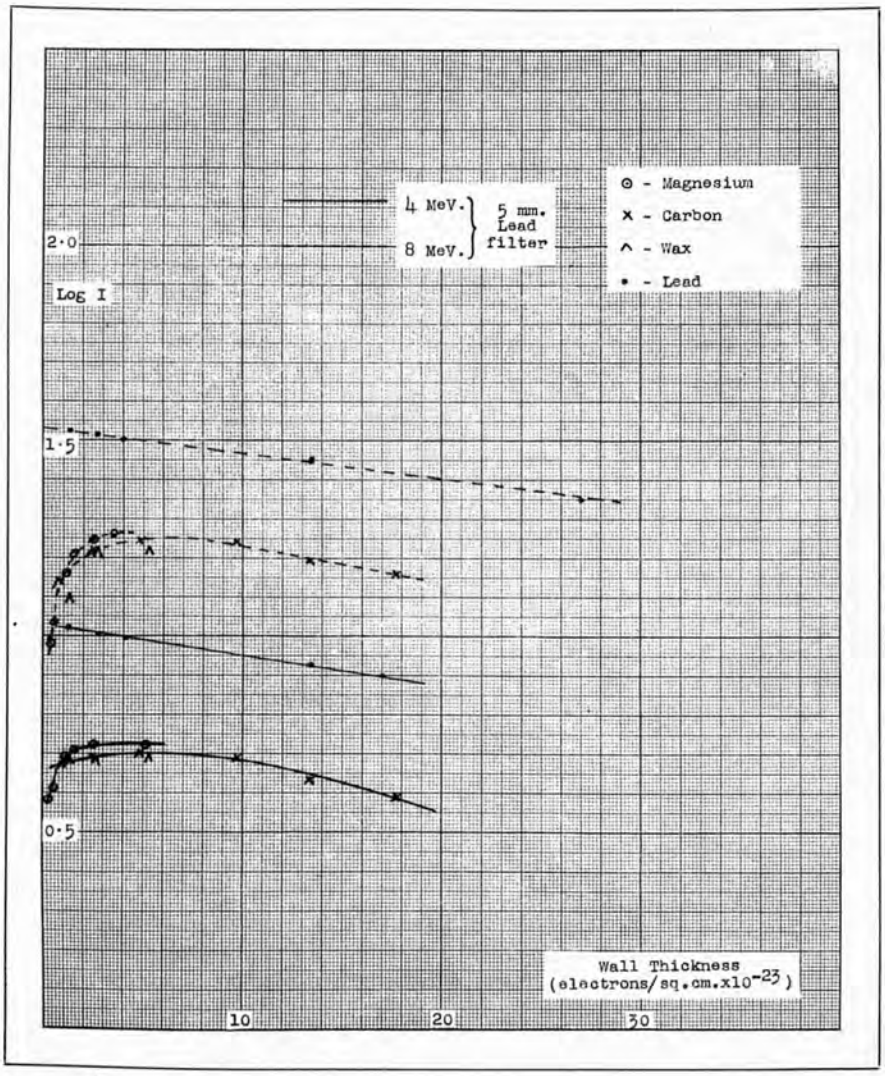
4 MeV.
8 MeV.
5 mm. Lead filter
⊙ - Magnesium
× - Carbon
^ - Wax
• - Lead
2·0
Log I
1·5
0·5
Wall Thickness
(electrons/sq.cm.x10-23)
10
20
30

Fig. 55

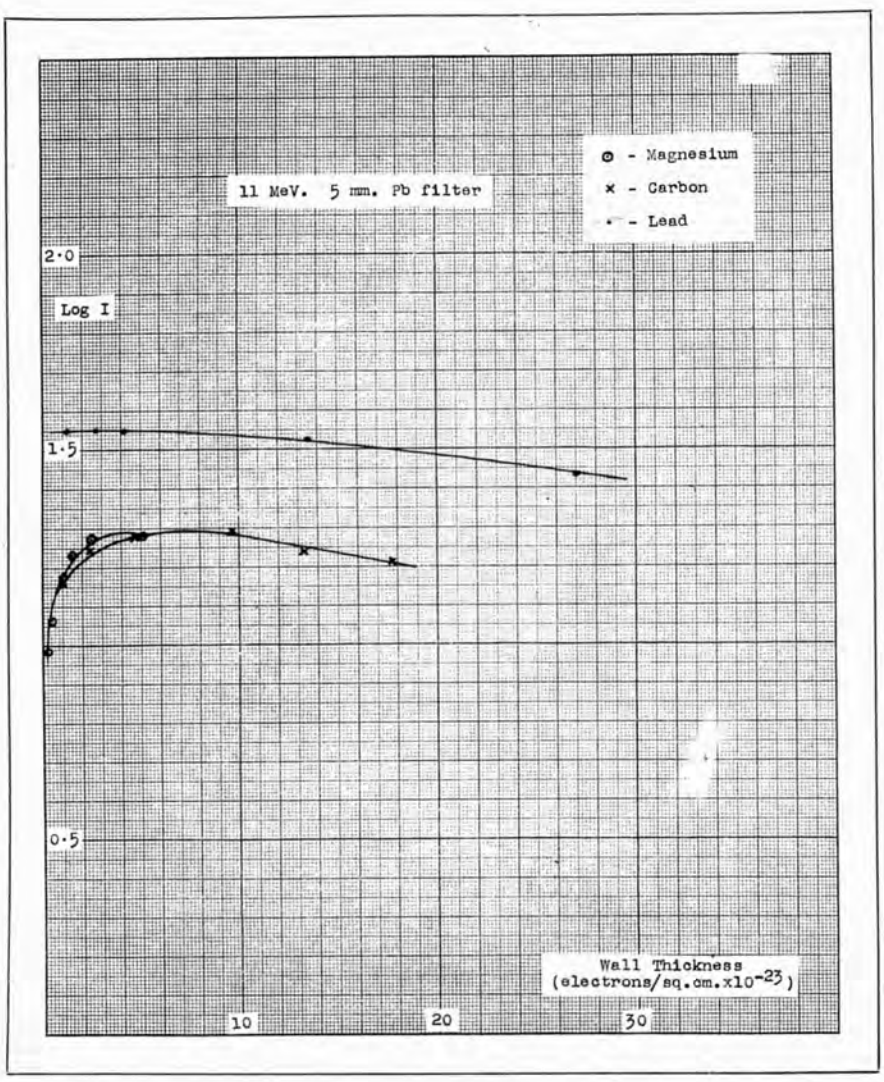
11 MeV. 5 mm. Pb filter
⊙ - Magnesium
× - Carbon
• - Lead
2·0
Log I
1·5
0·5
Wall Thickness
(electrons/sq.cm.x10⁻²³)
10
20
30

Fig. 56

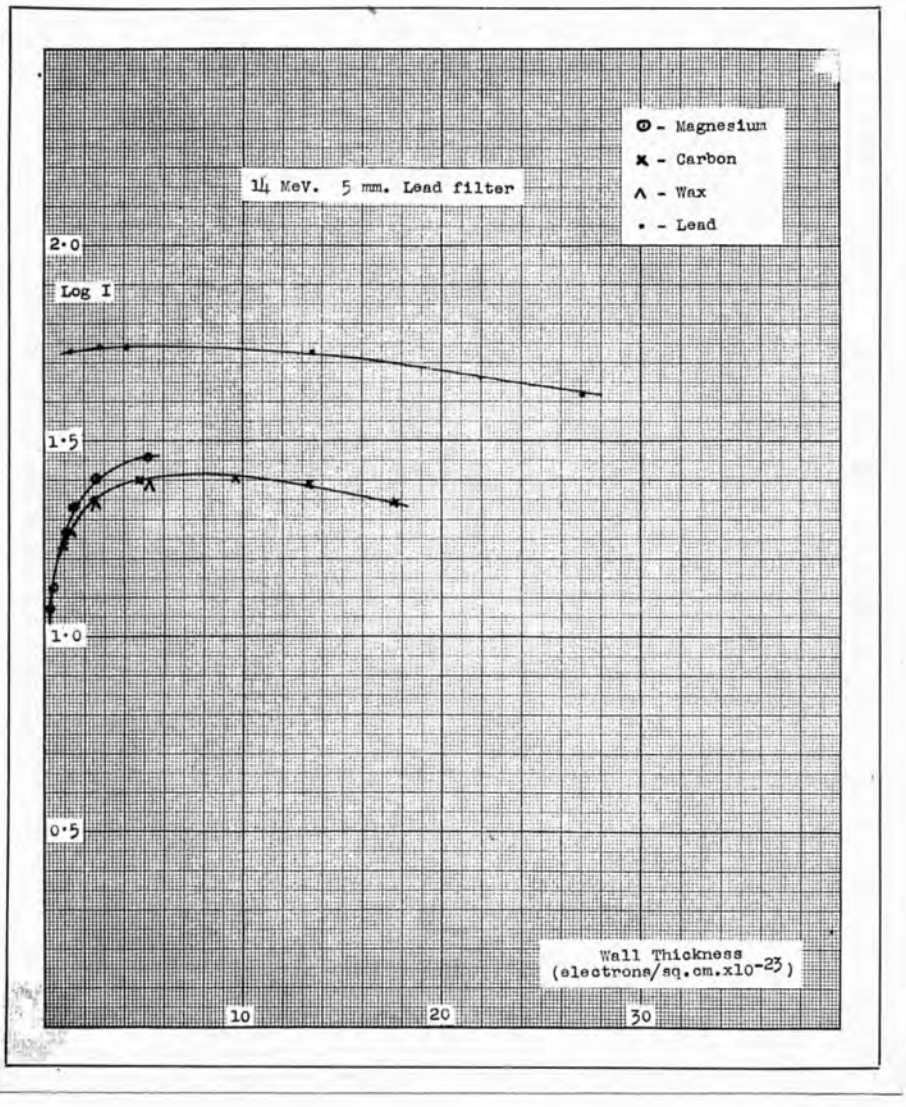
⊙ - Magnesium
✕ - Carbon
∧ - Wax
• - Lead
1¼ MeV. 5 mm. Lead filter
2·0
Log I
1·5
1·0
0·5
Wall Thickness
(electrons/sq.cm.x10⁻²³)
10
20
30

Fig. 57

"clean" beams.

(2) Effect of chamber wall material on ionisation current.

It is to be expected that the ionisation current observed would depend upon the atomic number of the wall of the chamber both because of the variation of real absorption coefficient and of stopping power of the material.

In Figs. 55, 56 and 57 the chamber wall thickness has been expressed in electrons/sq.cm. It will be seen here that in media of low effective atomic number such as carbon and wax the variation of ionisation current with wall thickness is approximately the same, but that for magnesium chambers higher currents are shown, the divergence increasing with energy.

Where the absorption of energy is predominantly by the Compton process, as is the case in low atomic number materials, similar ionisation currents are to be expected. The differences shown for magnesium chambers are due to pair formation which becomes significant in magnesium about 5 MeV. (approximately 25% of the Compton effect) and also to differences in stopping power.

The experimental ratios of ionisation currents in chambers of different materials over the energy range investigated have been obtained relative to that in carbon.

It is convenient as a first approximation to compare values of the ionisation currents at the maxima.

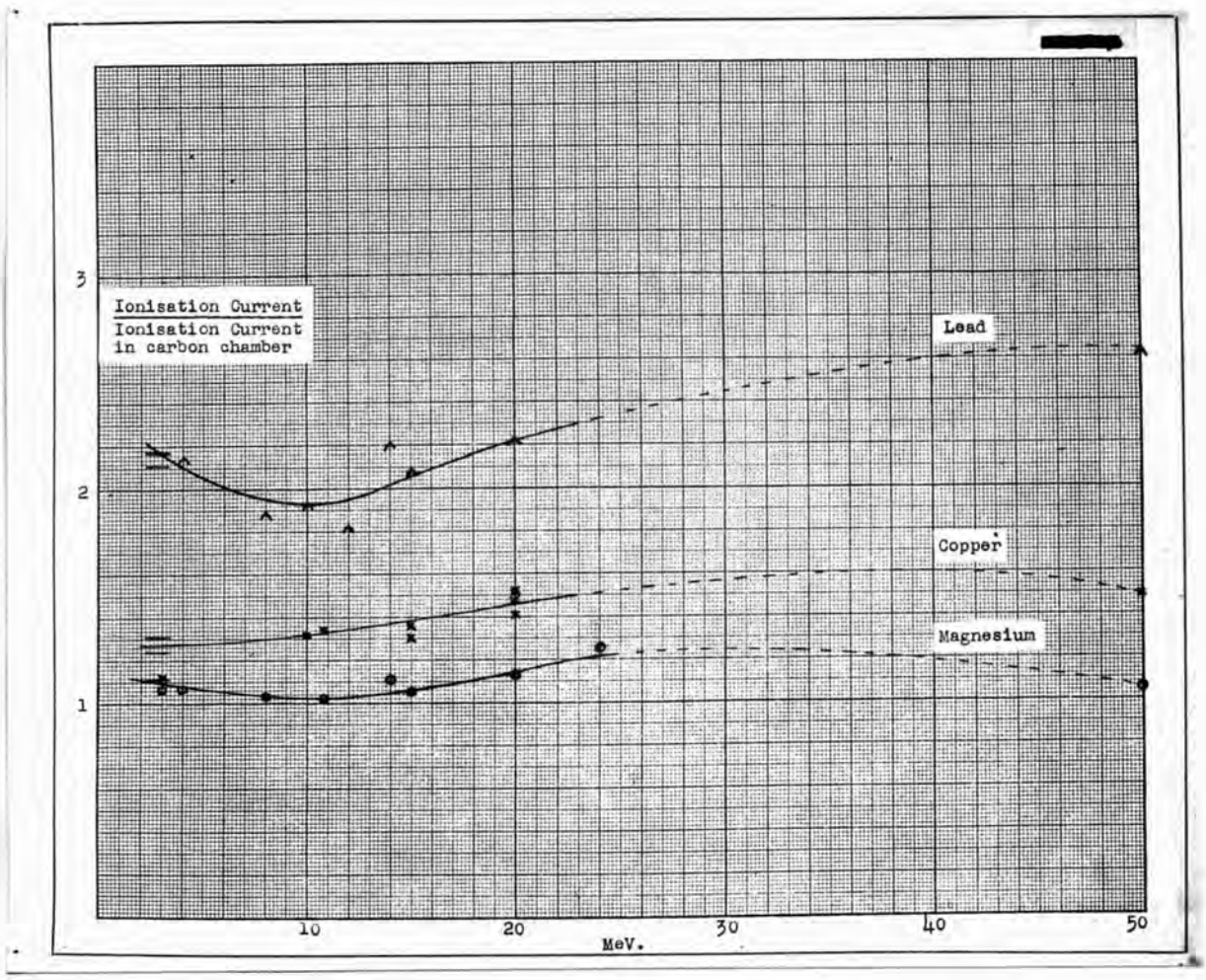
Ionisation Current
Ionisation Current
in carbon chamber
Lead
Copper
Magnesium
3
2
1
10
20
30
40
50
MeV.

Fig. 58

In Fig. 58 are plotted, against peak energy, the results of a comparison of maximum ionisation current in magnesium, copper and lead chambers relative to that in a carbon chamber. The results have been obtained with a wide variety of generators on both sides of the Atlantic and also include some values, to be described later, obtained with radioactive Co60 sources and they show the small differences to be expected, even over a wide range of energy, in the relative currents in various materials.

Gray[85] has shown that the relation between energy absorbed per unit volume of a medium and the ionisation current to be observed in a small cavity in the medium containing air is given by

$$E_v = 1.35 \times 10^{-31} f_z \, n \, J_v \text{ ergs/cc.}$$

where E_v = energy absorbed per unit volume of medium

f_z = function of atomic number representing the relative stopping powers of the medium and air

n = electronic density of the medium

J_v = ionisation current per unit volume.

The values of the energy absorbed can be calculated from a knowledge of the real energy absorption coefficient (μ) given by $\mu = \tau + \sigma_a + \pi$

where τ is the photoelectric absorption coefficient, σ_a is the real part of the absorption coefficient due to Compton scatter and π the absorption coefficient due to

the production of pairs. These coefficients can be calculated from the theories previously mentioned.[42, 43, 52] From the work of Bethe[93] and Gray[85] the stopping power relative to air is seen to be a very slowly varying function of Z and therefore a determination of the relative amounts of energy absorbed per electron in various materials over a range of energies would be expected to give a measure of the relative ionisation currents to be observed.

Mayneord[94] has calculated the relative energies absorbed up to 100 MeV. Using these values a ratio of about 6 to 1 would be expected between the ionisation currents to be observed in a lead and a carbon chamber exposed to a beam of radiation of peak energy 50 MeV. It is clear from Fig. 58 that the ratio is much smaller.

It should now be observed that at high energies electrons begin to lose energy by radiation. The cross-section for this process increases roughly proportional to the energy E and to Z^2 and is therefore most important in heavy elements. At energies about 20 $mc.^2$ an electron in lead loses about half its energy by radiation while in a light material such as carbon the process becomes significant much later at energies of the order of 200 $mc.^2$

At high energies, therefore, the wall of the chamber becomes the source of penetrating electromagnetic radiation which is relatively inefficient as an ionising

agent, while, of course, the electron range is relatively reduced in heavy elements. Thus, when this new mechanism of energy loss becomes important, the stopping power becomes dependent to a greater extent upon the energy with the result that the ionisation current observed is less than would be expected using the energy absorption theory.

(3) Measurement of Stopping Power.

The energy loss of charged particles when passing through matter is at low energies (< 5 mc.^{2} for electrons) mainly due to ionisation and excitation of the atoms of the substance traversed. The probability of these inelastic collisions depends on the velocity and charge of the particle and the atomic number of the material traversed. A great deal of work has been carried out on the rate of loss of energy of such charged particles in passing through matter beginning as early as 1895 with the experiments of Lenard. The early work is difficult to interpret on account of the complications which arise from the considerable scattering straggling of the particles, particularly beta particles, in their passage through the materials. Later measurements, first using thicknesses of material small compared with the range of the particles in the material concerned and secondly using cloud chamber techniques, have yielded more reliable results.

The theory for the loss of energy by moving

electric particles according to classical mechanics was considered by Bohr in 1913.[95] It is interesting that later treatments of the problem by quantum mechanics have not greatly altered the values obtained for the energy losses.

Later Bethe[93], using quantum mechanics, developed a theory for the energy losses due to such inelastic collisions based on Born's approximate treatment of the collision processes. The formula found by Bethe for the average rate of loss of energy (- dE/dx) for a particle of charge ze and velocity v is:-

$$-\frac{dE}{dx} = \frac{4\pi z^2 e^4}{mv.^2} \cdot NZ \log \frac{mv.^2}{I}$$

where I = average excitation potential of the atom

N = number of atoms per cc. of the material

Bethe's formula is valid only if the velocity of the impact is great compared with the orbital velocity of the electrons in the atom. Values obtained from Bethe's calculations show good agreement with experimental determina tions at low atomic numbers, reported by him. For higher atomic numbers the stopping powers per electron determined experimentally are lower than the theoretical values.

Williams[96] has considered the effect at relativistic energies of the change of impact parameter and shows that although the time integral of the force on the atomic electron is unaltered the atomic binding forces

alter the resulting energy transfer. He obtains a correction for the effect depending upon $\beta = v/c$ where v is the velocity of the incident beta particle. This correction to Bethe's formula occurs in the logarithmic term and is similar to a correction worked out by Bethe.[97]

The discrepancy between the experimental values and Bethe's calculated values for high atomic number materials is thought to be due to Bethe's assumptions in the evaluation of I. He has assumed that the wave function of a complicated atom can be considered as the sum of hydrogen wave functions of the same quantum number. This part of the problem has been investigated by Bloch[98] using the Fermi-Thomas model of the atom and also by Livingston and Bethe.[99] The latter workers have endeavoured to make a correction by determining the "effective" number of electrons involved in the stopping processes, since Bethe's calculations were made on the assumption that the velocity of the incident particle is large compared to the velocities of the electron in the atom, a condition which may not be fulfilled in all the levels of the atom.

All these corrections to the original Bethe formula are still uncertain, there being little or no experimental data with which to compare the calculated values. The corrections are also in most cases small, occurring in the logarithmic term only, and in the subsequent comparisons with experiment the original Bethe values have

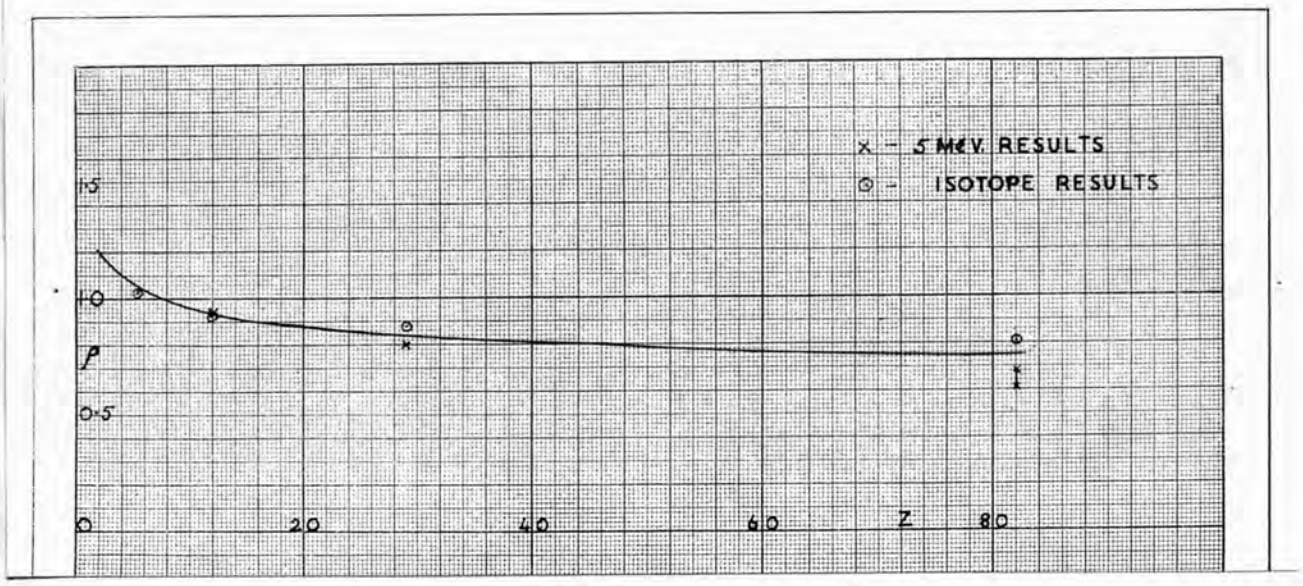

Fig. 59

been used.

In Fig. 59 is plotted curve of relative stopping power per electron (ρ) against atomic number as obtained from Bethe's calculations. The values so obtained have been checked against the corresponding values obtained at values of Z up to 82 from Bloch's formula as quoted by Heitler[52] and only very small deviations found.

Experimental values of stopping power have been obtained by Bragg[81], White and Millington[100], Williams[101] and Gray[89], among others. The experiments of Williams and Gray show good agreement with the values of Bethe given in Fig. 59, while the earlier work of Bragg also shows fair agreement. Gray's values do not lie accurately on a smooth curve and he is of the opinion that the irregularities are real. His measurements were made for light elements up to Z = 29 and he suggests that as the stopping power is a function of the ionisation potential of the individual electrons in the atom the stopping power may increase in passing from one row of the periodic system to the next rather than between neighbouring elements in the same row.

White and Millington's experiments show that the stopping power does not vary over a range of energies from 0.15 MeV. to 1.33 MeV.

The measurements with ionisation chambers of different atomic numbers reported above along with similar

measurements, to be presented later, obtained using radium and the radioactive isotopes Co60 and I131 have been used to calculate relative stopping powers.

As shown earlier, from a knowledge of the real energy absorption coefficients the ratio of the energy absorbed in various materials can be obtained. The values of the relative ionisation currents in ionisation chambers of these materials have been measured and we have therefore a means of measuring the effective stopping power using Gray's equation:

$$E = 1.35 \times 10^{-31} \rho J \text{ ergs}.$$

where E and J are the energy absorbed and ionisation current respectively per electron and ρ is the stopping power.

For two different materials we have:-

$$\frac{E'}{E''} = \frac{\rho' J'}{\rho'' J''} \qquad \therefore \frac{\rho'}{\rho''} = \frac{E' J''}{E'' J'}$$

From the calculated values of E'/E'' and measured values of J''/J' the value of the relative stopping powers ρ'/ρ'' can be obtained.

From the measurements made using radium and the radioactive isotope sources the relative stopping powers have been calculated and are shown in Table II. These experimental values are plotted in Fig. 59 and will be seen to be in good agreement with the values of Bethe.

A similar treatment has been used in obtaining

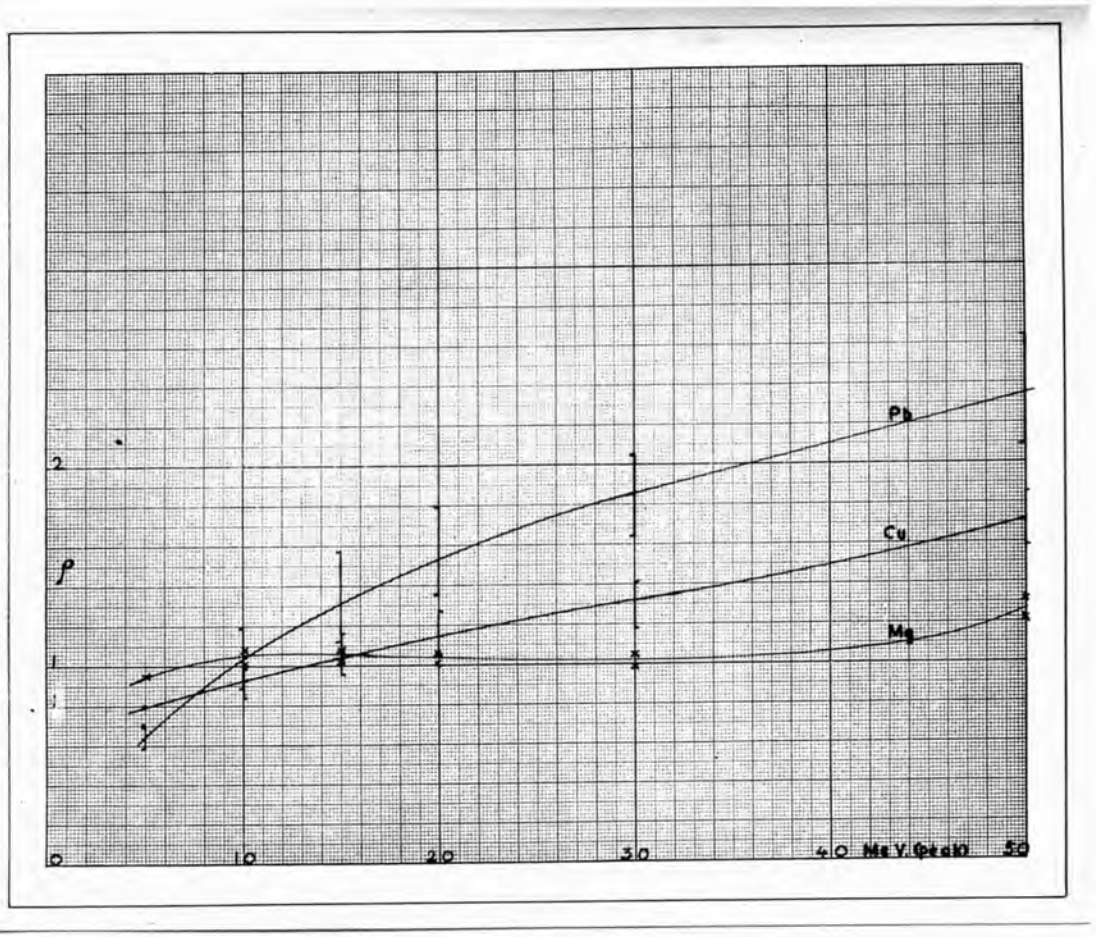

Fig. 60

the relative stopping power per electron at high energies (relative to carbon in this case) from the ratios of the ionisation currents plotted in Fig. 58 and the calculated real energy absorption values. The results are shown in Table III. The values obtained at 5 MeV. peak energy (corresponding to 1.3 to 2.5 MeV. mean energy) have also been plotted on Fig. 59. The agreement will be seen to be good confirming and extending to about 2 MeV. the result of White and Millington that the stopping power does not vary over a wide range of energies.

In Fig. 60 the results of Table III are plotted and show the variation with energy of the stopping power per electron relative to carbon for the three materials lead, copper and magnesium. A considerable variation with atomic number and energy is now evident. As mentioned earlier this is due to the advent of energy loss by radiation. In the theories of stopping power previously mentioned only the collisions processes have been considered. At energies above 5 $mc.^2$, however, the energy loss of electrons passing through matter, as the energy increases, arises more and more from radiation losses. The theory of the process has been discussed by Heitler.[52].

Reprinted from

THE BRITISH JOURNAL OF RADIOLOGY

Volume XXII, No. 253, January 1949

MARTIN (J.H.)
Ph. D.
(Physics)
1949.
JOHN COPY.

REPORT ON THE INSTALLATION OF A TEN GRAMME TELERADIUM UNIT

By J. H. MARTIN, B.Sc., A.Inst.P., T. J. TULLEY, B.Sc., A.Inst.P., E. B. HARRISS, B.Sc.

Physics Department, Royal Cancer Hospital (Free), London, S.W.3

INTRODUCTION

THE following report describes the conversion of a 5 gm. teleradium unit to a 10 gm. unit. The results are published in the hope that they may be of use to those faced with similar problems. The report covers the measurement of radiation in the primary beam, the investigation of stray radiation, and details of the transference of the radium.

A 5 gm. unit has been in use at this hospital since 1936, but for some time it has been apparent that a larger unit would have considerable advantages, such as the possibility of treating approximately twice the number of patients in a given time, or alternatively the attainment of greater effective penetration by the use of larger radium skin distances. The main problems were the packing of a large quantity of radium into a small bobbin and also the protection during the conversion and subsequently during use. Until recently it has been unusual to pack more than 200 mgm. of radium directly into a single tube, but with the availability of 400 mgm. tubes, the attainment of the concentration necessary is greatly facilitated.

Description of the unit

The unit is essentially similar to that described by Grimmett (1937), known as the Radium Beam Therapy Research 5 gm. Unit, No. 2. It incorporates pneumatic transference from a heavily protected safe located against a wall at a distance of 8 ft. from the head, protection from stray radiation being by means of lead and heavy tungsten alloys. The radium is contained in a spacer consisting of an elektron metal cylinder having holes drilled parallel to its axis to hold the radium tubes. This spacer fits inside a bobbin, in our own case constructed of light aluminium-magnesium alloy. The beam of radiation is parallel to the axes of the radium tubes. The mean radium-skin distance is fixed at approximately 8·3 cm., and various sizes and shapes of nozzles may be fitted to give different fields (Lederman, Clarkson and Mayneord, 1944). This radium-skin distance has been preserved with the 10 gm. loading.

The radium containers available for packing in the unit are shown in Table I.

It was thought necessary for the beam of radiation to have an axis of symmetry but found impossible to utilise all the radium and fulfil this condition. Brass models of tubes were used in experimental trials of possible arrangements, with the result that the arrangement shown in Fig. 1 was selected. Use was made of a group of seven closely packed 400 mgm. containers in the centre, surrounded immediately by twelve 200 mgm. containers and an outer ring of twenty-four 200 mgm. containers. It might have been preferable, given suitable strong sources, to have used a more peripheral arrangement of radium to obtain an approximately uniform radiation field

TABLE I

No. of tubes	Nominal content	Overall length	External diameter	Filtration	Ownership
25	200 mgm.	13·0 mm.	5·0 mm.	0·5 mm. monel metal	Royal Cancer Hospital
15	200 mgm.	14·5 mm.	4·5 mm.	0·5 mm. monel metal	Royal Free Hospital
8	400 mgm.	16·5 mm.	6·5 mm.	1·0 mm. monel metal	Nat. Rad. Commission

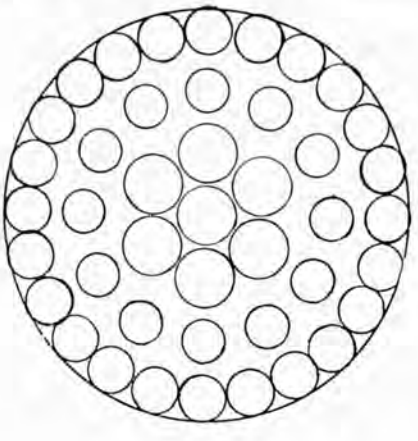

FIG. 1.

on the skin. However, this was not possible with the radium available and differences in distribution of radiation over the skin would in any case be small at this radium-skin distance.

The total nominal content is 10 gm. radium element, and the equivalent filtration was estimated at 1 mm. of platinum. It was found that the extra weight of the bobbin due to the radium did not seriously affect the pneumatic transference, although with the beam pointing vertically downwards, hesitation in starting was noticeable.

MEASUREMENT OF RADIATION

Before clinical use could be made of the apparatus it was important to solve two main problems: (*a*) the determination of absolute dosage-rate at the centre of the field on the skin of the patient and (*b*) the distribution of radiation inside tissues.

(*a*) *Absolute dosage rate*

For the measurement of absolute dosage-rate, reliance was placed on small condenser ionization chambers constructed as shown in Fig. 2. The air

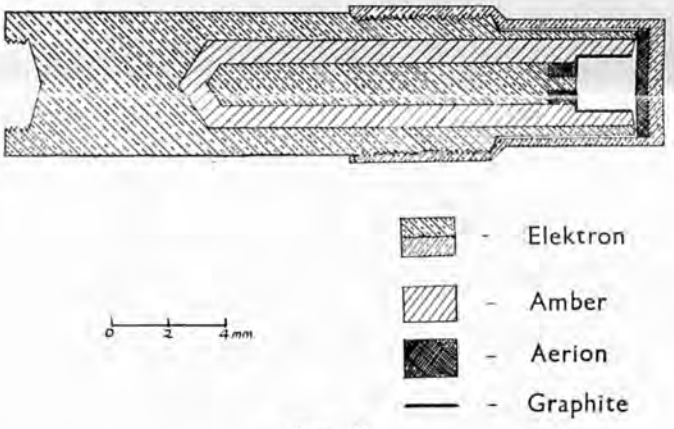

FIG. 2.

volume is cylindrical and approximately 2 mm. long and 2 mm. diameter, the walls being aerion and graphited amber with a central electrode of elektron metal. Similar chambers have been described by Farmer (1945).

Calibration. The chambers were calibrated with the help of a 400 mgm. tube of the type used in the teleradium unit. Its wall thickness is 1 mm. monel metal, the total absorption correction in salt and wall for radiation emerging at right angles to the length of the tube being estimated as 6 per cent. The loss of charge of the chambers during exposure was measured with a Lindemann electrometer connected in a compensating circuit employing a null method devised by Honeyburne and Strong (1943). Times of exposure during calibration were of the order of ten minutes.

The content of the tube was estimated by comparison with a 69·7 mgm. radium standard (Mayneord and Roberts, 1937), used for some years in this department and initially measured at the National Physical Laboratory. Two separate measurements yielded 395 mgm. and 402 mgm. respectively as the content of the tube. In the subsequent measurements it was assumed that within experimental error the content was 400 mgm. radium element at an equivalent filtration of 0·5 mm. Pt. During calibration seven chambers were exposed

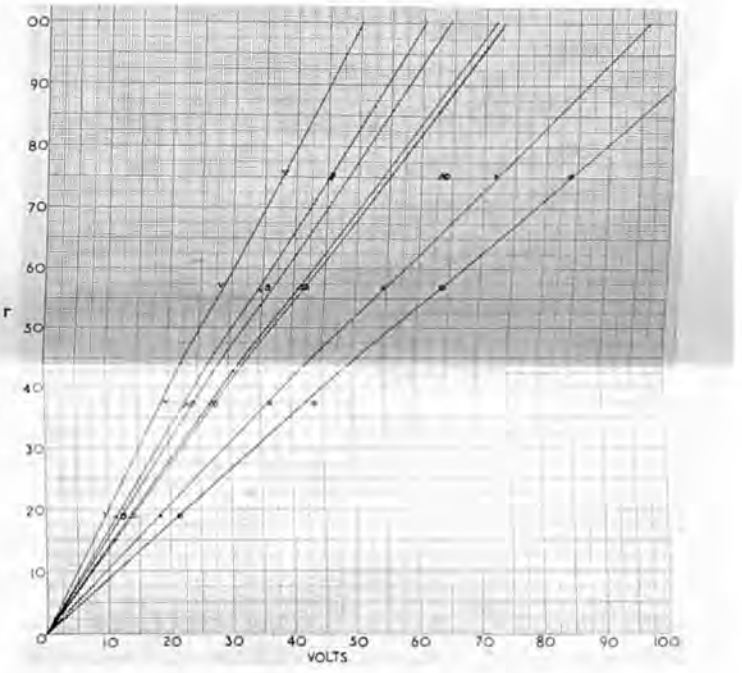

FIG. 3.

simultaneously in a specially designed perspex holder which fixed precisely their position with respect to the 400 mgm. radium source. The distance from the centre of the radium source to the centre of the measuring volume of each chamber was approximately 6·2 cm. and was measured accurately by means of a travelling microscope reading to 10^{-2} mm. The absolute sensitivities of the chambers differed considerably among themselves, but in each case the loss of charge increased linearly with dose within the limits of accuracy of the measurements (Fig. 3).

The chambers have been tested for wavelength independence over a wide range of quality and show

little variation for radiations whose half-value layers are sufficiently great to render negligible absorption in the walls of the chambers (Fig. 4). A correction has been made to the results for the fact that the source was not a geometrical point, and for lateral filtration, use being made of the experimental result (Mayneord and Roberts, 1937), that a point source of radium with a filtration of 0·5 mm. of platinum delivers 8·3 r per mgm. hour at a distance of 1 cm. In all, twenty-eight calibration exposures were made.

Measurement of surface dosage-rate. Measurements of the dosage-rate at the surface of the applicator of the 10 gm. unit were made by fixing seven small chambers in close contact with its chromium-plated brass end. The charge lost during a five-minute exposure was measured with the Lindemann electrometer as above, the number of röntgens received being estimated directly from the calibration curves. Three complete sets of experiments of this type were made. The resulting observations were corrected to the temperature and pressure obtaining during calibrations and a correction was also made for wall thickness of the chambers. The latter correction was made in accordance with previous investigations (Mayneord and Roberts, 1937). In addition, the backscatter was measured in a water phantom, and agreed with previous determinations (Mayneord and Honeyburne, 1938). This backscatter is small and estimated at 4 per cent. for an 8 cm. diameter circle field. In view of the finite size of the chambers a correction was also made according to the inverse square law in order to obtain the dosage rate in the plane of the end of the applicator.

In addition to these investigations with condenser chambers a direct comparison was made between the dosage-rates from the unit when loaded with 5 gm. and 10 gm. respectively, using an F.P.54 direct reading dosage-rate system described elsewhere (Mayneord and Cipriani, 1947: Mayneord, in press); this comparison gave a value approximately 9 per cent. higher than the condenser chamber measurements (*i.e.*, 1040 r per hour). The output of the 5 gm. unit was measured some years ago with larger Sievert condenser chambers, and the result was liable to more error than the present measurements. Also in view of the fact that the 5 gm. unit had been in use for several years and small changes in the position of the radium may possibly have occurred, this value has been included only once in assessing the final result. The three sets of measurements with condenser chambers made on separate days were treated separately, and three mean values of the dosage-rate at the surface of the unit thus obtained. These values were 961, 943 and 941 r/hr. respectively. The final weighted mean value thus obtained for the surface dosage rate was taken as 970 r/hr.

(*b*) *Distribution of radiation in a water phantom*

The distribution of radiation in a water phantom was measured using the remotely controlled dosefinder (tele-dosefinder) described elsewhere (Mayneord and Cipriani, 1947; Mayneord, in press). This consists of an F.P.54 D.C. amplifier (DuBridge-Brown, 1933, circuit), attached to an ionization chamber with an evacuated lead. The dosage rate is read directly on a Cambridge spot galvanometer.

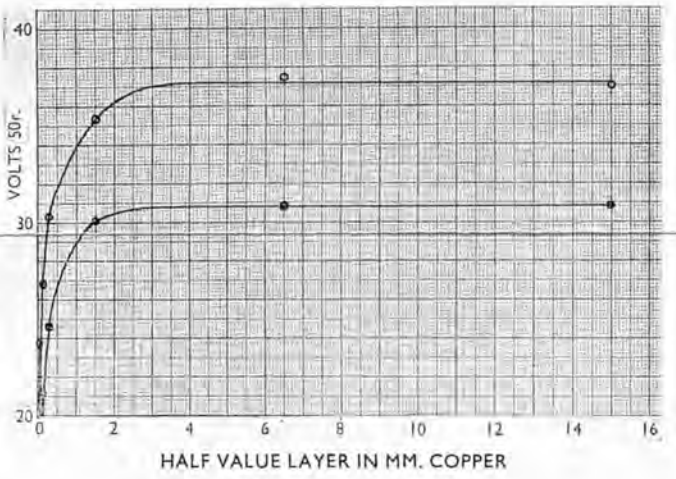

FIG. 4.

The ionization chamber is mounted on three slides at right angles to each other (Mayneord, 1939), and may now be controlled in position by means of three small electric motors. The position of the chamber may be read by balancing potentiometer systems at the control panel. The controls are connected to the measuring system by means of long screened cables and consequently measurements may be carried out at any required distance from the source of radiation, thus avoiding the necessity for removing the source or shutting off the plant each time a different measuring position is required. As used in work on the 10 gm. unit, the cables were 24 ft. long and enabled the operators to work at a distance where the dosage rate was 0·2 tolerance dosage-rate without extra screens. The cylindrical chamber used

for the distribution measurements was made of elektron metal and had internal dimensions of 6×6 mm. and wall thickness of 2 mm. With this chamber at the surface of the water phantom, a current of the order of two μA was observed, representing a current gain of 10^5. In determining the final distribution, appropriate corrections were made for the wall thickness and finite size of the chamber on the lines already indicated.

Measurements were made in the usual way along a number of carefully chosen vertical axes, and isodose curves were drawn by interpolation. It was found that the distribution of radiation with the 10 gm. loading was very similar to that obtained when the unit contained 5 gm. (except, of course, for a factor of two in the absolute dosage-rate), any slight discrepancies observed being probably attributable to the change of distribution of the radioactive sources. Two of the observed isodose curves are shown in Figs. 5 and 6. It is perhaps worth noting that during the distribution experiments, measurements of surface dose were noted to be constant to approximately 2 per cent., even after the bobbin had passed to and fro between safe and head of unit several times. It appears, therefore, that the bobbin returns accurately to the same position.

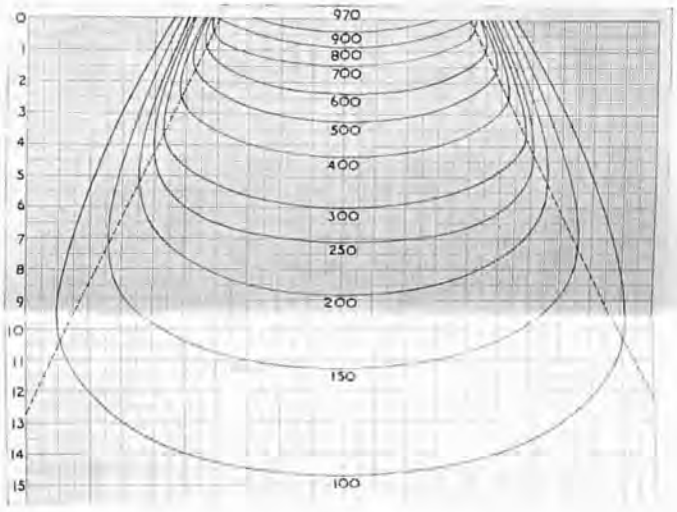

8 CM. DIAMETER CIRCLE FIELD
FIG. 5.

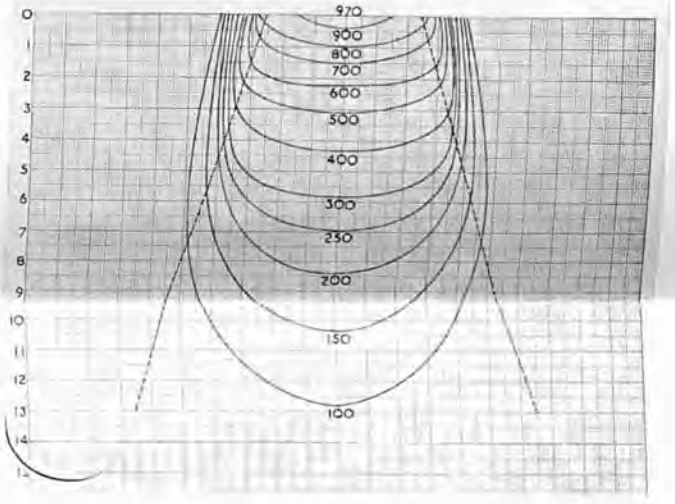

5 CM. DIAMETER CIRCLE FIELD
FIG. 6.

PROTECTION MEASUREMENTS

(*a*) *Doses received during loading*

It may be of interest to record the doses received during the loading of the bobbin. The bobbin was removed from the 5 gm. unit and manipulated on a well-protected radium table behind a thickness of lead increased for the purpose to approximately 5 in. The operations involved unscrewing the end of the bobbin, removing the 5 gm. of radium from the old spacer, transferring it to the new spacer and adding the extra 5 gm. of radium. The 10 gm. of radium in the new spacer had then to be placed back in the bobbin and the latter again sealed.

The operators carried "air-wall" ionization chambers, reading up to 2·5 r, in the breast pocket. The doses received during the operations, which took about a quarter-of-an-hour, were as follows:

Operator 1 0·9 r and 0·5 r

Operator 2 0·5 r and 0·2 r

In addition both the operators carried two condenser chambers, as used for the absolute dosage-rate measurements, strapped to the middle phalange of the first and second fingers of the right hand. Operator 1, who loaded the tubes into the bobbin, received 4·0 r and 11·6 r on the fingers, while Operator 2, who carried the bobbin to and from the safe, registered no measurable dose. The dose received on the fingers of Operator 1 was much higher than need be as some delay was caused by one of the fixing screws of the bobbin cap being faulty.

(*b*) *Investigation of stray radiation in the neighbourhood of the unit*

After the 10 gm. unit had been put into use a survey was made of the stray radiation to be found in its vicinity.

The measurements were made with a portable direct reading protection meter developed in the hospital. It consists of a simple D.C. amplifier coupled to an ionization chamber of approximately 1 litre capacity. The reading instrument, a standard microammeter reading to 50 μA, covers a range up to ten times tolerance dosage rate. (T.D.R.$=10^{-5}$ r/sec.)

The distribution of radiation is shown in Fig. 7.

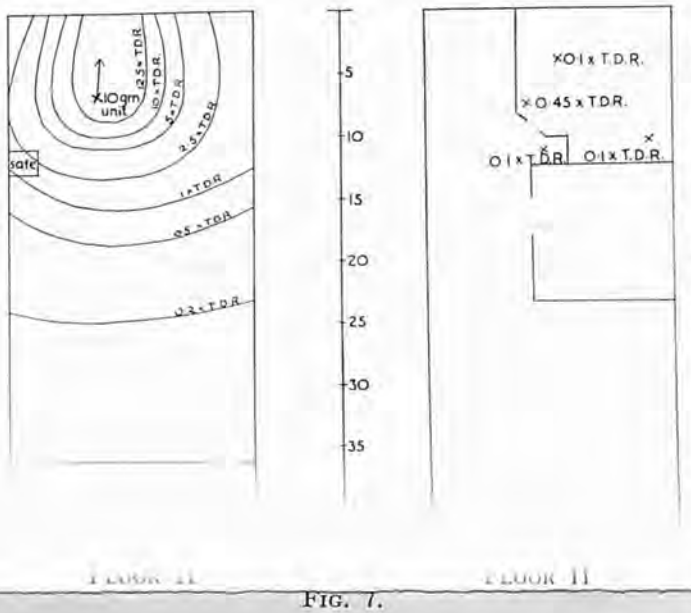

FIG. 7.

The measurements of radiation around the 10 gm. unit were made during the treatment of a patient with the beam pointing horizontally in the direction indicated. The dose received in the observation room is certainly below 0·01 $\times$ T.D.R., and too small to be measured accurately with the direct reading protection meter. It will be noted that tolerance dosage-rate is received at a distance of 9 ft. from the unit. The dosage rate approximately obeys the inverse square law. For details of thickness of protective material in the head reference should be made to Grimmett's (1937) paper. When the radium is in the safe, the radiation outside is never more than 0·2 $\times$ T.D.R. except in the immediate vicinity of the hand loading slot, where it is 1·0 $\times$ T.D.R.

With the radium in the head and the beam pointing vertically downwards, the dosage-rate immediately below on the next floor is 0·45 T.D.R. The distance is then approximately 16 ft., and the beam has passed through a floor of 11½ in. of concrete. The distribution of radiation on this floor is shown in Fig. 7.

The region of high dosage-rate (0·45 T.D.R.) is not normally entered by staff, being behind one of the X-ray plants. Surrounding this a dosage rate of 0·1 T.D.R. was recorded over a fairly large area. No radiation could be detected anywhere else on this floor or in the rooms on the ground floor.

It was therefore necessary to employ more sensitive means of detection in order to map the stray radiation on this floor completely (Turner and Sinclair, 1948).

SUMMARY

The report describes the conversion of a 5 gm. teleradium unit to a 10 gm. unit. A detailed description is given of the measurement of the output, and the determination of dosage distribution in a water phantom. The dosage distribution was measured with a new "teledosefinder" system which enables the operators to work at a safe distance from the unit. Protection measurements on the radiation in the neighbourhood of the unit were made, and the protection was found to be satisfactory.

REFERENCES

DUBRIDGE, L. A., and BROWN, H., *Rev. Scient. Inst.*, 1933, iv, 532.

FARMER, F. T., *Brit. Journ. Rad.*, 1945, xviii, 148.

GRIMMETT, L. G., *Brit. Journ. Rad.*, 1937, x, 105.

HONEYBURNE, J., and STRONG, J. A., 1943, unpublished.

LEDERMAN, M., CLARKSON, J. R., and MAYNEORD, W. V., *Brit. Journ. Rad.*, 1944, xvii, 115.

MAYNEORD, W. V., and ROBERTS, J. E., *Brit. Journ. Rad.*, 1937, x, 365.

MAYNEORD, W. V., and HONEYBURNE, J., *Brit. Journ. Rad.*, 1938, ii, 741.

MAYNEORD, W. V., *Brit. Journ. Rad.*, 1939, xii, 262.

MAYNEORD, W. V., and CIPRIANI, A. J., *Can. Journ. Research, A*, 1947, xxv, 303.

MAYNEORD, W. V., *Journ. de Radiologie et d'Électrologie*, 1948, xxix, 461.

TURNER, R. C., and SINCLAIR, W. K., *Brit. Journ. Rad.*, 1948, xxi, 632.

TABLE II

Source	Material	Relative Stopping power/air	Mean Value
Co 60	Carbon	1.02	1.02
Radium	Carbon	0.87	1.02
I 131	Carbon	0.84	1.02
Co 60	Magnesium	0.88	
Co 60	Magnesium	0.90	
Co 60	Magnesium	0.94	
Co 60	Magnesium	0.93	0.93
Radium	Magnesium	1.02	
Radium	Magnesium	0.87	
I 131	Magnesium	0.97	
Co 60	Copper	0.87	
Co 60	Copper	0.84	
Co 60	Copper	0.90	0.88
Radium	Copper	0.86	
Radium	Copper	0.86	
I 131	Copper	0.92	
Co 60	Lead	0.76	
Co 60	Lead	0.77	
Co 60	Lead	0.80	0.81
Radium	Lead	0.89	
Radium	Lead	0.78	
I 131	Lead	0.88	

TABLE III

E_{peak} MeV.	E_{mean} MeV.	Material	$\frac{\text{Energy absorbed}}{\text{Energy absorbed}_{carbon}}$	J/J_c measured	$\frac{\rho}{\rho_c} = \frac{E'J_c}{E_cJ}$
5	1.6-2.5	Lead	1.2 - 1.4	2.05	0.59 - 0.68
10	3.3 - 5.0	Lead	1.7 - 2.3	1.93	0.88 - 1.19
15	5.0 - 7.5	Lead	2.3 - 3.2	2.05	1.12 - 1.56
20	7.0 - 10	Lead	3.0 - 4.0	2.22	1.35 - 1.80
30	10 - 15	Lead	4.0 - 5.0	2.44	1.64 - 2.05
50	17 - 25	Lead	5.5 - 7.0	2.64	2.09 - 2.65
5	1.6 - 2.5	Copper	1.02	1.28	0.8
10	3.3 - 5.0	Copper	1.12 - 1.32	1.32	0.85 - 1.00
15	5.0 - 7.5	Copper	1.33 - 1.60	1.38	0.96 - 1.16
20	7.0 - 10	Copper	1.54 - 1.86	1.46	1.05 - 1.27
30	10 - 15	Copper	1.86 - 2.20	1.56	1.19 - 1.41
50	17 - 25	Copper	2.35 - 2.75	1.48	1.59 - 1.86
5	1.6 - 2.5	Magnesium	1.01	1.06	0.95
10	3.3 - 5.0	Magnesium	1.03 - 1.08	1.02	1.01 - 1.06
15	5.0 - 7.5	Magnesium	1.08 - 1.15	1.06	1.02 - 1.08
20	7.0 - 10	Magnesium	1.15 - 1.21	1.14	1.01 - 1.06
30	10 - 15	Magnesium	1.21 - 1.30	1.24	0.98 - 1.05
50	17 - 25	Magnesium	1.30 - 1.40	1.06	1.28 - 1.32

TABLE IV

Peak Energy	Material	Stopping Power relative to carbon
10 MeV.	Magnesium	1.03
10 MeV.	Copper	1.17
10 MeV.	Lead	1.62
20 MeV.	Magnesium	1.06
20 MeV.	Copper	1.42
20 MeV.	Lead	2.33
50 MeV.	Magnesium	1.23
50 MeV.	Copper	1.88
50 MeV.	Lead	3.60

Using Heitler's formula for the total energy loss of a fast electron in passing through matter the relative stopping power per electron has been calculated for a range of energies and atomic numbers. The effect of the heterogeneity of the incident radiation has been taken into account. The appropriate Heitler spectral distributions have been divided into a number of bands to which a mean energy has been assigned; the energy losses for these average energies have then been calculated and the values so obtained weighted according to the relative intensities at each energy. The relative stopping powers per electron for magnesium, copper and lead relative to carbon obtained in this way are given in Table IV. It will be seen that the values for the heavier elements are considerably higher than the experimental values obtained and plotted in Fig. 60. This is probably due to the fact that the incident radiation sets in motion electrons with a wide range of energies resulting in a lower average energy for the electrons traversing the material and hence a lower stopping power. Point is added to this explanation by the small deviation from theory found for the low atomic number material magnesium, where the change of stopping power with energy is small. To obtain the average energy of the electrons set in motion by the incident radiation a knowledge of their energy distribution is required. Calculations are in hand

to enable, in this way, a more exact comparison of theory and experiment to be made.

(4) Measurement of short wavelength X rays in rontgens.

To measure the flux of an electromagnetic radiation by the measurement of ionisation in a small cavity it has been shown that arbitrary measuring conditions must be imposed. In order to compare the above measurements with similar measurements at lower energies we naturally try to impose the same conditions relating to atomic number of gas and chamber walls, electronic equilibrium and scattered electromagnetic radiation as implied in the definition of the rontgen.

We must first have a wall thick enough to supply all the electrons crossing the cavity, which means the wall must be at least as thick as the range of the fastest secondary particles and since this thickness is seen (Figs. 32 to 52) to amount to several centimetres it must now be decided:-

(a) What correction must be made for the absorption of primary radiation in the wall?

(b) What correction must be made for the effects of the secondary electromagnetic radiations comprising scattered quanta, annihilation radiation and radiation loss by electrons?

(c) At what point in space is the electromagnetic radiation measured?

The best answer which can be given to (c) is that the measurement is made at the "centre of gravity of the 'build-up' portion of ionisation-wall thickness curve." Electrons enter the measuring cavity from elements of mass throughout the whole thickness of the wall required for build-up and any of these elements can influence the resulting ionisation. It seems, therefore, that the position of measurement may be best regarded as the "centre of gravity" of the electronic distribution reaching the cavity, the electrons arising in different elements of mass being suitably weighted as to their effectiveness. Since experiment shows the effectiveness to vary approximately linearly with distance from the cavity the centroid is a reasonable position at which the measurement of energy flux may be regarded as being made.

This decision determines the correction which need be applied for absorption of the primary radiation in the front wall of the chamber. A correction for absorption in a thickness of wall equal to the depth of the centroid from the front wall of the chamber must be made. This more exact correction differs little from that applied by Mayneord and Roberts[84] when the correction for the wall thickness from the front face to the position of maximum ionisation was applied.

This method of correction for absorption partially,

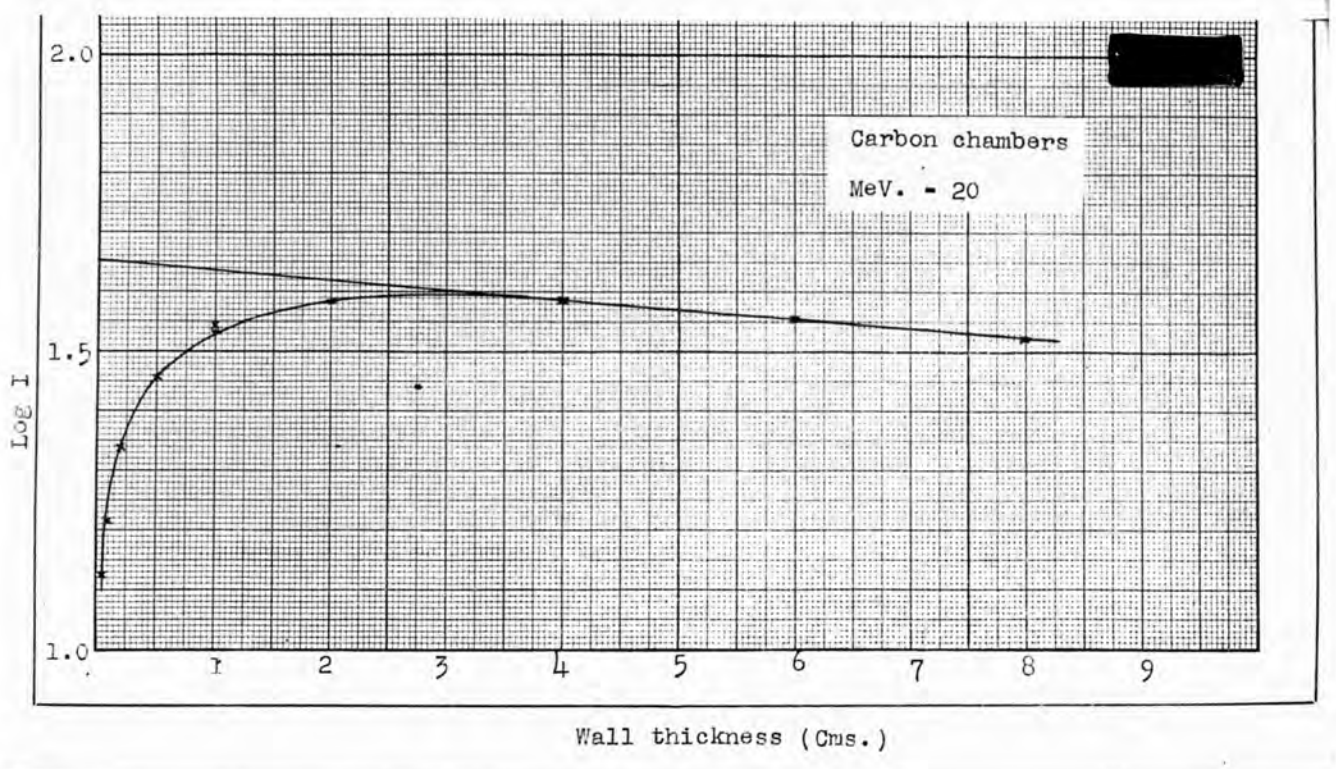
2.0
1.5
1.0
Log I
Carbon chambers
MeV. - 20
1
2
3
4
5
6
7
8
9
Wall thickness (Cms.)

Fig. 61

at least, takes care of the correction for scattered electromagnetic radiation.

In Fig. 61 is shown the curve of log. ionisation current against wall thickness obtained in a carbon chamber with the 20 MeV. betatron. The centroid of the build-up curve is found to lie 2.0 cms. from the front face. The slope of the curve beyond the maximum is taken as a measure of the absorption of the primary radiation in the material of the walls. Extrapolating, therefore, as shown the absorption correction is the ratio of the ionisation current at 2.0 cms. to that at zero wall thickness, that is 44.7 to 41.7. The maximum ionisation current (39.8) is then multiplied by this ratio so that the final current is

$$39.8 \times \frac{44.7}{41.7} = 42.7 \text{ e.s.u./cc./min.}$$

Three further corrections must be applied before the result is in rontgens. These are corrections for temperature and pressure of the air and atomic number since carbon is not strictly an "air-wall" material though the deviation is small. The final corrected value is 43.9 r/min. This was obtained at 125 cms. focal distance and therefore at 1 metre the dosage-rate is approximately 68.7 r/min., a good example of the order of dosage-rate consistently observed at 20 MeV. with this instrument. It will be shown later that this is in good agreement with Kerst's own measurements.

These results indicate that up to 20 MeV. at least, it is possible to obtain a reasonable estimate of dose in rontgens. Obviously, however, difficulties are appearing which as stated earlier make the rontgen an unsuitable unit in which to measure high energy radiations. The lack of knowledge as to what we may now interpret as "associated corpuscular emission" is aggravated by the great wall thicknesses required to establish equilibrium which may introduce unknown quantities of secondary scattered radiation and finally the difficulty of deciding where the measurement is taking place will increase the higher the energy.

It is quite clear also that inside a medium at points nearer the surface than the point of maximum ionisation current the measurements cannot possibly be called rontgens. Since a measurement at points nearer the surface than this are frequently of interest we are faced with the choice of making the measurement with a chamber of wall of sufficient thickness to measure in rontgens or of one whose wall is so thin that it contributes nothing to the observed ionisation. That is we have the choice between imposing unique measuring conditions in an endeavour to measure the primary radiation or making a measurement which characterises the conditions existing, however complex.

A modified approach to the problem of measuring the primary radiation is suggested by Lax.[102] Here an ionisation chamber whose wall thickness is considerably less than that required to build up electronic equilibrium is suggested. For measurements on the 100 MeV. betatron he uses a chamber consisting of two carbon plates separated by a thin gas layer. The thickness of carbon wall is 4.5 cms. He applies suitable corrections for the thickness of the wall, absorption of the beam of primary radiation in the wall, scattering and losses by radiation from the electrons in the wall and computes the sensitivity of such a chamber to an accuracy of 5%.

This solution is attractive for measurements at very high energies where, normally, very thick chamber walls would be required but for energies up to say 50 MeV. the introduction of the uncertainties due to calculations of scatter, losses by radiation and the possibilities of repeated Compton encounters of scattered quanta in the walls of the chamber make it preferable to use direct measurements as outlined above.

It seems possible then, from the experimental evidence obtained, that the definition of the rontgen may be sufficiently accurately fulfilled to enable an estimation of dosage-rate in primary beams to be made to an accuracy adequate for comparison of different pieces of apparatus.

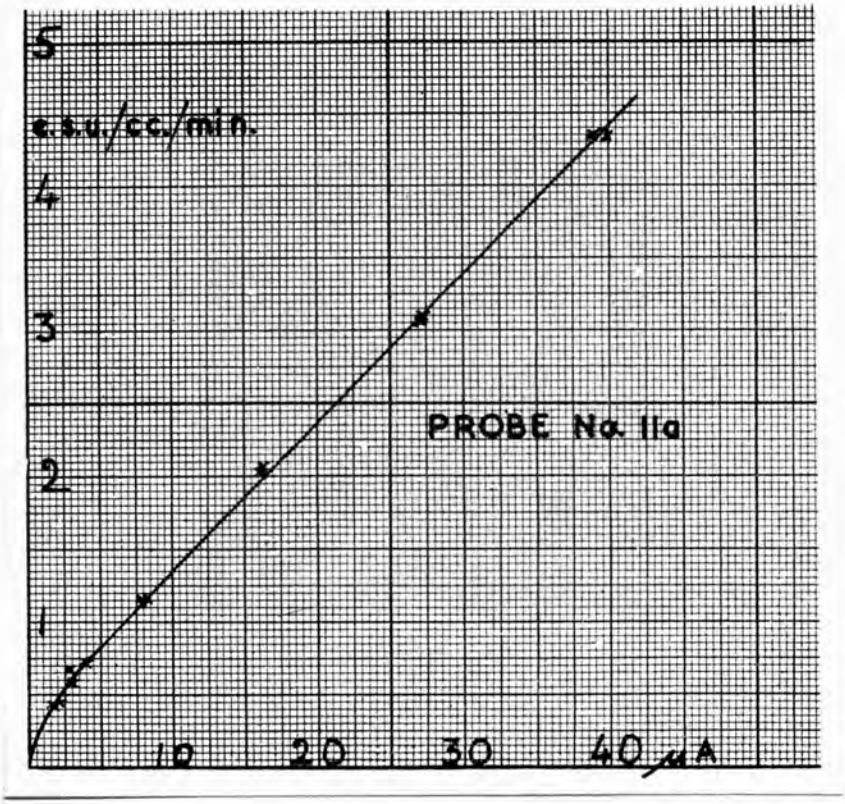

Fig. 62

(5) Comparison in rontgens of output of British and American high energy generators.

Using the above method an endeavour has been made to compare the output of American and British machines in rontgens as follows.

First, in the laboratories of the Royal Cancer Hospital the standard victoreen kept in the Physics Department of that hospital was used to calibrate, at 200 kV., the probe system with a 2 mm. wall carbon chamber. As stated earlier the victoreen, just prior to these measurements, had been standardised by the National Physical Laboratory over a range of qualities enclosing the one employed for the probe system calibration. The probes were, therefore, calibrated in e.s.u. of charge per cc. per minute, per division of scale. A typical curve is shown in Fig. 62. The carbon chamber probe system was then placed in the high energy beam to be measured, the variation with wall thickness of carbon observed and the value corrected as explained above. This reading was then corrected for temperature and pressure to the conditions under which the probe was calibrated. Finally, correction was made for the fact that carbon is not strictly "air-wall." This correction as will be seen from Fig. 58 is negligible at 10 MeV. and at 30 MeV. is estimated at only 3%, the carbon chamber reading too low. The resulting value of the ionisation

current is then in e.s.u./cc./min. under conditions appropriate to the definition of the rontgen. The dosage-rate is then known in r/min.

The measurements thus made were compared with values previously given as r/min. by the workers at Urbana and Schenectady. At Urbana, Kerst and his colleagues had used a victoreen condenser dosemeter inside a block of plastic to build up its wall thickness. This plastic cylinder had a wall of 5.7 cm. and was suitable for the purpose, but no correction had been made for absorption in its mass. The Urbana team now use the victoreen in a "pressdwood" phantom in which small animals had been irradiated.[103] This measurement of dose seems, therefore, to be valid when made at depths greater than the equilibrium thickness.

In order to compare the probe system measurements with those of Kerst it was first necessary to compare victoreens. This was effected by comparison of the Kerst victoreen and the carbon chamber probe system in a 200 kV. pulsating E.M.F. X-ray plant. It was thus found that the Kerst victoreen read 5% lower than the probe system. Experiments were then carried out with the two systems at 10 and 20 MeV.

It might be mentioned that a comparison of the naked victoreen and the probe system in the 20 MeV. beam showed that the victoreen read too low by a factor of 2.9

owing, of course, to lack of electronic equilibrium. This serves to emphasise the misleading and possibly dangerous results which would arise from the use of the instrument in this way to compare effects at high and low voltages.

Comparisons of the two systems under proper conditions were carried out by building up the wall thickness of both the victoreen and the probe unit chamber with the same blocks of carbon. Convenient blocks of carbon 6 cms. thick were available and therefore used for the experiment, the instruments being placed in the beam as close as possible behind the carbon blocks. The beams were monitored continually by a second victoreen dosemeter during the experiments. A sample of the observations made is given below.

20 MeV. 6 cms. carbon front wall for both instruments.

Kerst(s victoreen reads (mean value)	19.7 r/min.
Carbon probe system reads (mean value)	17.6 e.s.u./cc./min.
Carbon probe corrected to standard conditions of temperature and pressure	18.2 e.s.u./cc./min.
Corrected to value at centroid	21.6 e.s.u./cc./min.
Corrected for carbon to "air-wall" chamber	21.8 r/min.
Kerst victoreen corrected for temperature and pressure	20.4 r/min.

Thus the victoreen reading uncorrected differs by 7% from the r/min. estimated by the probe system. If a correction

for wall thickness be made to the victoreen it is found to read about 10% higher than the probe system. A similar comparison at 10 MeV. showed a difference in the same sense of 5%. Thus relative to the probe system the victoreen reads at 200 KV. 5% lower, at 10 MeV. 5% higher and at 20 MeV. 10% higher.

A comparison with the victoreen in the plastic shell was also made at 20 MeV. The composition of the shell was not known and the corrections to be applied were, therefore, uncertain but agreement in readings to within 10% was again obtained.

In view of preliminary nature of the results this comparison shows good agreement with Kerst's measurements and certainly it appears that at 20 MeV. agreement on a measurement in rontgens, to a reasonable accuracy, can be reached.

At Schenectady the method of measurement used had consisted in surrounding the chamber of a victoreen condenser dosemeter with a lead cap $\frac{1}{8}$" thick. A comparison of this system and the carbon probe system was made at 11 MeV. and at 47 MeV. It is found that the uncorrected readings of the victoreen in the lead cap read 1.50 times the estimated r/min. at 11 MeV. and 2.84 times the value at 47 MeV. Comparison with Fig. 58 shows that at 11 MeV. the ratio is less than that between pure lead and pure

carbon chambers, evidently due to absorption of electrons from the lead in the wall of the victoreen chamber. The ratio at 47 MeV. agrees roughly with that found in Fig. 58 for the ratio of maximum ionisation in pure lead and carbon chambers.

Similar measurements have been made at T.R.E., Malvern, on the 15 MeV. synchrotron and at 24 MeV. during the development of a 30 MeV. synchrotron in order to determine the true output in rontgens and to standardise measuring systems in use at T.R.E. The output of the 15 MeV. machine was very low and found to be at 1 metre approximately 0.2 r/min. at 15 MeV. The output varied little with energy. It was known, however, that this machine had not a very good field shape and it is probable that electrons were being lost as the energy increased, a possibility substantiated by the measurements reported earlier showing the large background of stray electrons found round the machine.

The output of the 30 MeV. synchrotron measured at 24 MeV. was 3 r/min. at a metre. This has subsequently been increased to 15 r/min. at 1 metre.

Two further possible difficulties arise in these measurements and comparisons. The radiation from betatrons and synchrotrons is emitted in bursts of the order of 1 - 5 μ sec. at intervals depending on the excitation frequency but usually of the order of 1/50 sec.

The instantaneous dosage-rate is therefore of the order of 10^4 times the mean value. The two difficulties introduced are first that of saturation ionisation current, there being a possibility of loss of ions by recombination and secondly possible errors due to the inability of a dosage-rate measuring system of relatively long time constant to follow the instantaneous variations. No effects have been observed which could be interpreted as lack of saturation. A direct test was made using the 4 MeV. linear accelerator at Malvern as source of radiation. The output pulses from this machine are of the order of 1 μ sec., at least as short as those from betatrons and synchrotrons. The voltage in the carbon probe chamber was changed in steps from 180 volts (the voltage usually employed) up to 300 volts at an observed dosage-rate of 15 r/min. No change greater than 2% was observed in the ionisation current with this change of field.

Mr. J.W. Boag of the Medical Research Council has carried out certain calculations on this problem and checked these with measurements using the 4 MeV. linear accelerator, obtaining very good agreement between the two. The writer is indebted to him for the use of the information by which it has been calculated that with the geometry and field strength used in the carbon chamber the error due to lack of saturation does not exceed 5%. The particular geometry used in the carbon probe system does

not allow the best application of Boag's theory but this value is in fair agreement with the value of 2% observed above.

No effects of wave form have been observed. The ratio of probe to victoreen readings (a condenser dosemeter with high field strength in the chamber) remained constant to within a few percent whether the comparison was made on a constant potential X-ray plant, a pulsating potential X-ray plant or a generator of the betatron type emitting very short pulses.

It therefore seems that the absolute values of dosage rate are acceptable to an accuracy of say 10%, no evidence having been obtained that either of the effects suggested has appreciably influenced the results given above.

MEASUREMENT OF RADIOACTIVE ISOTOPES

It is obviously of interest to be able to correlate the dosage-rate at a given distance from a known quantity of a radioactive isotope and that due to a beam of radiation. It is significant that the steps required to achieve correlation are to calculate the energy absorption in ergs/gm. from the radioactive source and then to relate this to the energy absorbed when 1 rontgen is delivered to 1 gramme of air or water. This might well be, and has no

doubt been, used as an argument for the adoption of energy absorption in ergs/gm. as a unit of measurement of radiation.

The preliminary theory has been developed very clearly for beta and gamma-ray emitters by Mayneord[94] and for beta-ray emitters by Marinelli.[104] Mayneord has shown that the theory leads to a satisfactory correlation between the experimental and calculated values for the dosage-rate at 1 cm. from 1 mgm. of radium (8.3 r/hr. when filtered with 0.5 mm. platinum) and the theory provides similar constants for other radioactive sources of different energies.

Using some sources of radioactive Co 60 and I 131 an endeavour was made to measure their value and also through the means adopted for this evaluation to provide a check on the theory by which the evaluation was made. The measurements were made using the F.P.54 system along with the set of ionisation chambers described earlier. Some difficulty was experienced in getting the requisite sensitivity with the F.P.54 system, the use of a 10^{12} resistor in the circuit resulting in a very long time constant. A few early results were, however, made with this arrangement (Series III) until a more sensitive galvonometer made the use of a 10^{11} resistor practicable. (Series I and II). The sensitivity of the system was approximately 4×10^{-6} r/sec. per cm. division of the

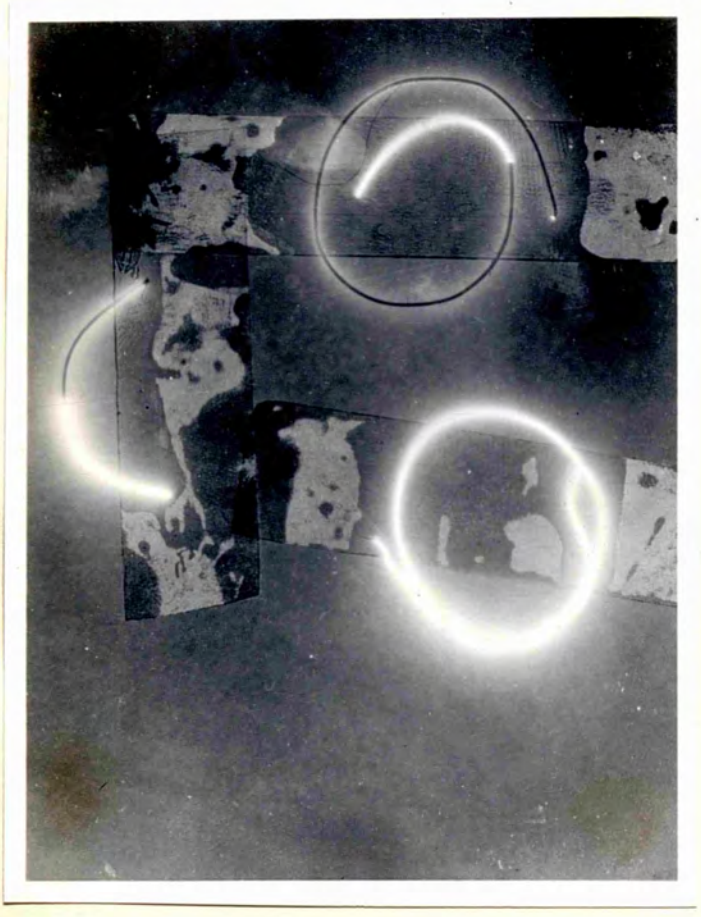

Fig. 63

galvonometer scale which, with the ionisation chamber volume used, corresponded to 8.4×10^{-15} amps. per cm. division of the scale. With some of the weaker sources the accuracy was, however, less than would be desired.

The sources available included a number of Co 60 sources comprising some granules enclosed in a thin celluloid tube, a 1" diameter cobalt 60 disc and a short length of cobalt wire which had been gold plated to absorb the 0.31 MeV. rays emitted in the disintegration. The range of these beta rays in gold is approximately 0.05 mm., so a comparatively thin coating of gold is an adequate filter. An autoradiograph of two lengths of the wire is shown in Fig. 63 along with that of a length of bare cobalt 60 wire. The beta radiation is clearly seen around the bare wire and also around the parts of the gold plated wire from which the plating had been stripped. In the case of the short length of wire no beta radiation can be seen to come from the end of the wire where it has been cut. No doubt the well known property of gold whereby it welds under pressure has resulted in a layer of gold plate at the end of the wire. This has, however, not happened in the case of the longer piece of wire and a "jet" of beta radiation can be detected coming out from the gold plated end of the wire. The effectiveness of the gold plating is clearly demonstrated. Other sources were a glass ampule containing a quantity of

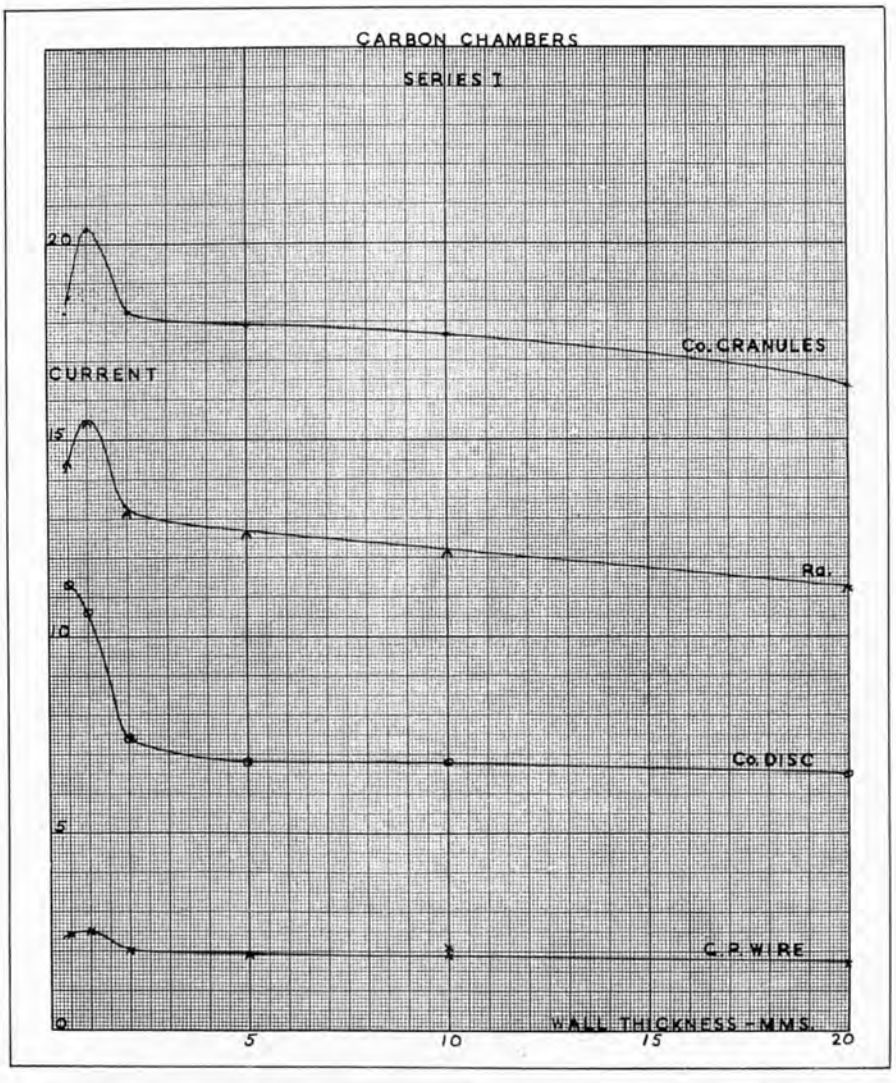
CARBON CHAMBERS
SERIES I
20
15
10
5
0
CURRENT
Co. GRANULES
Rd.
Co. DISC
C. P. WIRE
5
10
15
20
WALL THICKNESS - M.M.S.

Fig. 64

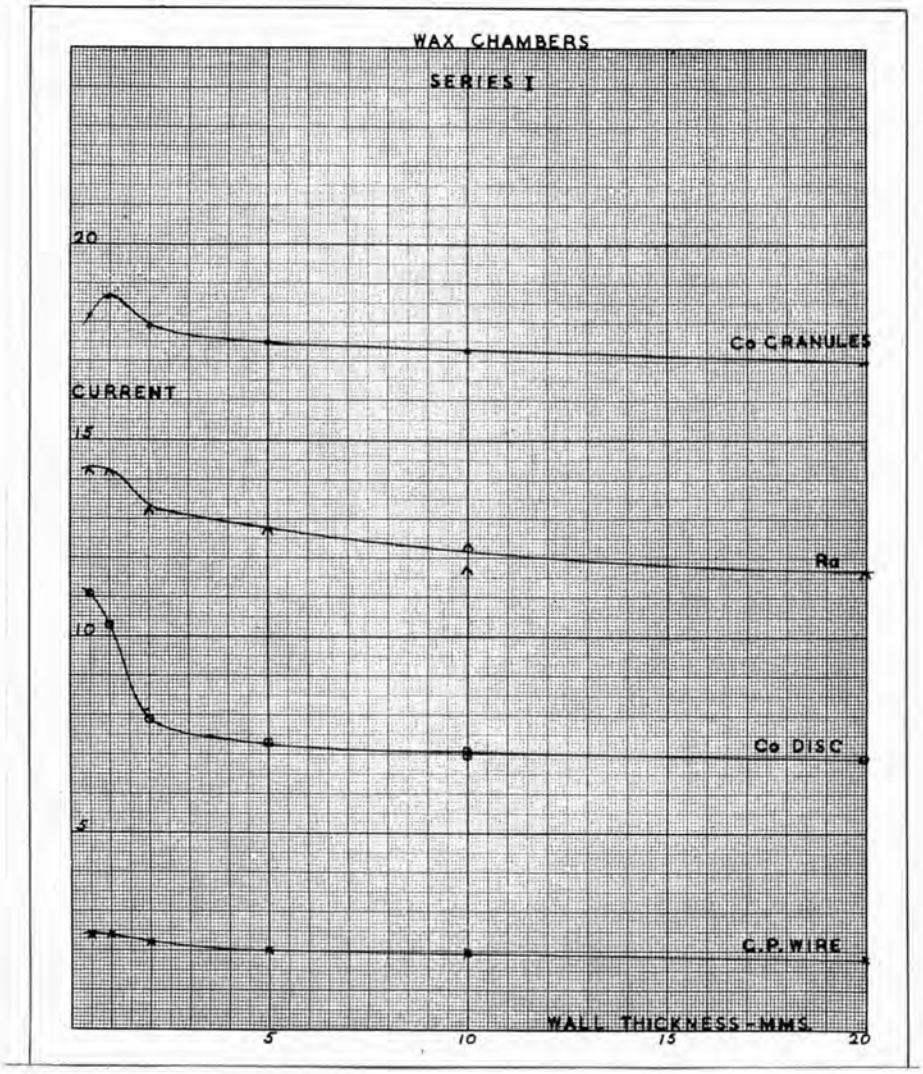
WAX CHAMBERS
SERIES I
20
CURRENT
15
10
5
Co GRANULES
Ra
Co DISC
C.P. WIRE
5
10
15
20
WALL THICKNESS - MMS.

Fig. 65

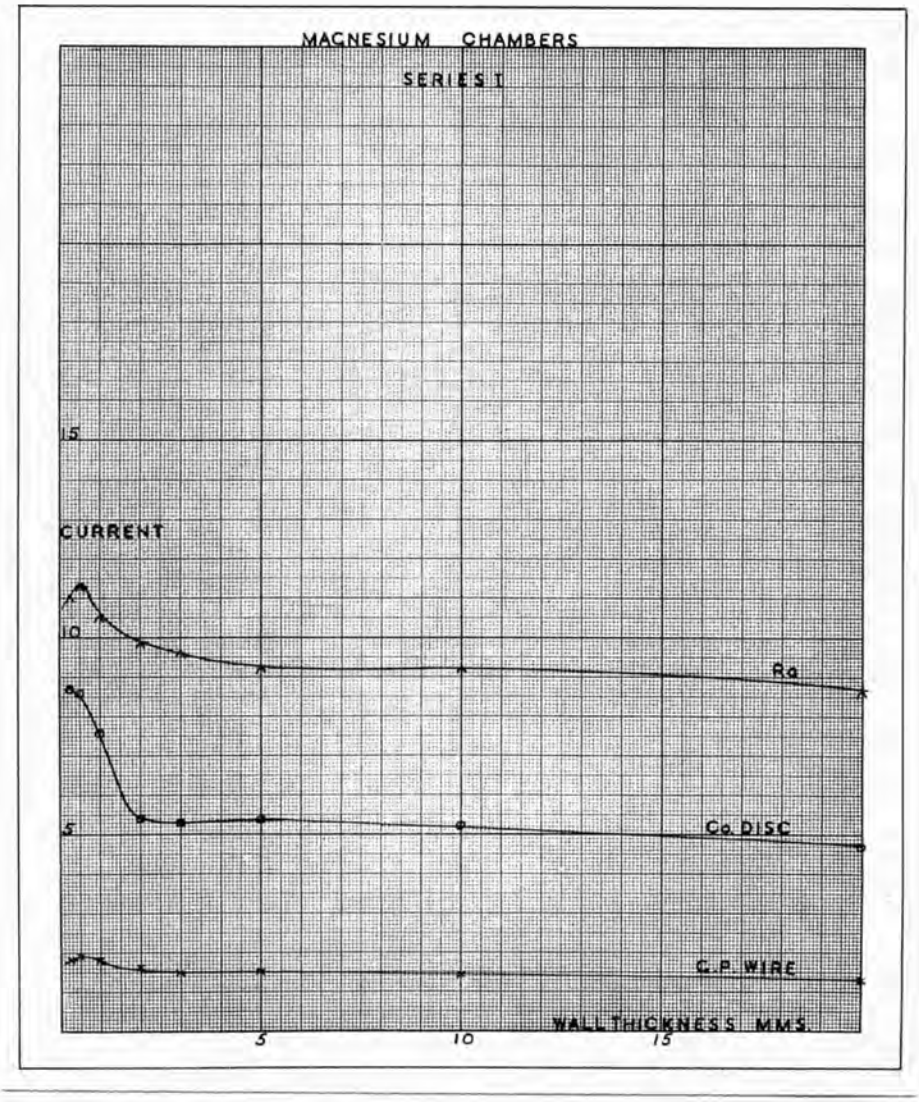
MAGNESIUM CHAMBERS
SERIES I
15
CURRENT
10
5
Ro
Co. DISC
C.P. WIRE
WALL THICKNESS MMS.
5
10
15

Fig. 66

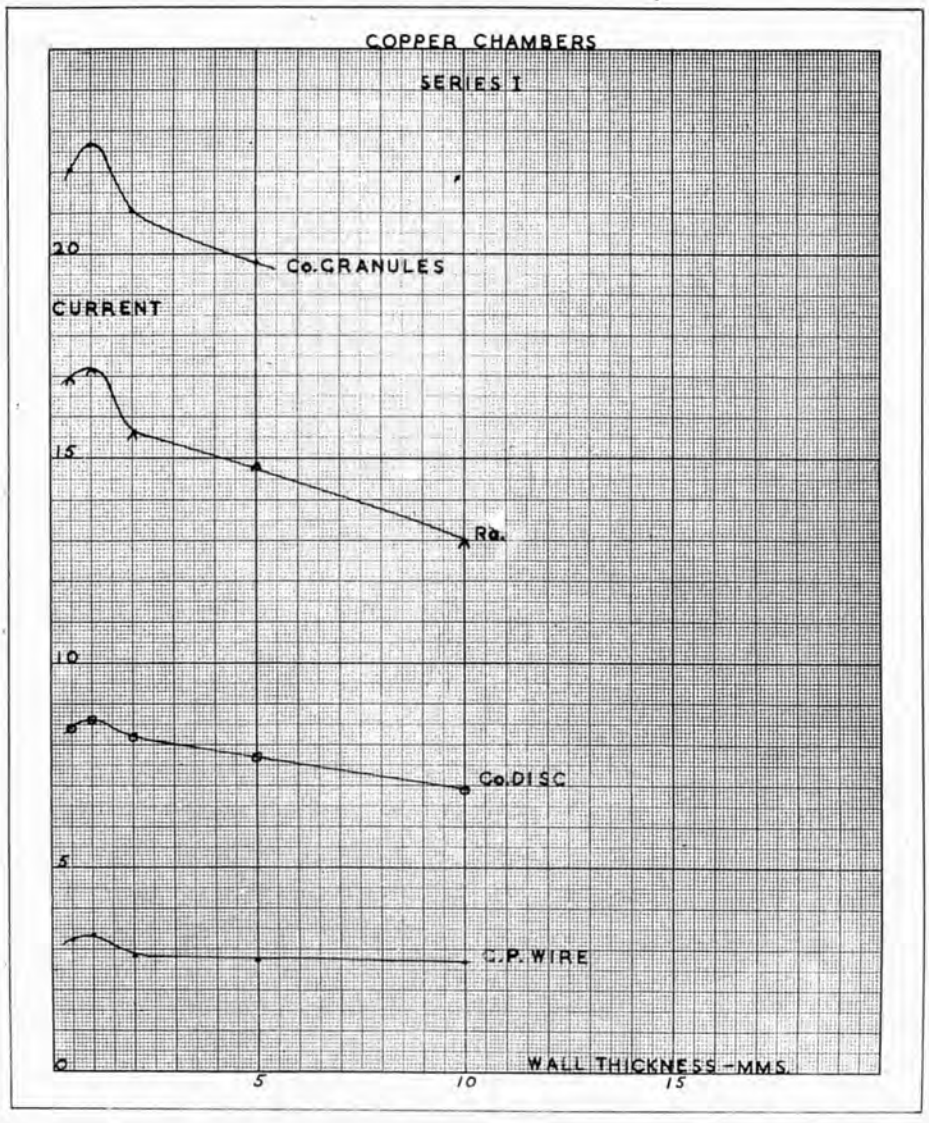
COPPER CHAMBERS
SERIES I
20
Co. GRANULES
CURRENT
15
Ra.
10
Co. DISC
5
C.P. WIRE
0
5
10
15
WALL THICKNESS - MMS.

Fig. 67

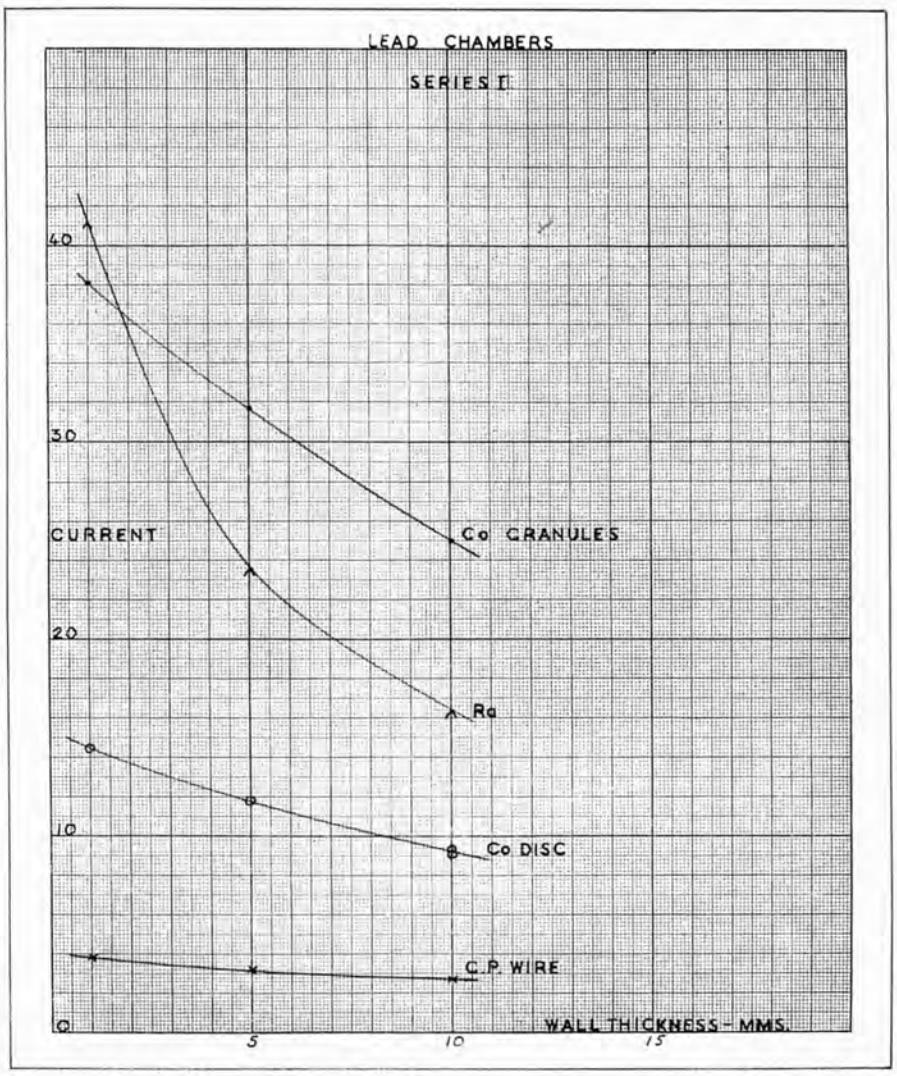
LEAD CHAMBERS
SERIES I
40
30
CURRENT
20
10
0
5
10
15
Co GRANULES
Ra
Co DISC
C.P. WIRE
WALL THICKNESS - MMS.

Fig. 68

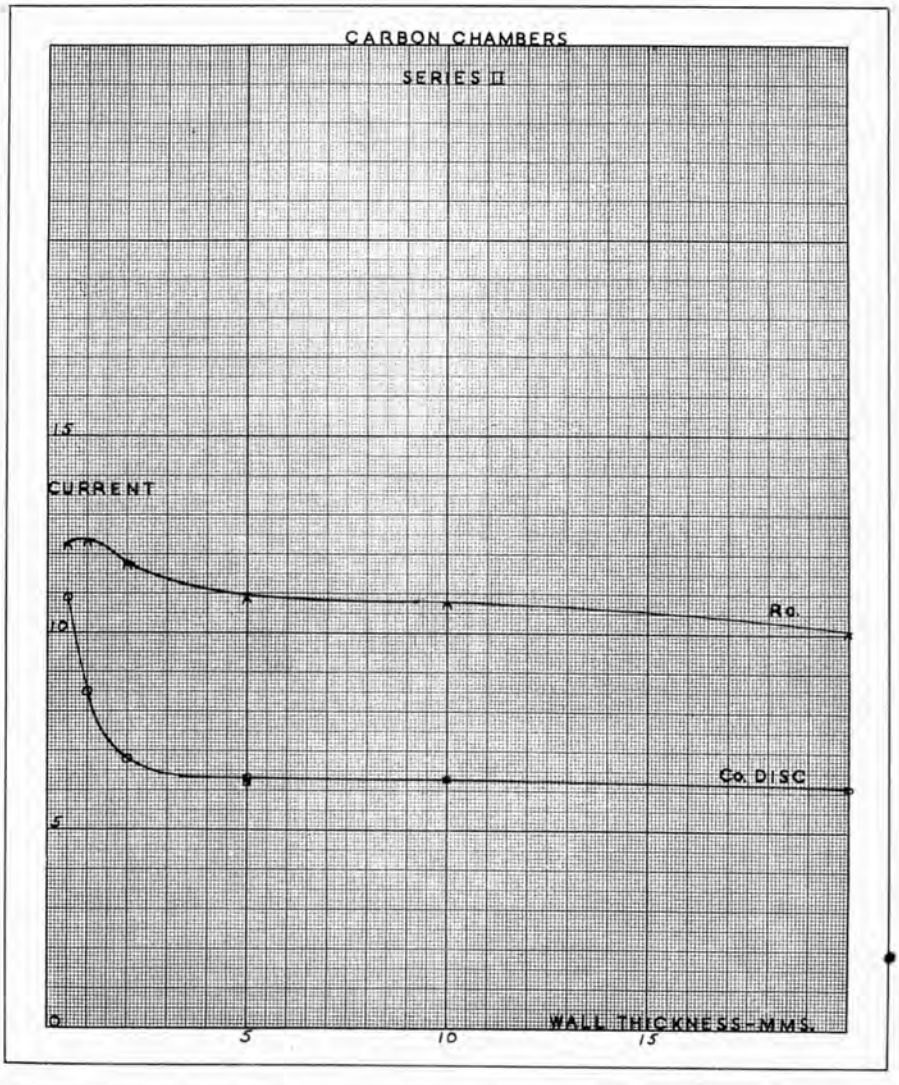
CARBON CHAMBERS
SERIES II
15
CURRENT
10
5
0
5
10
15
WALL THICKNESS-MMS.
Ro.
Co. DISC

Fig. 69

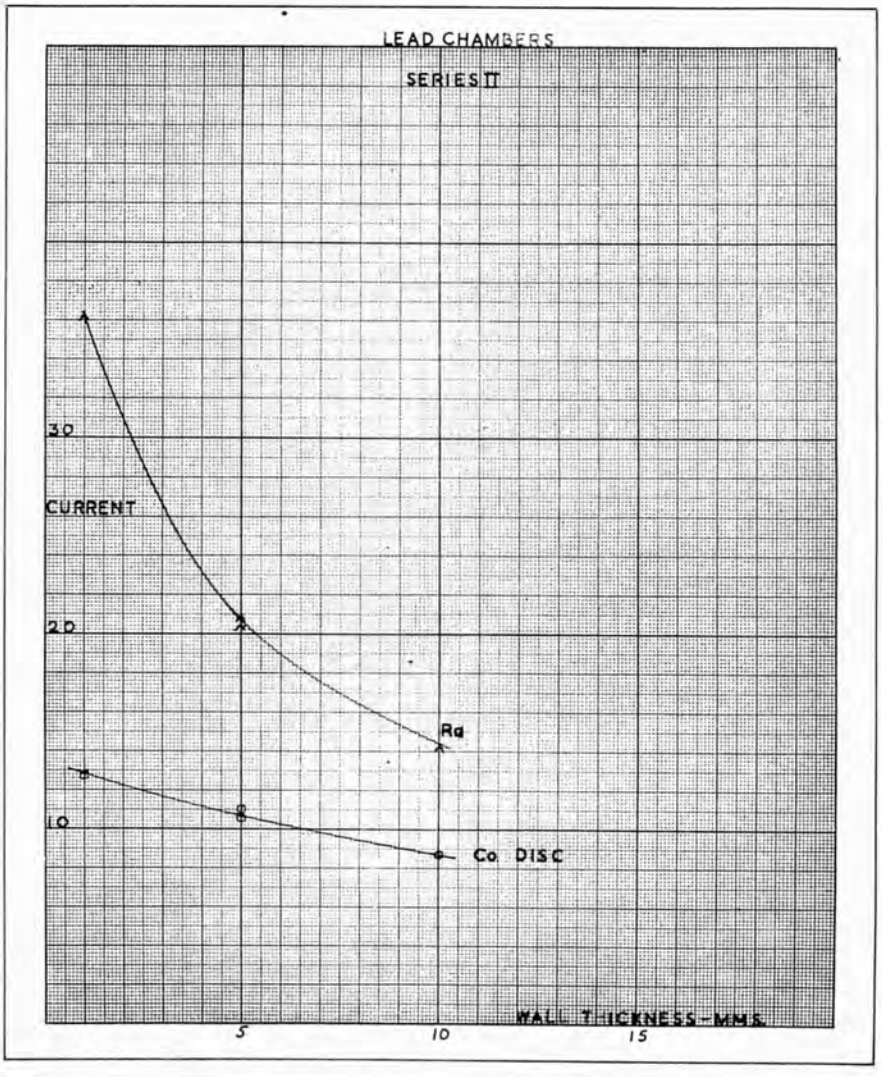
LEAD CHAMBERS
SERIES II
30
CURRENT
20
10
Ra
Co DISC
5
10
15
WALL THICKNESS - MMS.

Fig. 70

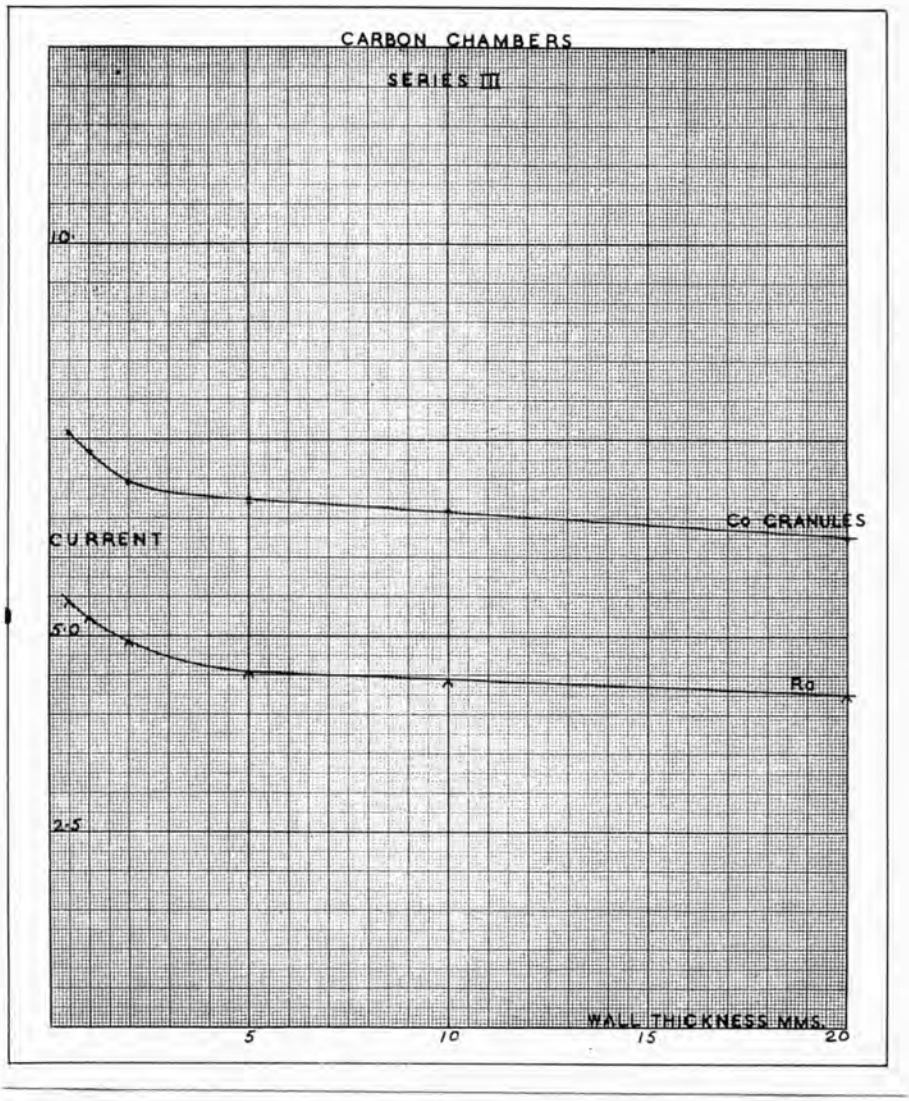
CARBON CHAMBERS
SERIES III
10·
5·0
2·5
CURRENT
Co GRANULES
Ro
5
10
15
20
WALL THICKNESS MMS.

Fig. 71

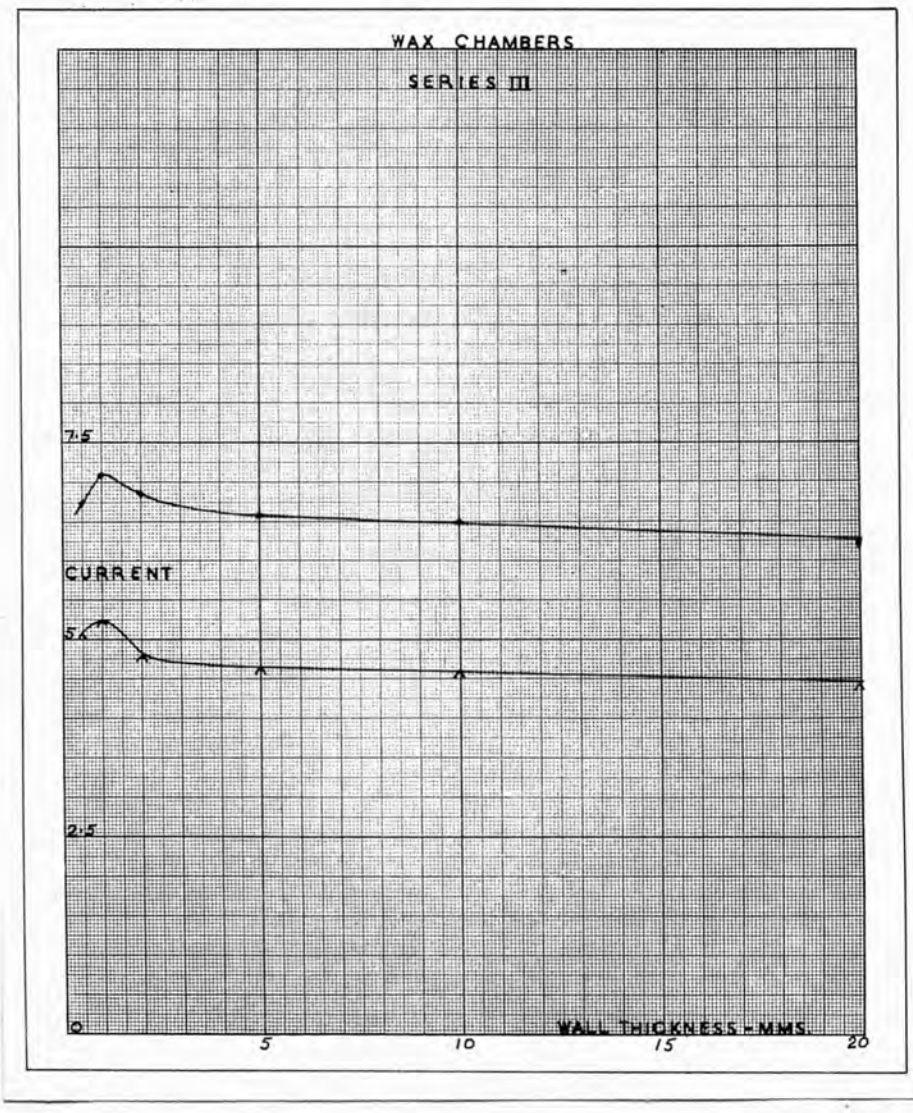
WAX CHAMBERS
SERIES III
7·5
CURRENT
5
2·5
0
5
10
15
20
WALL THICKNESS - MMS.

Fig. 72

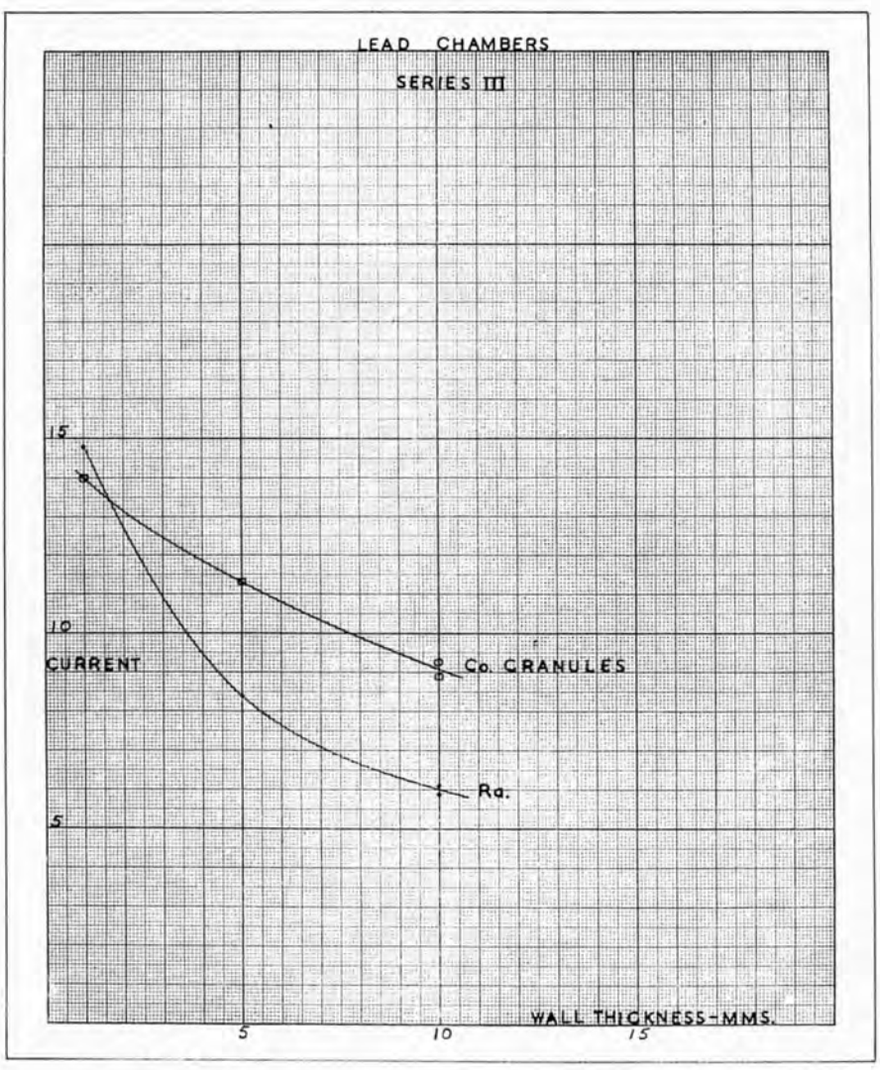
LEAD CHAMBERS
SERIES III
15
10
CURRENT
Co. GRANULES
Ra.
5
5
10
15
WALL THICKNESS-MMS.

Fig. 73

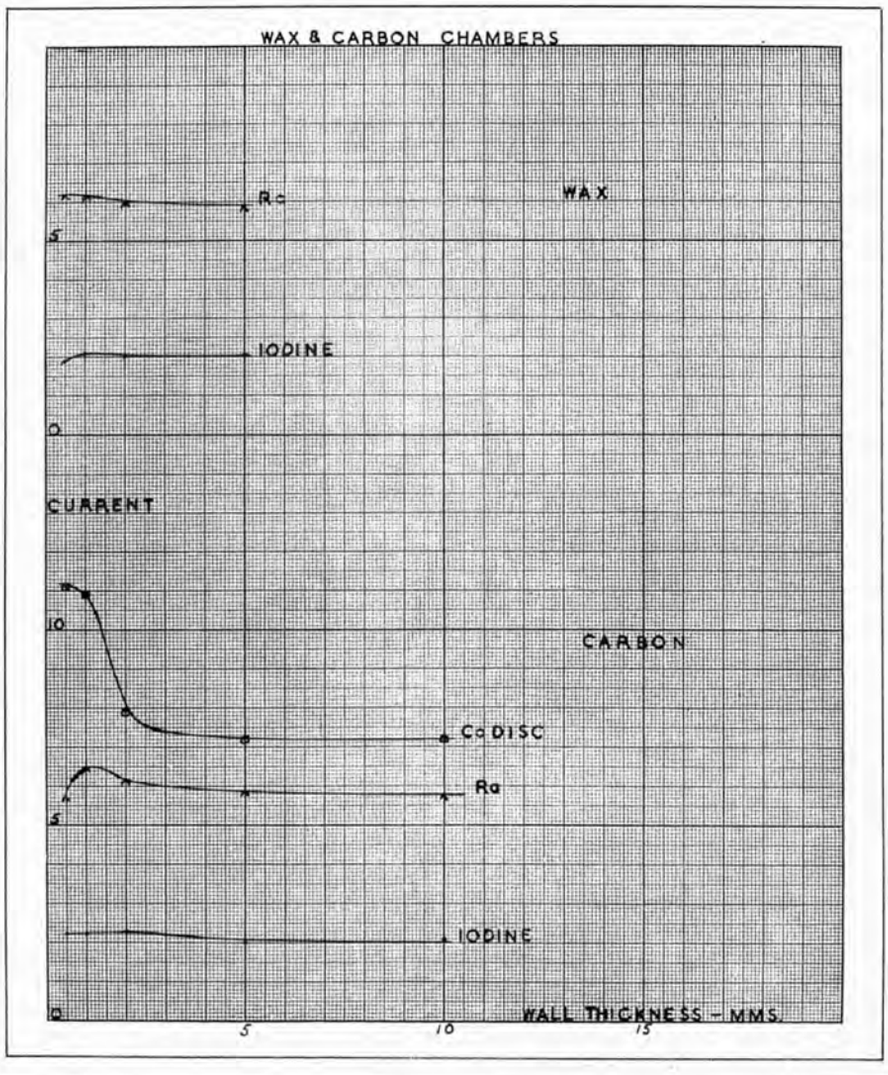
WAX & CARBON CHAMBERS
WAX
Ra
IODINE
CURRENT
CARBON
Co DISC
Ra
IODINE
WALL THICKNESS - MMS.
5
10
15

Fig. 74

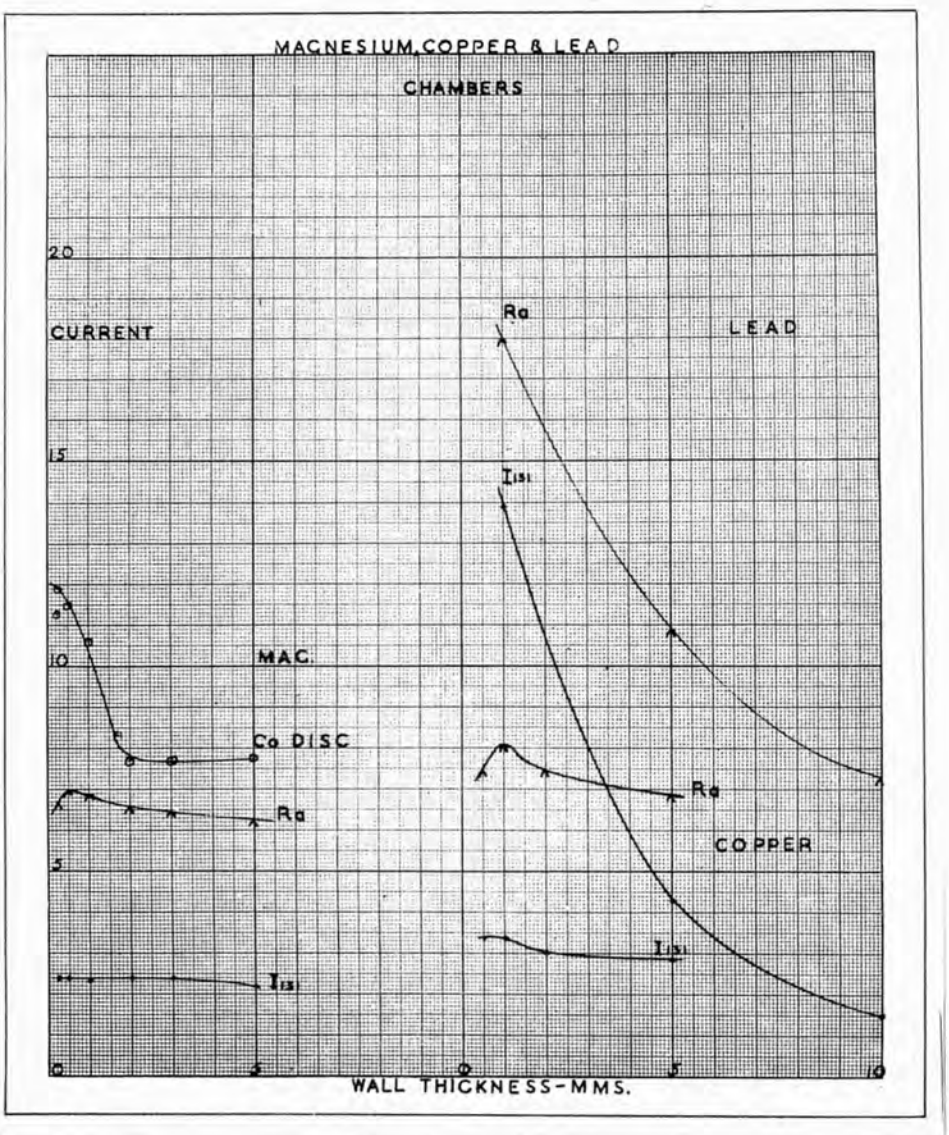
MAGNESIUM, COPPER & LEAD
CHAMBERS
CURRENT
20
15
10
5
0
MAC.
Co DISC
Ra
I131
LEAD
Ra
I131
Ra
COPPER
I131
0
5
10
WALL THICKNESS-MMS.

Fig. 75

I 131 in a sodium iodide solution and two radium needles of 2.11 mgm. and 0.5 mgm. value kept in the Physics Department of the Hospital as standards.

The comparisons were effected by measuring the ionisation currents in ionisation chambers of different wall thickness and different materials with the sources placed one at a time at a distance of 11.0 cms. from the measuring volume. This distance was chosen as a compromise between that required to obtain a deflection of sufficient magnitude to ensure accuracy and that to give uniform primary radiation throughout the irradiated material as well as to ensure that each source could be regarded as nearly a point source. The error involved in the latter was negligible. The largest linear dimensions of any of the sources was 2.5 cms. and the error involved in regarding this as a point source is therefore less than 1%. For the iodine measurements a distance of 8 cms. had to be used but the error involved is still small enough to be neglected. The curves obtained from these measurements are shown in Figs. 64 to 75. The rather odd maxima shown are thought to be due to the electronic build-up for the gamma rays on which is superimposed the effect of the beta rays emitted from the sources. This latter effect would explain the sharp drop of the curve occurring at a thickness equal to the range of the electrons. The 0.3 MeV. electrons from

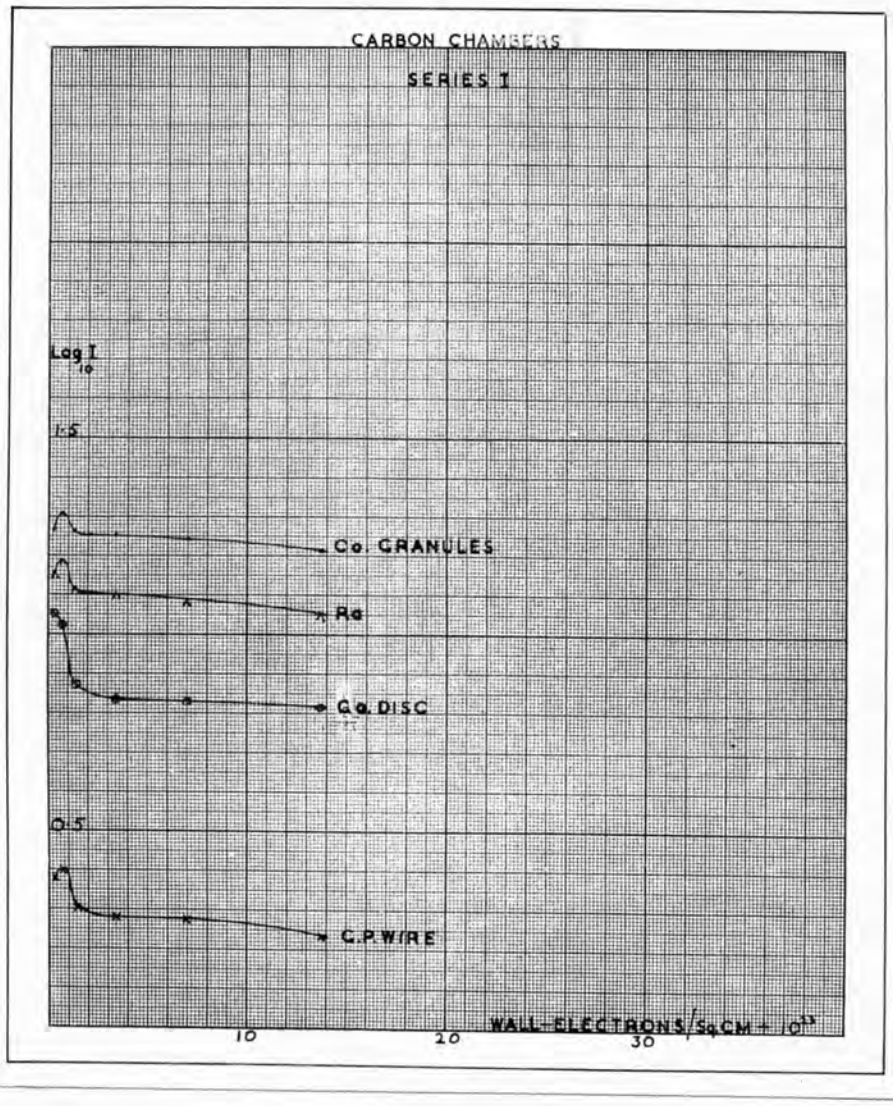
CARBON CHAMBERS
SERIES I
Log I10
1·5
Co GRANULES
Ra
Co DISC
0·5
C.P.WIRE
10
20
30
WALL-ELECTRONS / Sq CM × 10¹³

Fig. 76

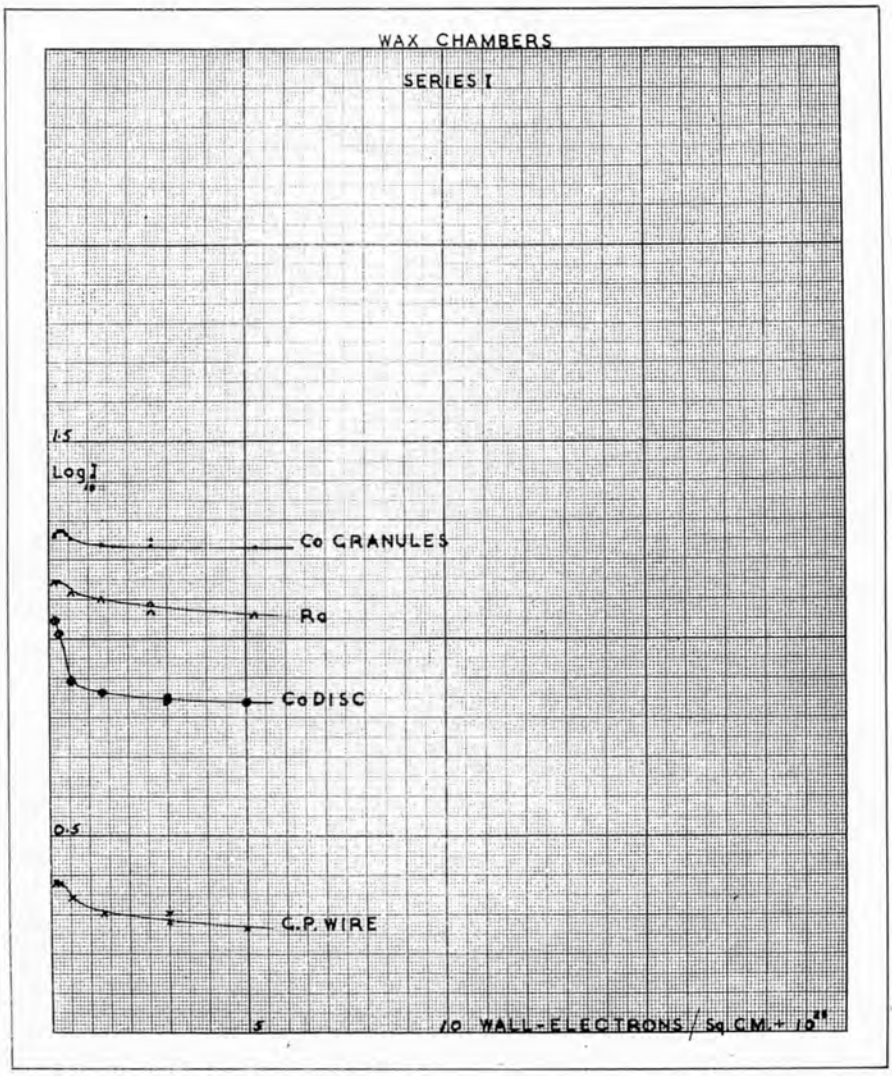
WAX CHAMBERS
SERIES I
1·5
Log I/I₀
Co GRANULES
Ra
Co DISC
0·5
C.P. WIRE
5
10 WALL-ELECTRONS / Sq CM. ÷ 10²²

Fig. 77

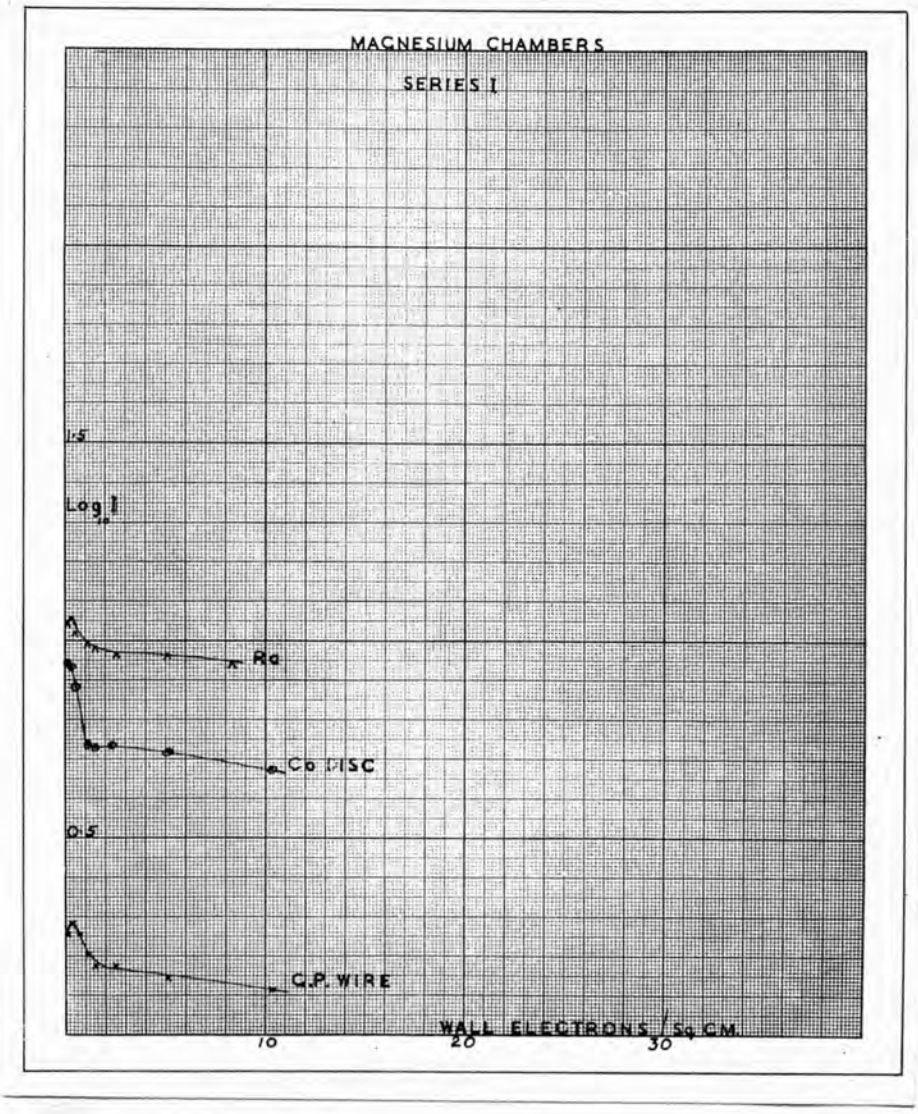
MAGNESIUM CHAMBERS
SERIES I
1·5
Log I
Rd
Co DISC
0·5
C.P. WIRE
WALL ELECTRONS / Sq. CM.
10
20
30

Fig. 78

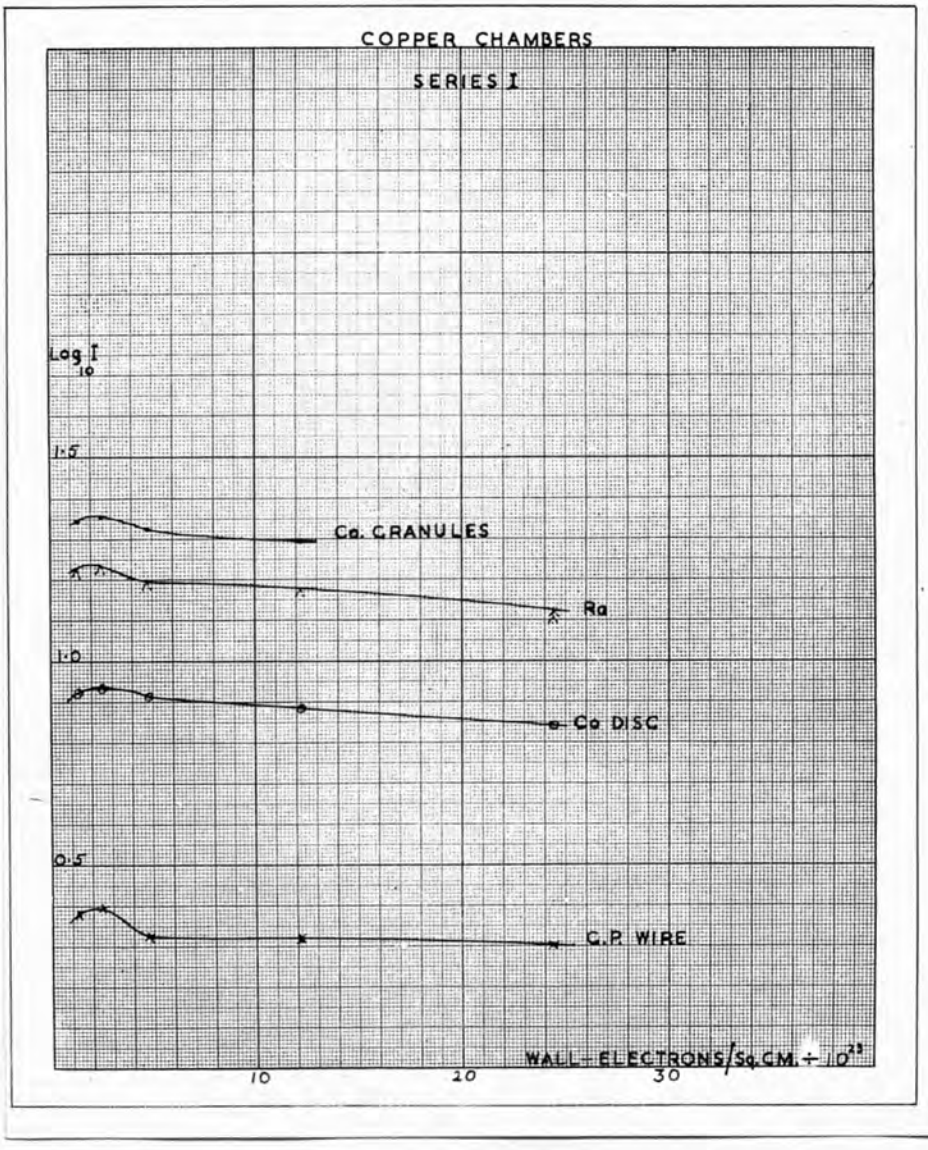
COPPER CHAMBERS
SERIES I
Log I
10
1·5
Co. GRANULES
Ra
1·0
Co DISC
0·5
C.P. WIRE
WALL - ELECTRONS/Sq.CM. ÷ 10²³
10
20
30

Fig. 79

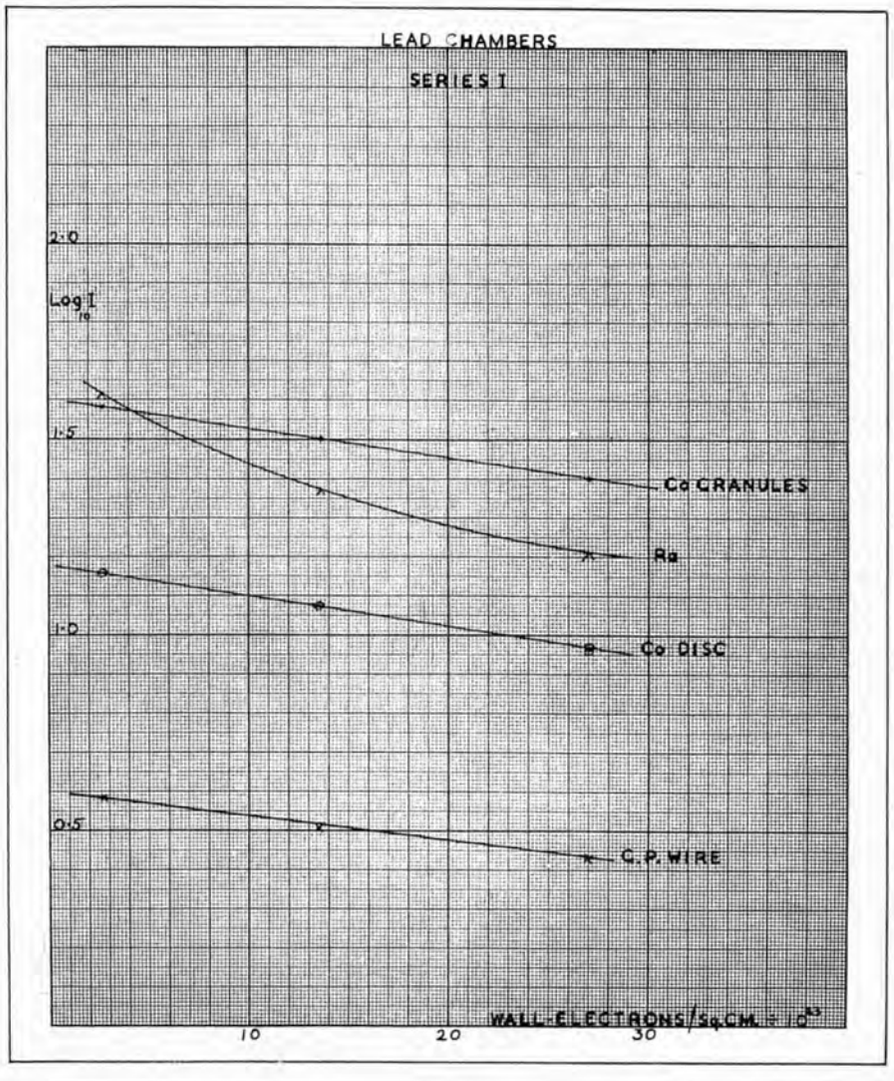
LEAD CHAMBERS
SERIES I
2·0
Log I
1·5
1·0
0·5
Co GRANULES
Ra
Co DISC
C.P. WIRE
10
20
30
WALL-ELECTRONS/sq.CM. = 10^23

Fig. 80

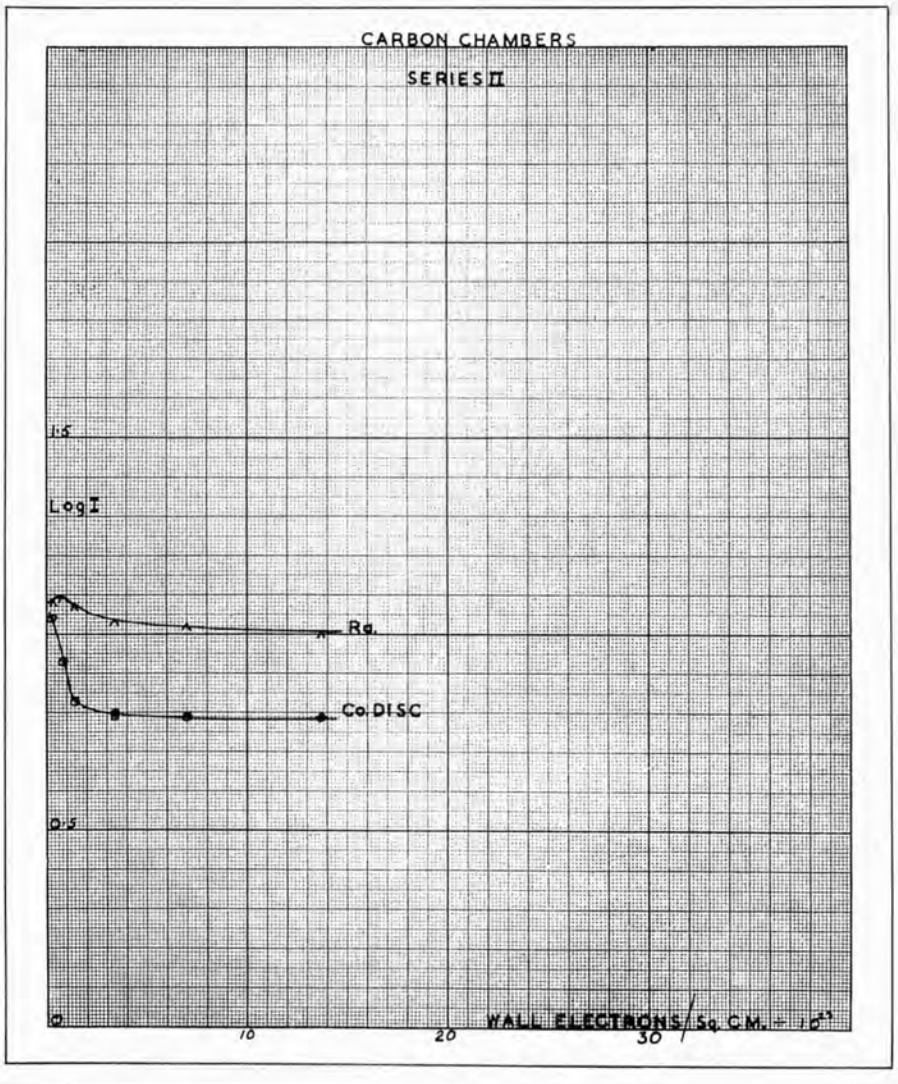
CARBON CHAMBERS
SERIES II
1·5
Log I
Ra.
Co. DISC
0·5
0
10
20
30
WALL ELECTRONS / Sq. C.M. = 10

Fig. 81

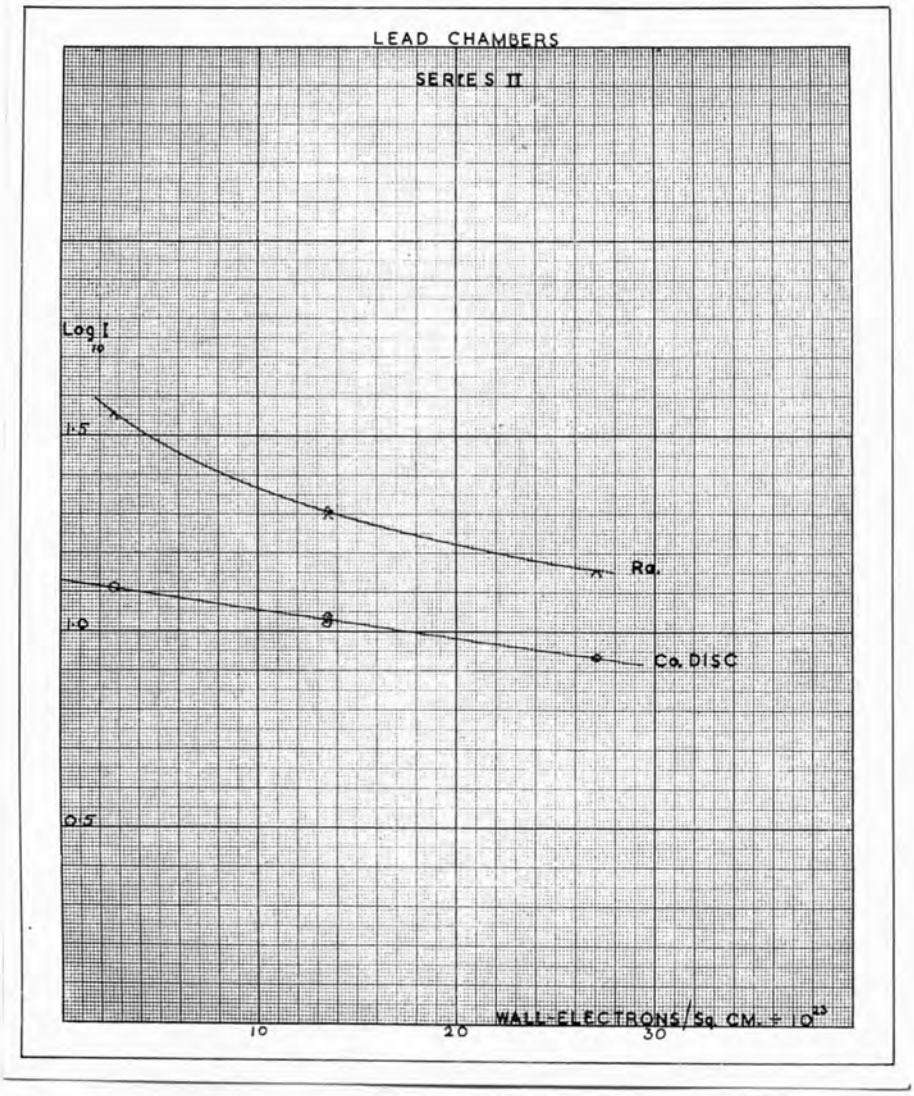
LEAD CHAMBERS
SERIES II
Log I
10
1·5
1·0
0·5
Ra.
Co. DISC
10
20
30
WALL-ELECTRONS/Sq CM. = 10^23

Fig. 82

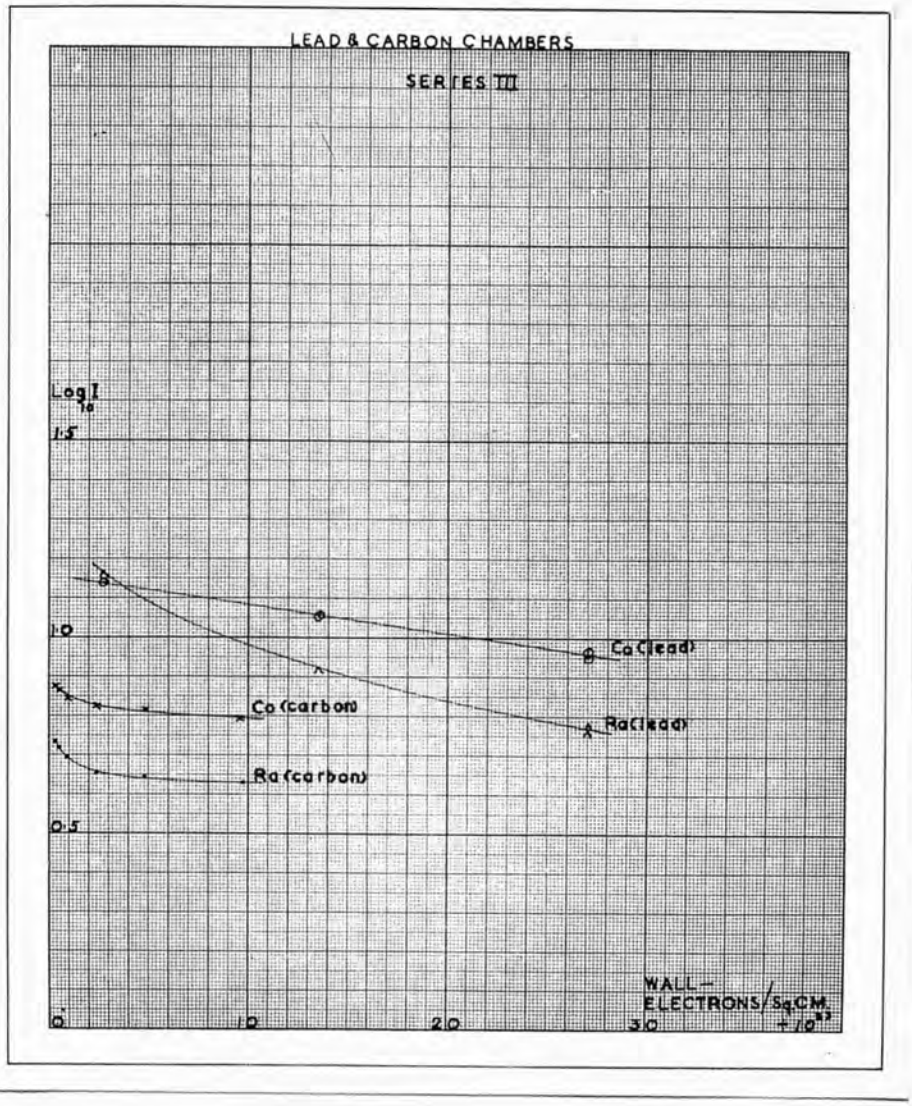
LEAD & CARBON CHAMBERS
SERIES III
Log I
10
1·5
1·0
0·5
0
10
20
30
WALL-
ELECTRONS/SqCM.
Co(lead)
Co(carbon)
Ra(lead)
Ra(carbon)

Fig. 83

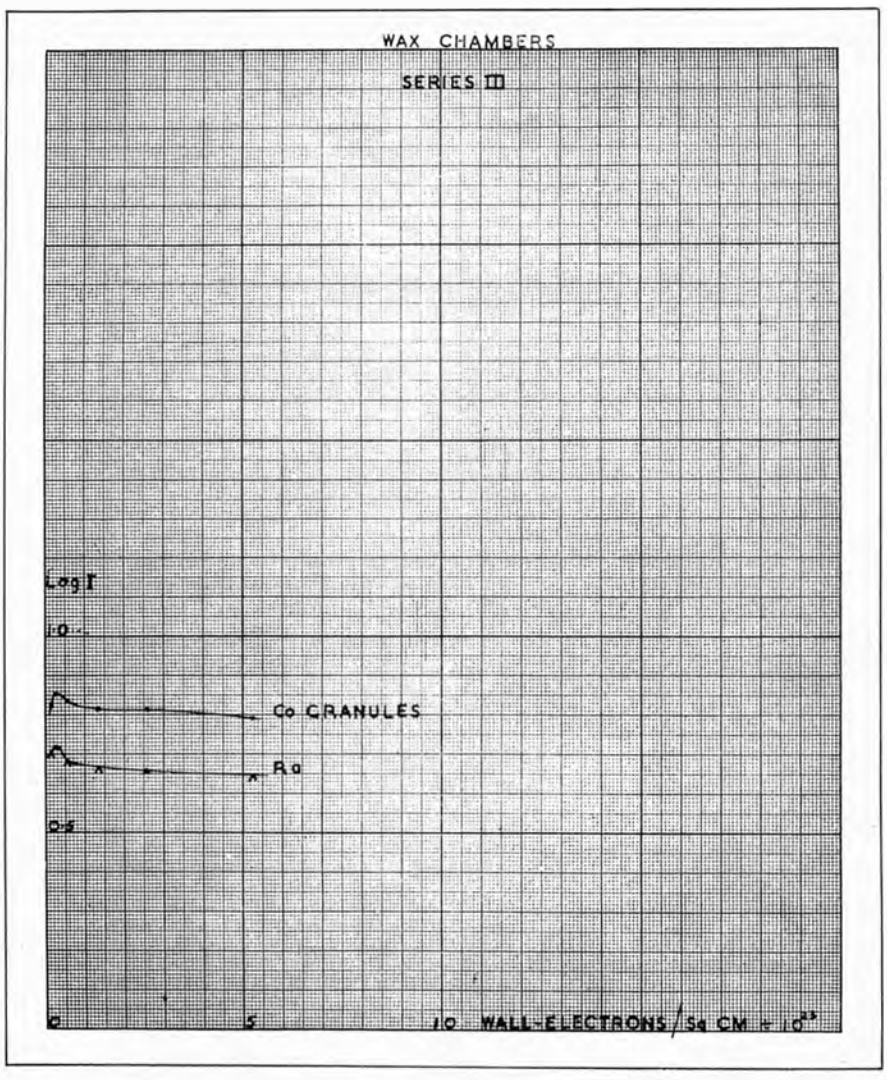
WAX CHAMBERS
SERIES III
Log I
10
Co GRANULES
Ra
0·5
0
5
10 WALL-ELECTRONS / Sq CM ÷ 10²³

Fig. 84

Co 60 have a range of approximately 1 mm. in a light material such as carbon. The subsequent fall of the current measured as the wall thickness is increased is due to absorption of the primary radiation.

To interpret the results the measurements were plotted as in Figs. 76 to 84, showing $\log_{10}$ (ionisation current) against wall thickness in electrons per sq. cm. The value of the ionisation current in conditions appropriate to measurement in rontgens was obtained by the method adopted by Mayneord and Roberts,[86] the curve being extrapolated back to zero wall thickness thereby correcting for absorption in the walls of the chamber and at the same time satisfying the condition that electronic equilibrium should be built up. The very small difference between this correction and the true one described earlier is neglected.

Unfortunately the value of the high resistor was not known to any accuracy and the absolute values of these currents could not be obtained.

The values of the isotope sources could be obtained as follows. The rontgen as explained earlier is essentially a unit of energy absorption in a given mass of air. For our purpose it is important to determine the energy flux, in beams of quanta of various energies, required to record one rontgen. The theory has been discussed by Mayneord.[94] The fraction of the incident energy converted

into energy of electronic motion may be written

$$(\tau + \sigma_a + \pi)\, N.\, dm$$

where τ, σ_a and π are the usual real absorption coefficients expressed per atom and N dm is the number of atoms in the mass dm.

If E_F is the energy flux of the radiation per $cm.^2$ per rontgen we have in air

$$E_F\,(\tau + \sigma_a + \pi) \;=\; 84 \text{ ergs.}$$

Mayneord has calculated the values of E_F over a range of energies and finds the energy flux is roughly constant at 3000 ergs/sq.cm./r from 0.1 to 1.0 MeV., thereafter rising slowly to about twice the value at 10 MeV.

If we now consider a point source of 1 curie strength of any gamma-ray emitting substance, emitting for simplicity one quantum of energy E MeV. per disintegration the intensity of the radiation at 1 cm. from the point source will be

$$I \;=\; \frac{1}{4\pi}\,(3.7 \times 10^{10} \times 3600 \times E_{MeV.} \times 1.59 \times 10^{-6})$$

$$=\; 1.685 \times 10^{7}\, E_{MeV.} \quad \text{ergs/sq.cm./hr.}$$

where the number 3.7×10^{10} represents the number of disintegrations per second from a source of 1 curie strength. From the previous calculations we obtain the dosage-rate in r/mc.hr.:-

$$D \;=\; 1.685 \times 10^{4}\, \frac{E_{MeV.}}{E_F}$$

From Mayneord's calculations a value of 13.55 r/hr. from a point source of 1 mc. of Co 60 at 1 cm. is obtained.

Using this value and the known value for the dosage-rate at 1 cm. from 1 mgm. of radium filtered by 0.5 mm. Pt, we have:-

Value of Co 60 source in mc. $= \frac{J_{Co}}{J_{Ra}} \times \frac{8.3}{13.55} \times$ (mgm. of Ra)

where J = current measured.

$\therefore$ Value of granule source $= \frac{18.2}{13.34} \times \frac{8.3}{13.55} \times 2.11 =$ 1.76 mc.

Similarly the value of the disc source (No. 11) = 0.68 mc.

and the value of the gold plated wire source = 0.19 mc.

In order, however, to verify the validity of these calculations the following method was used.

Gray's equation for the ionisation current per unit volume in an ionisation chamber gives:-

$$E_v = 1.35 \times 10^{-31} \, n \, f(Z) \, J_v \text{ ergs/cc.}$$

where as before E_v = energy absorbed per unit volume.

n = electronic density of medium in which measurement is made.

f(Z) = slowly varying function of Z depending on the relative stopping powers of the medium and air.

It is possible, knowing the appropriate absorption coefficients, to calculate E_v for any given material and it should therefore be possible to show that the different ratios of ionisation current for say a cobalt source and radium source obtained in chambers of different materials do, in fact, represent the same relative activities.

$$E_{Co} \propto n\, f(Z)\, J_{Co}$$

$$E_{Ra} \propto n\, f(Z)\, J_{Ra}$$

For a chamber of the same material we, therefore, have:-

$$\frac{E_{Co}}{E_{Ra}} = \frac{J_{Co}}{J_{Ra}}$$

But the rate of energy absorption is given by

$$E = 1.685 \times E_{MeV.} \times 10^7 (\tau + \sigma_a + \pi) \text{ X ergs/cc./hr.}$$

where X = strength of source.

$$\therefore \frac{J_{Co}}{J_{Ra}} = \frac{1.685 \times E_{MeV.\,Co} \; (\tau_{Co} + \sigma_{a\,Co} + \pi_{Co}) \times (\text{mc. of Co})}{1.685 \times E_{MeV.\,Ra} \; (\tau_{Ra} + \sigma_{a\,Ra} + \pi_{Ra}) \times (\text{mgm. of Ra})}$$

$\therefore$ Strength of cobalt source in mc.

$$= \frac{J_{Co}}{J_{Ra}} \; \frac{E_{Ra} \; (\tau_{Ra} + \sigma_{a\,Ra} + \pi_{Ra}) \times (\text{mgm. of Ra})}{E_{Co} \; (\tau_{Co} + \sigma_{a\,Co} + \pi_{Co})} \quad \ldots (1)$$

The values of the real energy absorption coefficients for cobalt, a source of almost monochromatic radiations, are easily and accurately calculated as before from the Klein-

Nishina values for σ_a, Fowler-Hulme values for τ and the Heitler-Bethe values for π. The values for radium and iodine are, however, much more difficult to calculate owing to the width of the energy spectrum in their disintegration scheme. To obtain the appropriate value of the real energy absorption for each material, the absorption coefficient appropriate to each spectral line was calculated and the overall value obtained by weighting the individual values in relation to the intensity of each particular line. The spectral distribution used for radium is that of Ellis and Aston[105] and the one for iodine that of Deutsch and Mitzger.[106] Allowance has been made for the filtration of 0.5 mm. Pt in the case of the radium source and 1 mm. glass in the case of iodine source.

The values for paraffin wax have been calculated using an "effective" atomic number calculated from its proportional composition.

The results of calculations of the values of the various sources based on the theory above and those values thus obtained of the energy absorption coefficients are shown on Tables V and VI. It will be seen that on this basis there is fair agreement between the comparison (in chambers of different materials) of radium and cobalt, radium and iodine, and cobalt and iodine sources. The comparisons in lead chambers are somewhat uncertain owing

to the difficulty in estimating the true current due to the radium and iodine sources, the quality of the radiation, from these sources, changing rapidly with the thickness of the chamber wall.

It will be seen, however, that the measurement of the activity of radioactive materials by comparison with a standard source when the two sources differ in the energy of their gamma-ray emission may be satisfactorily carried out by an ionisation current comparison in an air wall chamber of suitable design.

Disagreement still exists between the absolute values obtained as above and shown in Tables V and VI and the values obtained using the "k" factor of Mayneord. This is certainly due to differences in the value of the absorption coefficients adopted. Since the divergences are all in the same direction and of the same order the disagreement undoubtedly arises from the values of the coefficients calculated for radium.

The ionisation current ratios for chambers of different materials have been used in the calculation, earlier, of relative stopping powers and are found to agree well with the values obtained by Bethe and Gray. In consequence the above measurements can be regarded as a demonstration of the validity of Gray's equation

$$E_v = 1.35 \times 10^{-31} \, n \, f(Z) \, J_v \text{ ergs/cc.}$$

As will be seen from Table VII there is agreement between the values in the column showing the relative energy absorbed as calculated from the real energy absorption coefficients and these in the column showing the relative energy absorbed as calculated from Gray's equation.

From the slope of the curve of log ionisation current against wall thickness the value of the real energy absorption coefficient may be obtained. It is unfortunate that the extended series of chambers giving large wall thicknesses was not available during these experiments since the small number of points (often only two) after the maximum of a curve makes the measurement of the slope of low accuracy. The values obtained have, however, been given in Table VII and these will be seen to be of the right order but tend to be higher than the theoretical values computed as described above. As already stated, the number of points available to determine the slopes of the curves was small and it is, further, possible that some scattered radiation is being recorded. The distances from possible scattering objects were as large as possible but no collimating system was available for the various sources.

TABLE V.

Source	Chamber Material	J	x mc.	
Radium 2 mgm. standard needle = 2.11 mgm.	Carbon	13.34	-	
	Wax	12.70	-	
	Magnesium	13.50	-	
	Copper	16.22	-	
	Lead	55.00	-	
Cobalt 60 granules	Carbon	18.20	2.16	
	Wax	17.50	2.16	
	Magnesium	-	-	
	Copper	21.88	2.32	
	Lead	39.80	2.59	Series I
Cobalt 60 disc No. 11	Carbon	6.99	0.84	
	Wax	7.32	0.88	
	Magnesium	8.18	0.97	
	Copper	8.61	0.91	
	Lead	15.24	0.96	
Gold plated Co 60 wire	Carbon	1.95	0.23	
	Wax	2.00	0.24	
	Magnesium	2.22	0.26	
	Copper	2.16	0.23	
	Lead	4.07	0.25	
Radium 2 mgm. needle	Carbon	11.05	-	
	Lead	46.80	-	Series II
Cobalt 60 disc No. 11	Carbon	6.30	0.90	
	Lead	13.50	1.00	
Radium 2 mgm. needle	Carbon	4.60	-	
	Lead	19.95	-	Series III
Cobalt 60 granules	Carbon	6.85	2.36	
	Lead	14.45	2.51	

TABLE VI

Source	Chamber Material	J	x mc.	
Radium 0.5 mgm. standard needle	Carbon	6.03	-	
	Wax	6.09	-	
	Magnesium	6.87	-	
	Copper	7.94	-	
	Lead	28.20	-	
I 131 source	Carbon	2.27	1.63x0.5	Iodine-Radium Comparison
	Wax	2.09	-	
	Magnesium	2.40	1.62x0.5	
	Copper	3.46	1.66x0.5	
	Lead	32.30	1.77x0.5	
Co60 disc No.5 = y mc.	Carbon	7.16	0.89x0.5	Cobalt-Radium Comparison
	Magnesium	7.83	0.87x0.5	
	Carbon		1.89 x y	Iodine-Cobalt Comparison
	Magnesium		1.82 x y	

By "k" factor:

$$x_I = \frac{2.27}{6.03} \times \frac{8.3}{2.1} \times 0.5 = 1.49 \times 0.5 \text{ mc.}$$

$$x_{Co} = \frac{7.16}{6.03} \times \frac{8.3}{13.55} \times 0.5 = 0.73 \times 0.5 \text{ mc.}$$

$$x_I = \frac{2.27}{7.16} \times \frac{13.55}{2.1} \times y = 2.04 \times y$$

where y = strength of cobalt source

TABLE VII

Source	Chamber Material	J	Stopping power ρ from Fig.52	Real absorption coefficient $u_e \times 10^{25}$	Ratio $\frac{J}{J}_{carbon}$	Ratio $\frac{\mu_e}{\mu_e}_{carbon}$	$\frac{E}{E}_{carbon} = \frac{\rho J}{1.02J}$	Slope of curve per electron
Cobalt	Carbon	18.20	1.02	0.907	1.00	1.00	-	0.922
	Wax	17.50	1.04	0.906	0.96	0.997	0.98	-
granules	Copper	21.90	0.85	0.923	1.20	1.02	1.00	0.935
	Lead	39.80	0.75	1.491	2.19	1.65	1.61	1.730
	Carbon	6.99	1.02	0.907	1.00	1.00	-	0.610
Cobalt	Magnesium	8.18	0.94	0.907	1.17	1.00	1.08	1.340
disc	Wax	7.16	1.04	0.906	1.02	0.997	1.04	-
No. 11	Copper	8.61	0.85	0.923	1.23	1.02	1.02	0.905
	Lead	15.24	0.75	1.491	2.18	1.65	1.60	1.880
	Carbon	1.95	1.02	0.907	1.00	1.00	-	1.020
G.P.	Magnesium	2.22	0.94	0.907	1.14	1.00	1.05	1.150
	Wax	1.99	1.04	0.906	1.02	0.997	1.04	-
Co wire	Copper	2.16	0.85	0.923	1.16	1.02	0.97	-
	Lead	4.07	0.75	1.491	2.08	1.65	1.53	1.440
	Carbon	13.34	-	0.880	1.00	1.00	-	0.880
Radium	Magnesium	13.50	-	0.870	1.01	1.01	0.93	0.750
2 mgm.	Wax	12.70	-	0.890	0.95	0.99	0.97	-
needle	Copper	16.22	-	0.971	1.32	1.10	1.10	0.920
	Lead	55.00	-	3.160	4.14	3.60	-	-
Cobalt	Carbon	6.30	-	0.907	-	1.00	-	-
disc No.11	Lead	13.50	-	1.491	2.15	1.65	1.58	1.69
Radium	Carbon	11.05	-	0.880	-	-	-	-
2mgm.needle	Lead	46.80	-	3.160	4.24	3.60	3.10	-
Cobalt	Carbon	6.85	-	0.907	-	-	-	-
granules	Wax	6.70	-	0.906	0.98	0.997	1.00	-
	Lead	14.45	-	1.491	2.11	1.650	1.55	1.76
Radium	Carbon	4.60	-	0.880	-	-	-	-
2 mgm.	Wax	4.70	-	0.870	1.02	0.990	1.04	-
needle	Lead	19.95	-	3.160	4.34	3.600	3.20	-
	Carbon	2.27	-	0.968	1.01	1.000	-	-
I 131	Magnesium	2.40	-	1.000	1.06	1.010	0.98	-
	Wax	2.09	-	0.960	0.92	0.992	0.94	-
ampoule	Copper	3.46	-	1.285	1.39	1.260	1.160	-
	Lead	32.30	-	11.950	14.20	12.800	10.500	-
Co 60	Carbon	7.16	-	0.907	1.00	1.000	-	-
disc No.5	Magnesium	7.83	-	0.907	1.09	1.000	1.00	-
	Carbon	6.03	-	0.880	1.00	1.000	-	-
Radium	Magnesium	6.87	-	0.890	1.19	1.010	1.10	-
0.5 mgm.	Wax	6.09	-	0.870	1.01	0.990	1.03	-
needle	Copper	7.94	-	0.971	1.32	1.100	1.10	-
	Lead	28.20	-	3.160	4.70	3.600	3.50	-

MEASUREMENTS IN A SCATTERING MEDIUM

The X radiation measured at a depth in a scattering medium comprises primary radiation which has penetrated to the point of measurement and radiation which has been scattered to the point of measurement from adjacent elements of medium. The scattered radiation will reach the point of measurement from all directions and the relative amounts of forward, side and backscatter will depend upon the conditions pertaining. For primary radiation of low energy, say 200 kV., a large fraction of the radiation will be scattered back, the percentage back-scatter being of the order of 40%. As the primary energy is increased the scattered radiation, due mainly to Compton encounters, tends to go more and more in the forward direction and the percentage backscatter rapidly decreases.

Where back and sidescatter are important the dose of radiation measured at a point in a scattering medium will depend greatly on the volume of medium irradiated since the amount of scattered radiation received will increase as the number of possible scattering elements increases. The limit to the increase is reached when the edge of the irradiated volume is at a distance from the point of measurement greater than the range of the scattered radiation. At 200 kV. this condition is reached when the

irradiated field on the surface of the scattering medium has a diameter of approximately 22 cms. When the energy of the primary radiation is high the scattered radiation goes, predominantly, forward and consequently the amount of scattered radiation received at a point in a scattering medium depends to a smaller extent on field area.

As the radiation received at any point comprises both primary and scattered radiation the quality of the radiation will depend in a complex way on the relative amounts of primary radiation and of forward, back and sidescattered radiation received. The change in wavelength due to a Compton encounter resulting in scatter backwards is large (0.048Å) but decreases as the scattering direction approaches that of the primary quantum. Further, in the case of a heterogeneous primary beam the medium will act as a filter transmitting the more penetrating wavelengths. Mayneord and Clarkson[107] have studied extensively the variations of quality of the radiation in a scattering medium for energies up to approximately 350 kV. These workers used a double ionisation chamber, the two parts of which were of different materials. A comparison of the relative ionisation currents in the two parts served as an indication of the mean quantum energy of the beam being investigated. They found that, at the energies they investigated, the scattering effects masked the filtration effect and the beam of radiation became softer as depth in

the scattering medium was increased.

A number of measurements of the distribution and quality of radiation in and around a scattering medium have been made. Measurements of backscatter have been made on the surface of "pressdwood" phantoms, one at 3 MeV. using the Van de Graaff generator and one at 4 MeV. with the Malvern synchrotron.

The former measurement was made using the carbon chamber probe system, a value first being obtained for the dosage-rate in air and then values for the dosage-rate for various field sizes, obtained with the chamber lying close against the surface of the phantom. A similar measurement using the small condenser chambers described was made using the open filtered beam of the Malvern synchrotron. In both cases the generator output was independently monitored during the experiments.

The value of percentage backscatter obtained at 3 MeV. was 5%, apparently independent of field size as expected, and the value at 4 MeV. was 3%. The back-scatter is certainly low at these energies and the values obtained are in approximate accordance with theory.[108]

Some measurements of the distribution of radiation inside a "pressdwood" phantom were made with the open beam of the Malvern synchrotron at 4 MeV. The "pressdwood" phantom consisted of a number of 40 cm. square blocks of

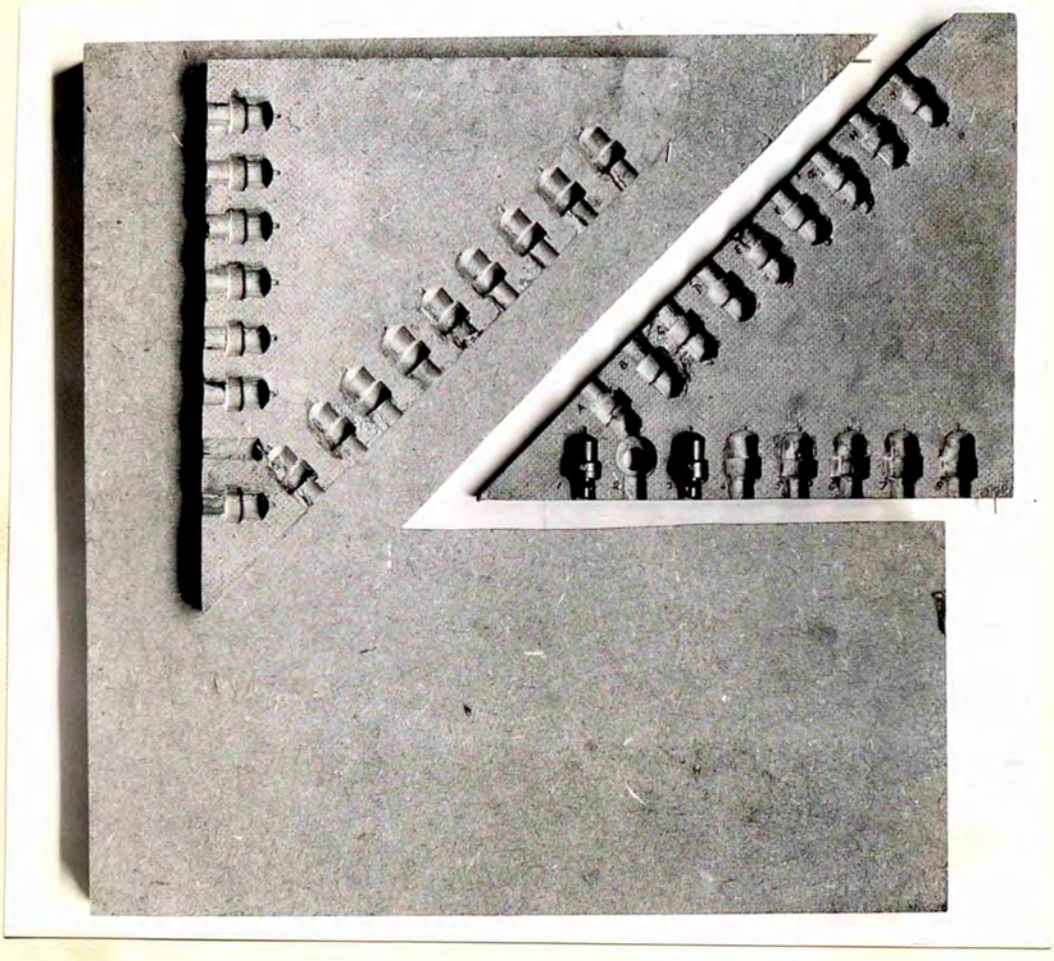

Fig. 85

thickness varying from 1 cm. to 10 cms. Two blocks of 1.5 cms. thickness had a 45° sector cut out as shown in Fig. 85 and the inside faces of these two sectors were machined by a special cutter to hold the small ionisation chambers described earlier. When filled with chambers the sectors could be refitted to the blocks from which they were cut and the whole 3 cms. thick block placed at any depth in the phantom so that measurements from 1.5 cms. to some 40 cms. depth were obtained. Surface values were obtained by using only the back half of the block and fixing the chambers, buried to half their depth, in the face of this half. By rotating the block, at each depth, 90° at a time through 270° distributions along eight radial lines 45° apart were obtained. The distribution measurements were made before the presence of the electron background in the beam was realised. The curves (Figs.86, 87, 88) show three of these distributions in parallel planes at depths of 0, 5.5 and 25.5 cms. at right angles to the direction of the beam, points at which equal doses were observed being joined to form isodose curves. Fig. 86 serves to emphasise the asymetry of the beam already noted in Fig. 7, while Figs. 87 and 88, where the electrons have been filtered out by the surface layers of the phantom, show that in a "clean" beam symetrical distributions may be expected.

In Fig. 89 can be seen the distribution in a plane containing the centre axis in which the above features

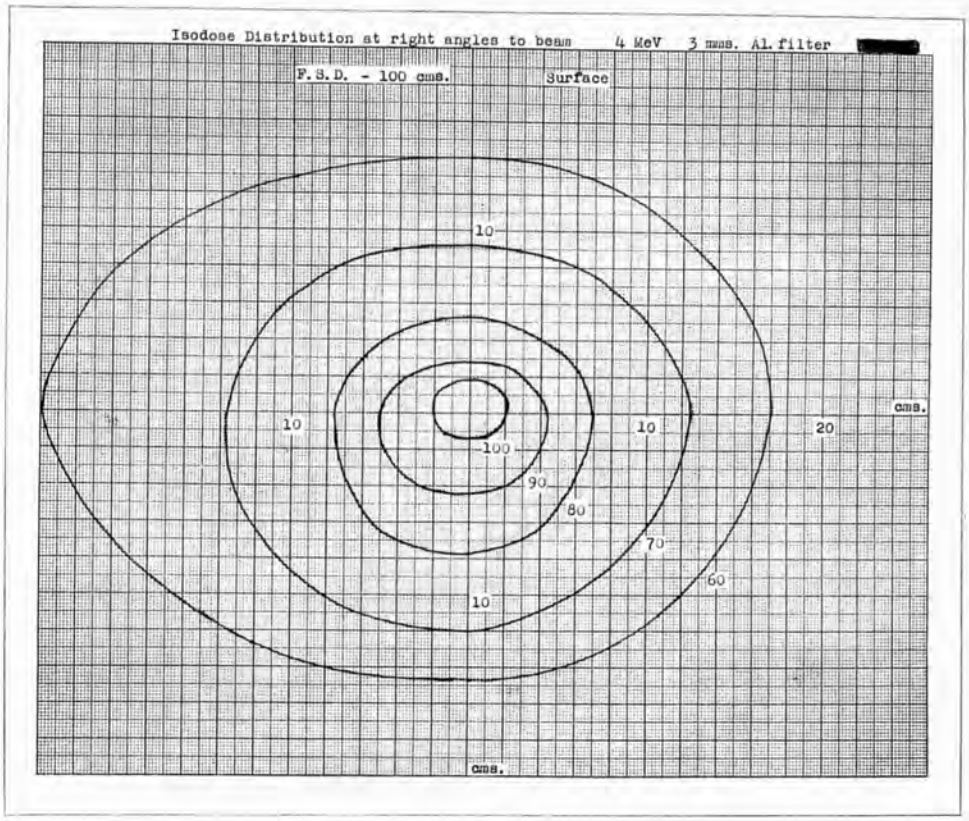
Isodose Distribution at right angles to beam 4 MeV 3 mms. Al. filter
F.S.D. - 100 cms.
Surface
10
10
10
10
20
cms.
100
90
80
70
60
cms.

Fig.86

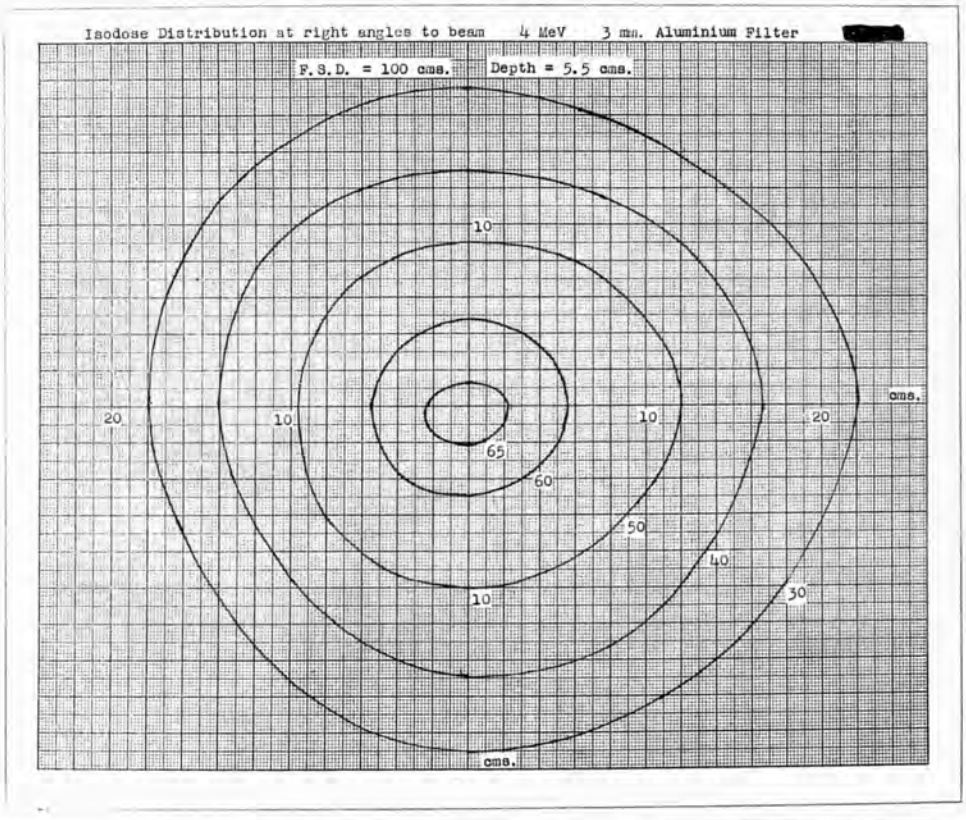
Isodose Distribution at right angles to beam 4 MeV 3 mm. Aluminium Filter
F.S.D. = 100 cms.
Depth = 5.5 cms.
10
20
10
10
20
cms.
65
60
50
40
30
10
cms.

Fig.87

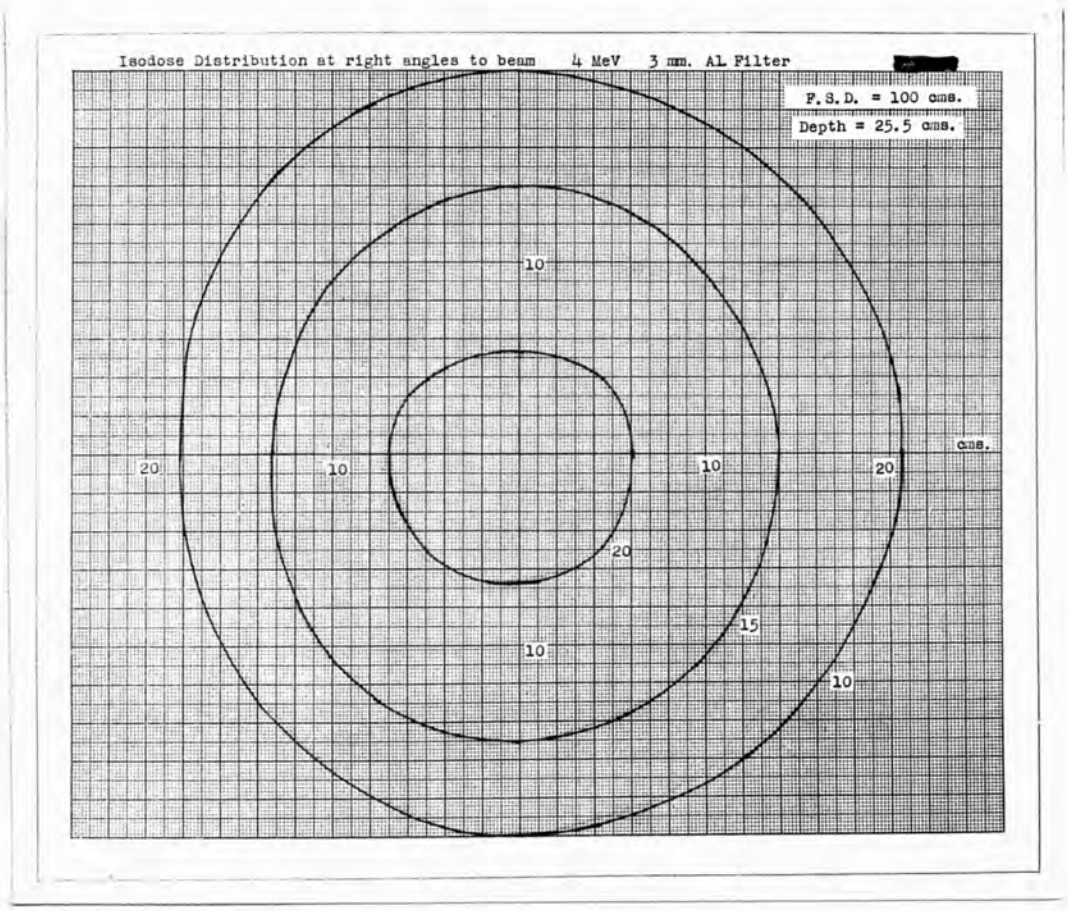
Isodose Distribution at right angles to beam 4 MeV 3 mm. Al Filter
[redacted]
F.S.D. = 100 cms.
Depth = 25.5 cms.
10
20
10
10
20
cms.
20
15
10
10

Fig. 88

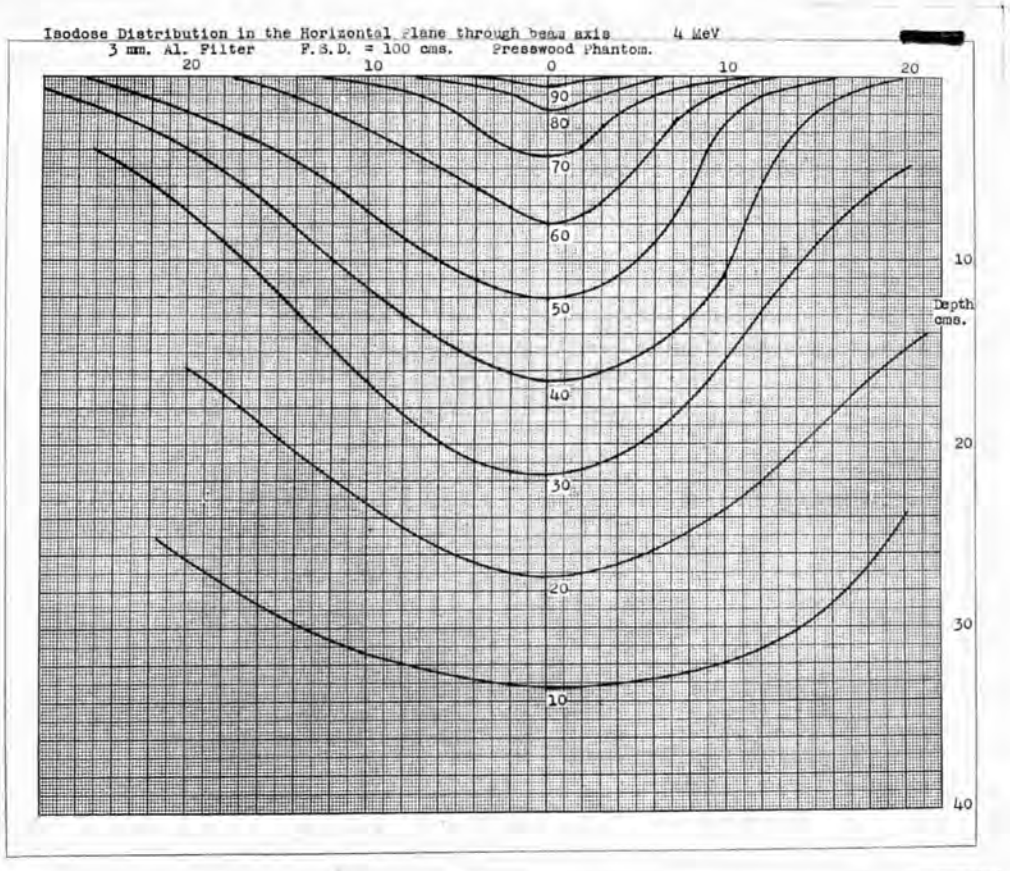
Isodose Distribution in the Horizontal Plane through beam axis 4 MeV
3 mm. Al. Filter F.S.D. = 100 cms. Presswood Phantom.
20
10
0
10
20
90
80
70
60
50
40
30
20
10
10
20
30
40
Depth cms.

Fig. 89

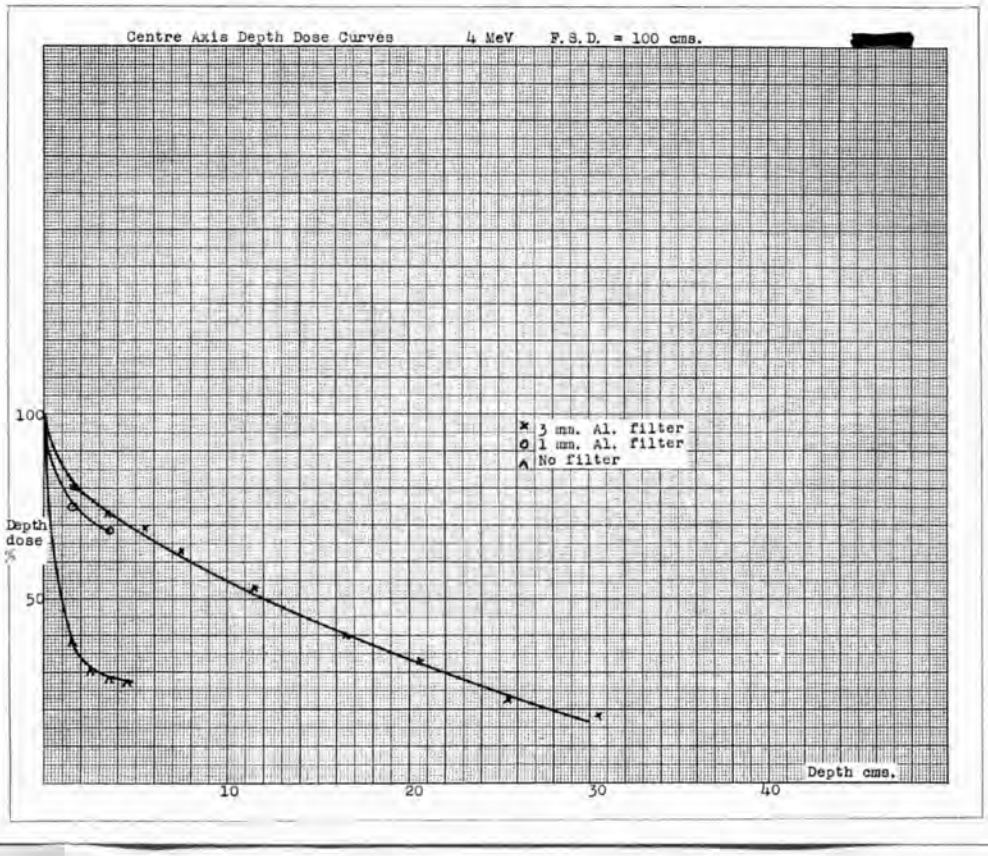
Centre Axis Depth Dose Curves 4 MeV F.S.D. = 100 cms.
3 mm. Al. filter
1 mm. Al. filter
No filter
100
50
Depth dose %
10
20
30
40
Depth cms.

Fig. 90

are again evident. In Fig. 90 the centre axis depth dose is shown. The initial sharp drop here represents, clearly, the removal of the electrons from the beam. The subsequent slope of the curve, however, is about that to be expected at an energy of 4 MeV.

These distributions serve to emphasise the erroneous interpretations, and in the case of the medical use the danger to a patient, which could, in adverse conditions, result from lack of care in determining the nature of the radiation emitted by a generator of the type used and also from dosage measurements made without an understanding of types of radiation emitted.

Distributions have been measured by Kerst and his collaborators[40] at 20 MeV. showing the possibilities of well defined beams with sharp edges and flat fields obtained by differential filtration. Their centre axis depth dose distributions are in accord with what would be expected judging from the observations reported above in carbon chambers of varying wall thickness. A number of distributions over a range of energies have also been made by Charlton and Breed[36] using the 100 MeV. betatron. Their distributions, certainly at lower energies, show that they have not taken adequate precautions to remove the electrons present in the beam. Their maxima, therefore, appear closer to the surface.

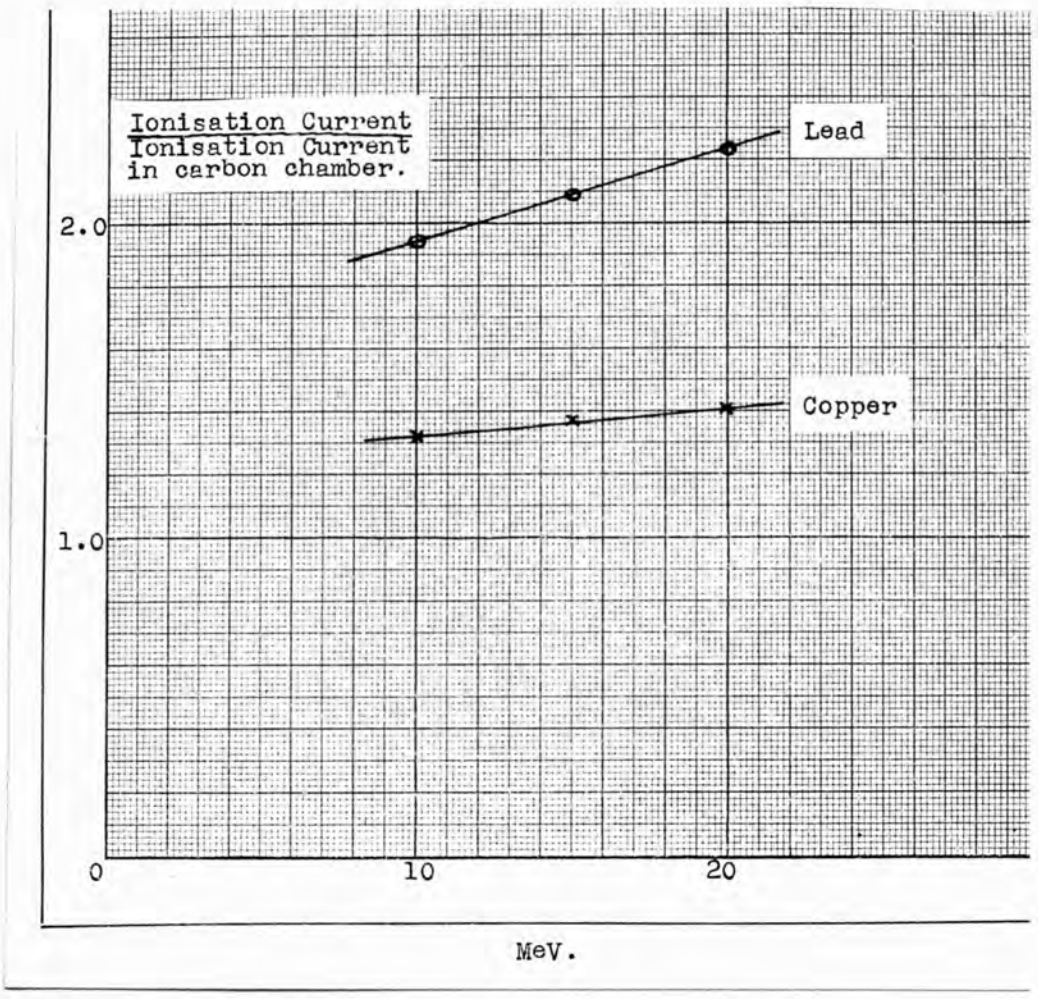
Ionisation Current
Ionisation Current
in carbon chamber.
Lead
Copper
2.0
1.0
0
10
20
MeV.

Fig. 91

While in Urbana and Cambridge, Massachusetts, a short study was made of the variation of quality of radiation inside a "pressdwood" phantom.

It was desired to find out if the presence of secondary scattered radiation appreciably alters the mean energy of the electromagnetic radiation received at a given point. The technique used was that of Mayneord and Clarkson.[102] The type of double ionisation chamber made of two materials which they used was not available for these experiments but the ratios of maximum currents in lead and copper chambers to that in a carbon chamber was determined and plotted in Fig. 91 showing the variation as the peak energy is increased from 10 to 20 MeV. Measurements of the ratio of the ionisation current in two chambers of different materials evidently serve to indicate whether the radiation in a phantom is changing in "quality" at different depths.

The values of copper-to-carbon and lead-to-carbon ratios obtained at different depths are given in Table VIII. The chamber wall thicknesses used have been chosen to give approximately maximum ionisation in each material. It will be seen that at 20 MeV. the ratio of Copper/carbon increases with depth indicating a slight hardening of the radiation and at a depth of 60 cms. the filtration effect is evidently predominant. It is interesting that, using

a 24 cms. carbon filter at a distance of 84 cms. from the measuring chamber, a much more marked change in quality is produced than is produced by 60 cms. of "pressdwood" when the chamber is in contact with the scattering medium.

TABLE VIII

	Depth in phantom	Ratio $\frac{\text{copper}}{\text{carbon}}$	Ratio $\frac{\text{lead}}{\text{carbon}}$
MeV. = 20	Zero-in air	1.41	2.23
	7 cms.	1.50	
	14 cms.	1.55	
	23 cms.	1.46	
	60 cms.	1.67	2.43
	24 cm. carbon filter		2.69
MeV. = 3	Zero-in air	1.12	
	4.6 cms.	1.11	
	9.2 cms.	1.17,1.18	
	18.4 cms.	1.12	
	29.0 cms.	1.04	

As shown by Mayneord and Clarkson, at lower voltages, the filtration and degradation effects are struggling for mastery and at the higher energies the filtration effect wins in contrast with the result found by Mayneord and Clarkson at say 350 kV. This is undoubtedly due to the smaller amounts of back and sidescatter at higher energies, the scattered radiations going predominantly forward. Also, the phantoms, being of low atomic number materials,

were the type of filter which would most readily transmit the hard components of the beam. At 3 MeV. using the Van de Graaff generator it is difficult to draw any conclusions owing to the small rate of change of the ratio with quality. It would seem that the two effects of filtration and degradation just balance at this energy which must represent the energy region in which the transition from increasing dominance of scatter to increasing dominance of high energy components takes place.

PROTECTION FROM STRAY RADIATION

It is important to measure the stray radiation in the vicinity of high energy machines in order to provide a sound basis for adequate protection for users of the equipment. A survey has therefore been made around the 15 MeV. synchrotron in Malvern, certain measurements around Kerst's 20 MeV. betatron and observations near the 3 MeV. Van de Graaff at the Massachusetts Institute of Technology, Cambridge.

During the experiments at Malvern where a larger number of observations were made, condenser chambers were carried by all personnel to assess the stray radiation received.

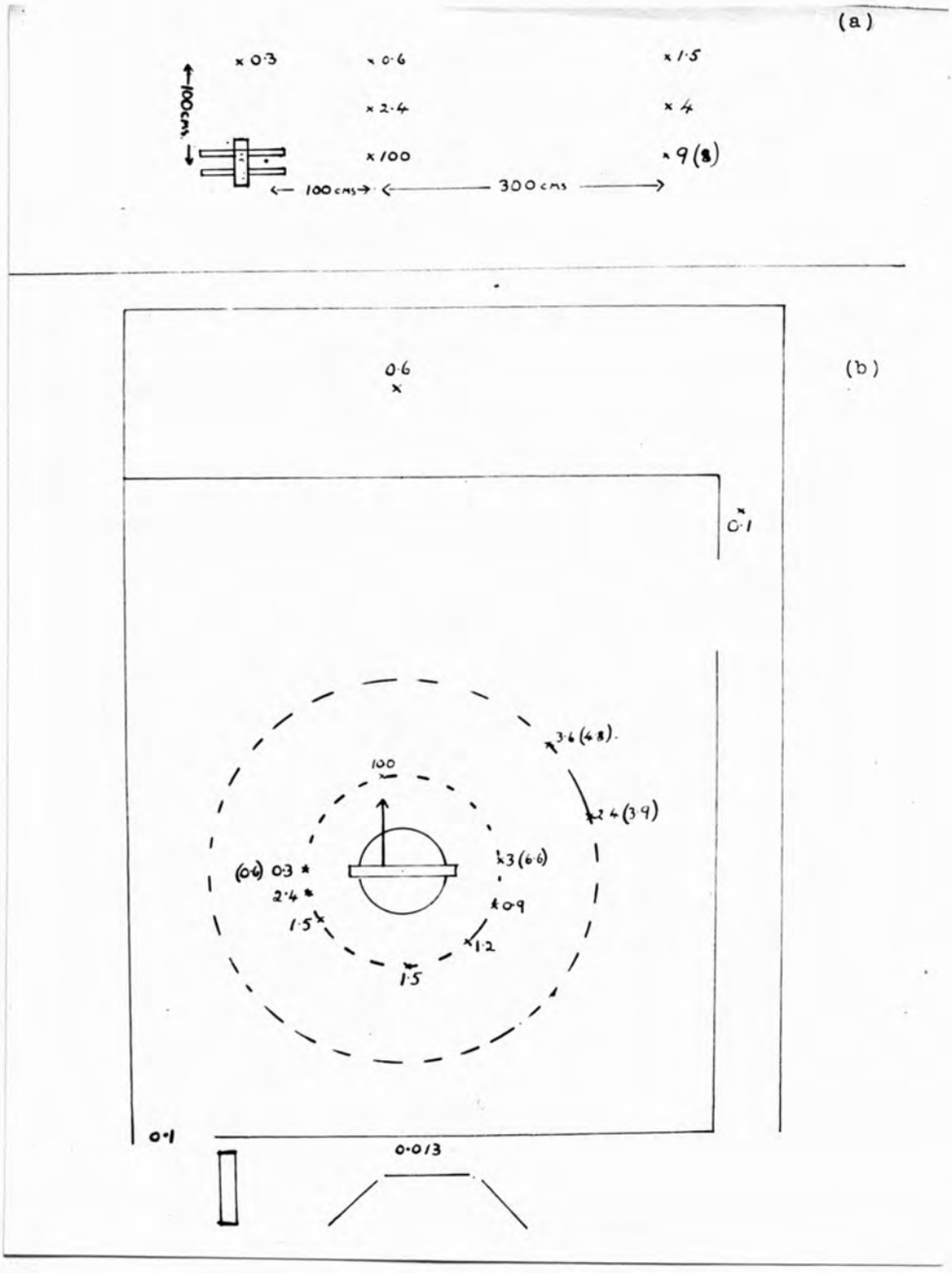
(a)
×0·3
×0·6
×1·5
×2·4
×4
×100
×9(8)
100cms
100cms
300cms
(b)
0·6
0·1
3·6(4·8)
2·4(3·9)
100
(0·6) 0·3
2·4
1·5
3(6·6)
0·9
1·2
1·5
0·1
0·013

Fig. 92

(1) Stray Radiation Measurements.

Malvern Synchrotron.

The measurements in the vicinity of the synchrotron were made with the direct reading monitoring system described. The wall of the chamber of this instrument was ordinarily 1 cm. thick but the figures in brackets in Fig. 92 give the values observed when the end of the chamber was removed and an openwork graphited gauze front substituted. Thus even low energy electrons were recorded.

The distribution of stray radiation round the synchrotron as shown in Fig. 92 is based on values observed at 1 and 2 metres radius from the target in the plane of the donut, as well as at several points above the plane and also points in adjacent rooms.

The values are quoted in terms of the dosage-rate at 1 metre from the target in the primary beam as 100%. The absolute value of this dosage-rate was approximately 0.2 r/min. The values observed here are in good agreement with measurements made at the edge of the coils and shown in Fig. 8.

During the observations in the vertical plane the effect of the shadow of the magnet was obvious, while in the horizontal plane that of the yoke is evident.

The quality of the radiation in different directions varies. For example, on thickening the wall of

the recording chamber to 1 cm. of carbon the ionisation drops to approximately one half at positions at the side or behind the plant, but in the direct beam on thickening the chamber wall the ionisation current rises in the way already discussed in detail. As already emphasised the radiation near these instruments contains many high speed electrons which constitute a serious problem in its vicinity but, of course, little difficulty behind reasonable protective walls.

Assuming an output of 1 r/min. at 1 metre in the primary beam, the dosage-rate 1 metre sideways behind the yoke is 10 "tolerance dosage-rates," the tolerance dosage-rate being taken as 10^{-6} r/sec. At 1 metre behind the synchrotron the value is 50 T.D.R. Near the operator's controls, at a distance of about 3 metres behind the synchrotron and behind a 13" brick wall, there was difficulty in measuring the radiation with the system available but the value is certainly not greater than 0.5 T.D.R.

The quantities of radiation recorded by the protection condenser ionisation chambers carried by personnel working on this instrument were very small. In most cases no detectable radiation was found during an intermittent days working and values never exceeded 0.002 r in this time. Two members of the team recorded 3×10^{-3}r in a days working on the plant room at about 6 feet behind the apparatus. Two members of the team performing experiments which involved working for about half an hour at the edge of the beam

received a dose of 6×10^{-3} r/hour.

The National Physical Laboratory have carried out a survey of the stray radiation received by all workers with high energy generators at Malvern using films carried by those workers. These films are partly covered by 2 mm. lead and partly uncovered apart from the light-tight holder. Thus they will record the beta radiation as well as the hard X-radiation. The blackening of the film per rontgen was determined by exposure to gamma rays from radium. Evidence will be given later that the sensitivity of film to radiation does not appear to alter greatly as the energy is increased to 12 MeV. and the values obtained by densitometer measurement of the films carried by these workers should be a reasonable guide to the true doses received in rontgens. The author is indebted to Mr. W. Binks and his colleagues of the Physics Department at the National Physical Laboratory, who carried out this survey for information about their findings. Their figures are in approximate agreement with the values obtained and given above using condenser ionisation chambers. The weekly values of dose received lie between 0.01 and 0.05r for a 5 day week which compares well with a value of 0.002 r/day recorded by the condenser chambers. Since the small change in film sensitivity is found to be in such a direction as to lead to an overestimation of the dose received when the sensitivity

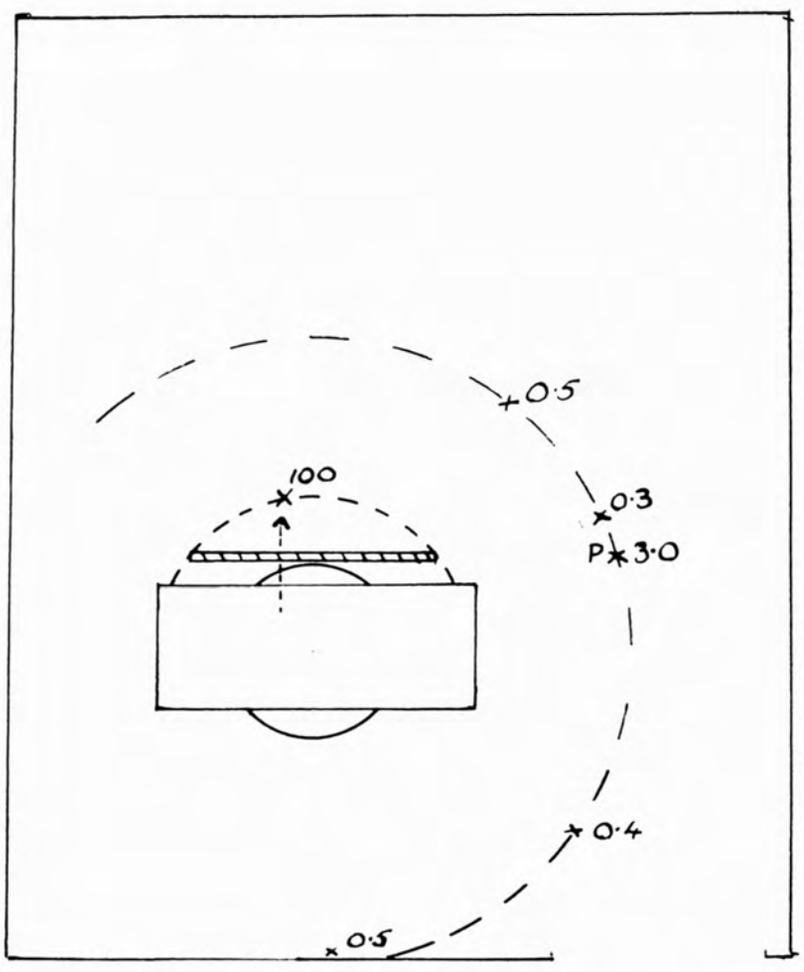

Fig. 93

to radium gamma rays is used to interpret the blackening, the agreement is rather better than appears. Both systems are working at their lower limit and the absolute values are, therefore, not regarded as very accurate, but it is certain that stray radiation received does not exceed these figures.

The doses recorded are low but it must be pointed out that with higher primary beam dosage-rates they will become significant and even dangerous. For example, a dosage-rate of 20 r/min. at 1 metre is of the order which might reasonably be required for some purposes. This is 100 times the output of the machine during these measurements and, assuming the other figures rise proportionately, operating personnel would receive about 0.2 r/day which exceeds considerably the present figure for maximum permissible daily dose (0.03 r/day or 10^{-6} r/sec.)

20 MeV. Betatron

Measurements were made in the vicinity of Kerst's 20 MeV. betatron running at 20 MeV. and delivering approximately 60 r/min at 1 metre. The measurements were made with the probe system using the large volume "Perspex" chamber having a 6 mm. wall. Unfortunately, no measurements with a very thin wall were possible. In Fig. 93 the dosage-rates at a radius of 2 Metres from the target are shown expressed as percentages of the value at 1 metre in the primary

beam. Behind the betatron the dosage-rate, due to stray electrons as mentioned before, is approximately 5000 T.D.R. An even more spectacular demonstration of the presence of these electrons is given by the measurement at point P shown on the diagram. This value (of the order of 3×10^4 T.D.R.) was observed when in line with the back face of a block of wood placed in front of the betatron and used to deflect the electrons from the direction of the primary beam. Evidently these electrons are deflected into a narrow angle between the back face of the wood block and the yoke of the magnet. These measurements emphasise the danger of remaining in the vicinity of such installations without special precautions.

In particular, machines for therapeutic use will require careful preliminary study of these dangers and continuous monitoring during use, especially as the intensity of soft radiation may change from time to time, for example, with the state of the vacuum in the donut, the scattered electrons increasing in number as the vacuum deteriorates.

The intensities of radiation in adjacent rooms is low; Kerst himself records that "operating personnel outside the room receive less than 0.01r even on very prolonged runs with a beam intensity about 50 r/min. at 1 metre" and measurements made substantiate this claim.

It is worthy of note that the percentage of stray radiation around both the Malvern synchrotron and the

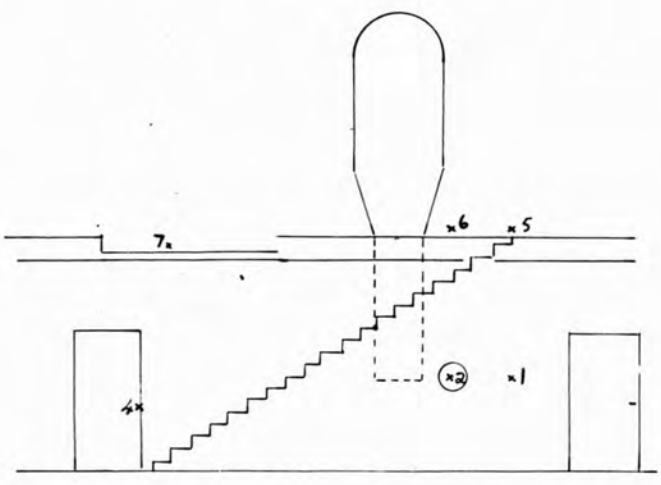

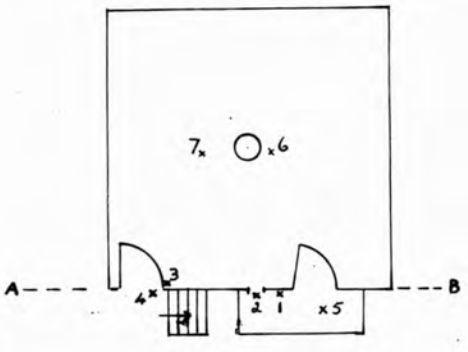

Position		Energy	Dosage Rate ÷10⁻⁶/sec
1	Behind	3 MeV	60
1	9" wall	2 MeV	30
2	Behind gap	3 "	1040
2	In wall	2 "	700
3	Inside	3	1160
3	Door	2	880
4	Outside ½" steel	3 "	120
4	½" Pb door	2	60
5	Top of	3	<40
5	stairs	2	<40
6	Above set	3	80
6	6" concrete	2	60
7		2	300

Fig. 94

20 MeV. betatron are similar in value. For example, at 2 metres behind both plants the dosage-rates for stray radiation are 16 and 13 T.D.R. respectively per r/min. at 1 metre in the primary beam.

3 MeV. Van de Graaff

Similar stray radiation measurements made around the 3 MeV. Van de Graaff are shown in Fig. 94. As will be seen from the diagram the unit is mounted above floor level but the accelerator tube goes through into an underground room, the only access to which is by a $\frac{1}{4}$" steel + $\frac{1}{2}$" lead door located at the bottom of a flight of steps leading to the room. It will be seen that there is a very high background of radiation all round the generator. The output during these measurements was, at 3 MeV., approximately 50 r/min. and, at 2 MeV., approximately 25 r/min. In the room itself a large fraction of this stray radiation is due to electrons. The X-ray tube has a thin window and an external transmission target is used and this gives rise to a large amount of scattered electrons. The stray high energy radiation measured above the plant is probably due to the target acting partially as a reflection target and giving a beam of radiation vertically up through the floor. At the control desk located on ground level some 15 feet from the generator and partially shielded from the generator tank by a wall, no detectable dosage-rate was observed.

As a matter of interest it was found that when the X-ray tube, which was continuously evacuated, went "soft" the background of scattered radiation round the tank on the ground floor may rise by a factor of 10 or more. This is due to electrons scattered out of the beam in the tube.

(2) Sensitivity of photographic films to short wavelength X rays.

To assist in the use of photographic film in monitoring stray radiation and for other purposes, a number of measurements were made to determine the sensitivity of film at these high energies. A number of strips of "Ilfex" film was exposed at 4, 8 and 12 MeV. and the doses received recorded simultaneously by ionisation chambers. The blackening of these films was measured by my colleague Dr. G. Spiegler, who had previously considerable experience of the blackening of X-ray films by lower energy radiations. It was found that the sensitivity, as judged by density of film per rontgen, remained approximately constant at all energies investigated. The values obtained were in fair agreement with the sensitivity for the gamma rays of radium. (Table IX). The results are preliminary and the opportunity has not occurred to carry out the considerable amount of further work required but there is certainly no evidence of falling sensitivity in the higher energy region and, in fact, at 12 MeV. the blackening per rontgen as shown in Table IX is some 20%

higher. This result is to be expected theoretically since the energy loss of high speed electrons per centimetre of path shows a minimum at about 2 MeV. and then remains fairly constant, there being a very slow rise with energy above 2 MeV. At 12 MeV. for small densities it will be seen that the blackening rises approximately linearly with dose, a result previously well established for gamma rays from radium and 200 kV. X rays.

TABLE IX

Radiation	Dose	Blackening	Blackening/r
12 MeV.(3 mm. Al filter)	0.15r	0.17	1.14
	0.175r	0.23	1.31
	0.18r	0.23	1.28
	0.35r	0.44	1.26
4 MeV.(3 mm. Al filter)	0.25r	0.40	1.60
Radium gamma rays	0.13r	0.11	0.85
	0.26r	0.25	0.76
	1.04r	1.00	0.76

Charlton and Breed[36] use photographic measurements in some of their work with the 100 MeV. betatron. Their tests of Kodak film at 200 kV. and 100 MeV. show almost identical sensitivity as well as a linear relation between density and dose. The former result is surprising and may be fortuitous since the energy loss per cm. of path given by Heitler[52] at 100 MeV. does not differ greatly from that at 200 kV.

At energies up to say 20 MeV., however, the values of radiation recorded by photographic films are capable of fairly accurate interpretation and the agreement between the National Physical Laboratory film survey and the condenser ionisation chamber measurements for stray radiation received by workers at Malvern gains in significance thereby.

It should be pointed out that considerable care must be taken in the choice of conditions under which the measurements of stray radiation are made. It has been clearly demonstrated that electrons scattered around these machines may well constitute one of the main dangers. To record these, as we must, a thin walled ionisation chamber is required while to measure correctly the hard X radiation a chamber of some centimetres wall thickness is required. The corresponding difference for use of films has not been investigated yet but such a condition no doubt applies. In practice it is suggested that two condenser chambers be carried, one with a thin and the other a thick wall. It would obviously be inconvenient to carry a chamber whose wall thickness was say 6 cms. as required to obtain complete build-up for 30 MeV. radiation. The correction required to the reading obtained with a chamber of 1 cm. wall thickness at this energy is small (a factor of about 1.3) and since this thickness is great enough to avoid errors due to variations in scatter caused by different geometrical layouts of plant it is suggested that

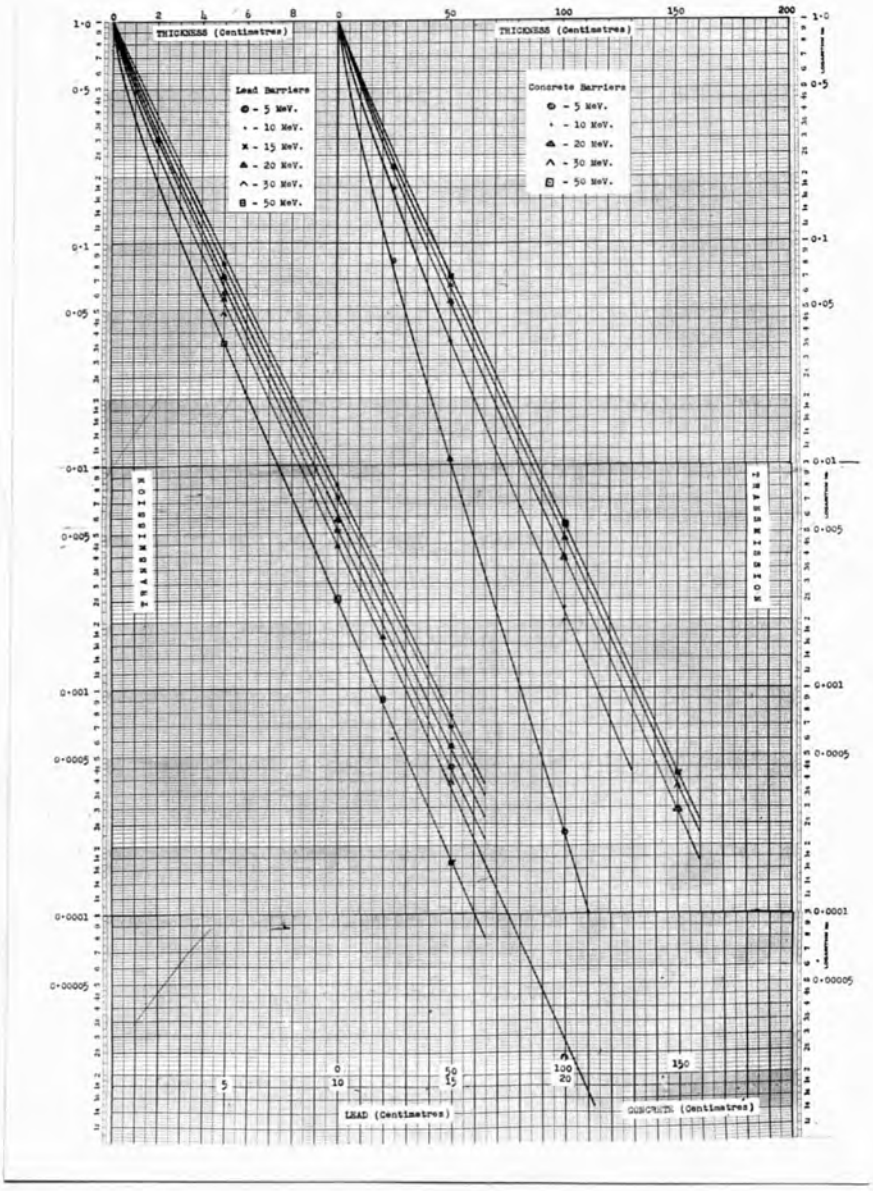
THICKNESS (Centimetres)
Lead Barriers
5 MeV.
10 MeV.
15 MeV.
20 MeV.
30 MeV.
50 MeV.
THICKNESS (Centimetres)
Concrete Barriers
5 MeV.
10 MeV.
20 MeV.
30 MeV.
50 MeV.
TRANSMISSION
TRANSMISSION
LEAD (Centimetres)
CONCRETE (Centimetres)

Fig. 95

a condenser ionisation chamber of 1 cm. wall thickness be used for energies up to 30 MeV. to measure the dose of hard X radiation received.

(3) Protective materials.

The problem of protecting personnel working with high energy generators obviously requires considerable study. The curves of Fig. 10 and 11 give preliminary guidance as to the protective barriers required at various energies and dosage-rates. Hitherto, lead has been the material principally used as a protective screen, at any rate in the energy range up to 500 kV., and despite the sharp drop in its linear coefficient of absorption to a minimum at 3 - 4 MeV. it is still the most effective barrier per unit mass.

The curves of Fig. 95 have been calculated using the Heitler energy distributions and the appropriate absorption coefficients thus calculating the spectral distribution after filtration through the barrier. The areas under these curves have been used to calculate the fractional transmissions for various thicknesses of material and these are plotted in Fig. 95 for various energies.

It will readily be seen that the thickness of lead required, at these energies, would be prohibitive from the point of view of cost and possible difficulty of assembly. For example, at 30 MeV. for a plant giving say 50 r/min. at

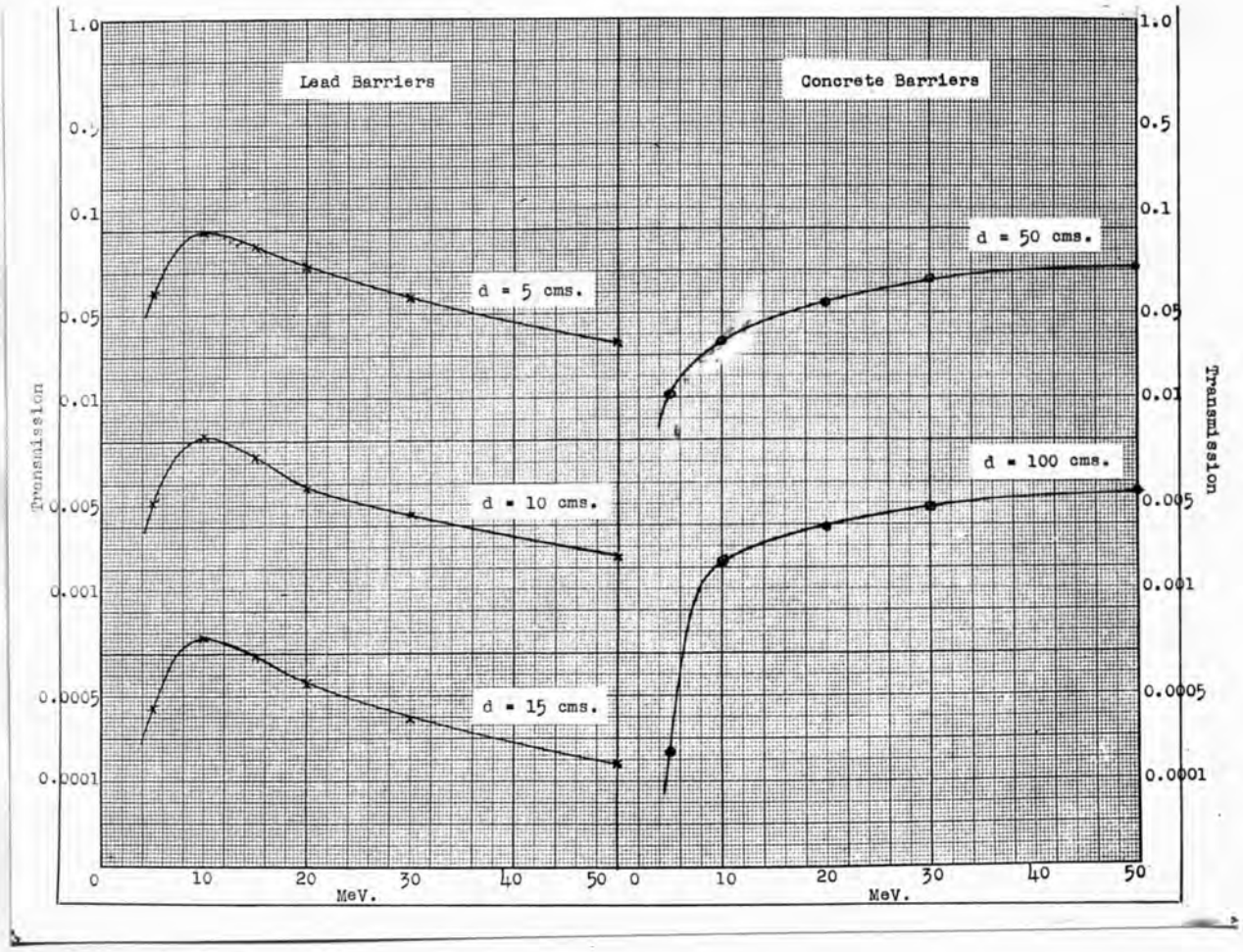
Lead Barriers
Concrete Barriers
d = 5 cms.
d = 10 cms.
d = 15 cms.
d = 50 cms.
d = 100 cms.
Transmission
MeV.
1.0
0.5
0.1
0.05
0.01
0.005
0.001
0.0005
0.0001
0
10
20
30
40
50

Fig. 96

1 metre, to reduce the dosage-rate to 10^{-6} r/sec. at a distance of 4 metres from the plant in the direction of the beam would require about 20 cms. of lead. To obtain corresponding protection with concrete some 200 cms. is required. Where space is unimportant a concrete barrier is to be recommended since it is structurally self-supporting and relatively inexpensive.

An interesting result emerges from a plot of the variation of transmission of radiation against energy through a fixed thickness of lead and concrete absorber shown in Fig. 96. The peak value of transmission for lead corresponds to its minimum absorption coefficient which occurs at 3 - 4 MeV. The maximum transmission calculated from the spectral distribution curves occurs about 10 MeV. i.e. at between two and three times the energy at which lead has its minimum absorption coefficient. As the values of the transmission were calculated from the spectral distribution of the radiation this is an interesting demonstration that the mean energy corresponds to between a half and a third of the peak energy.

No comparable measurements exist but some observations at lower energies on the transmission through lead and concrete barriers have been made notably by Wyckoff and Braestrup[109,110] and their colleagues, in which they have studied the effects of broad and narrow beams on the

radiation transmitted. Part of the radiation measured on the far side of the barrier from the source comes as scattered radiation from a large volume of the barrier, thereby reducing the apparent absorption coefficient. At the energies up to 1400 kV. at which these measurements have been carried out the scattered quanta have higher absorption coefficients than the primary beam and the volume of material from which scattered radiation can contribute to the transmitted dose is, therefore, limited as shown by Wyckoff and his co-workers,[109] in particular for lead where the absorption coefficient rises rapidly with λ. At energies above 4 MeV., however, this condition no longer holds for lead and the scattered quanta may well have greater penetrating power than the primary radiation. In the case of concrete this does not arise until the primary energy exceeds about 30 MeV.

The problem is further aggravated by the effect of the distance of the measuring system from the barrier, i.e. the angle which the irradiated area of the barrier subtends at the chamber of the measuring system.

The reduction factor in dosage-rate which a barrier must introduce is so great that the radiation undergoes repeated changes in wavelength and direction and it becomes well-nigh impossible to allow suitably in calculation for all these variations, any necessary

simplifying assumptions reducing the value of the result. Further, a protective barrier should not be reduced to such fine limits that all these factors require to be considered. Failla[111] in discussing the problem has suggested a simple method of computing the required barrier thicknesses by means of half value layers. These, of course, must first be measured under the appropriate conditions. Failla suggests that the most appropriate type of absorption curve to use would be one in which the measurements were made with the absorbing material completely surrounding the measuring chamber. Braestrup[112] has obtained an absorption curve in lead for gamma rays from radium under these conditions and shown the greater transparency as compared with "narrow beam" measuring conditions. This method is akin to measurements made in ionisation chambers of varying wall thickness. It will, therefore, tend to underestimate the effective absorption coefficient of the barrier.

Circumstances will vary so much between installations that a complete answer to the problem is not easy but it is to be recommended that where the excitation energy exceeds this value, the barrier should be designed for the energy of its minimum absorption coefficient. For protective barriers, concrete in the form of loose readily transportable blocks which can be built up to make thick barriers, as used in some existing installations, is considered the most practical method of solving the problem. The beam of the

generator should be directed away from adjacent rooms and buildings and where a separate building is not available the installation should be below ground level and the beam fired horizontally into a "black body" cut under the ground.

REFERENCES

1. Van de Graaff R.J., Compton A.T. and Van Atta L.C. — Phys.Rev., 43, 149, 1933.
2. Trump J.G. and Van de Graaff R.J. — Phys.Rev., 55, 1160, 1939.
3. Kerst D.W. — Phys.Rev., 58, 841, 1940.
4. Kerst D.W. — Phys.Rev., 59, 110, 1941.
5. Kerst D.W. — Phys.Rev., 60, 47, 1941.
6. Kerst D.W. — Phys.Rev., 61, 93, 1942.
7. Kerst D.W. — Rev.Sci.Inst., 13, 387, 1942.
8. Kerst D.W. — Amer.J.Phys., 10, 219, 1942.
9. Kerst D.W. — Radiology, 40, 115, 1943.
10. Kerst D.W. — Nature, 157, 90, 1946.
11. Goward F.K. and Barnes D.E. — Nature, 158, 413, 1946.
12. Fry D.W. et al. — Nature, 161, 504, 1948.
13. Elder F.R. et al. — J.App.Phys., 18, 810, 1947.
14. Sloan D.H. and Lawrence E.O. — Phys.Rev., 38, 2021, 1931.
15. Fry D.W. et al. — Nature, 160, 351, 1947.
16. Walkinshaw W. — Proc.Phys.Soc., 61, 246, 1948.
17. Harvie R.B. — Proc.Phys.Soc., 61, 255, 1948.
18. Mullett L.B. and Loach B.G. — Proc.Phys.Soc., 61, 371, 1948.
19. Westendorp W.F. — J.App.Phys., 16, 657, 1945.
20. Westendorp W.F. — Phys.Rev., 71, 271, 1947.
21. Du Bridge L.A. and Brown H. — Rev.Sci.Inst., 4, 532, 1933.

22. Mayneord W.V. and Roberts J.E. — Brit.J.Rad., 60, 365, 1937.

23. Mayneord W.V. — Proc.Phys.Soc., 54, 405, 1942.

24. Newbery S.P. — In publication.

25. Turner R.C. and Newbery S.P. — In publication.

26. Turner R.C. — In publication.

27. Stokes G. — Proc.Manch.Lit.&.Phil.Soc., 1898.

28. Thomson J.J. — Phil.Mag., 45, 172, 1898.

29. Sommerfeld A. — Atomic Structure and Spectral Lines - Methuen 1923.

30. Bethe H. and Heitler W. — Proc.Roy.Soc., 146, 83, 1934.

31. Sommerfeld A. — Ann.d.Phys., 11, 257, 1931.

32. Schiff L.I. — Phys.Rev., 70, 87 , 1946.

33. Williams E.J. — Phys.Rev., 58, 292, 1940.

34. Appelyard R.K. and Allen-Williams D.T. — Brit.J.Rad., 22, 106, 1949.

35. Westendorp W.F. and Charlton E.E. — J. App.Phys., 16, 581, 1945.

36. Charlton E.E. and Breed H.E. — Amer.J.Roent., 60, 158, 1948.

37. Buechner W. et al. — Phys.Rev., 74, 1348, 1948.

38. Chien-Shiung Wu — Phys.Rev., 59, 481, 1941.

39. Ivanov L. et al. — J.Phys.,U.S.S.R., 4, 319, 1941.

40. Kerst D.W. et al. — Amer.J.Roent., 60, 153, 1948.

41. Compton A.H. and Allison S.K. — X Rays in Theory and Experiment, MacMillan 1935.

42. Hulme H.R. et al. — Proc.Roy.Soc.A, 149, 131, 1935.

43. Klein O. and Nishina Y. — Zeit.f.Phys., 52, 853, 1929.

44. Dirac, P.A.M. — Quantum Mechanics - Oxford 1935.

45. Oppenheimer J.R. and Plesset M.S. — Phys.Rev., 44, 53, 1933.

46. Curie I. and Joliot F. — Comptes Rendus, 196, 1105, 1933.

47. Chadwick J. et al. — Proc.Roy.Soc., 144, 235, 1934.

48. Heitung Th. — Zeit.f.Phys., 87, 127, 1933.

49. Wheeler J.A. and Lamb W.E. — Phys.Rev., 55, 858, 1939.

50. Watson K.M. — Phys.Rev., 72, 1060, 1947.

51. Votruba V. — Phys.Rev., 73, 1468, 1948.

52. Heitler W. — Quantum Theory of Radiation - Oxford 1946.

53. Lawson J.L. — Phys.Rev., 75, 433, 1949.

54. Tarrant G.P. — Proc.Camb.Phil.Soc., 28, 475, 1932.

55. Adams G. — Phys.Rev., 74, 1707, 1948.

56. Cowan C.L. — Phys.Rev., 74, 1841, 1948.

57. Jones M.T. — Phys.Rev., 50, 110, 1936.

58. Cork J.M. and Pidd R.W. — Phys.Rev., 66, 227, 1944.

59. Alburger D.E. — Phys.Rev., 73, 344, 1948.

60. Groetzinger G. and Smith L. — Phys.Rev., 67, 53, 1945.

61. Cork J.M. — Phys.Rev., 67, 53, 1945.

62. Mayneord W.V. and Cipriani A.J. — Canadian J. of Res. A., 25, 303, 1947.

63. Petrauskas A.A. et al — Phys.Rev., 63, 389, 1943.

64. McMillan E. Phys.Rev., 46, 325, 1934.

65. Delsasso L.A. et al. Phys.Rev., 46, 1109, 1934.

66. Delsasso L.A. et al. Phys.Rev., 51, 389, 1937.

67. Delsasso L.A. et al. Phys.Rev., 51, 527, 1937.

68. Halpern J.A. and Crane H.R. Phys.Rev., 55, 258, 1939.

69. McDaniel B.D. et al. Phys.Rev., 72, 985, 1947.

70. Stahel E. Strahlentherapie, 31, 50, 1929.
Strahlentherapie, 33, 296, 1929.

71. Murdoch J. et al. Acta Radiologica, 11, 350, 1930.

72. Behnken H. Z.Tech.Phys., 5, 3, 1924.

73. Behnken H. Strahlentherapie, 29, 192, 1928.

74. Duane W. Amer.J.Roent., 19, 461, 1928.

75. Taylor L.S. Radiology, 16, 1, 1931.

76. Kaye G.W.C. and Binks W. Brit.J.Rad., 2, 553, 1929.

77. Failla G. Amer.J.Roent., 21, 47, 1929.

78. Mayneord W.V. and Roberts J.E. Brit.J.Rad., 7, 158, 1934.

79. Failla G. and Henshaw W. Radiology, 17, 1, 1931.

80. Kaye G.W.C. and Binks W. Proc.RoylSoc.A., 161, 564, 1937.

81. Bragg W.H. Studies in Radioactivity, 1912.

82. Fricke H. and Glasser O. Fort.Rontgen Strh., 33, 239, 1925.

83. Gray L.H. Proc.Roy.Soc.A., 124, 647, 1929.

84. Bruzau M. Ann.de.Phys., 11, 5, 1929.

85. Gray L.H. Brit.J.Rad., 10, 600, 1937.
Brit.J.Rad., 10, 721, 1937.

86. Mayneord W.V. and Roberts J.E. — Brit.J.Rad., 10, 365, 1937.

87. Kaye G.W.C. et al. — Rep.Prog.Phys., 6, 95, 1939.

88. Rutherford E, Chadwick J. and Ellis C.D. — Radiations from radioactive substances - Cambridge 1930.

89. Gray L.H. — Proc.Roy.Soc.A., 156, 578, 1936.

90. British Committee for Radiological Units. — Memorandum B.R.U./13, May 1948.

91. Kerst D.W. — Radiology, 40, 120, 1943.

92. Trump J. — Paper before Amer.Rontgen Ray Society 1942 (quoted by Kerst 91)

93. Bethe H. — Ann.d.Phys., 5, 325, 1930.

94. Mayneord W.V. — Nat.Res.Council of Canada, C.R.M.315.

95. Bohr V. — Phil.Mag., 25, 10, 1913. Phil.Mag., 30, 581, 1915.

96. Williams E.J. — Proc.Roy.Soc., 130, 328, 1931.

97. Bethe H. — Zeit.f.Phys., 76, 293, 1932.

98. Bloch F. — Zeit.f.Phys., 81, 363, 1933.

99. Livingston M.S. and Bethe H. — Rev.Mod.Phys., 9, 245, 1937.

100. White M. and Millington S. — Proc.Roy.Soc.A., 120, 701, 1928.

101. Williams E.J. — Proc.Roy.Soc.A., 135, 113, 1932.

102. Lax M. — Phys.Rev., 72, 61, 1947.

103. Quastler H. and Clark R.K. — Amer.J.Roent., 54, 723, 1945.

104. Marinelli L.D. — Amer.J.Roent., 47, 210, 1942.

105. Ellis C.D. and Aston F. — Proc.Roy.Soc.A., 129, 180, 1930.

106. Deutsch M. and Mitzger F. — Phys.Rev., 74, 1640, 1948.

107. Mayneord W.V. and Clarkson J.R. — Brit.J.Rad., 12, 168, 1939.

108. Lamerton L.F. — Brit.J.Rad., 21, 352, 1948.

109. Wyckoff H.O. et al. — J. of Res. of Nat. Bureau of Standards, 41, 223, 1948.

110. Braestrup C.B. and Wyckoff H.O. — Radiology, 51, 840, 1948.

111. Failla G. — Amer.J.Roent., 54, 553, 1945.

112. Braestrup C.B. — Quoted by Failla, Ref.111.

SUMMARY OF THESIS

The work described covers an investigation of some of the physical problems associated with short wavelength X rays.

The radiations emitted from high energy generators are discussed and it is found that the experimental results of the writer and the small number of other experimental results available do not agree with theoretical predictions for the angular distribution of the radiation. Possible explanations are given.

A number of measurements of absorption coefficients of high energy radiations in various materials are reported. Values of the coefficients calculated from the theories for the various absorption processes are also given and the agreement between theory and experiment is, in general, good. A review of other measurements of absorption coefficients using various techniques and at energies up to approximately 90 MeV. show that generally speaking the theories for the various processes are substantiated. Some effects are demonstrated resulting from the change from a decrease of absorption coefficient with increasing energy to an increase with increasing energy resulting from the advent of the pair formation process.

The problem of the measurement of high energy X radiation is discussed and experimental results presented

which indicate that it is possible to measure the radiations in rontgens up to an energy of approximately 30 MeV. Some comparative measurements with American workers show satisfactory agreement with the dosage measuring technique of one team and demonstrate the errors introduced by the method adopted by another team.

New processes which alter the effective stopping power of the materials become evident from the experimental results and values of these stopping powers are deduced.

The problem of measurement of the radiation from radioactive isotopes has also been investigated and measurements made with ionisation chambers of different materials show that a satisfactory system of measurement of the dosage-rate for radiations emitted from these isotopes can be worked out from considerations of the energy absorbed. Values of stopping power calculated from these measurements show good agreement with the values given by Bethe and Gray. Measurements and calculations pertaining to the protection requirements for personnel operating high energy generators are given along with recommendations on the solution of the problem.

Some photographic dosage measurements are also presented from which it is concluded that the sensitivity of photographic film measured in "blackening per rontgen" changes very slowly in this high energy region, a result to be expected theoretically.

Some measurements of the distribution of radiation in and around a scattering medium and the variation of quality of the radiation inside the mass are also presented.

British Journal of Radiology, Vol.XIX, No. 223, July 1946.

A NOTE ON THE AMOUNT OF RADIATION INCIDENT IN THE DEPTHS OF THE PELVIS DURING RADIOLOGICAL PELVIMETRY

By J.H. Martin, B.Sc.,A.Inst.P. and E. Rohan Williams, M.D., F.R.C.P.

Physics Department, Royal Cancer Hospital (Free), London,S.W.3. and Radiological Department, Queen Charlotte's Maternity Hospital, London, W.6.

Amongst radiologists there has always been some unease in carrying out major radiological investigations during pregnancy, especially in its earlier stages. It has seemed desirable actually to measure the amount of radiation incident in the depths of the pelvis during the performance of radiological pelvimetry. This has recently been done at Queen Charlotte's Hospital, and the results are recorded below.

Two patients were selected for the investigation of similar general build, one being fourteen weeks pregnant, the other thirty-seven weeks pregnant. In each patient the ionisation chambers were placed in the postero-superior limits of the vaginal vault by Miss K. Robinson, F.R.C.S., the Resident Surgeon at the Hospital. On each patient, a full standard pelvimetric technique was carried out appropriate to the stage of pregnancy. Briefly, the technique used is as follows:-

(1) Antero-posterior, patient supine, centring in mid-line 2 in. above symphysis pubis, cone covering circle of 17 in. diameter at 37 in.

(2) Supero-inferior, patient sitting inclined backwards, plane of inlet parallel to film, centring 2 in. behind symphysis, cone covering circle 10 in. diameter.

(3) Lateral, patient erect, centring 2 in. above upper margin of greater trochanter, cone covering circle 14 in. diameter.

(4) Subpubic arch projection, patient sitting inclined forwards, centring approximately over spinous process of third lumbar vertebra, cone as in (2).

The focus-film distance used in projections 1, 2 and 3 is 37 in., and in projection 4 is 30 in.

In relation to the bony walls of the pelvis, the chamber in each patient was 1.5 in. anterior to the sacro-coccygeal junction and approximately 1.0 to 1.5 in. below and behind the mid-point of the true pelvic cavity.

The table below is given to show the general build of the two patients chosen.

In order to measure the doses received in the depths of the pelvis during the pelvimetric examination, use was made of "thimble" ionisation chambers. The chambers used were made at the Royal Cancer Hospital (Free). They are pressed out of a bakelite-graphite mixture which gives a

very satisfactory "air-wall." The chambers were charged to a potential of 165 volts, enabling doses up to about 1.3 rontgens to be measured. Measurements were made using a Lindemann electrometer system.

For these experiments, although their wavelength dependence is small, the chambers were calibrated for the wavelength range to be used in the radiographic examination.

In use the chambers were encased in a thin rubber sheath, inserted as described above and left in position during the radiographic examination.

For the measurements made on the patient fourteen weeks pregnant, the chamber was removed after two exposures (projections 1 and 4) and another substituted as slightly higher doses were expected which might have led to the complete discharge of the one chamber if left in position for all four exposures.

The various physical and technical factors, and the results of the measurements, are tabled on page 5.

Comments. It is somewhat gratifying to note that even with this somewhat extensive pelvimetric examination (admittedly without the duplicated exposures of a stereoscopic technique) the dose received at the vaginal vault was less than 0.9 rontgen both early and late in pregnancy.

Patient	Maturity	Height fundus above symphysis	Girth and A-P thickness at different levels above symphysis							
				0 in.	2 in.	4 in.	6 in.	8 in.	10in.	12in.
A	14 weeks	5.5 ins.	Girth	34	33	32	29	27.5	29	30
			Depth	7	7.5	7.75	6.5	6.5	6.75	7
B	37 weeks	9.25 in.	Girth	37.5	35.5	35.5	35.75	36	34	33
			Depth	7.5	8.5	9.5	10.25	10	10	10

Patient	Maturity	Projection	kV.	mA.	Time	F-F distance	Radiation measurement
						in.	
A	14 weeks	1	70	40	2.5	37	0.39r
		4	82	40	3.5	30	0.86 rontgens
		2	92	40	8.0	37	0.47r
		3	92	40	5.0	37	
B	37 weeks	1	77	40	2.5	37	0.80 rontgens
		4	85	40	3.5	30	
		2	100	40	8.0	37	
		3	88	40	6.0	37	

Reprinted from
THE BRITISH JOURNAL OF RADIOLOGY

AUGUST 1946

A COMPUTOR FOR X-RAY ISODOSE CURVE PRODUCTION

By J. H. MARTIN, B.Sc., A.Inst.P.

Physics Department, Royal Cancer Hospital (Free), London, S.W.3

INTRODUCTION

THE distribution of X radiation in planes at various depths below the surface of the skin is frequently required in order to build up volume distributions.

A considerable amount of work has been carried out on the measurement of depth doses under a variety of conditions and as a development of the work done (Mayneord and Lamerton, 1941) Clarkson (1941) used a means of constructing the necessary isodose curves using graphical integration. The method has been further developed by Meredith and Neary (1944).

The method (Meredith and Neary, 1944) is rapid for circular fields but for rectangular fields where the contribution of eight triangular areas to the dose at a point is required in each case it becomes involved and is not sufficiently straightforward to be performed by an unskilled person. The method is illustrated in Fig. 1. The values of p and α are measured for each of eight triangles covering the area of the field; p is then multiplied by a factor $\lambda^{\frac{(f+d)}{f}}$ depending upon the half-value layer of the radiation and the depth of the point O below the surface, the values of the appropriate "scatter integral" for the particular $\lambda^{\frac{(f+d)}{f}}$. p and α involved being obtained from a table and these added to give the total "scatter integral" at the point P.

It will be seen from Fig. 2 that the scatter contribution of area ONM at O is given by

$$\int_{\theta=O}^{\alpha} \int_{r=O}^{p\,Sec\,\theta} \frac{1}{2\pi r} \frac{d}{dr} f(r) r dr \; . \; d\theta$$

It is therefore possible to consider the area $ABCD$ (Fig. 1) to be divided into triangles of 10° angle (Fig. 3) and to integrate over each of these triangles and sum as before. The advantage is that α is constant ($= 10°$) and only p varies. In order to obtain the "scatter integral" for these triangles it is required to measure p in each case and multiply it by a factor $\lambda^{\frac{(f+d)}{f}}$, which is fixed for set conditions of half-value layer and depth below the surface. This product then corresponds to a particular "scatter integral" since α is constant.

In practice the length of the bisector OS should be measured since this will give an integration over OQR, a close approximation to $OQ'R'$ in which we are interested. Performing the integration in this

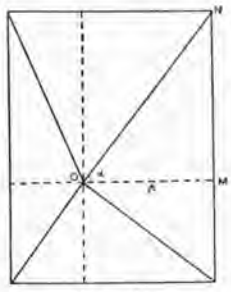

FIG. 1.

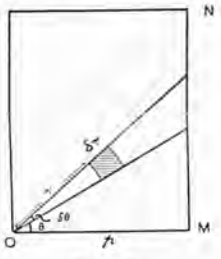

FIG. 2.

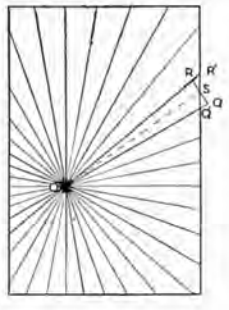

FIG. 3.

way enables the method to be used without further modification for fields of any shape. The above process can obviously be performed by a slide-rule on which $\lambda^{\frac{(f+d)}{f}}$ is multiplied by p and the answer read on a scale on which the graduations are determined by values of the product $\lambda^{\frac{(f+d)}{f}} p$

but which is actually marked in values of the corresponding "scatter integral".

A linear slide-rule was first designed, but owing to difficulty in correlating a linear scale on which to measure p with a log scale for p with which to carry out the multiplication this was abandoned and recourse made to a circular slide-rule of the type shown complete in Fig. 4A and in an exploded view in Fig. 4B.

The part A has a curved edge which has the form $\theta = k \log. p$ where k is an arbitrarily determined constant. The straight edge continued passes through the pivot point. At a radial distance of 10 cm. (the radius of part B) a scale D is fitted to the

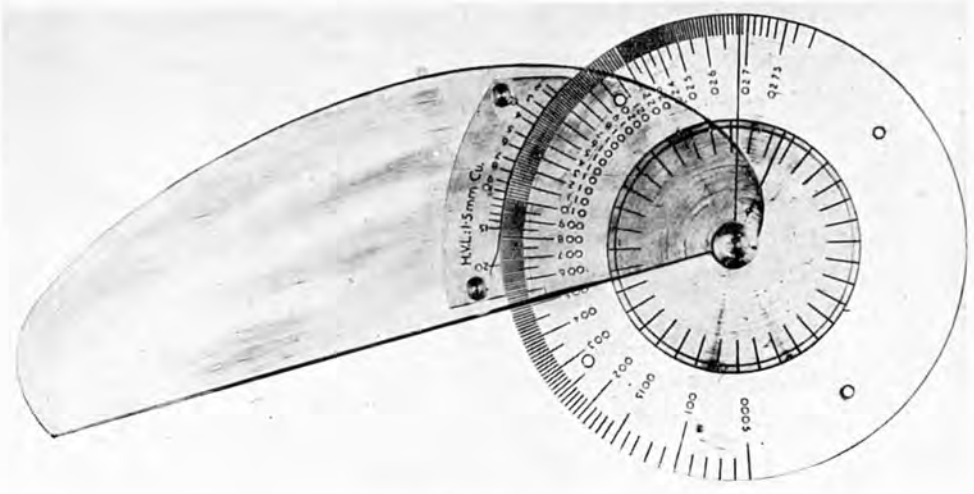

FIG. 4A.

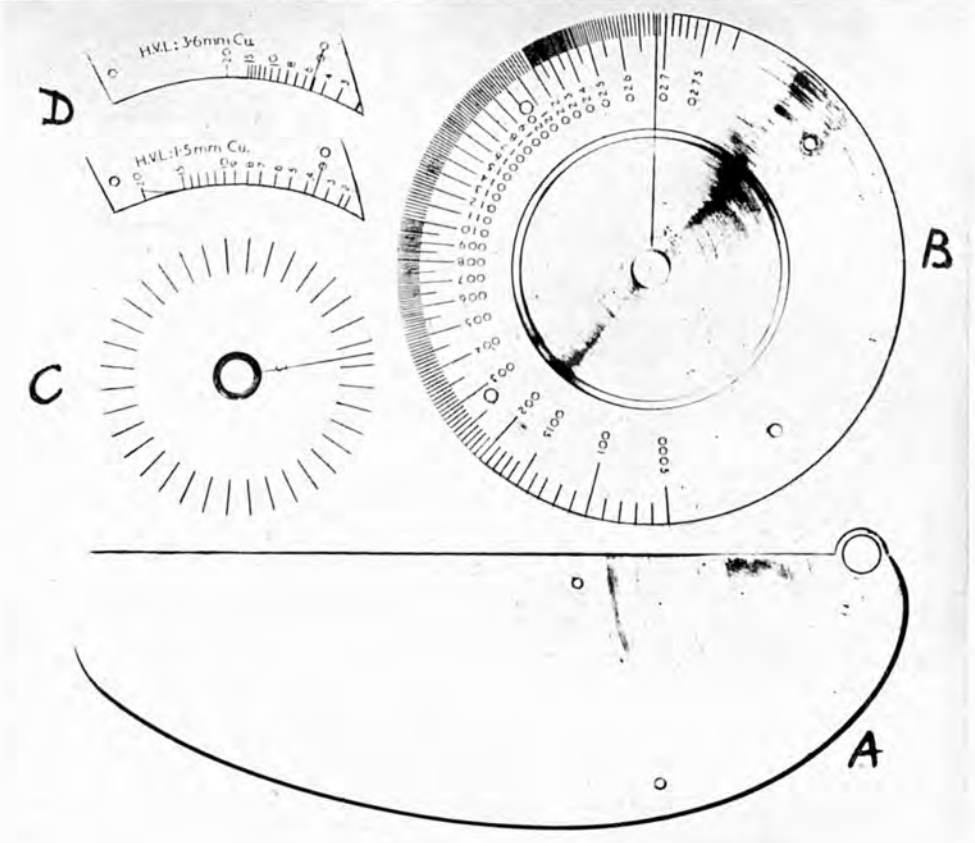

FIG. 4B.

underside of part A such that it moves round flush with part B. This scale is graduated in values of $\lambda^{\frac{(f+d)}{f}}$ at angles given by $\psi = k \log. \lambda^{\frac{(f+d)}{f}}$. The scale is removable, the reason being that for any half-value layer the values of $\lambda^{\frac{(f+d)}{f}}$ vary only with depth so that for a known half-value layer this scale can be graduated in depth, a different scale

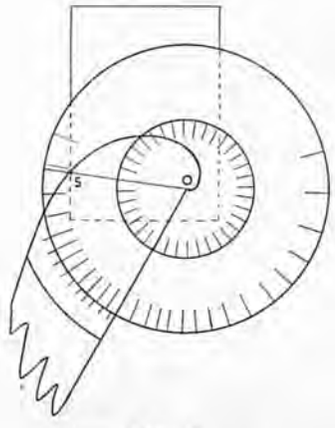

FIG. 5.

being used for each half-value layer. We have made scales for the two half-value layers which we require, namely 1·5 mm. and 3·6 mm. copper. Part B has the values of $\lambda^{\frac{(f+d)}{f}p}$ plotted (corresponding values of "scatter integral" are actually marked) at angles given by $\phi = k \log. \lambda^{\frac{(f+d)}{f}p}$. Part C is merely a protractor marked off in angles of 10° with one intermediate line at 5°. It fits flush into the under surface of B. The three parts when assembled rotate about a central pivot O (Fig. 5).

In use O is placed over the point under consideration (the hollow boss fitted with a central spot facilitates this), the 5° line on C being set parallel to one edge of the field. This enables the computor to be set up in the same position again if checking is required. The field is now divided into triangular areas of 10° apex angle of which the divisions on C are the bisectors.

The base line of the scale B is moved to the first 10° line on C and A rotated until the curved edge is at the intersection of the edge of the field and the base line of scale B (point S, Fig. 5). The rotation of the part A to this point has rotated it through an angle proportional to log.(OS), namely log. p. All that now remains to be done is to multiply by $\lambda^{\frac{(f+d)}{f}}$. This is done by the scale D on part A. The value of the scatter integral is read off on scale B under the appropriate point on the scale D. The process is now repeated, the base line of B is moved to the next 10° line on C and A rotated to the intersection again, and so on right round the field. Obviously at each setting of A the values of the scatter integral for all the depths in which we are interested can be read off against the graduations on the scale D. In this way we obtained for each depth a column of thirty-six figures which are summed on an adding machine. Obtaining the values at all

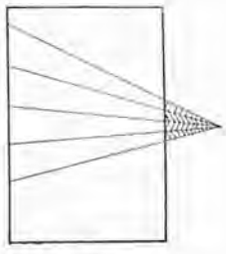

FIG. 6.

depths simultaneously in this way facilitates the calculation of a volume distribution. The radius of B is 10 cm. and consequently for the field sizes generally in use the base line will intersect the edge of the field. If this is not so the straight edge of A can be used to determine the intersection by laying it along the base line of B and in this way it is possible to deal with greater values of p.

From Fig. 3 it will be seen that at the corners of the field discontinuities occur. These discontinuities have been ignored, the triangle being regarded as normal and the resultant error found to be negligible. For points outside the field the method is similar, the triangular areas outside the field (shaded Fig. 6) being subtracted from the total.

Examples

A few examples have been worked out using a 10 × 6 cm. rectangular field; focal-skin distance 50 cm. and half-value layer 3·6 mm. Cu.

The points chosen, when the isodose curves in a plane are desired, are taken one centimetre apart, starting from the axes of the field up to a distance of 1 cm. outside the geometrical edge of the field. Three such points A, B, and C have been selected

(Fig. 7) and the scatter contribution for these points on the surface determined using the computor.

Point *C* is completely inside the field and consequently thirty-six readings will be obtained, all positive:—

0·0143	0·0197	0·0067	0·0143
0·0147	0·0201	0·00685	0·0147
0·0155	0·0172	0·0075	0·0156
0·0169	0·01295	0·0085	0·0169
0·0187	0·0102	0·0099	0·0189
0·0213	0·00865	0·0123	0·0169
0·0210	0·00755	0·0156	0·0155
0·0202	0·00695	0·0147	0·0147
0·0197	0·0067	0·0143	0·0147

Total scatter integral = 0·5105

To obtain the actual "scatter contribution" it is now necessary to multiply by a factor *M* (Table IV, Meredith and Neary, 1944). For half-value layer 3·6 mm. Cu. and focal-skin distance 50 cm. the value of *M* at the surface is 30·5. Therefore the total "scatter contribution" for 100 r primary radiation is 30·5 × 0·5105 = 16·1 r.

Point *B* is at the geometrical corner of the field and consequently only nine readings will be obtained, all of them positive:—

0·0197
0·0201
0·0209
0·0220
0·0235
0·02525
0·0257
0·0253
0·02505

Total scatter integral = 0·2075

Therefore total "scatter contribution" for 100 r primary radiation is 0·2075 × 30·5 = 6·3 r.

Point *A* is outside the geometrical edge of the field and in consequence two columns of figures are obtained. The positive column represents the whole triangles subtended by the far edges of the field at *A* and the negative column those subtended by the near edges. The difference of these figures gives the contribution at *A* due to the field. The figures

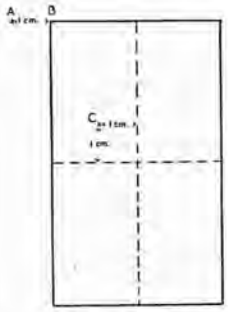

Fig. 7.

obtained using the method described above are as follows:—

Positive	Negative
0·0216	0·0031
0·0219	0·00315
0·0226	0·0035
0·0236	0·0038
0·0248	0·00455
0·0261	0·0058
0·02575	0·00825
0·0253	0·0131
0·19165	0·04525

Therefore total scatter integral = 0·1464

Therefore "scatter contribution" of *A* for 100 r primary radiation is 30·5 × 0·1464 = 4·5 r.

Acknowledgments

I am indebted to Professor W. V. Mayneord for drawing my attention to the possibilities of the method and for his help and interest in developing it; also to Mr. H. Hodt, Jr., who showed considerable patience, ingenuity, and skill in constructing the computor.

References

Clarkson, J. R., *Brit. Journ. Rad.*, 1941, xiv, 265.

Mayneord, W. V., and Lamerton, L. F., *Brit. Journ. Rad.*, 1941, xiv, 255.

Meredith, W. J., and Neary, G. J., *Brit. Journ. Rad.*, 1944, xvii, 75.

Reprinted from
THE BRITISH JOURNAL OF RADIOLOGY
JULY 1947

RADIATION DOSES RECEIVED BY THE SKIN OF A PATIENT DURING ROUTINE DIAGNOSTIC X-RAY EXAMINATIONS

By J. H. MARTIN, B.Sc., A.Inst.P.

Physics Department, Royal Cancer Hospital (Free), London, S.W.3

INTRODUCTION

THERE is a growing tendency in diagnostic X-ray practice either to forget the dose received by the skin of the patient or to dismiss it as being negligible. At first sight it may appear strange that plants of low kilovoltage and exposures of the order of fractions of a second or possibly seconds should result in doses of even a few röntgens. A little reflection, however, will draw the attention to the fact that, although diagnostic plants are of low kilovoltage, high currents are employed and, more important still, low filtration and often short focal-skin distance, the result of which is an output in r/min. often several times that of a therapy plant of higher kilovoltage.

Several workers (Braestrup, 1942; Smedal, 1942; Jäderholm, 1935; Stevenson and Leddy, 1937; Turnbull and Leddy, 1935, Holmgren, 1945; Zimmer, 1935) have realised the possible dangers, especially in unfavourable conditions, and have in many cases measured the doses and indicated the factors which influence the surface dose.

So far, however, no really systematic investigation has been made indicating the average doses received in various examinations and estimating the improvements which may be expected. It is the purpose of this paper to present the available information in this way.

Influence of filter and focal-skin distance factors

In order to assess the effect of filtration and focal-skin distance as factors influencing the skin damage, the output of a diagnostic plant run at 70 kV was measured. This value was selected as being a mean. The output was measured under several conditions of filtration and focal-skin distance, using a 25 r Victoreen condenser chamber. This chamber had been calibrated by the National Physical Laboratory down to a half-value layer of 0·33 mm. Al. The values of the outputs in r/sec./mA plotted against filtration for several focal-skin distances are shown in Fig. 1. The curves have been drawn through the points measured, which do not appear on the diagram. Marked on the diagram are values obtained from other sources (Braestrup, 1942; Smedal, 1942; Stevenson and Leddy, 1937; Barclay and Mayneord). As the filtration used in diagnostic work is so low, the inherent filtration of the tube plays an important part and these curves have, consequently, been plotted against total filtration, *i.e.*, inherent + extra filter. Inherent filtration has been estimated where possible using published curves (Thoraeus, 1940). Since, obviously, no tube can have exactly zero filtration, it has been assumed that the minimum possible filtration is 0·2 mm. Al. The outputs are plotted with backscatter which, however, only amounts to 10–15 per cent. under the conditions used.

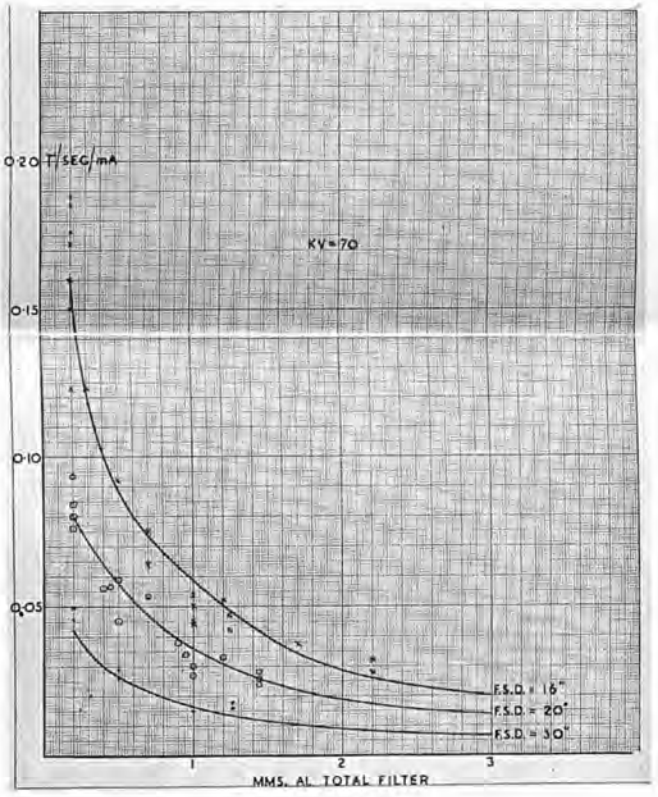

FIG. 1.

It will be seen that the values obtained from other sources fall fairly well on the curves so that they may be used, without errors of magnitude, to assess the

output of a tube under given conditions and they have been so used at a later stage.

Some values of the order of things may be obtained by examining the curves. At 16 in. focal-skin distance a tube with minimum inherent filtration run at, say, 20 mA, gives an output of some 175 r/min., while with a 0·5 mm. Al filter the output falls to 90 r/min. At minimum inherent filtration, increasing the focal-skin distance from 16 in. to 30 in. reduces the output from 175 r/min. to some 50 r/min.

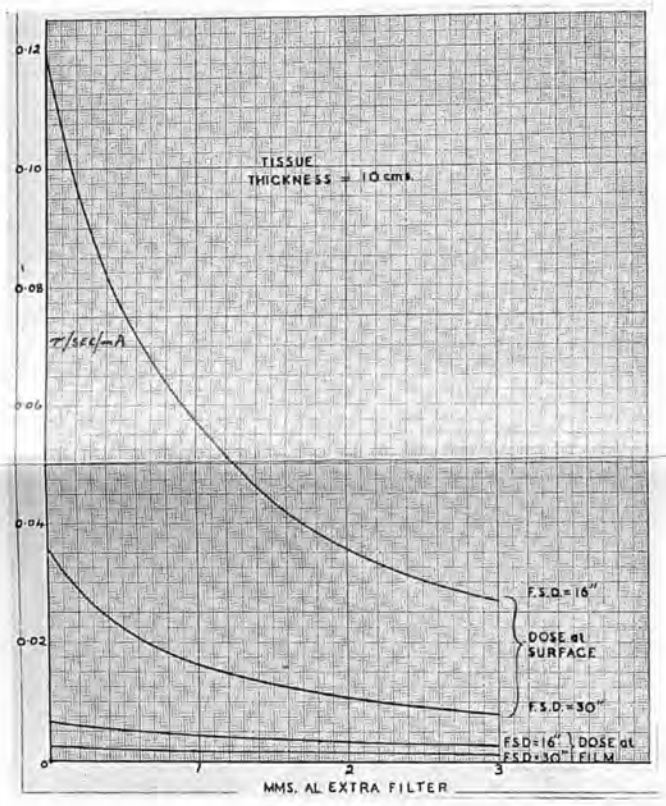

FIG. 2.

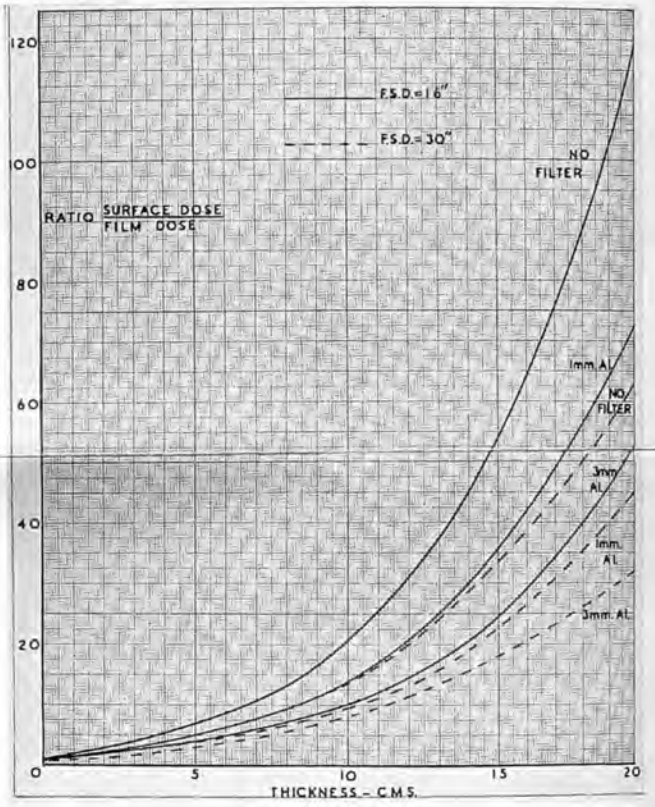

FIG. 3.

These effects are, of course, well realised and are of little value in diagnostic procedures unless, at the same time, the effects of these factors on the dose at the film are studied.

Using a wax phantom and correcting for the wax absorption (Spiers, 1946), values of r/sec./mA at the surface and at the film have been obtained for a tissue thickness of 10 cm. and are shown in Fig. 2 plotted against extra filter thickness at two focal-skin distances, *viz.*, 16 in. and 30 in. Again, calibrated Victoreen chambers were used.

Considering first the 16 in. focal-skin distance case it will be seen that 0·5 mm. Al added filter reduces the surface dose from 0·119 r/sec./mA to 0·075 r/sec./mA, a drop of some 40 per cent. The dose at the film is reduced from 0·0065 r/sec./mA to 0·0052 r/sec./mA, a drop of only 20 per cent. With 1 mm. Al added filter the surface dose is reduced by about 55 per cent., while the film dose is reduced by just over 30 per cent. In the 30 in. focal-skin distance case the inverse square law gives us a further gain and while the 0·5 mm. Al filter reduces the surface dose by 40 per cent. again, the film dose only drops by 13 per cent. With 1 mm. Al filter the surface dose is reduced by 55 per cent. and the film dose by 27 per cent.

A variation of up to 30 per cent. in film dose will in general be undetected on a diagnostic film and in fact as much as 100 per cent. variation will be found in the films used by a single radiologist. Accepting, however, the 30 per cent. drop, it will be seen that, while obtaining a satisfactory radiograph, a reduction in skin dose of over 50 per cent. may be effected by increasing the extra filtration from 0 to 1 mm. Al, no other change in conditions being necessary.

Considering a tube with 0·5 mm. Al extra filter, which is the thickness normally employed, an

increase to 1 mm. Al will reduce the skin dose by 26 per cent., other conditions again remaining the same.

Now investigating the effect of focal-skin distance only it will be seen that, at zero extra filter, by increasing the focal-skin distance from 16 in. to 30 in. the skin dose is reduced by 71 per cent. and the film dose by only 65 per cent. In this case, of course, increased tube loading will be required to keep the film dose within 30 per cent. of the original figure, and so the improvement is not so great as with filtration.

One other case should be considered—the use of a fairly heavy filter of 3 mm. Al. This produces a reduction of about 75 per cent. in the skin dose and about 55 per cent. in the film dose. Assuming that the permissible drop in film dose is only 30 per cent., the exposures will have to be increased 1·8 times and the resultant drop in skin dose will now be just over 60 per cent. It seems, therefore, since the further gain is so small and results in an increased tube loading, that it is not economic to increase the extra filtration beyond 1 mm. Al.

The data may be presented in another and more direct way. The entry dose (*i.e.*, surface dose) can be divided by the exit dose (*i.e.*, film dose) and this ratio plotted against the thickness of tissue involved for various conditions (Fig. 3). These curves represent a kind of inverted percentage depth dose curve series. The measurements have been extended up to 20 cm. tissue thickness. These thicknesses are measured from the film as zero at which, of course, the dose ratio is unity. In the worst case measured, *viz.*, 16 in. focal-skin distance and no extra filter for a tissue thickness of 20 cm., the surface receives 120 times the film dose. The tube used for these measurements had an inherent filter of 0·4 mm. Al, so this ratio might well be greater in other circumstances. Zimmer (1935), in making similar measurements during routine radiography of pregnancy cases, obtained a value of about 100 for this ratio. The conditions are not detailed, but this is interesting verification of the magnitude of the ratio under normal diagnostic conditions.

The order of the dose required at the film when no screens are used is 0·05–0·1 r. The use of screens will enable the dose to be cut by a factor of 10 or more. It would, therefore, be expected that skin doses should not exceed, say, 12 r, and generally to be of the order of 1–2 r. Another factor, however, enters in when use is made of a Potter-Bucky grid. This will increase the surface film dose ratio required.

Effect of Potter-Bucky

The effect of a Potter-Bucky grid has been measured using a Victoreen condenser chamber and bakelite-graphite wall ionization chambers made in this hospital. These have been calibrated against the Victoreen. The ratio of the surface to film dose was again measured (*a*) using the Potter-Bucky, (*b*) without Potter-Bucky, but with the ionization

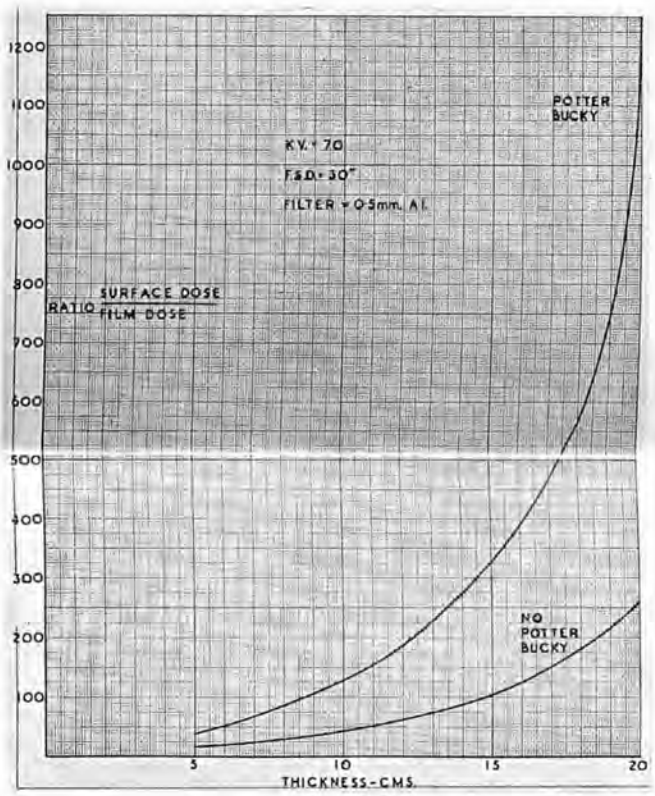

FIG. 4.

chamber measuring the film dose at the same level as in (*a*). This was done for several tissue thicknesses and the ratios plotted as shown in Fig. 4.

Case (*b*) immediately brings out an important point. The ratios here are some three times those shown in Fig. 3. The reason for the difference is that in the cases of Fig. 3 the film dose was the dose at the rear surface of the phantom, while in Fig. 4 the film dose is the dose some 5–7 cm. from the rear surface and with the filtration of the table top, which in this case was 1 mm. Al. As the table top accounts for a 20–30 per cent. drop in the emergent radiation, the thickness and composition of the table top are

obviously of importance (Stevenson and Leddy, 1937). Considering case (*a*) it will be seen that between 5 and 15 cm. tissue thickness the skin to film dose ratio is roughly three times that of case (*b*). Thereafter it rises rapidly until at 20 cm. tissue thickness it is about six times. As the values in case (*b*) are three times those in Fig. 3 it would be expected that the exposure time required to take a radiograph using a Potter-Bucky would be nine times that required for the case without Potter-Bucky. In practice a factor of about 3 is used.

To investigate this discrepancy, three radiographs were taken of the phantom. First without Potter-Bucky and then with the Potter-Bucky grid, using three times and then four times the first exposures. After photometering the films it was found that to obtain equal blackening in the two cases the exposure factor should be about 5. The discrepancy is explainable by the action of the screens. The contribution to the blackening by the screens increases markedly with the hardness of the radiation. Since when employing a Potter-Bucky only primary radiation is used, and is filtered by the table top, the source of discrepancy becomes apparent.

Surface doses in routine practice

So far only the factors affecting the surface dose have been considered. It is now required to obtain an estimate of the values of these doses. Data has been collected for a number of techniques from various sources, including the diagnostic departments of the Royal Cancer Hospital, Royal Free Hospital, Moorfields Eye Hospital, and Queen Charlotte's Hospital, and from published papers (Braestrup, 1942; Smedal, 1942; Jäderholm, 1935; Turnbull and Leddy, 1935; Holmgren, 1945; Zimmer, 1935; Kolbow, 1940). In some of the published work the actual surface doses have been measured, but in the majority of cases the doses have been estimated, using the curves of Fig. 1 along with a curve of output variation with kilovoltage. The results are tabulated below. They represent average values found for the various techniques, but in many cases values well outside these limits have been found.

Chest: The chest is an interesting case as it demonstrates the value of a long focal-skin distance. It would be expected that because of the thickness of the part that a relatively high surface dose would result. That this is not so is due to use of very long focal-skin distance, usually of the order of 5–6 ft. Extreme values are 0·04 r–0·4 r per exposure. Mean value is about 0·2 r/exposure. This value also covers chest tomographs. These figures represent the lowest surface doses found although the thickest filter used was 0·5 mm. Al.

Heart: 0·1 to 0·4 r/exposure.

Heart kymography: Approximately 2 r/exposure.

I.V.P.: Doses range from 0·5 to 1·5 r/exposure.

Skulls, Sinuses: Approximately 4 r/film for A.P. and 1–2 r/film for laterals.

Gastro-intestinal examination (including barium meal work): Range 1 to 8 r/film. Average value is 5 r/film.

Spine: Range 2 to 34 r/film. Average value 5 r/film.

Gall bladder cholecystograms: Average 1·5–4 r/film.

Dental work: Owing to the short focal-skin distance and low filter used these units are very dangerous. The output of the unit used in this hospital is about 250 r/min. Values vary from 1 to 15 r/exposure. The average value is 5 r/film. The danger here lies in the large number of films required with the consequent dangers of overlap.

Pregnancy: The range here is wide. One case of a supero-inferior radiograph resulted in a surface dose of 65 r per film. Average value for this projection is 24 r. Average value for other projections is 10 r/exposure. These high values result from the short focal-skin distance used, rarely more than 20 in.–25 in., and the low filtration.

Some work has been done in connection with this technique to assess the dose received at the ovaries. The author recently made measurements of this (Martin and Williams, 1946) and found a dose of approximately 0·2 r per film. Kolbow (1940) gives a value of 0·1 to 0·5 r/film, while earlier works by Zimmer (1935) and by Witte (1933), and Neef (1934) give estimates of 0·4 to 0·5 r/film for the dose, all of which, considering the variation in techniques used, is in good agreement.

Screening: The variation in surface dosage-rate here is considerable, rising in cases of short focal-skin distance and low filtration to 40 r/min., and Braestrup (1942) quotes a case measured by him in which the dosage-rate was 127 r/min.

Most examinations seem to result in dosage-rates between 10 and 20 r/min. at the skin so that a

screening time of a few minutes will administer quite a heavy dose. An average screening time seems to be 5 minutes. Increased filtration and focal-skin distance are certainly to be recommended.

X-ray Cinematography: Two types of this apparatus were met. One in Sweden (Holmgren, 1945) which photographs the image on the fluorescent screen, and one at the Nuffield Institute at Oxford which takes true radiographs. The two plants seem under the conditions used to give roughly the same dosage-rate of between 4 and 8 r/sec. At Oxford the practice is to expose for about 80 frames which results in a dose to the skin of an average patient of 64 r. The apparatus is already well filtered with 2 mm. Al, but the focal-skin distance is only 17 in.

CONCLUSIONS

It will be apparent from the above data that the skin doses received in these diagnostic examinations must not be neglected, especially if multiple films or repeats are required. Greatest care seems to be necessary in dental and pregnancy radiography and during screening, it being possible in unfavourable screening conditions to deliver an erythema dose in between 2 and 5 minutes.

In almost every case the skin doses could be cut by 50 per cent. by increasing the focal-skin distance or the filter or both, and it would certainly be advisable if the filtration of all diagnostic plants in use were checked and fixed at a definite value, the value to be recommended being 1 mm. Al.

SUMMARY

The paper draws attention to the relatively high output of diagnostic plants under the conditions normally used. The influence of various factors in reducing the surface dose for given conditions at the film is also discussed and finally a table is given indicating (for a number of parts of the body) the order of dose to be expected on the skin during an X-ray examination.

ACKNOWLEDGMENTS

I am indebted to Professor W. V. Mayneord who pointed out the lack of correlated information on the subject and suggested the investigation. I am also grateful to Dr. G. Spiegler and Mr. Leslie Smith, of this hospital, for their assistance in making some of the measurements; also to Miss Mount and Miss Lloyd-Jones, of the X-ray departments of the Royal Free Hospital and Moorfields Eye Hospital respectively, for information regarding techniques used.

REFERENCES

BARCLAY, A. E., and MAYNEORD, W. V., unpublished.
BRAESTRUP, C. B., *Radiology*, 1942, xxxviii, 207.
HAWLEY, S. J., *Radiology*, 1943, xl, 387.
HOLMGREN, B. S., *Acta Rad.*, 1945, xxvi, 286.
JÄDERHOLM, K. B., *Acta Rad.*, 1935, xvi, 518.
KOLBOW, H., *Strahlentherapie*, 1940, lxviii, 620.
MARTIN, J. H., and WILLIAMS, E. R., *Brit. Journ. Rad.*, 1946, xix, 297.
NEEF, TH. C., *Fortschritte a.d. Geb. d. Rönt.*, 1934, I, 86.
SMEDAL, M. D., *Amer. Journ. Roentgenol.*, 1942, xlviii, 807.
SPIERS, F. W., *Brit. Journ. Rad.*, 1946, xix, 52.
STEVENSON, C. A., and LEDDY, E. T., *Amer. Journ. Roentgenol.*, 1937, xxxvii, 70.
THORAEUS, R., *Acta. Rad.*, 1940, xxi, 603.
TURNBULL, A., and LEDDY, E. T., *Amer. Journ. Roentgenol.*, 1935, xxxiv, 258.
WITTE, E., *Fortschritte a.d. Geb. d. Rönt.*, 1933, xlvii, 302.
ZIMMER, K. G., *Fortschritte a.d. Geb. d. Rönt.*, 1935, 51, 418.

6610

6610

Report No.Aero 1801

Report No.Aero 1801

February, 1943.

ROYAL AIRCRAFT ESTABLISHMENT, FARNBOROUGH

Flight measurements of the hinge moments on single ailerons of the Spitfire. Part I. Tests on port aileron No.I

by

D.J. Lyons, B.Sc.(Eng.)
J.H. Martin, B.Sc., A.Inst.P.
and
C.H. Naylor, B.Sc.

M.A.P. Reference:Nil
R.A.E. Reference:Aero/1130.R/28
Item No. :50(6)/1/38

R

SUMMARY

Reasons for enquiry

Flight measurements of the hinge moments of a single aileron of the Spitfire were required to help in the investigation of Spitfire accidents. Comparisons of wind tunnel and flight measurements of aileron hinge moments were also required.

Range of investigation

Measurements of hinge moments on port aileron No.I were made over a speed range from 150 - 400 m.p.h.,A.S.I. The effect of a 'pull-out' on the aileron hinge moments was also determined.

Results

The maximum cable tension recorded was 330 lb. Agreement with wind tunnel tests was excellent up to flight speeds of 200 m.p.h.,A.S.I., but as the speed increased after this, both b_0 and b_2 became more negative than in the tunnel.

Further investigation

Records of stick forces are to be taken simultaneously with the single aileron forces, and the characteristics of other ailerons are to be investigated.

1. Introduction

The hinge moment characteristics of the Frise ailerons on the Spitfire have been thoroughly investigated in the tunnel using both models[1,2] and actual full scale ailerons on full scale wings[3]. These tests have shown large variations in the hinge moment characteristics, especially in the degree of balance and the value of b_0 (the hinge moment coefficient at zero angle of incidence and zero aileron angle). In flight, however, although much evidence was available on both fabric[4] and metal[5,6] covered ailerons, this was all obtained in terms of pilot's stick force,

and thus, only the total hinge moments of both ailerons taken together could be deduced. There was, therefore, no means of obtaining, other than from wind tunnel tests, which as pointed out above showed considerable variation, the tensions which were occurring in the aileron operating cables.

In connection with the investigation of Spitfire accidents, however, it was considered important to have flight measurements of the cable tensions. It was decided therefore, to measure in flight the hinge moments on an individual aileron on the Spitfire to obtain this information and at the same time to investigate the following points:-

(a) The degree of agreement between the aileron hinge moments measured in flight and the wind tunnel measurements.

(b) The change in aileron characteristics with aircraft speed with especial reference to compressibility effects.

To provide the wind tunnel comparisons, tests were to be made of the same wing-aileron combination in the large tunnel.

2. Description of apparatus

A G.A. of the Spitfire II used for these tests is given in Fig.1 and a drawing of the port, metal-covered aileron used for the tests, with three specimen sections in Fig.2. This aileron will be designated as port aileron No.I as it is intended to test more ailerons. A table is included giving relevant details of the aileron and aircraft.

On the normal Spitfire, the control column is connected by a chain drive to a shaft about 6 in. long, at the end of which is fixed a double drum to which the aileron wires are attached. To obtain the hinge moments on one aileron, this double drum was split into two, and effectively separated by a solid torque shaft (see Fig.3A) so that the rear drum drove the port aileron, and the front the starboard aileron. The torque on this torque shaft is then solely due to the port aileron, and the deflections of it give a direct measure of the difference in the tension of the cables in the port circuit.

The deflections of the torque shaft were measured by a Micro-desynn system in the following manner. An arm (see Fig.3B) which was fixed to the rear or port aileron drum, passed through a large clearance hole in the front aileron drum, and was connected with the operating needle of the Micro-desynn transmitter. The transmitter itself was attached firmly to the front end of the torque shaft. The effective length of this torque shaft was about 3 in. and the point at which the deflections were measured was about $2\frac{1}{2}$ in. from the shaft centre line. The Micro-desynn system was found to be capable of measuring the deflections to an accuracy of $\pm 1/4000$ in., and the accuracy of the torque measurement (static conditions) was thereby about ± 3 lb. in.

To obtain the greatest possible accuracy in the measurements, the friction in the aileron circuit was reduced, as far as possible, by careful attention to the circuit, and by slackening the cables as far as was consistent with safety. The measured friction in the port aileron circuit on the ground (static and unloaded conditions) was ± 1 lb. at the stick top.

The measuring unit was first calibrated by itself, so that the cable tensions could be directly obtained from the Desynn indication, and then the whole system was calibrated in place on the aircraft, by applying known moments to the aileron itself with varying aileron angle. This method eliminated changes in the gearing between the aileron drum and the aileron due to distortion of the circuit when loaded, which, incidentally were found to be quite large, and a chart could be drawn from which the hinge moments could be read directly knowing the Desynn indication and aileron angle only, and without reference to the aileron stick gearing curve (Fig.4). The friction which was found to alter slightly with aileron load was allowed for by taking measurements of the moving friction under all loading conditions and including it in the chart mentioned above. The friction in flight was assumed, for want of better information, to be the same as on the ground.

The indicator of the Micro-desynn system was mounted on an instrument panel, together with the indicator of another Desynn system, which measured the aileron angle at the inboard end of the aileron relative to the wing chord, and a timing device was also included. This panel was photographed with a ciné camera so that simultaneous records of aileron angle, hinge moment and time were taken.

3. Method of test

The hinge moment coefficients measured on an aileron during a pure rolling manoeuvre can be expressed by the following equation, assuming, for the present, linear coefficients, and the usual conventions:-

$$C_H = b_0 + b_1(\alpha' + \Delta\alpha_1 + \Delta\alpha_2) + b_2\zeta$$

where α' = wing incidence at the mid-aileron position corresponding to straight flight at the forward speed considered,

and $\Delta\alpha_1$ = change in wing incidence at mid-aileron due to the instantaneous rate of roll,

$\Delta\alpha_2$ = change in wing incidence at mid-aileron due to the wing twist.

To compare these hinge moments measured in flight with wind tunnel curves obtained at constant α, the value of the term $b_1(\Delta\alpha_1 + \Delta\alpha_2)$ must be determined as this part of the α term varies with ζ. Now during the series of flight tests, it was decided that the hinge moment should always be measured whilst the pilot was steadily applying aileron, at as near a constant a rate as possible, for the following reasons:-

(i) It is possible to know in which direction the friction was acting, so that full advantage could be taken of the friction measurements described in §2.

(ii) During one application of aileron a considerable number of points were obtained (determined by the number of ciné frames taken), as against the one point per application that would be obtained, if as is usual, the hinge moment at a steady rate of roll was measured.

(iii) If the rate of aileron application is fairly high, the $b_1 \Delta\alpha_1$ term is kept small.

The inertia of the aileron and circuit will alter the apparent hinge moments during the period in which the pilot is accelerating the stick, but ground tests have shown that the effect is small for the rates of applications used even at low speeds.

To obtain the $b_1 \Delta\alpha_1$ term under these conditions, calculations were made of the instantaneous values of the rate of roll during the steady application of the aileron. The theory of these calculations is given in the Appendix. It was necessary for these calculations, however, to know the values of $d\alpha/d\zeta$ for the steady rate of roll conditions ($d\alpha/d\zeta_0$), and these were obtained from measurements previously made on the same aircraft[6]. These are plotted in Fig.5. Fig.6 gives the calculated values of $d\alpha/d\zeta$ against time for a series of forward speeds. It will be noted that after one second from the start of application of the control, there is extremely little lag behind the maximum value of $d\alpha/d\zeta$ especially at high speed, in fact as shown in the Appendix the lag in $\Delta\alpha_1$ becomes constant and equal to a constant times A/L_p

where A is the rolling moment of inertia.

and L_p is the damping moment due to unit rate of roll.

The change in incidence of the wing, $\Delta\alpha_2$, arising from wing twist due to aileron angle, was calculated using the method described in Ref.7, and values of the constants for the Spitfire wing supplied by S.M.E. Department of the Royal Aircraft Establishment.

Therefore for any given conditions of aileron angle, time from start of application, and forward speed, the values of C_H, ζ and α at the mid-aileron position can be found, and by using the results obtained for varying forward speeds it was possible to construct C_H, α curves for constant values of ζ, and from them to deduce C_H, ζ curves for constant values of α.

4. Range of investigation

Records of aileron forces were taken at an average height of 5,000 ft., under the following conditions:-

(a) In straight flight at the following range of speeds, 150, 200, 250, 300, 350 and 400 m.p.h., A.S.I., with varying rate of application of the ailerons.

(b) During a pull out at 4g at 300 m.p.h., A.S.I., with varying rate of application of the ailerons.

During all flights the aircraft was trimmed laterally level stick free by adjustment of the radiator flap before the commencement of aileron application.

5. Results

5.1. Cable tensions

The highest tension ever recorded during the tests was 330 lb. It is here assumed that one cable is slack, but this is quite justified as the cables were not unduly taut on the ground.

It would be possible however to reach a higher cable tension with the same aerodynamic stick forces by pretensioning the cables greater than 165 lb. when the maximum cable tension would be

$(T_o + 165)$lb. where T_o is the initial tension in the cable circuit.

It is however extremely unlikely that such an excessive pretensioning would occur, as tests have shown the friction forces on the control column became unduly high when T_o is greater than 60 lb. and the greatest ever recorded during a survey of Service Spitfires was about 110 lb.

The nominal breaking load of the cables in the Spitfire aileron circuit is 15 cwt.

5.2. Hinge moments uncorrected for incidence changes

In Figs.7-12 are given the hinge moment curves as deduced directly from the records taken, over the range of speeds from 150 - 400 m.p.h.,A.S.I., and for different rates of aileron application. They represent the actual contribution to the pilot's stick force, in terms of C_H, made by the port aileron. There is no large variation in the C_H, ξ curves with change in rate of application of the aileron, though in general as the aileron moved up, increase in rate of application decreased the value of Kb_2 and where the aileron moved down, increase in rate of application increased the value of Kb_2

where, as is conventional, $Kb_2 = b_2\left(1 + \frac{\Delta\alpha}{\Delta\xi}\frac{b_1}{b_2}\right)$.

It will also be seen that the balance of the aileron decreases with increase in speed, the aileron being almost overbalanced at low speed for small negative values of ξ.

Fig.13 shows the hinge moment curves as measured during a "4g" pull out at 300 m.p.h.,A.S.I. It will be seen that there is little difference from the curves recorded in level flight.

A further point of interest in Fig.10, is that the maximum value of C_H of -0.094 on the port aileron corresponds to a stick force of approximately 110 lb. The pilot was, therefore, either putting on far more stick force than the usually accepted maximum of 60 - 80 lb., or the starboard aileron was supplying at the corresponding aileron angle (about -14^0), a contribution to the stick force of the order of -30 to -50 lb.

Later tests have shown that pilots have actually applied stick forces of 90 - 100 lb. at the aileron control of this aircraft in flight.

5.3. Aileron vibration and compresibility effects

During the tests the pilots reported that at 200 m.p.h., A.S.I., and above, as a certain aileron angle was reached (this angle varied with speed) a vibration of slow frequency occurred on the aileron. The approximate aileron angle at which this occurred, as judged by the oscillation of the hinge moment readings, is marked on each of the Figs.7-13. The vibration was found to worsen with speed, being decidedly unpleasant to the pilot at 400 m.p.h. It will be noticed that

as the aileron angle is increased after the vibration has started, there is a tendency for the C_H, ζ points to scatter, and in Fig.3 the curve is clearly seen to flatten out or even show reversed slope. It was considered that the explanation of these phenomena was that the local flow round the aileron nose, projecting from the lower wing surface, was reaching the critical speed for compressibility effects. Previous evidence has shown that both vibration and overbalance of controls can be encountered when shock waves are generated[8].

To demonstrate the probability that shock waves are causing the trouble, a curve showing the peak suction on the aileron nose, plotted against aileron angle has been given in Fig.14a for a typical Spitfire aileron tested in the large wind tunnel (metal-covered aileron No.4), and in Fig.14b the deduced curve showing the aileron angle at which the local flow around this particular aileron would reach the critical Mach number. This angle is plotted against the indicated speed at 5,000 ft., the average height of the tests. Also given in Fig.14B is the experimental curve for the aileron angle at which the vibration began in flight. The curves, although for different ailerons, show similar tendencies, and agree fairly well at the high speeds where the accuracy of the experimental readings is greatest.

It would also be expected from Fig.14A, that the shock wave effect would disappear on passing a further aileron angle, for the peak suction diminished after $\zeta = 18^0$ for the No.4 metal aileron. One curve in Fig.10 does show this, a steady hinge moment curve recommencing at about $\zeta = 16^0$, but as this angle is rather low it is a possibility that a stable shock wave formation is arising instead.

5.4. Change of droop with speed

The aileron angle relative to the wing chord in straight flight changes considerably with speed, due to

(a) the circuit stretching as the load increases.
(b) any change in lateral trim of the aircraft.

It is not possible to separate these two effects, so the combined effect has been called the aileron droop, and has been measured when the stick force was zero by trimming out any roll caused by release of the control column by means of the radiator flap. The amount of droop for any forward speed is marked on all the figures from 7-12 and in Fig.15 the aileron droop has been plotted against speed.

5.5. Comparison with wind tunnel tests

By use of the method described in §3 curves of C_H against α for constant values of ζ have been constructed in Fig.16. Also included are the similar curves obtained from wind tunnel tests on the same aileron-wing combination[9].

There are therefore three types of C_H, α curves in Fig.16,

(i) for a constant speed of 68 m.p.h. (tunnel tests).
(ii) for a constant speed of 303 m.p.h. in flight, obtained by varying the wing loading, by varying the "g" on the aircraft.

(iii) for a constant wing loading, and therefore for a varying speed in flight.

For the sake of clarity, the curves for condition (iii) have been repeated in Fig.16A, with forward speeds in m.p.h.,A.S.I., spotted along the curves to illustrate the speed alteration along these constant wing loading curves.

Examination of a particular family of these curves in Fig.16, for the value of $\zeta = 0^{\circ}$, shows that,

(a) $dC_H/d\alpha$ (i.e. b_1) is reasonably the same for the conditions of (i) and (ii) above and for (iii) up to 200 m.p.h.,A.S.I.

(b) the C_H, α curves from the tunnel tests and for the condition (iii) up to 200 m.p.h. are reasonably the same.

(c) above 200 m.p.h. the C_H, α curves for condition (iii) change slope abruptly and become very positive in slope.

From these facts it follows that the value of $-b_0$ must increase with speed, for b_1 is the same at 68 m.p.h. and 303 m.p.h. and yet there is a large interval in C_H, between the C_H, α curves for these two conditions. Now by using the curve for condition (iii) in Fig.16 for $\zeta = 0^{\circ}$, and the assumption that b_1 is constant over the whole speed range from 150 - 400 m.p.h., A.S.I., the actual variation of b_0 with speed can be obtained. This is plotted in Fig.17. The increase in $-b_0$ with speed is an important factor in the determination of the cable tension, and though the reason for it has not been established, much is probably due to a change in boundary layer conditions. A small increase of about -0.003 in b_0 would be expected from compressibility consideration, by assuming Glauert's law that the forces increase in ratio of $1/\sqrt{1 - m^2}$. Further experiments are to be made on this point, including the testing of a number of other ailerons on this aeroplane.

Direct comparisons of the C_H, ζ curves, obtained from flight with the curves obtained from wind tunnel tests are given in Figs.18 and 19. In both these figures, the flight curves are deduced from Fig.16 or 16A, by assuming b_1 constant for a given ζ, but allowing for the variation in b_1 with change in ζ. An example of the method used is shown in Fig.16A, where the point for $\zeta = +8^{\circ}$ at 400 m.p.h.,A.S.I. (A) is corrected from the flight incidence to a standard incidence of -2.3° (point B), by drawing the line AB parallel to the mean b_1 curve for $\zeta = +8^{\circ}$. The point B is then plotted on the C_H, ζ curve (see Fig.19). Fig.18 shows the variation in the hinge moment curves with speed for a constant wing incidence of 0°, and Fig.19 gives a comparison of the C_H, ζ curves for three flight speeds with the wind tunnel curves taken at the corresponding wing incidences. Both these figures show the excellent agreement of flight tests with the wind tunnel tests up to 200 m.p.h., after which the curves separate due to the increase in $-b_0$ and steepen in slope. The reason for the increase in slope of the C_H, ζ curves is not fully known, but again, the effect of compressibility would be to increase the slope in the ratio of $1/\sqrt{1 - m^2}$. This does account for much

of the increase when large ζ variations are considered, but does not account for the "flat" on the curve at small negative ζ values at low speeds, disappearing as the speed is increased.

The errors in the final curves in Figs.18 and 19 can be divided into two parts (a) experimental, (b) theoretical in the corrections for the $\Delta\alpha$ changes. The experimental errors can be seen in the scatter of the points in Figs.7-13, the accuracy increasing rapidly as the speed is increased. The errors due to the theoretical corrections should also be quite small, for the value of b_1 is low and therefore the true value of α does not need to be known to any great accuracy.

6. Conclusions

(i) The cable tensions in the port aileron circuit never exceeded 330 lb. during the whole series of tests. But it should be noted that for this aileron the b_0 was low in comparison to the tunnel range of -0.01 to -0.05, and that the aileron was quite well balanced, Kb_2 being about -0.1 at 400 m.p.h.,A.S.I.

(ii) The aileron hinge moment characteristics agreed well with the tunnel tests on the same aileron wing combination at low flight speeds, but as the speed increased both the b_0 and the b_2 became more negative. At 150 and 200 m.p.h.,A.S.I. the b_0 was -0.013, but by 400 m.p.h. this had increased to -0.026. A little of both these variations can be attributed to compressibility effects.

(iii) A slow period vibration occurred on the aileron at an angle which varied with speed. This vibration was probably due to a shock wave coming off the aileron nose and when it occurred there was considerable scatter of the points on the C_H, ζ curve, especially at high speeds, and in one case in which more than the usual amount of aileron was applied, the curve was clearly seen to be flattening out in this region.

7. Further investigation

(i) Tests are being made with the aircraft and ailerons in the same condition as in the experiments described here, but measuring both the stick force and the port aileron hinge moments. The starboard hinge moments will thus be determinable.

(ii) Tests are to be made of a number of port ailerons, to check the variation of b_0 and b_2 on these ailerons with speed and obtain information on the consistency of the characteristics from aileron to aileron.

REFERENCES

No.	Author	Title, etc.
1	Nivision, Nicholson and Gray	Spitfire aileron tests in the 24 ft. tunnel. Part I - Half scale tests. R.A.E. Report No.Aero 1775. September, 1942.
2	Somerville and Jefferies	Comparative tests in the 24 ft. and 7 ft. tunnels on a ½ scale Spitfire aileron. R.A.E. Technical Note No.Aero 1009 (Wind Tunnels). August, 1942.
3	Nicholson, Gray and Roe	Spitfire aileron tests in 24 ft. tunnel. Part II - Full scale tests. R.A.E. Report Not yet published.
4	Morris and Morgan	Aileron tests on Spitfire K.9944. R.A.E. Report No.B.A.1667. April, 1941.
5	-	A collection of aileron data. R.A.E. Report No.Aero 1708. October, 1941.
6	-	Interim note on fighter aileron comparison, Spitfire and Mustang. R.A.E. Technical Note No.Aero 1001 (Flight). August, 1942.
7	Pugsley and Roxbee Cox	The aileron power of a monoplane. R. & M. No.1640. April, 1934.
8	Young	A survey of compressibility effects in aeronautics. R.A.E. Report No.Aero 1725. (5749). February, 1942.
9	Gray	Tunnel tests on a "Spitfire" aileron for direct comparison with hinge moments in flight. R.A.E. Technical Note No.Aero 1050 (Large Tunnel). October, 1942.

Appendix

The estimation of rate of roll during steady application of the ailerons

The general equation of motion in roll during application of aileron, assuming no yaw, is as follows,

$$A\dot{p} = L_t + L_p.p \qquad \ldots \ldots \ldots \ldots \quad (1)$$

where A is the rolling moment of inertia.
p is the angular velocity in roll.
L_p is the rolling moment due to roll.
L_t is the applied aileron rolling moment.

Now let us assume that the aileron is applied at a steady rate and that we can represent L_t by $R.t$ where R is a constant varying with the rate of application of the control. This also assumes that there is no delay in the building of the rolling moment.

Then we can write

$$\frac{dp}{dt} - \frac{L_p}{A}.p = \frac{R.t}{A} \qquad \ldots \ldots \ldots \ldots \quad (2)$$

$$\text{and hence } pe^{-\frac{L_p t}{A}} = -\frac{R}{A}\left[\frac{t}{L_p/A}e^{-\frac{L_p t}{A}} + \frac{e^{-\frac{L_p t}{A}}}{(L_p/A)^2}\right] + C$$

now $p = 0$ when $t = 0$

$$\therefore C = \frac{R\,A}{L_p^2}$$

$$\therefore p = \frac{R}{A}\left[\left(\frac{A}{L_p}\right)^2 e^{\frac{L_p t}{A}} - t\left(\frac{A}{L_p}\right) - \left(\frac{A}{L_p}\right)^2\right] \qquad \ldots \ldots \ldots \quad (3)$$

$$\text{and } \frac{dp}{dt} = \frac{R}{A}\left[\frac{A}{L_p}e^{\frac{L_p t}{A}} - \frac{A}{L_p}\right] \qquad \ldots \ldots \ldots \quad (4)$$

Now the sign of L_p is negative

$$\therefore \text{ when } t = 0 \quad \frac{dp}{dt} = 0.$$

$$\text{and when } t = \infty \quad \frac{dp}{dt} = -\frac{R}{L_p}$$

Now if A is assumed equal to zero from equation (2) it follows that $dp/dt = -R/L_p$.

Therefore the curves of p against time for any moment of inertia become parallel at ∞.

Now if we call the rate of roll assuming no inertia p^1.

Then the lag in the rate of roll due to inertia

$$p^1 - p = \frac{R}{A}\left[\left(\frac{A}{L_p}\right)^2 - \left(\frac{A}{L_p}\right)^2 e^{\frac{L_p t}{A}}\right] = \frac{RA}{L_p{}^2}\left[1 - e^{\frac{L_p}{A}t}\right]$$

which tends to $RA/L_p{}^2$ as $t \longrightarrow \infty$.

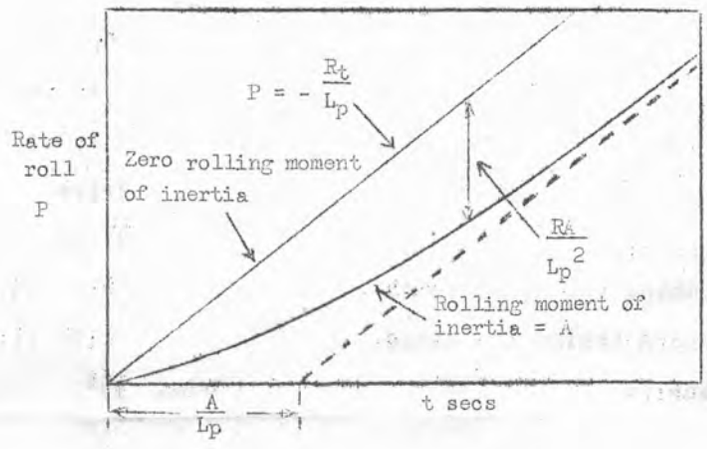

Now the change in incidence $\Delta\alpha$, at mid-aileron due to rate of roll is equal to $p\ell/V$.

where ℓ is the distance of the mid-aileron point from the C.L. and V is the forward speed of the aeroplane.

$\therefore$ from equation (3)

$$\Delta\alpha = \frac{\xi}{V} \cdot \frac{R}{A}\left[\left(\frac{A}{L_p}\right)^2 e^{\frac{L_p t}{A}} - t\left(\frac{A}{L_p}\right) - \left(\frac{A}{L_p}\right)^2\right] \quad \ldots \quad \ldots \quad \ldots \quad (5)$$

When the aeroplane has a steady rate of roll at a given value of ξ, let us call the change in α at the mid-aileron position $\Delta\alpha_o$.

$$\text{Then } \Delta\alpha_o = -\frac{L_T \ell}{L_p V} = \frac{Rt.\ell}{L_p V} \quad \ldots \quad \ldots \quad \ldots \quad (6)$$

$$\therefore \text{ from (5) and (6) } \Delta\alpha = \Delta\alpha_o\left[1 + \frac{A}{tL_p}\left(1 - e^{\frac{L_p t}{A}}\right)\right] \quad \ldots \quad (7)$$

Then from equation (7) knowing the value of A, L_p and $\Delta\alpha_o$, it is possible to deduce the value of $\Delta\alpha$, for any rate of application of the control, at any particular value of ξ.

Table

Aileron and aircraft data

Weight during tests.		6,000 lb.
Wing area (gross).		242 sq.ft.
Wing loading.		24.8 lb./sq.ft.
Span.		37.0 ft.
Aspect ratio.		5.7
Dihedral.		6.0°
Wing section	Root	N.A.C.A.2213
	Tip	N.A.C.A.2205
Aileron type.		Frise
Percentage balance.		37.9%
Aileron area behind the hinge (each).		6.86 sq.ft.
Aileron mean chord behind the hinge.		1.00 ft.
Aileron max. angles	Down	19°
	Up	25°
Maximum stick travel.		±8.0 in.
Droop.		+1.8°
Aileron area/wing area.		0.078
Aileron chord/wing chord.		0.174
Aileron span/wing span.		0.37
Wing thickness/wing chord.	Inboard end of aileron	0.106
	Outboard end of aileron	0.075

FIG. 1

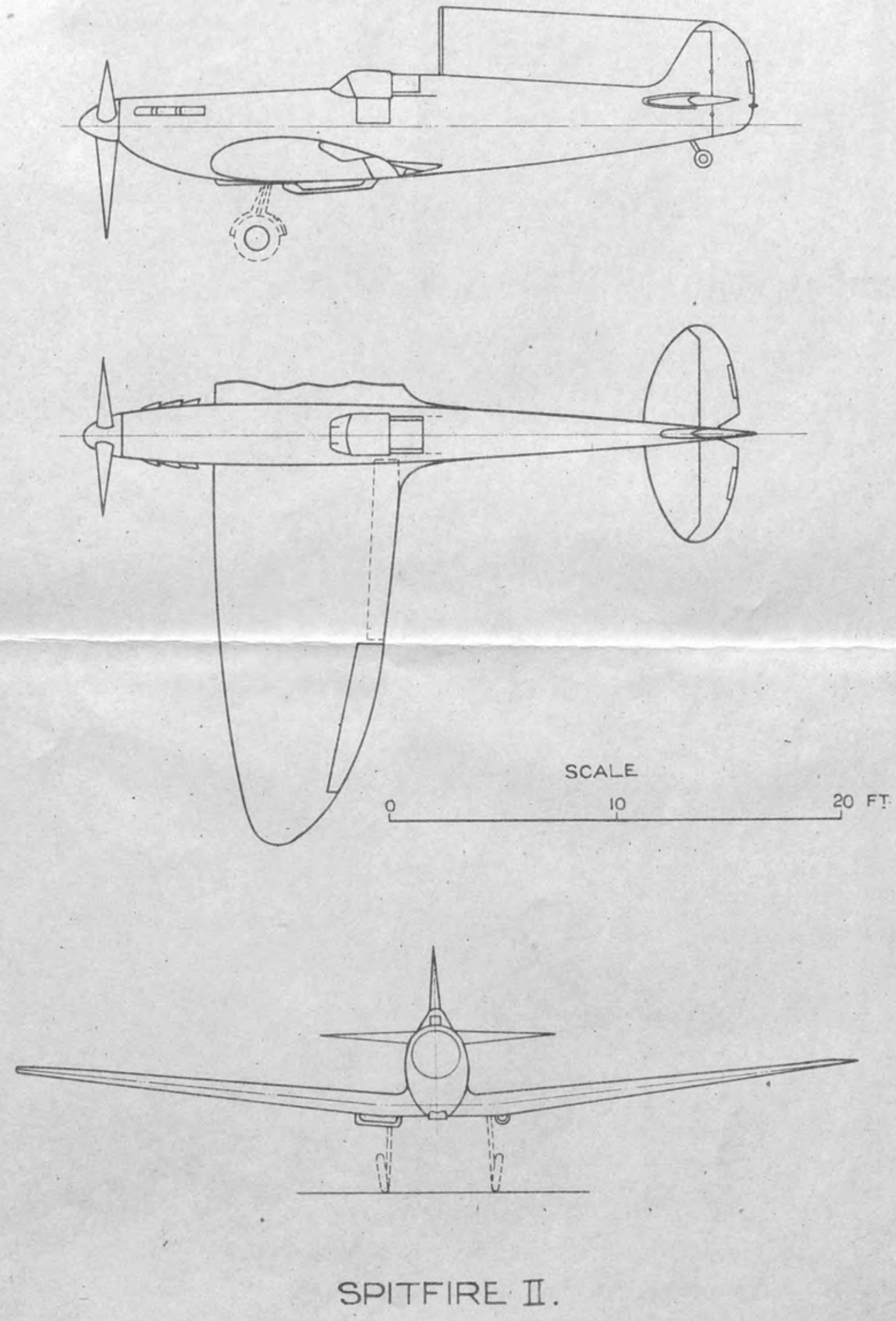

SPITFIRE II.

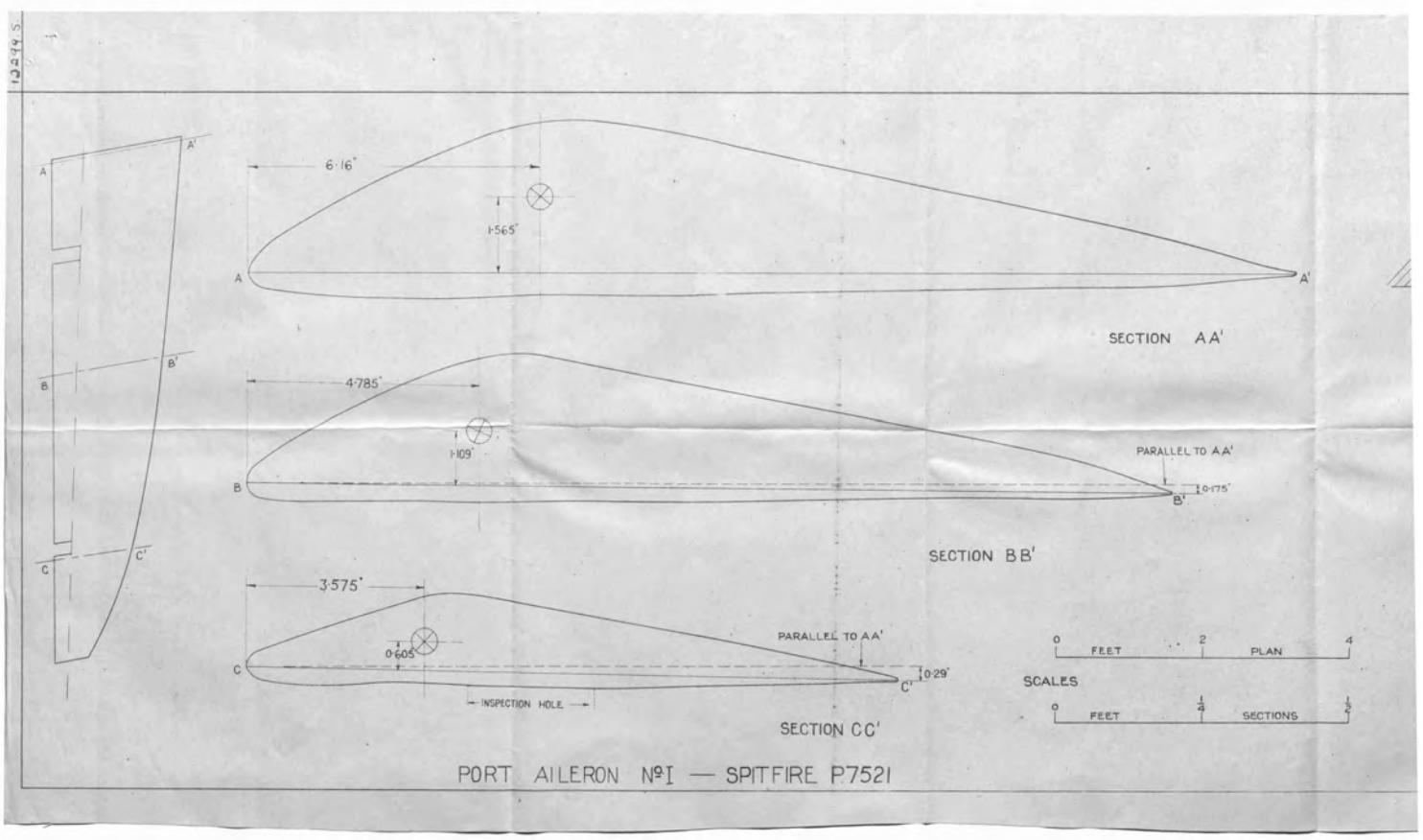
10279 S.
A
A'
B
B'
C
C'
6·16"
1·565"
SECTION AA'
4·785"
1·109"
PARALLEL TO AA'
0·175"
SECTION BB'
3·575"
0·605"
PARALLEL TO AA'
0·29"
INSPECTION HOLE
SECTION CC'
0 FEET 2 PLAN 4
SCALES
0 FEET SECTIONS
PORT AILERON Nº I — SPITFIRE P.7521

FIG. 2

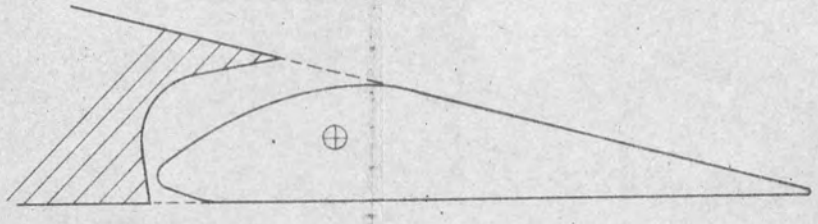

INBOARD SECTION

OUTBOARD SECTION

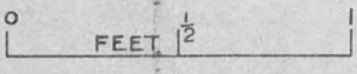

SKETCH OF SHROUD SECTIONS

12300.S.

FIG. 3

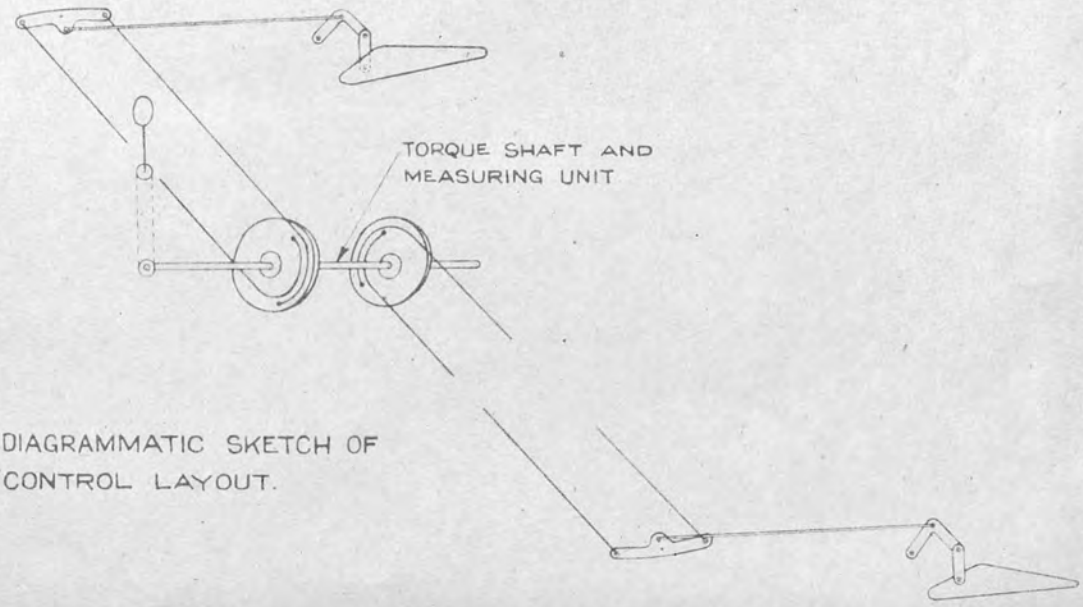

(A) DIAGRAMMATIC SKETCH OF CONTROL LAYOUT.

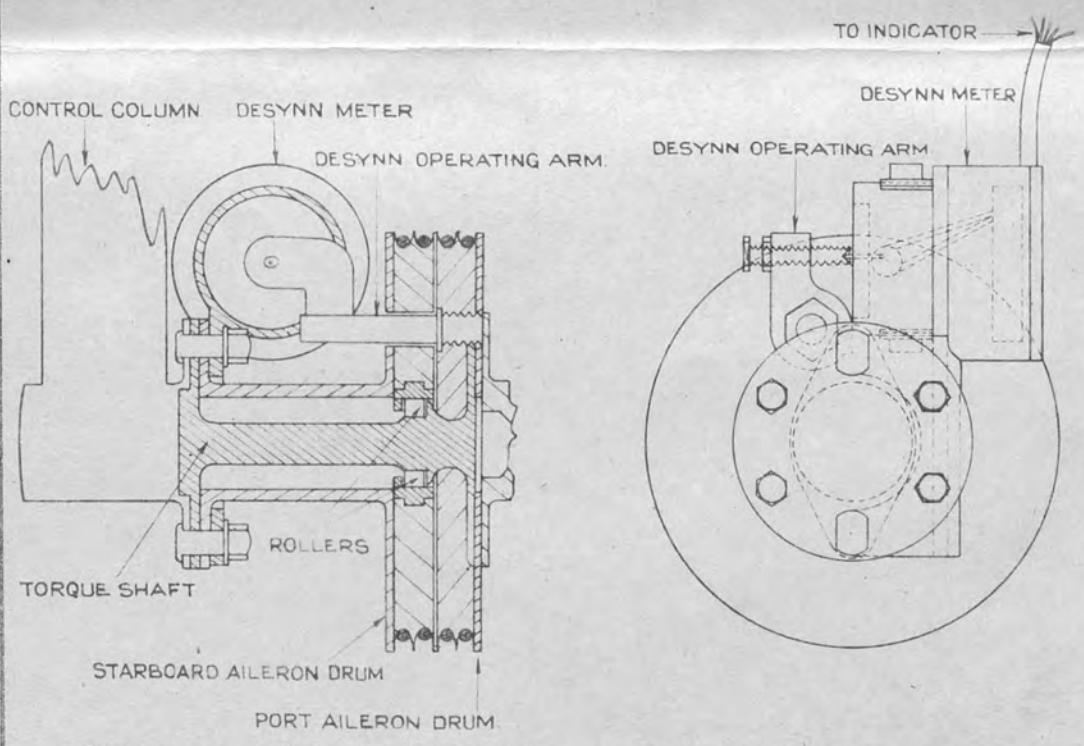

(B) GENERAL ARRANGEMENT OF TORQUE MEASURING UNIT
SKETCHES OF HINGE MOMENT MEASURING APPARATUS
FOR SPITFIRE AILERONS.

FIG.4

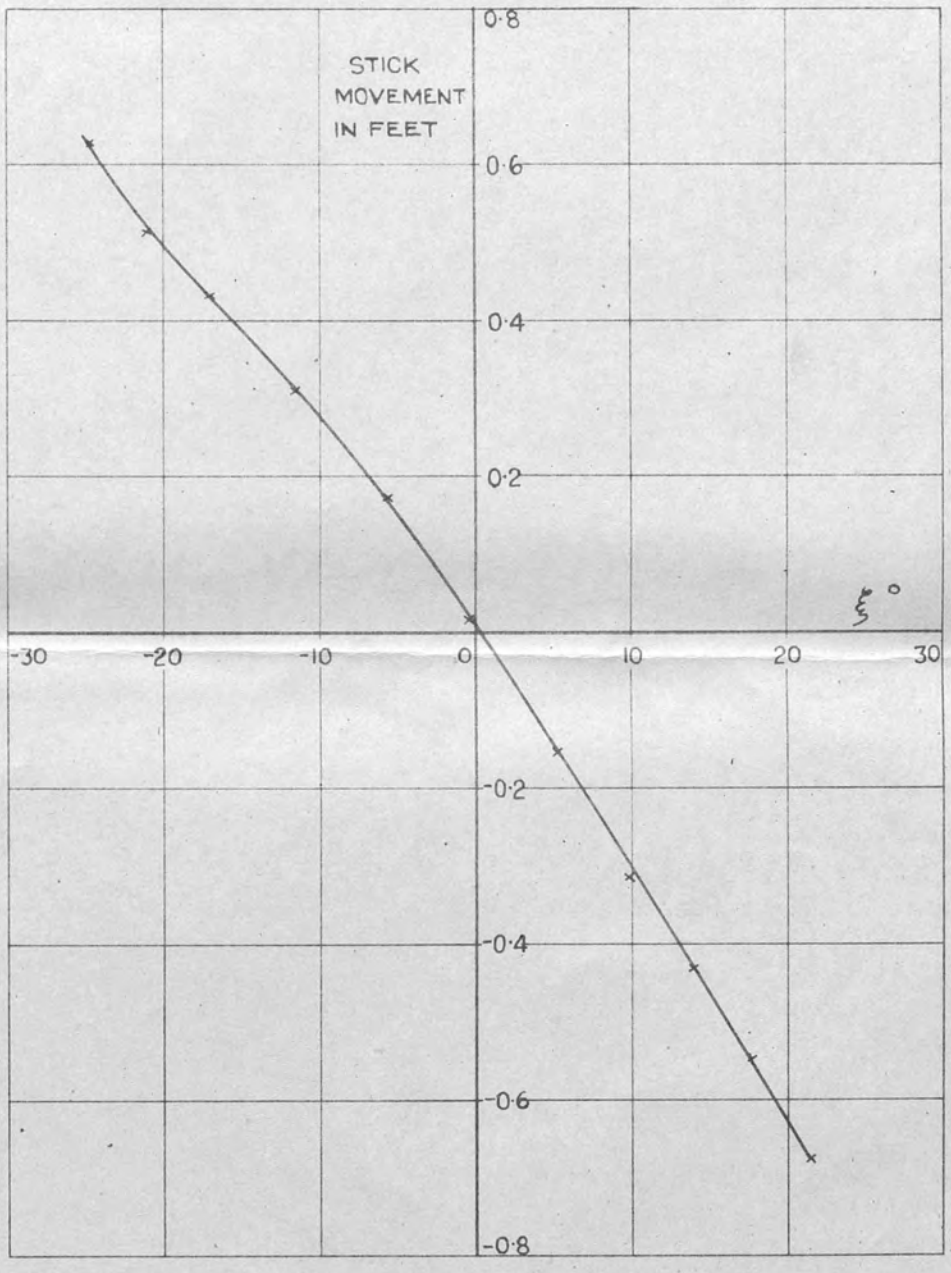

STICK-GEARING CURVE FOR THE PORT AILERON (NO LOAD)

SPITFIRE P.7521

12,302.5

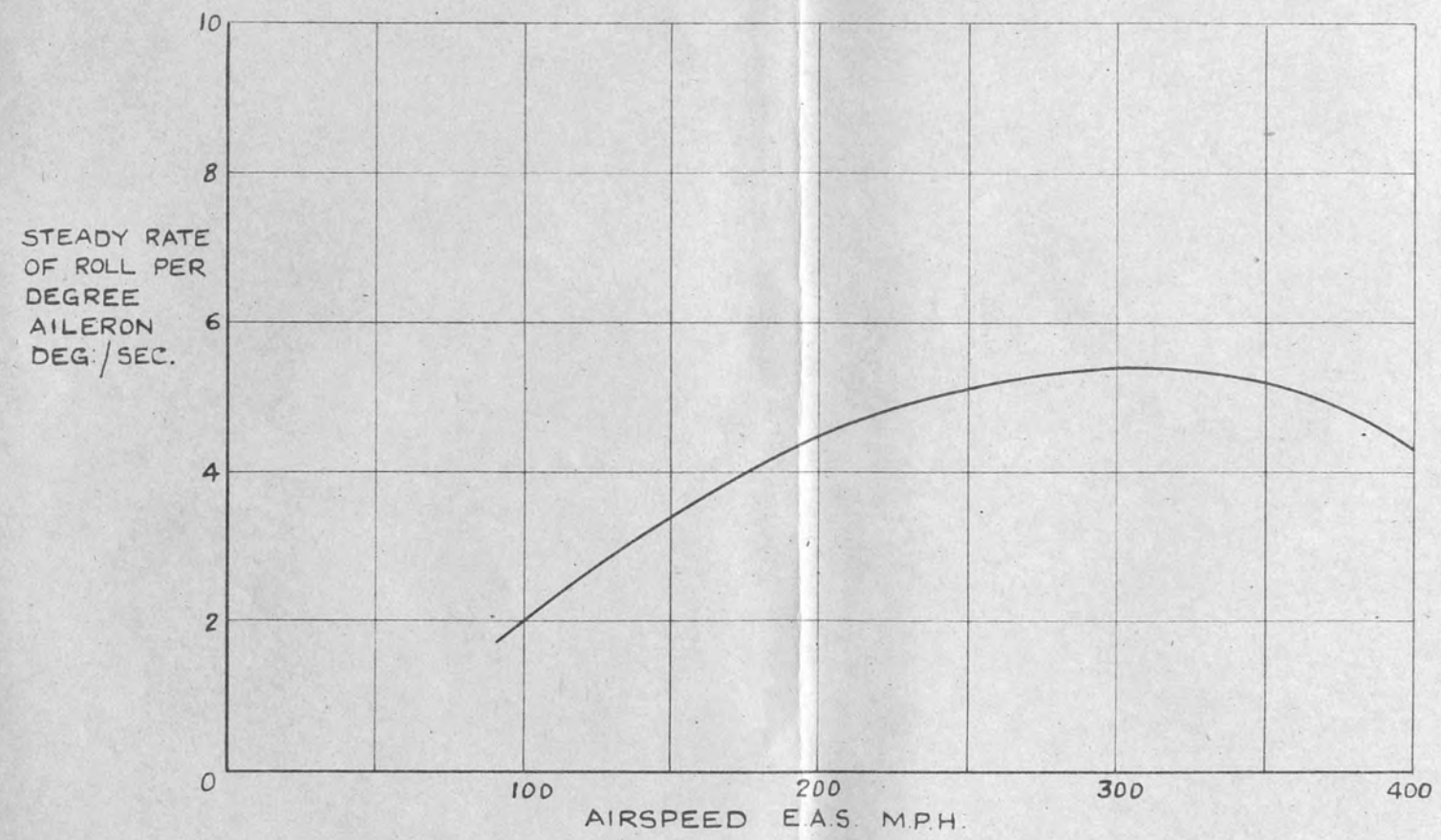

MEAN STEADY RATE OF ROLL PER DEGREE OF AILERON
(MEAN AILERON ANGLE.)

FIG. 5.

12,303.S.

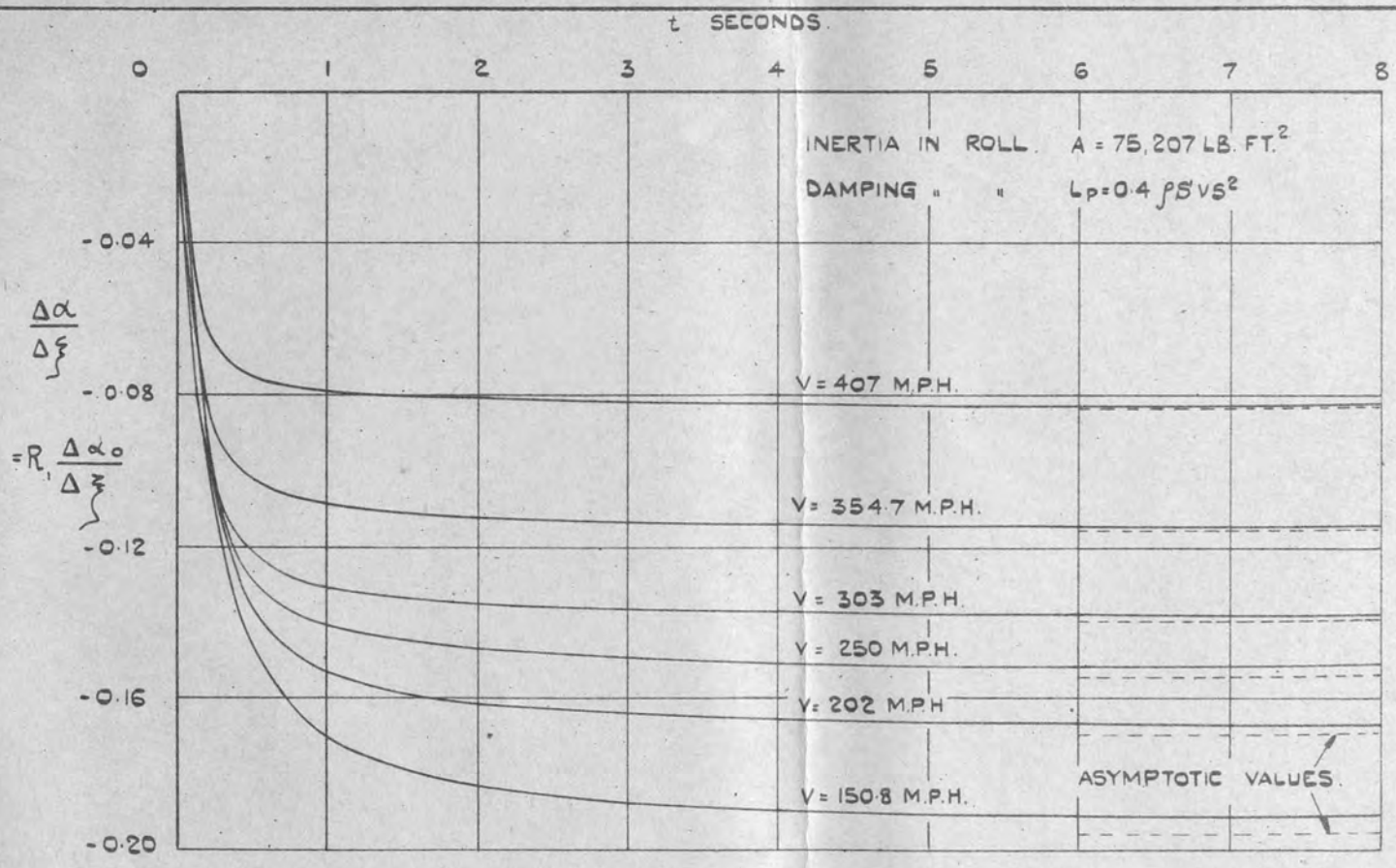

CALCULATED VARIATION OF $\Delta\alpha$, WITH TIME, DURING STEADY APPLICATION OF CONTROL.

FIG. 6.

12304:S.

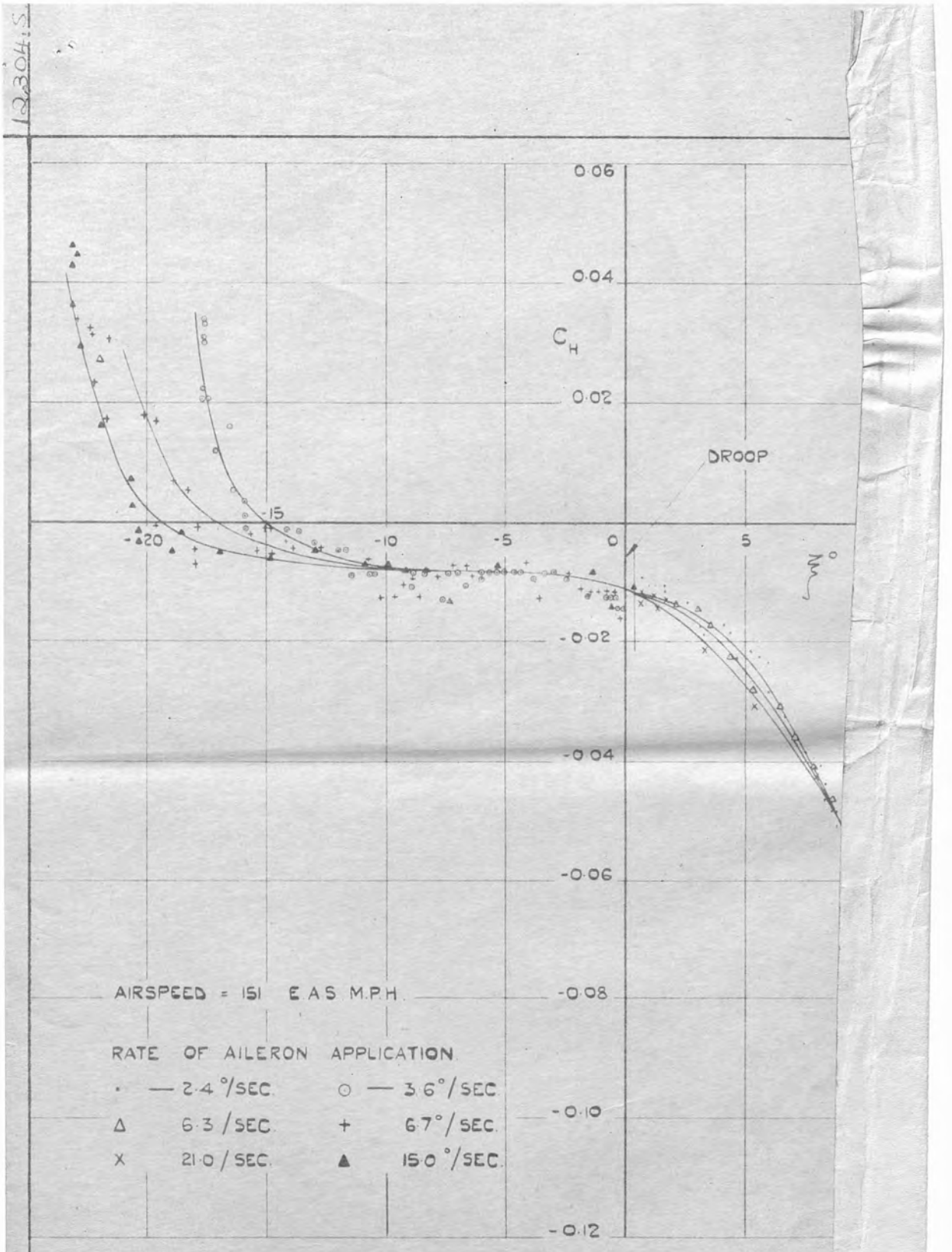

INSTANTANEOUS VALUES OF HINGE MOMENT COEFFICIENTS
STEADY APPLICATION OF AILERON IN STRAIGHT FLIG

SPITFIRE P.7521 (AILERON I.)

12,305.S

FIG. 8.

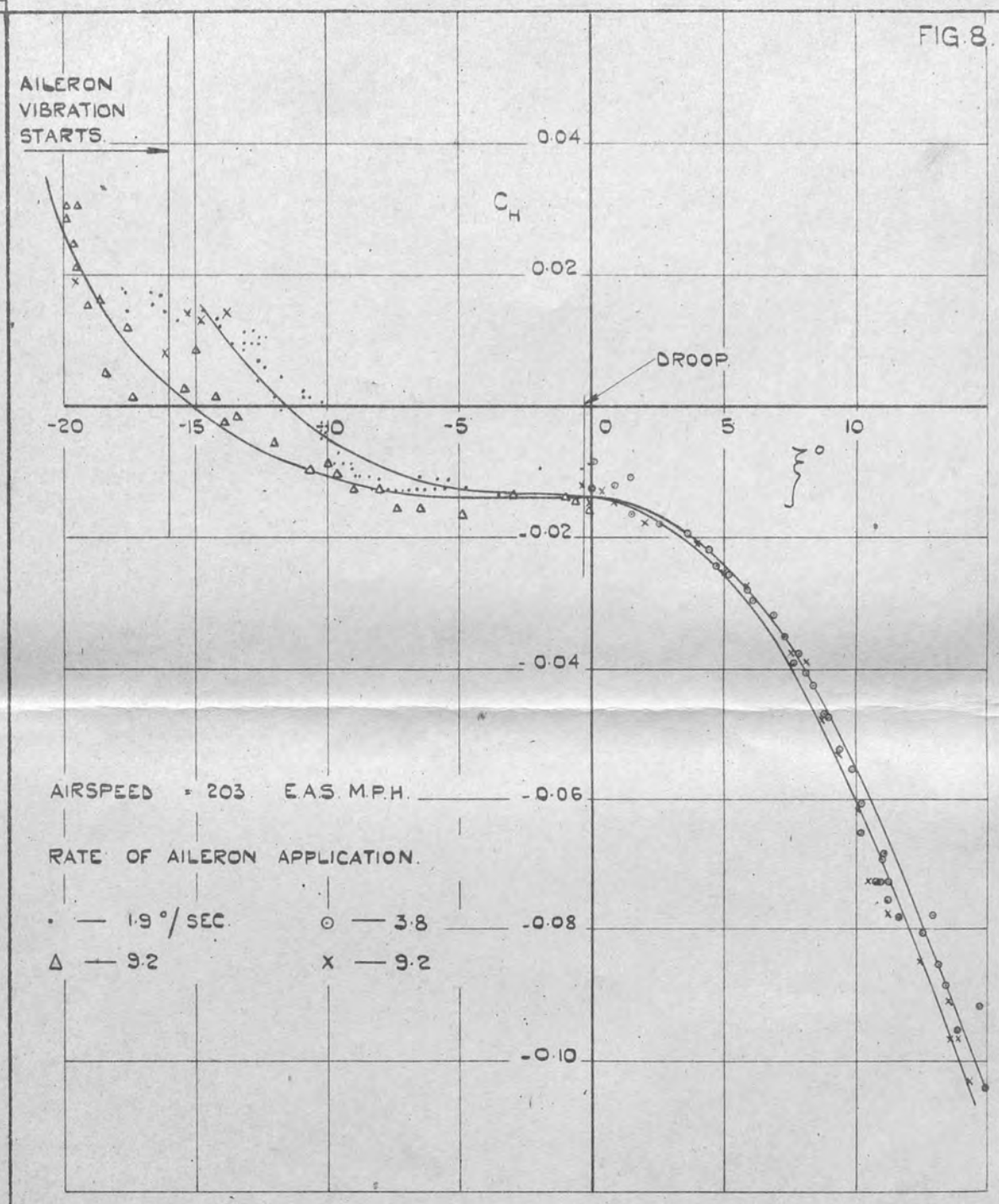

INSTANTANEOUS VALUES OF HINGE MOMENT COEFFICIENTS DURING STEADY APPLICATION OF AILERON IN STRAIGHT FLIGHT.

SPITFIRE P.7521 (AILERON I)

12306.S

FIG. 9

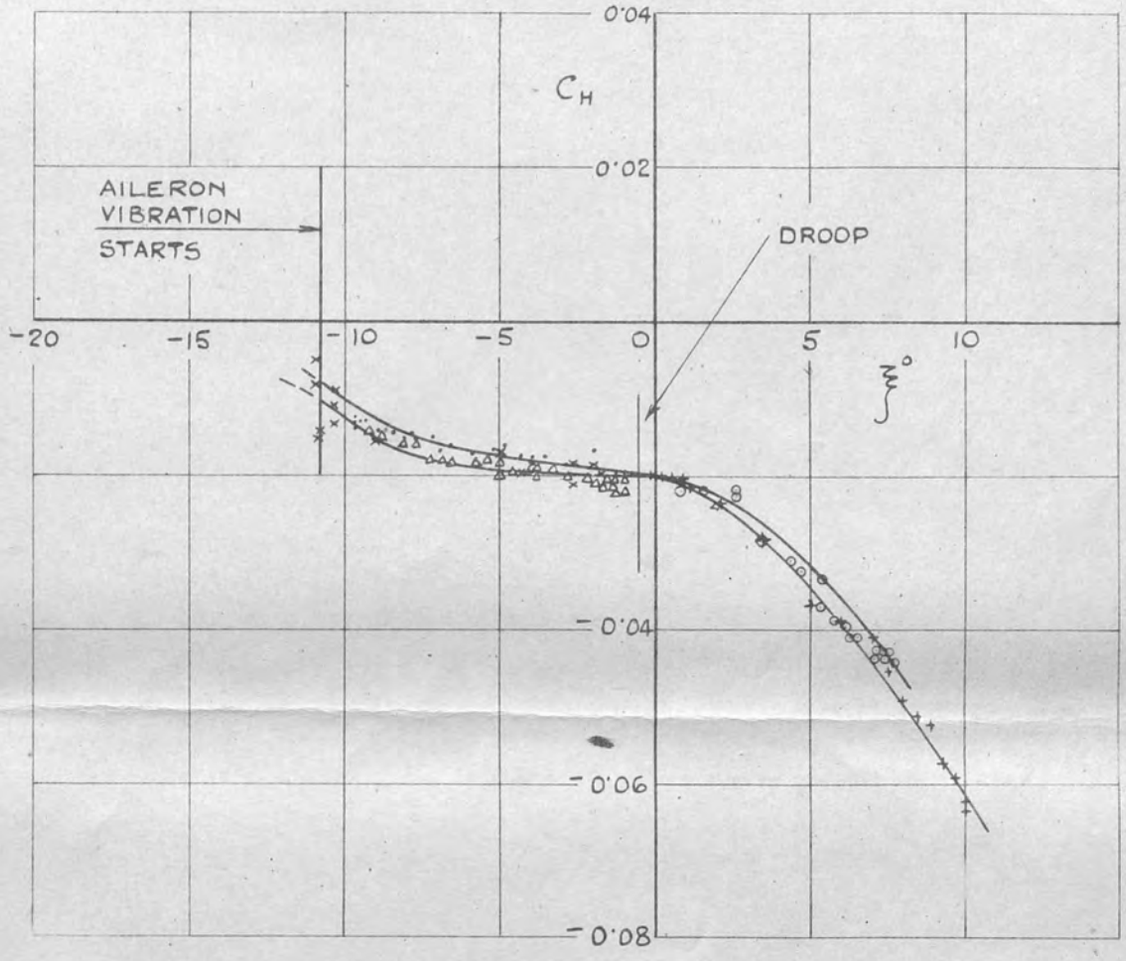

AIRSPEED = 250 E.A.S. M.P.H.

RATE OF AILERON APPLICATION

• —— 3·3°/SEC. ⊙ —— 3·3°/SEC.

Δ —— 3·7° " + —— 8·1°/SEC.

× —— 7·1° "

INSTANTANEOUS VALUES OF HINGE MOMENT COEFFICIENTS DURING STEADY APPLICATION OF AILERON IN STRAIGHT FLIGHT.

SPITFIRE P7521. (AILERON I)

12307.S

FIG. 10

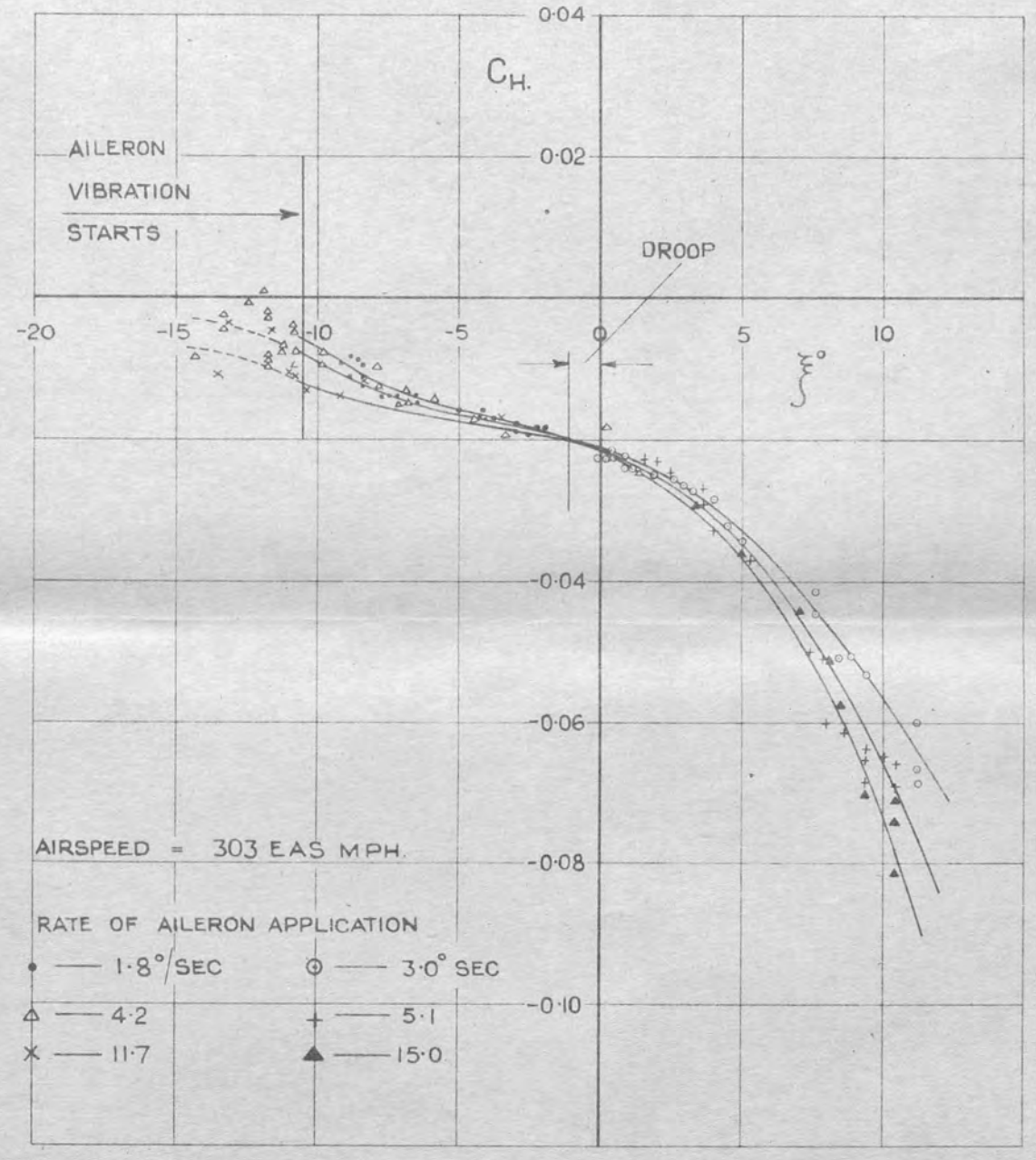

INSTANTANEOUS VALUES OF HINGE MOMENT COEFFICIENTS DURING STEADY APPLICATION OF AILERON IN STRAIGHT FLIGHT

SPITFIRE P7521 (AILERON 1.)

12,308.5

FIG.11

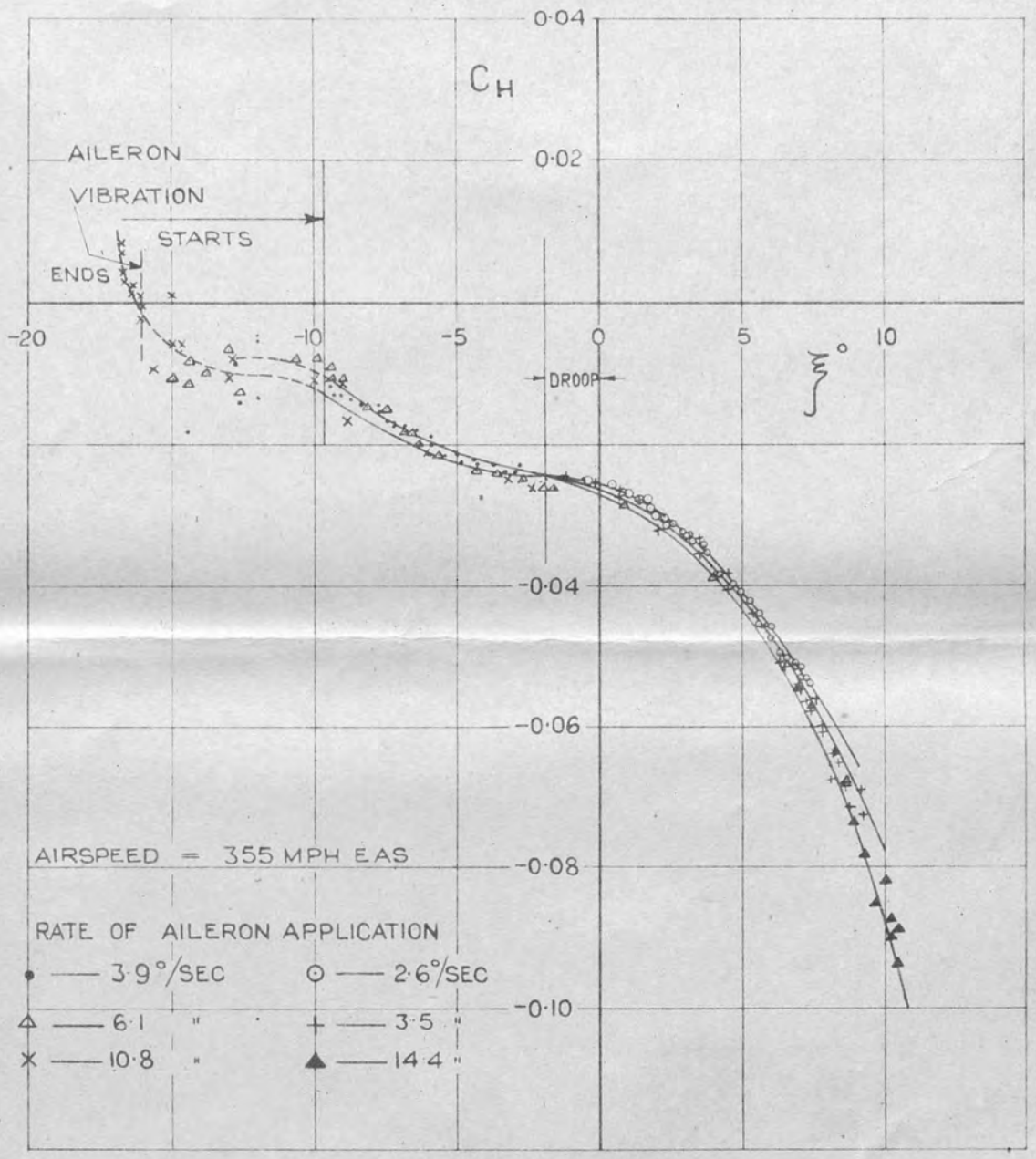

INSTANTANEOUS VALUES OF HINGE MOMENT COEFFICIENTS DURING STEADY APPLICATION OF AILERON IN STRAIGHT FLIGHT

SPITFIRE P7521 (AILERON 1)

12309.5

FIG.12

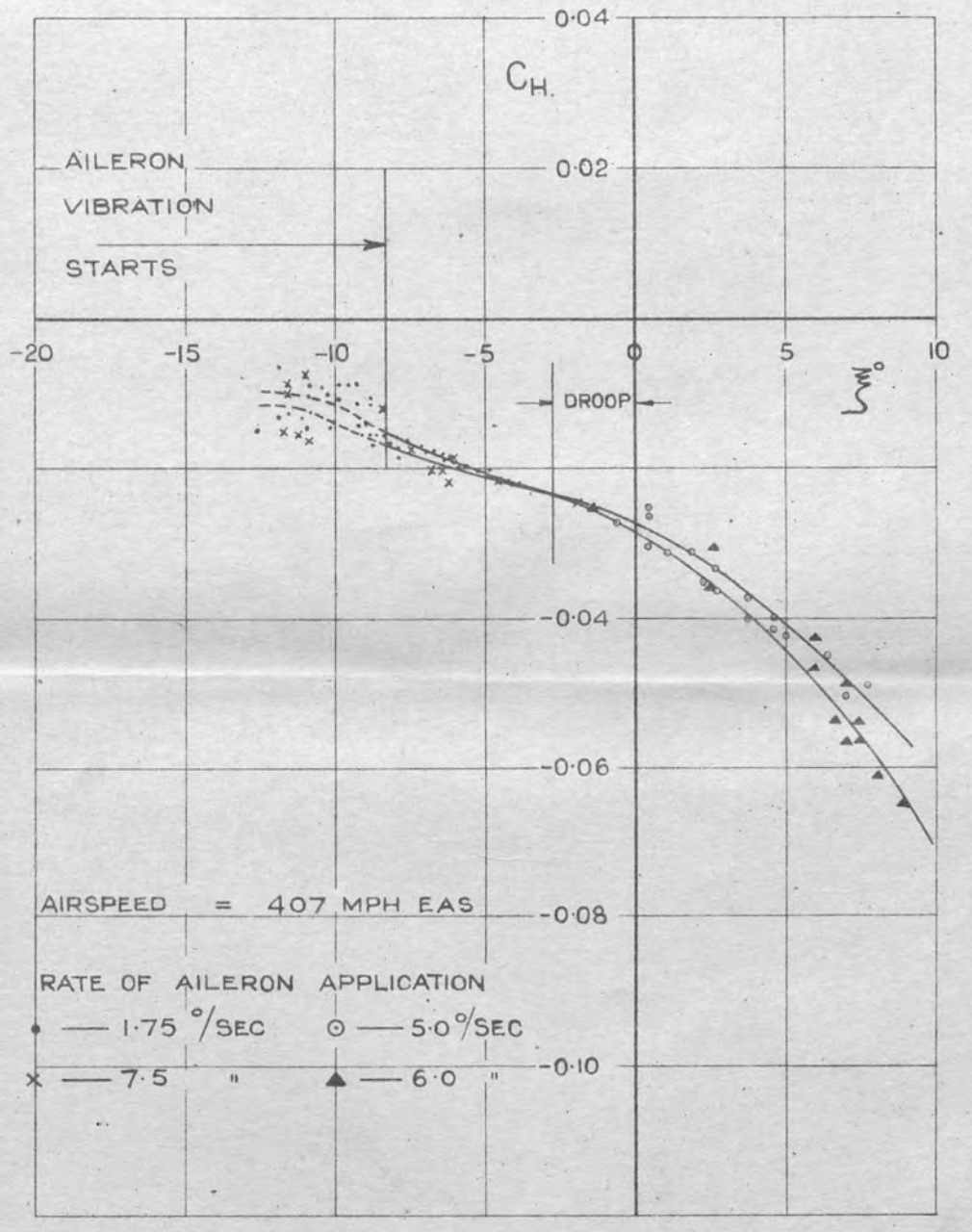

INSTANTANEOUS VALUES OF HINGE MOMENT COEFFICIENTS DURING STEADY APPLICATION OF AILERON IN STRAIGHT FLIGHT

SPITFIRE P 7521 (AILERON 1)

12310.S.

FIG. 13

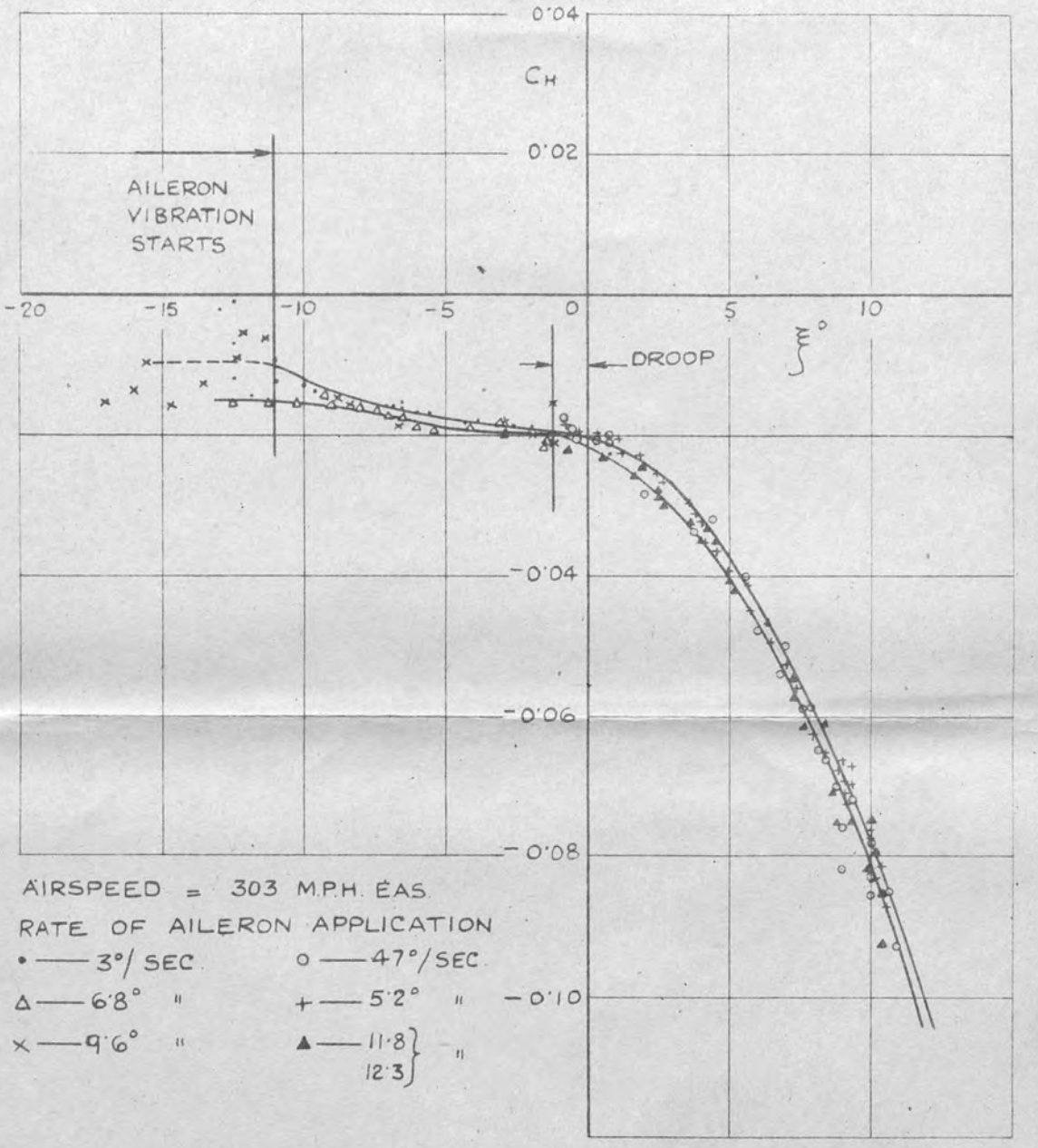

INSTANTANEOUS VALUES OF HINGE MOMENT COEFFICIENTS DURING STEADY APPLICATION OF AILERON DURING A 4g PULL OUT.

SPITFIRE P7521. (AILERON I)

1231.S.

FIG: 14

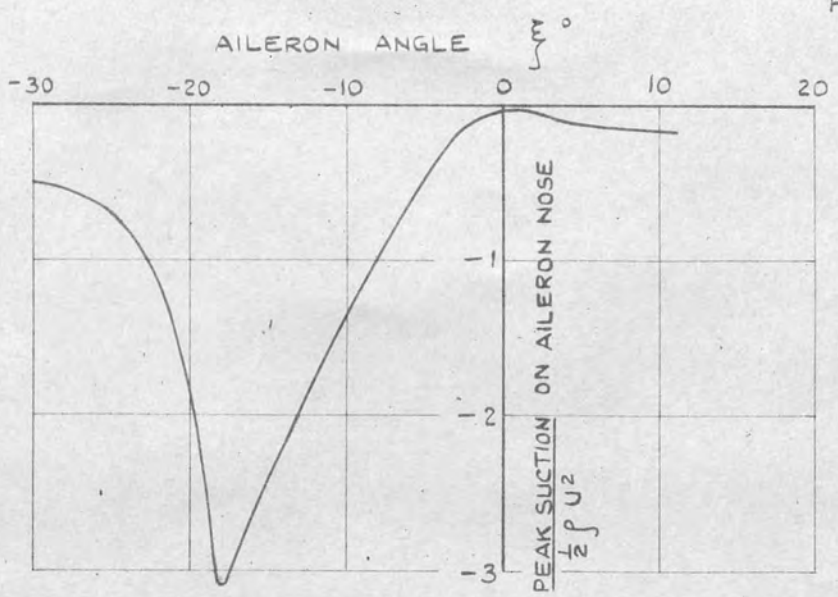

(A)

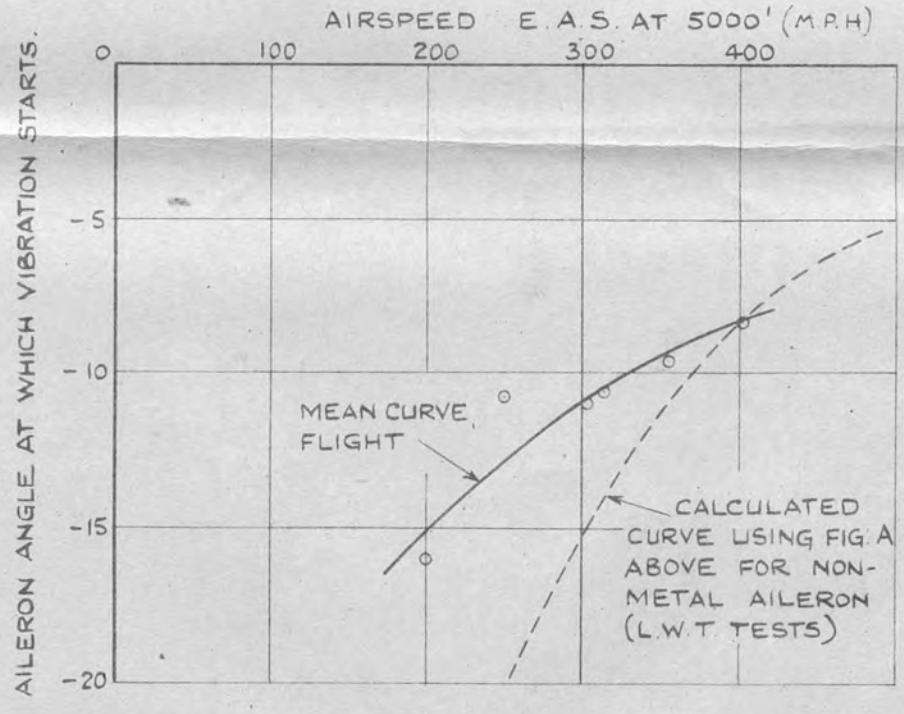

(B)

FIG. A. VARIATION OF MAXIMUM PRESSURE COEFFICIENT ON AILERON NOSE WITH AILERON ANGLE (L.W.T. TESTS METAL AILERON Nº 4.)

FIG. B. AILERON ANGLE AT WHICH BUMPING STARTS; COMPARED WITH CALCULATED ANGLE AT WHICH THE CRITICAL MACH. Nº FOR THE NOSE OF THE AILERON IS REACHED.

12312.5

FIG: 15.

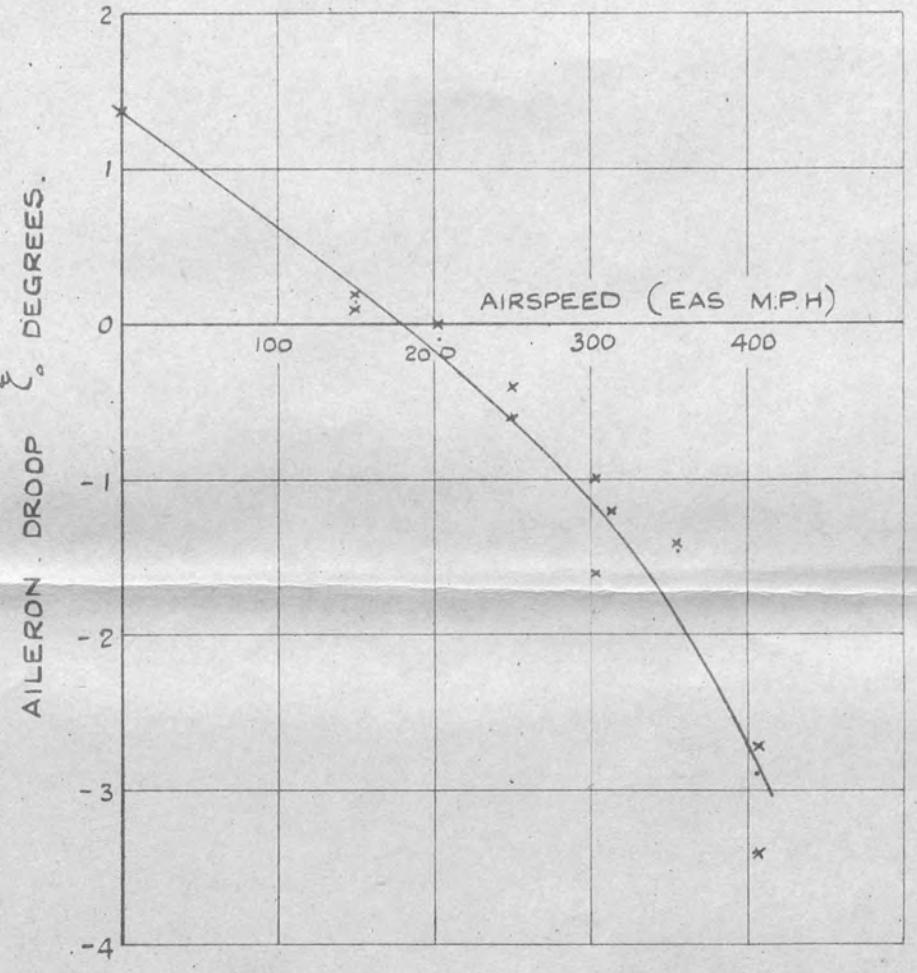

VARIATION OF AILERON DROOP WITH FORWARD SPEED FOR AILERON I.

SPITFIRE. P7521.

FIG. 16

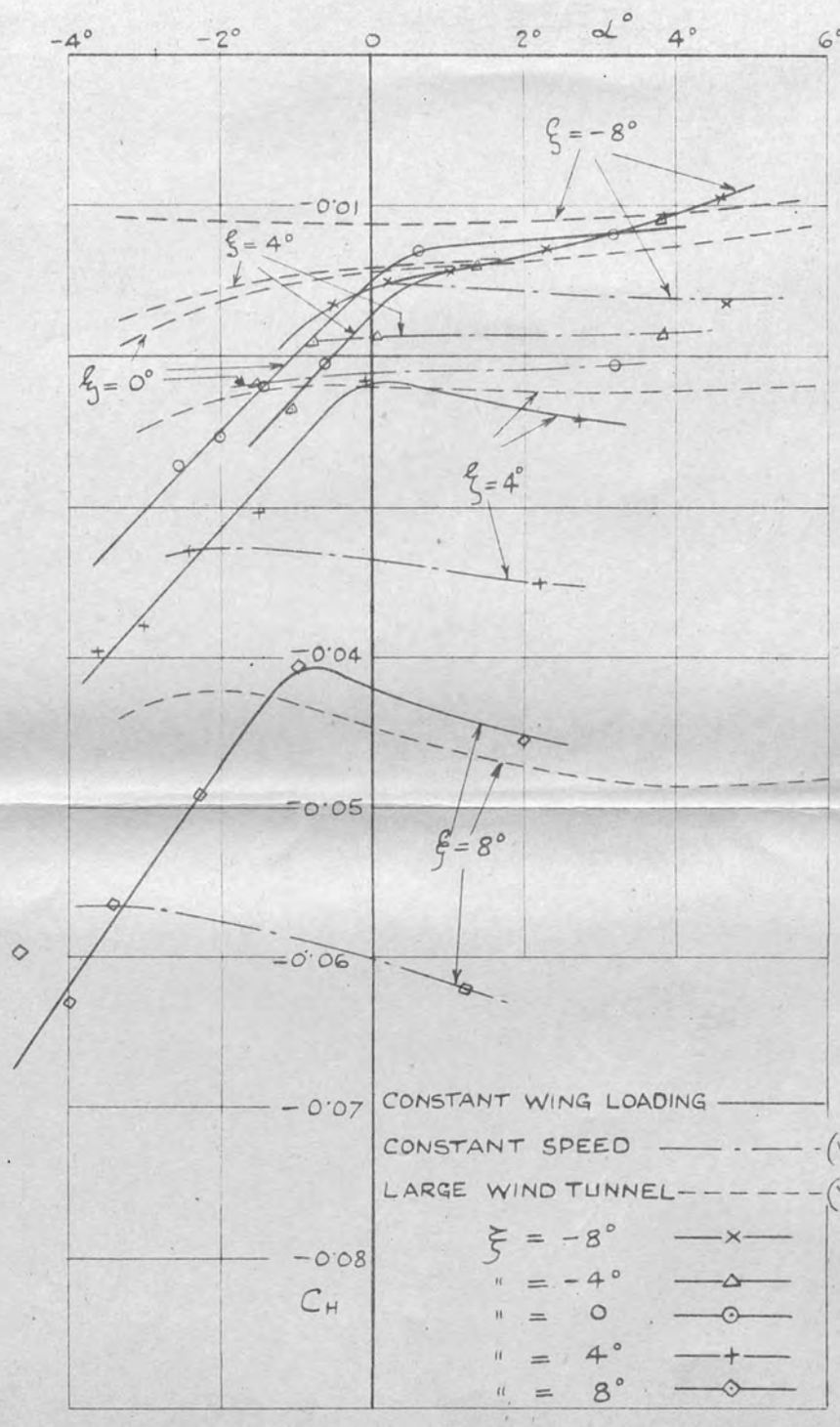

VARIATION OF AILERON HINGE MOMENT WITH INCIDENCE.

FIG. 16A

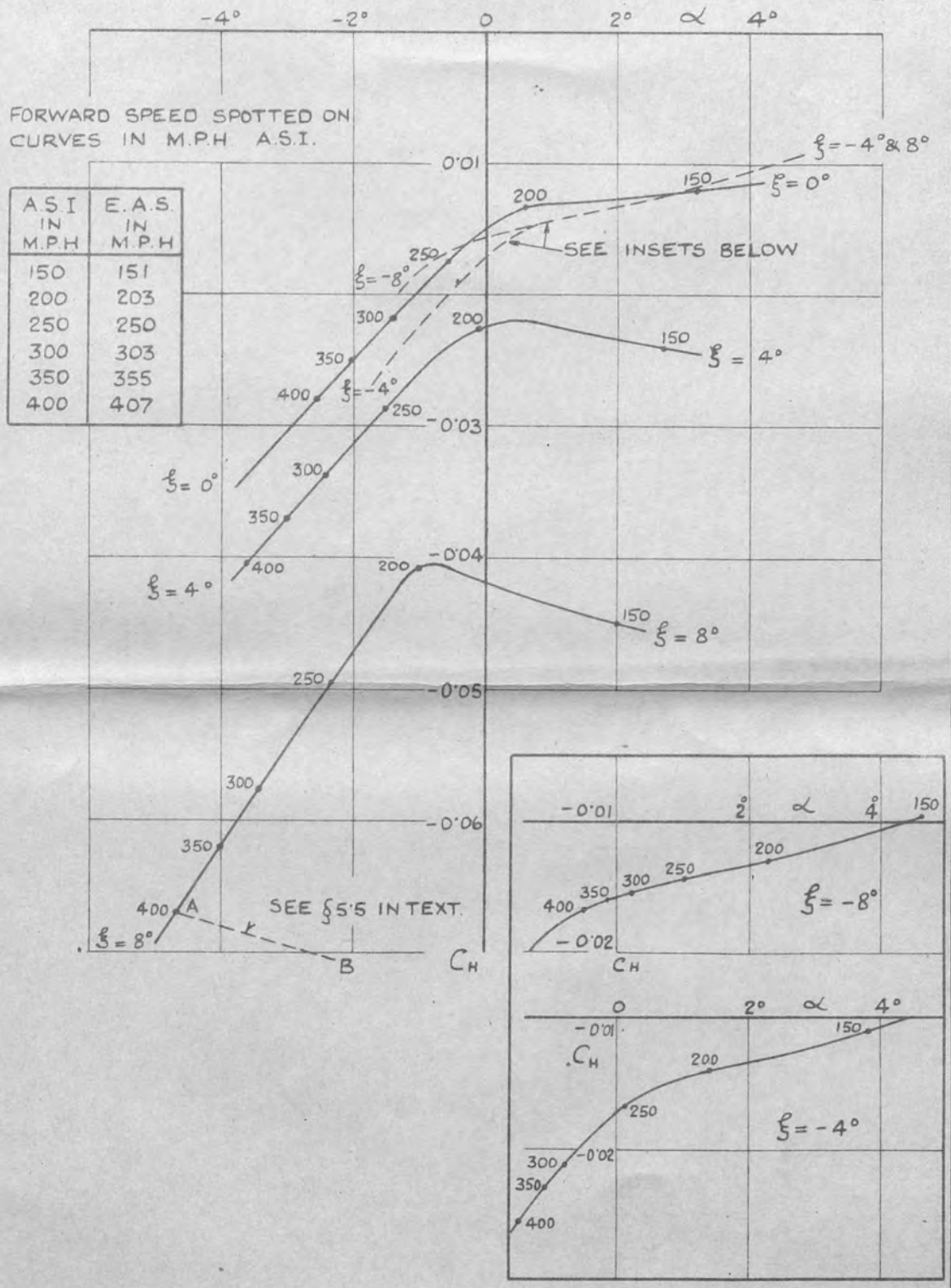

VARIATION OF AILERON HINGE MOMENT WITH INCIDENCE FOR CONSTANT WING LOADING CONDITIONS IN FLIGHT.

12315.S

FIG. 17

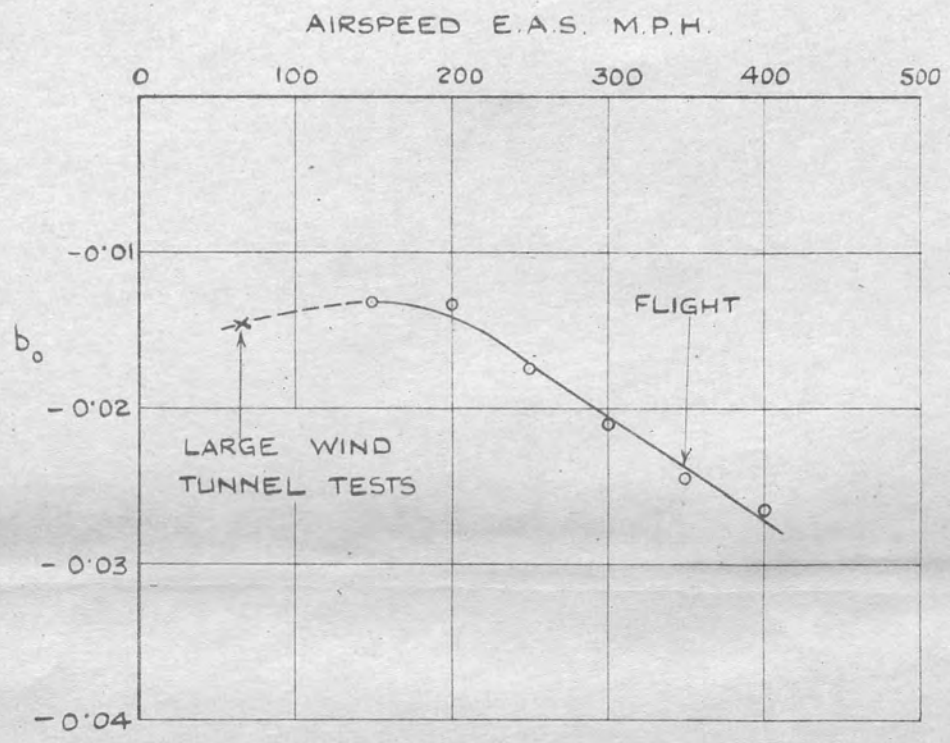

THE VARIATION OF b_o WITH FORWARD SPEED.

SPITFIRE P7521. (AILERON I)

12319.S.

FIG. 18

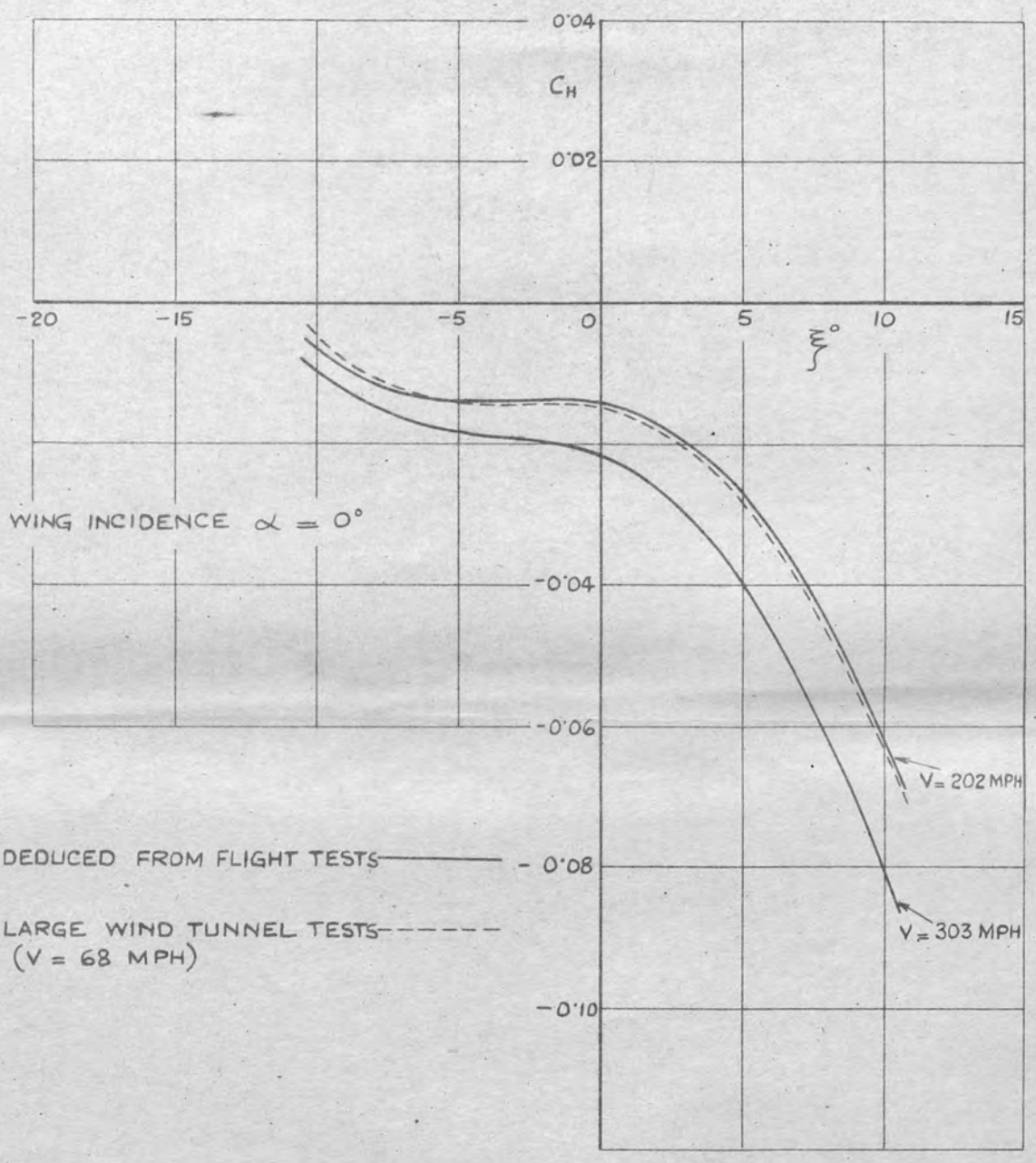

VARIATION OF HINGE MOMENT CURVES WITH FORWARD SPEED, WING INCIDENCE CONSTANT

SPITFIRE P7521 (AILERON I)

12317.5

FIG. 19.

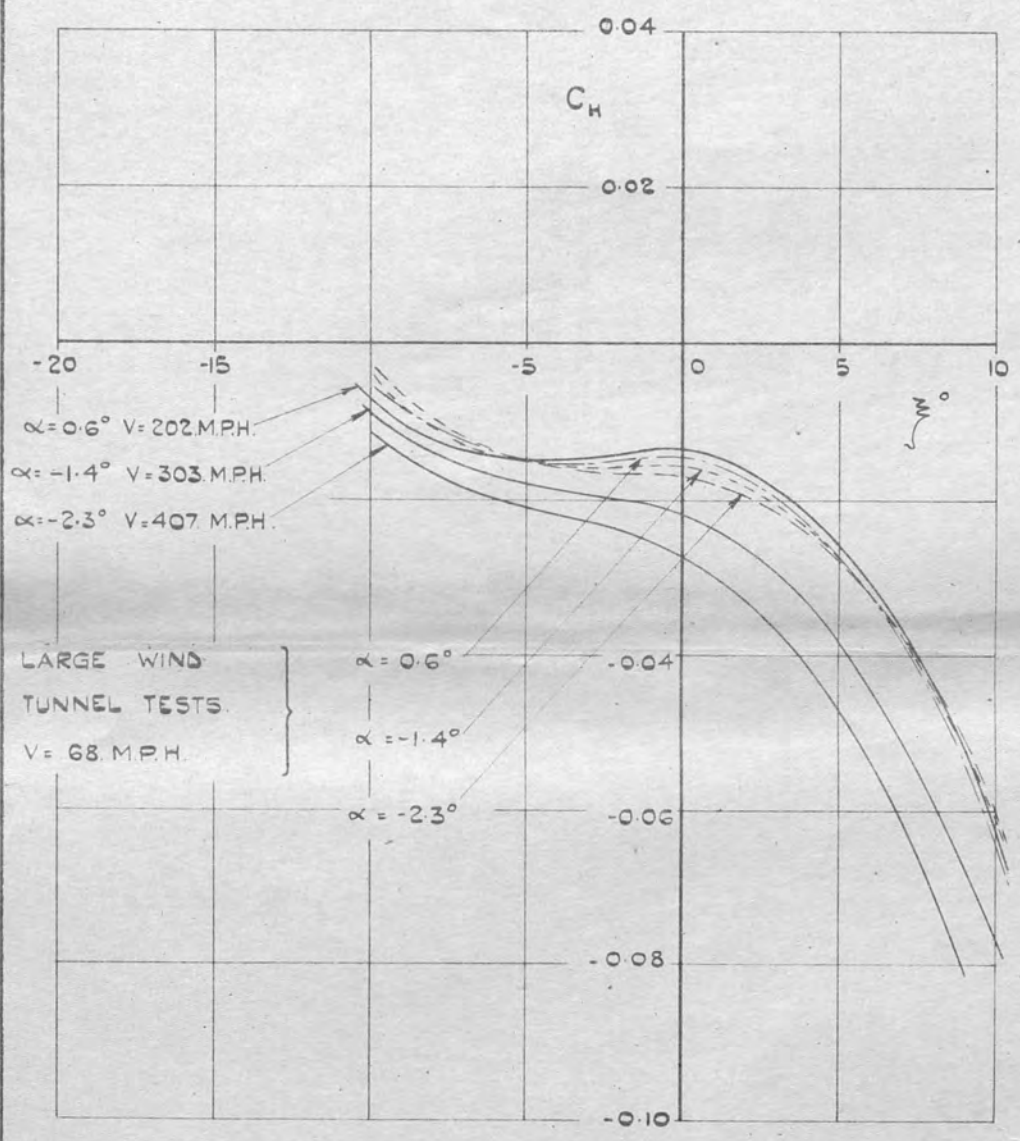

AILERON HINGE MOMENT CURVES AT CONSTANT INCIDENCES AND CONSTANT SPEEDS FOR AILERON I

SPITFIRE P.7521.

Report No. Aero 1799

January, 1943

CONFIDENTIAL

ROYAL AIRCRAFT ESTABLISHMENT, FARNBOROUGH

Diving and stability tests on the Lancaster

by

D.J. Lyons, B.Sc., (Eng.)
G.H. Naylor, B.Sc., D.I.C.
and
J.H. Martin, B.S.C. A.Inst.P.

M.A.P. Reference: Res/Air/707/R.D.L.3.b
R.A.E. Reference: Aero/1137.R/30
Item No. : 5J/5/42

S U M M A R Y

Reasons for enquiry

Trouble had been experienced in recovering from a dive, due to the large stick forces required to prevent the dive from steepening on a Lancaster at the A.A.E.E.

Range of investigation

Measurements were made of the following:-

(i) Static stability stick fixed and free up to a maximum diving speed of 365 m.p.h. E.A.S.
(ii) The effect of slipstream on stability.
(iii) The variation with speed, in stick force per "g" in a pull out.
(iv) The variation in aileron droop with speed.

Measurements or calculations were also made of the tail plane twist, elevator twist and fuselage bending.

Results

The neutral point in the glide stick fixed at low speeds was at approximately 0.40$\bar{c}$. The stick forces reversed in the dive, but the degree of stick free instability was fairly small over the centre of gravity range 0.25 to 0.35$\bar{c}$ and no difficulty was experienced in any of the considerable number of dives made.

The tail plane was found to twist inappreciably in flight, but both the elevator twist and fuselage bending were calculated to be appreciable but small. The elevator b_2 was found to be unexpectedly large and to increase considerably with speed.

---

1. Introduction

The Lancaster I aircraft has been dived to high speeds from very early in its career (the limiting diving speed is 360 m.p.h. A.S.I.) and during the turret operation trials at high speed[1] it was reported that during a dive at increasing speed, the stick force reversed from a push to a pull. This

reversal of stick force did not seem to be considered dangerous at that time and no further mention of this instability was made until considerable difficulty in recovering from a dive was experienced by a pilot of the intensive flying unit at the A.A.E.E. This pilot reported that the stick forces reversed in the region of 320 m.p.h. A.S.I. and that as the speed increased considerable force backwards was required on the control column, and that recovery was only obtained by full force back on the control column assisted by the winding back of the trimmer tabs.

It was pointed out by Messrs. A.V. Roe Ltd. at this time that due to the centre of gravity being very low in relation to the mean chord, there would be an appreciable loss in stability at high speed compared with a lower speed; the calculated loss in stability for the Lancaster, between C_L values of 0.5 and 0.14, would correspond to a shift of the neutral point of $0.03\bar{c}$ forwards (assuming the centre of gravity is $0.21\bar{c}$ below the mean wing chord). The reversal of stick forces, however, was first noted[1] with the centre of gravity at $0.26\bar{c}$, when, assuming a neutral point stick fixed of $0.42\bar{c}$ (this is the value given by the wind tunnel tests[2]), the aircraft should have a margin of stability stick fixed equivalent to $0.16\bar{c}$ at a C_L of 0.5 and $0.13\bar{c}$ at a C_L of 0.14. Therefore, unless freeing the stick has a very large effect on the stability, there must be a large change in static stability stick fixed to account for the reversal of stick forces.

It was decided to investigate fully the static stability of the Lancaster both stick fixed and free, with especial attention to the stability in high speed flight, to measure the degree of reversal of the stick forces and to find whether the reason for the instability lay in the static stability of the aircraft stick fixed or in the elevator characteristics.

This report gives the results obtained, with a partial investigation into the basic causes.

2. Method of test

To obtain the necessary information to assess the static stability stick fixed and free, the following measurements were made:-

(a) Elevator angles to trim with varying tab angle.
(b) Stick forces to trim with varying tab angle

and these measurements were made under the following conditions,

(i) Centre of gravity forward at $0.255\bar{c}$, engines throttled back,
(ii) Centre of gravity forward at $0.255\bar{c}$, engines on, boost + 6 lb. sq.in. 2,600 r.p.m.
(iii) Centre of gravity back at $0.35\bar{c}$, engines throttled back
(iv) " " " " " " , engines on, boost + 6 lb./sq.in., 2,600 r.p.m.

The stick force per "g" was also measured at 200, 250 and 320 m.p.h. A.S.I. with the centre of gravity at $0.26\bar{c}$.

On all these tests the main landing flaps were fully up, and the radiator flaps, though under automatic control, remained fully closed.

The elevator position was measured at the torque tube of the elevator inside the fuselage (the torque tube of the elevators is continuous right through the fuselage) and transmitted to the cabin by a Desynn system. The tab angle was measured at the tail, by recording the movements of the balance cable which directly connects the two trimming tab operating mechanisms; this was again transmitted to the cabin by means of a Desynn system. The stick forces were measured by the standard R.A.E. type stick force indicator on the control column, and the friction error should be fairly small as the whole control system is made up of push and pull rods.

A sketch of the Lancaster is given in Fig.1 and relevant details of the tail plane etc. in Fig.2.

3.1. General

A considerable number of dives were made to high speeds (the highest recorded was 365 m.p.h. E.A.S.) and although the stick forces reversed at high speeds for the range of centre of gravities tested, when trimmed for cruising flight, there was never any dangerous building up of stick forces, and no difficulty was ever experienced in pulling out of the dive. During the tests listed in the first part of §2, however, some peculiarities were noticed in the trim curves obtained, such as the crossing of the curves recorded for two centre of gravity positions before the C_L = 0axis was reached. It was thought that much of this would be explained by tail plane, elevator and fuselage distortion. Accordingly measurements or calculations of these distortions were made.

3.2. Tail plane, elevator and fuselage distortion

3.21. Tail plane twist

The twist of the tail plane was measured photographically with a cine camera over a range of speeds up to 340 m.p.h. E.A.S. with the centre of gravity at 0.27$\bar{c}$.

The camera was fixed firmly to the tail plane rear spar just inside the fuselage, and the twist of the fixed part of the tail plane was obtained from the movement of a line on the fin relative to the side of the frame of the film.

The twist was found to be negligible over the whole speed range. The calculated twist due to elevator lift deduced from wind tunnel tests[2] and measured stiffnesses was -0.1° at 340 m.p.h. E.A.S. but the drag of the end fin and rudder at this speed would be expected to twist the tail plane through about +0.1°, thus giving a total estimated twist of zero. The agreement between model and full-scale is therefore satisfactory.

Early tests of tail plane twist made with the camera mounted in the rear gun turret showed that the rear portion of the fuselage (i.e. from the tail plane to the rear turret) flexed considerably, so that between 150 and 340 m.p.h. E.A.S., the fuselage at the turret rotated -0.7° in pitch relative to the fuselage at the tail plane.

3.22. Elevator twist

Measurements of the elevator twist were made in flight by a method similar to that used for the tail plane twist measurements, but these were invalidated by the fact that the linkage

of the Desynn system used to measure the inboard elevator angle, was considerably affected by the bending of the elevator torque tube. This bending of the torque tube was fairly large due to the fact that the inboard hinges on either side were about 7 ft. apart and the arm to the pilot's control was attached only about 1½ ft. from the centre line of the fuselage. The elevator twist, due both to tab and elevator movement, was therefore determined by a graphical method. The hinge moment characteristics used in the calculations were taken from flight measurements at low speeds, and although the b_2 for the elevator varied considerably with flight speed, only slight error was introduced as the elevator angles at high speed were small. An allowance was made for the spanwise variation of b_2.

The stiffness in torsion assumed for the calculations was 100 lb.ft./^{o} for 90% of the elevator overall span, which corresponds to a value of approximately 0.012 for the stiffness criterion

$$\frac{1}{V} \cdot \frac{1}{S_E} \sqrt{t_e \cdot b_e} ,$$

where V = design speed in f.p.s. (400 m.p.h.)
S_E = elevator area behind hinge.
t_e = elevator stiffness in lb.ft./radian (measured from 5% to 95% of the overall elevator span).
b_e = overall elevator span.

The stiffness used was the mean between the results of the official tests and the measured stiffness of the elevator on the aircraft during the tests, and it was assumed that the stiffness of unit length was constant across the span.

The calculations showed the difference, $\Delta\eta$, between the measured inboard elevator angle and the mean elevator angle to be approximately equal to

$$-(0.014\ \eta_I + 0.0125\beta)\ (\frac{V}{100})^2$$

where η_I = inboard elevator angle in degrees
β = trimmer tab angle in degrees
V = flight speed in m.p.h.

At high speeds this correction was found to be quite appreciable, reaching as much as ½^{o} with the centre of gravity at 0.35$\bar{c}$, mainly due to the large trimming tab angle.

3.23. Fuselage bending.

The effect of fuselage bending on trim has been calculated, by use of wind tunnel tests[2] to obtain the tail loads, and a value of the flexural stiffness obtained from unpublished strength tests on a Manchester fuselage. The value of the stiffness figure was fairly high at 0.08^{o} tail movement per ton tail load measured relative to the root wing chord. The results of these calculations are given in Fig.3 and show the effect to be small, i.e. less than 0.2^{o} change in elevator angle below 400 m.p.h. E.A.S., but in the direction to account for a reduction in stability at high speeds.

3.3. Static stability stick fixed (Figs.4-9)

In Figs.4 and 5 the elevator angles to trim are plotted against C_L, for the glide and engine on conditions. All the

points are corrected for tab lift, and the elevator angle is that measured at the centre of the torque tube inside the fuselage corrected for the bending of the torque tube (see §3.22). The curves for the two centre of gravity positions, both for engines on and off, cross at a C_L of 0.14, instead of at the theoretical value of $C_L = 0$, and there is a large reduction in apparent stability at high speed with centre of gravity aft. Both these effects are due to the elevator twist, mainly as a resultant tab setting, which is far more negative for the centre of gravity aft than the centre of gravity forward condition. In Figs.6 and 7, the curves of Figs.4 and 5 are shown corrected for the calculated elevator twist (see §3.22), the mean elevator angle to trim being plotted against C_L. The trim curves, thus obtained, conform much better to the theoretical form, in that all the curves for both varying centre of gravity position and engine conditions can be made to intersect at the same value of η on the $C_L = 0$ axis. There is still, however, a decrease in stability at the very high speeds, and in Fig.8 it is shown that this is due to the effect of fuselage bending.

It is thus apparent, that at high speeds, it is possible to obtain three different values of dC_m/dC_L with elevator fixed, for a given centre of gravity position,

(i) Varying speed conditions (i.e. as measured).
(ii) Constant speed conditions in flight.
(iii) Constant speed conditions with no fuselage bending as in the wind tunnel tests.

The neutral points have been calculated completely for condition (i) and are given in Fig.9. These are comparable to the wind tunnel tests except at high speeds, and on the glide the neutral point is in fair agreement with the wind tunnel[2] neutral point of $0.42\bar{c}$.

The effect of the fuselage being non-rigid is to move the neutral point forwards about $0.01\bar{c}$ to $0.03\bar{c}$ (varying with centre of gravity position) for both the varying speed and constant speed condition at a C_L of 0.15. For instance the neutral point with a rigid fuselage, engines on at a C_L of 0.15, would be at $0.37\bar{c}$.

It therefore appears that even with a rigid fuselage, the neutral point moves slowly forward with decrease in C_L. This is in agreement with the calculated effect of centre of gravity height (see §1). It should be noted that during the flight tests the distance of the centre of gravity below the mean wing chord was $0.15\bar{c}$, which was equivalent to $0.20\bar{c}$, as the aerodynamic centre of the Lancaster wing section is $0.05\bar{c}$ above the chord line. This should move the neutral point 0.02 to $0.03\bar{c}$ forwards, between C_L values of 0.5 and 0.14, and from the flight tests we deduce a movement of $0.02\bar{c}$ forwards.

The effect on the neutral point of opening the throttle is small, this is good agreement with wind tunnel tests on four engined aircraft[3].

3.4. Stability stick free and elevator characteristics

3.41. Stability stick free (Figs.9 - 12)

The curves in Figs.10, and 11 give the stick forces to trim, with varying tab angle and centre of gravity position, in terms of C_H,

where $C_H = \dfrac{\text{Stick force in lb.} \times \frac{dx}{d\theta}}{\frac{1}{2}\rho V^2 S_\eta c_\eta}$

where $\frac{dx}{d\theta}$ = stick elevator gearing in ft./radian

V = forward speed in ft./sec.

S_η = elevator area aft of the hinge

c_η = mean elevator chord aft of hinge

Considerable trouble was experienced in obtaining these curves, especially where the stick forces were small, due to the scatter of the points; and the recording of different but parallel curves on different days and with different pilots. This was considered to be due to the following factors.

(a) There was a 0.5° backlash in the trimmer tab circuit from the irreversible unit to the tab itself.

(b) The stick force per 'g' being so large, in a pull out for this aircraft especially at high speeds, it is quite possible for the pilot to include an appreciable contribution due to 'g' in the stick force, while unaware that he is departing slightly from straight flight.

The curves have been drawn, however, as well as possible in the circumstances, but it is evident that the accuracy of the curves, and the deductions from them is not great. It was considered that the greatest accuracy in determining the neutral point would be obtained by deducing the tab angles to trim from Figs 10 and 11, and estimating the neutral points from the value of $d\beta/dC_L$ for the two centre of gravity positions. The tab angles to trim plotted against C_L are given in Fig.12, and the corresponding neutral points are included in Fig.9. It is possible to draw the following broad conclusions, and it should be noted that the curves only apply to varying speed conditions.

(i) There appears to be little change in the position of the neutral point at low speeds on freeing the stick when gliding, though there is a forward movement of about $0.03\bar{c}$ with engines on.

(ii) As the speed is increased there is an apparent movement of the neutral point rapidly forward, which is shown up by the fact that there is little effective change in stability at high speed with change in centre of gravity position, over the range tested. It is obvious that under the conditions which exist in the high speed dive on this aircraft, the standard method of determination of the neutral point breaks down, and in fact the use of the neutral point in assessing the margin of stability has little meaning, due to the insensitivity of the stability to the centre of gravity position.

Examination of the Figs.10-12 shows that there was no sudden change in static stability stick free at high speeds, although the aircraft was unstable below a C_L of about 0.20 over the whole range of centre of gravity tested. The amount of instability was quite small and the pull on the stick would not build up quickly with increase in speed unless the dive was entered with the trimmer wound forward from the cruising or top speed trimming position. This position might possibly arise if the trimmer were wound forward to overcome the large forces necessary to increase the speed of the aircraft in the dive.

The stick forces per 'g' were measured during the pull out, and the following table shows the large increase in this with speed.

Speed m.p.h. A.S.I.	200	250	320	Conditions
Stick force per 'g' (lb.)	88	106	200	Engines on C.G. at 0.20$\bar{c}$.

Thus, if the pilot winds the trimmer forward to overcome some of the stick force necessary to increase the speed at a reasonable rate, on attempting to straighten out and hold this speed in a dive he will get a feeling of a sudden reversal of stick force.

The stick free stability under constant speed conditions will differ from the stability under varying speed conditions due to an increase of $-b_2$ with increase in speed, but it has not been assessed owing to the difficulties in estimating the values of b_2 and b_1 for the elevator from the flight results. (See §3.42).

3.42. Control force characteristics

The average value of b_3 for the trimming tabs during the glide was found to be -0.175. This compares with the value of -0.16 which would have been estimated from reference 4, assuming an 80% tail efficiency factor. This means that the trimming tabs are very effective at high speed in producing large changes in stick force.

The values of b_2 deduced from the stick force curves and the corrected elevator angle to trim curves in Figs.6 and 7, are plotted in Fig.13. The method used is that given in reference 7. The value of b_2 is high, even at low speeds where the effect of distortion should be small. The measured value at a C_L of 0.7 was -0.18 (-0.22 allowing an 80% tail efficiency factor). The elevator (see Fig.2) has 42.5% forward balance (i.e. area forward of hinge/area aft of hinge) and a 6 2/3% balance tab with a gearing of roughly 0.5 to 1 for the central elevator angles. The balance of the elevator, however, varies to a considerable extent across the span, from 29.6% inboard to 74.4% outboard, and this does reduce the effective balance to a small extent[5]. The elevator has six cut-outs in the nose to accommodate the hinge attachments, and these, when large, have been shown to reduce the balance considerably[6]. The estimated b_2 for this elevator with the balance tab out without taking into account the effect of the cut-outs would be about +0.06. The difference between this estimated b_2 and the measured b_2, i.e. -0.28, is possibly due to:-

(a) Cut-outs in the elevator nose.
(b) Possible concavity in the elevator surface due to distortion of the fabric.
(c) The elevator shape departing too rapidly, and too far aft, from the section shape, and thus making the elevator nose too sharp (see Fig.2). Wind tunnel tests would settle this point.

Though it is difficult to detect any fabric distortion in flight to the degree of accuracy required, ciné photographs of the top surface of the elevator did suggest that some concavity might be occurring.

Fig.13 also shows that as the speed increases the estimated value of $-b_2$ increases rapidly. The rapid build up of stick force per 'g' in the pull out (see §3.41) also indicates a large increase of $-b_2$ with speed. It is not known exactly how this increase arises but there are three possible causes:-

(a) Increase in concavity of the elevator surface with speed.
(b) The effect of compressibility. This is estimated by Glauert's law to be responsible for about a 20% increase in $-b_2$.
(c) Increasing error in estimating the mean angle of the elevator as the speed is increased.

It is probable that the increase in $-b_2$ with increase in speed will account for much of the variation in stick free stability characteristics at high speed, but a full analysis cannot be made without a knowledge of the value of b_1, and its variation, if any, with C_L. It is impossible, however, to get any reliable values of b_1 from the flight curves due to the variation in b_2 with C_L.

4. Change in aileron droop with speed

The change in droop with speed was found to be small, the aileron trailing edges rising between 0.1 in. and 0.2 in. from rest to 340 m.p.h. E.A.S. (i.e. less than 0.5°).

5. Conclusions

(i) There has been no sign of any sudden change of stick force during the dive in a large number of dives on Lancaster h.5692, with the centre of gravity ranging between $0.25\bar{c}$ and $0.35\bar{c}$. There was, however, a small variation of stick force from day to day. This variation might be due to the small amount of backlash in the very effective trimming tabs, and it is possible that backlash might cause a variation during a dive.

(ii) The aircraft was stick free unstable in the dive (considering the varying speed conditions) over the range of centre of gravity tested, $0.25\bar{c}$ to $0.35\bar{c}$. This instability was, however, quite small and almost independent of centre of gravity position. Large pulls on the control column would only be encountered should the trimmer be wound forward from the top speed trimming position in order to help the aircraft into the dive. The increase in the stick force per 'g' with speed, which at 320 m.p.h. reaches 200 lb. (centre of gravity at $0.26\bar{c}$, engines on), would tend to make the pilot wind the trimmer forward. A reduction in stick free stability was measured as the speed was increased and this is probably due to the large measured increase in $-b_2$ with speed.
(iii) The b_2 for the elevator measured in flight at low speeds, -0.22 (allowing 80% tail efficiency), indicated much more unbalance than given by the estimated value of +0.06. The difference is possibly due to:-

(a) Cutouts in the elevator nose.
(b) Possible concavity in the elevator surface.
(c) Too rapid departure of the elevator shape from the section shape producing too sharp a nose.

(iv) There was no appreciable tail plane twist on this aircraft over the speed range tested, but both the elevator twist and the

angular bending of the fuselage were appreciable though small at high speeds. The position of the neutral point stick fixed in the glide at low speeds, 0.40$\bar{c}$, was in fair agreement with the wind tunnel value of 0.42$\bar{c}$. The neutral point moved forward at high speed but never went further than 0.52$\bar{c}$.

(v) It is probable that the diving characteristics of the Lancaster would improve on stiffening the elevator with a metal covering, due both to the prevention of surface distortion and the reduction in twist. It should be stressed, however, that even in its present condition the aircraft appears quite satisfactory up to 360 m.p.h. to most pilots in spite of the small degree of stick free instability at high speeds and the large stick force per "g".

REFERENCES

No.	Authors	Title, etc.
1	-	Part 7 of A.A.E.E. Report No. 766.
2	Seddon and Haile.	Wind tunnel tests on the Lancaster. R.A.E. Report No. B.A. 1672. April, 1941.
3	Brown and Hills.	The effect of slipstream on the longitudinal stability of four-engined monoplanes. R.A.E. Report No. B.A. 1675. (5238) May, 1941.
4	Lyons.	Note on the analysis of experimental data on the hinge moments of control surfaces due to tabs. R.A.E. Report No. Aero 1747. (5864) April, 1942.
5	Priestley and Warren.	The calculation of effective values of b_2 of set-back hinge controls for which the local balance varies across the span. B.A. Departmental Note - Performance No. 46. May, 1941.
6	Nivison.	Effect of hinge gaps on control characteristics. R.A.E. Technical Note No. Aero 983. (Large Tunnel). July, 1942.
7	Morgan and Morris.	Flight tests to investigate the lightness of the unbalanced elevator on the Lockheed 12A. R.A.E. Report No. B.A. 1574. (4532). January, 1940.

11995.S

FIG: 1

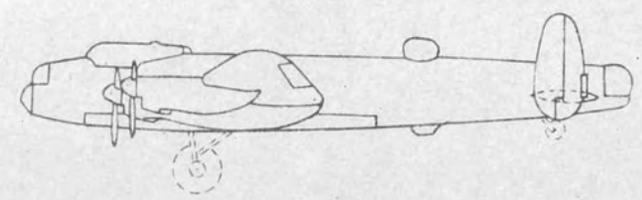

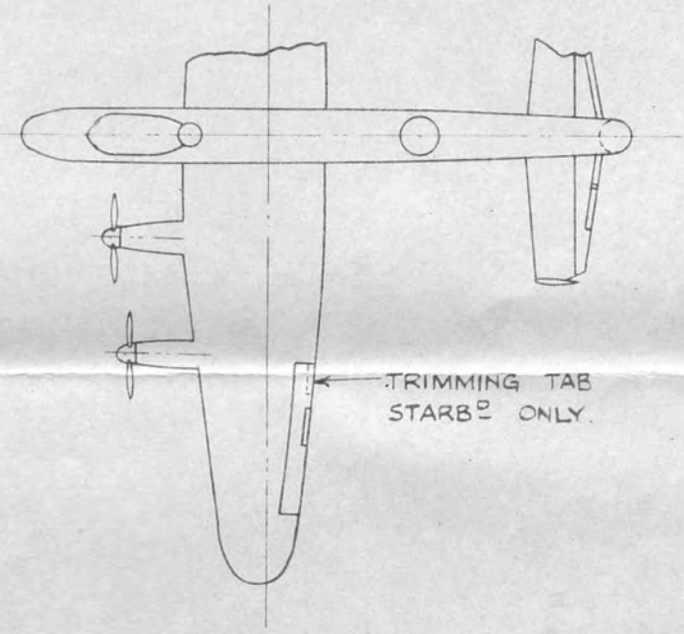

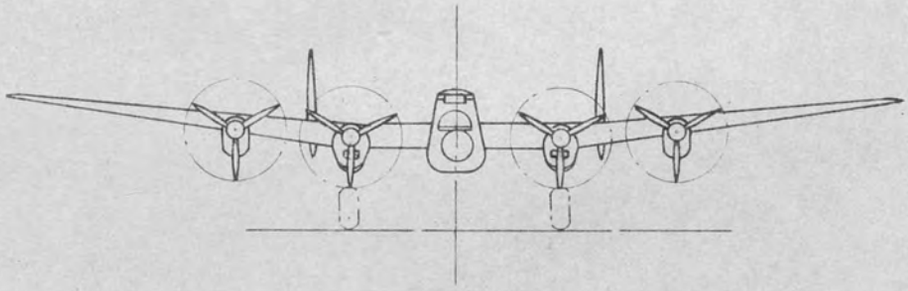

WEIGHT	LBS	60,000 APP
GROSS WING AREA	SQ.FT.	1300
SPAN		102'-0"

0 50

SCALE - FEET.

LANCASTER I R5692.

R5692

FIG. 2

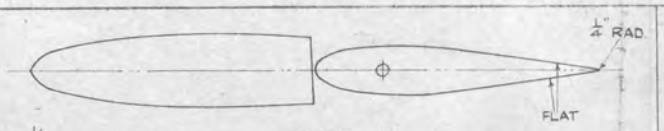

SCALE 1/16 SECTION AA

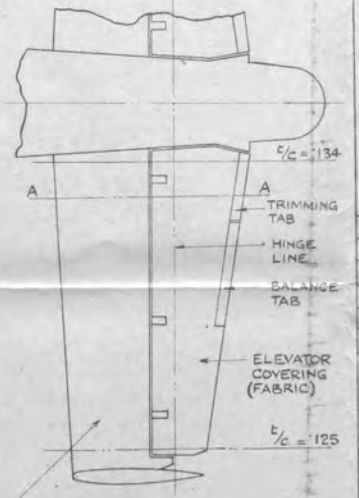

SCALE :- 1/48

TAIL SURFACE AREA (GROSS) SQ FT		237·0
ELEVATOR AREA / TAIL SURFACE AREA		·256
ELEVATOR RANGE	UP	28°
	DOWN	14¾°
PERCENTAGE BALANCE		39·50
STICK GEARING DEG / INCH		2·72
TRIMMING TAB	RANGE	6° EACH WAY
	CHORD / ELEVATOR CHORD	15·1%
	SPAN / ELEVATOR SPAN	22·6%
	AREA / ELEVATOR AREA	4·4%
BALANCE TAB	CHORD / ELEVATOR CHORD	18·7%
	SPAN / ELEVATOR SPAN	33·6%
	AREA / ELEVATOR AREA	6·68%
	GEARING	SEE GRAPH

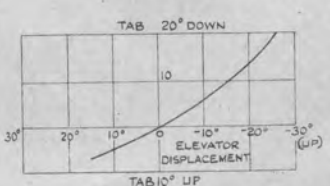

BALANCE TAB GEARING

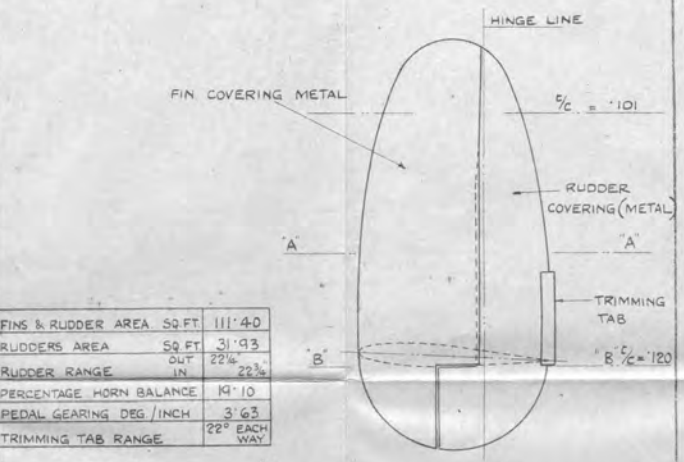

SCALE :- 1/32

FINS & RUDDER AREA SQ FT		111·40
RUDDERS AREA	SQ FT	31·93
RUDDER RANGE	OUT	22½°
	IN	22¾°
PERCENTAGE HORN BALANCE		19·10
PEDAL GEARING DEG / INCH		3·63
TRIMMING TAB RANGE		22° EACH WAY

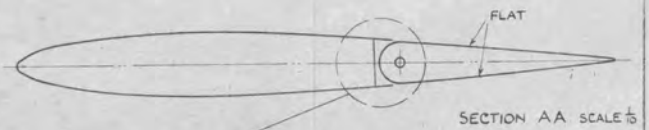

SECTION A A SCALE 1/8

SECTION B B
SCALE :- 1/16

SCALE :- ¼

SCALE :- 1/32 1/10 1/4 1/16.

LANCASTER I R5692. TAIL UNIT.

12252.S

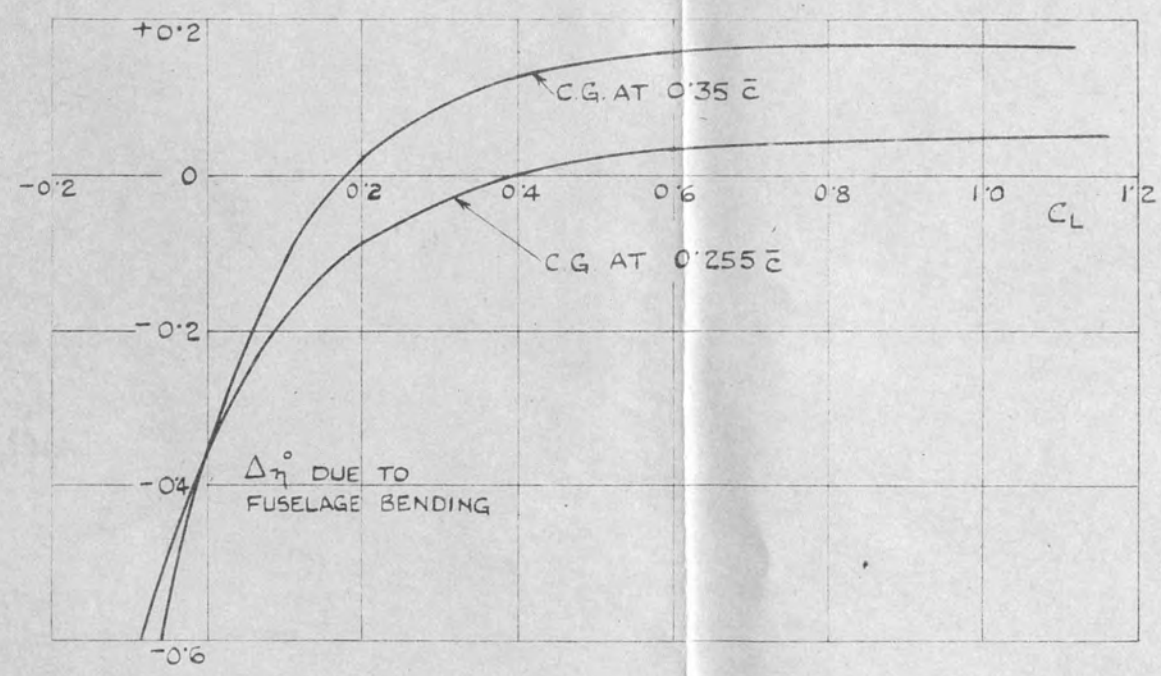

CALCULATED EFFECT ON ELEVATOR ANGLE TO TRIM DUE TO FUSELAGE BENDING

LANCASTER.

FIG. 3

1225 S

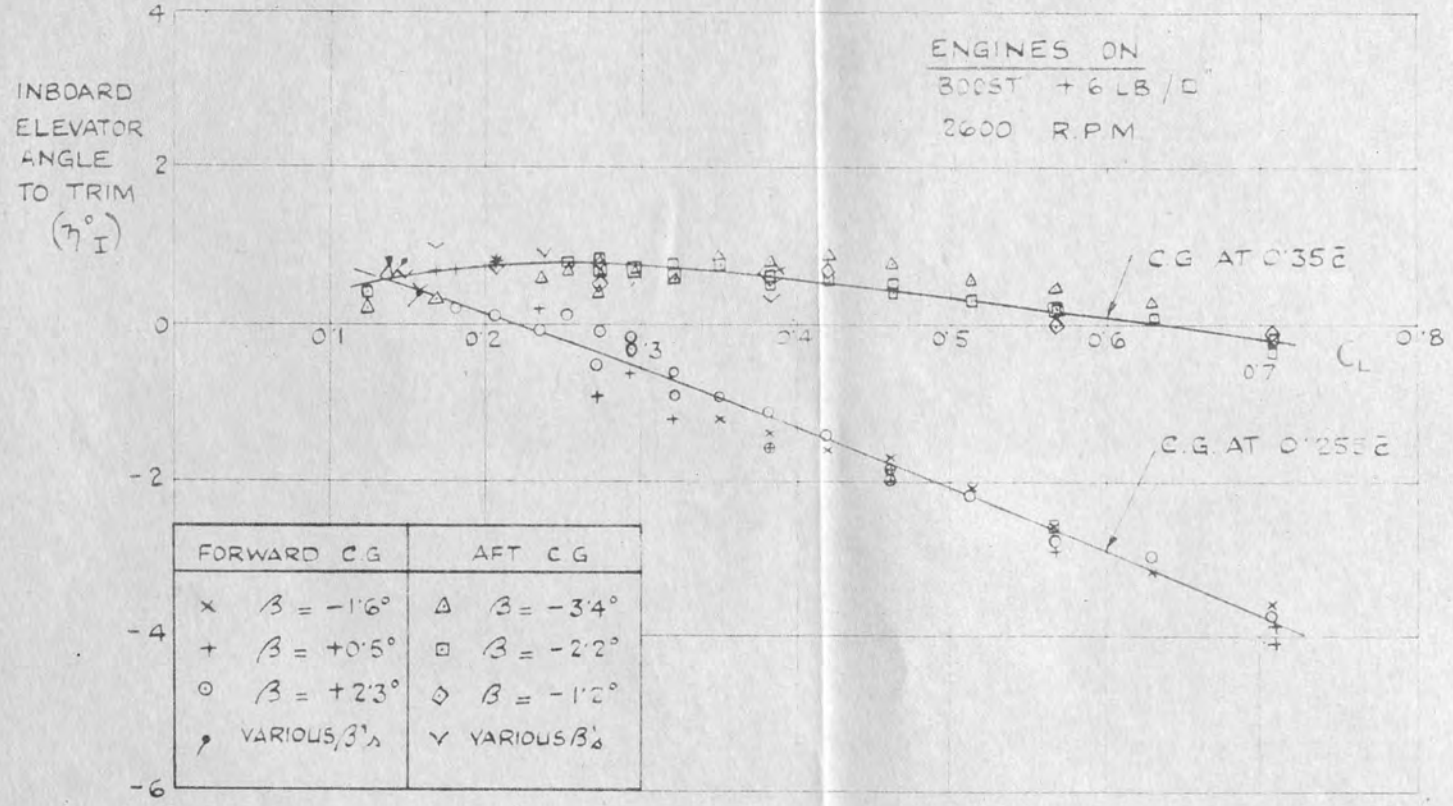

ELEVATOR ANGLE TO TRIM CURVES, CORRECTED FOR TAB LIFT
(ELEVATOR ANGLE MEASURED AT CENTRE OF TORQUE TUBE)

LANCASTER. R.5692.

FIG. 4

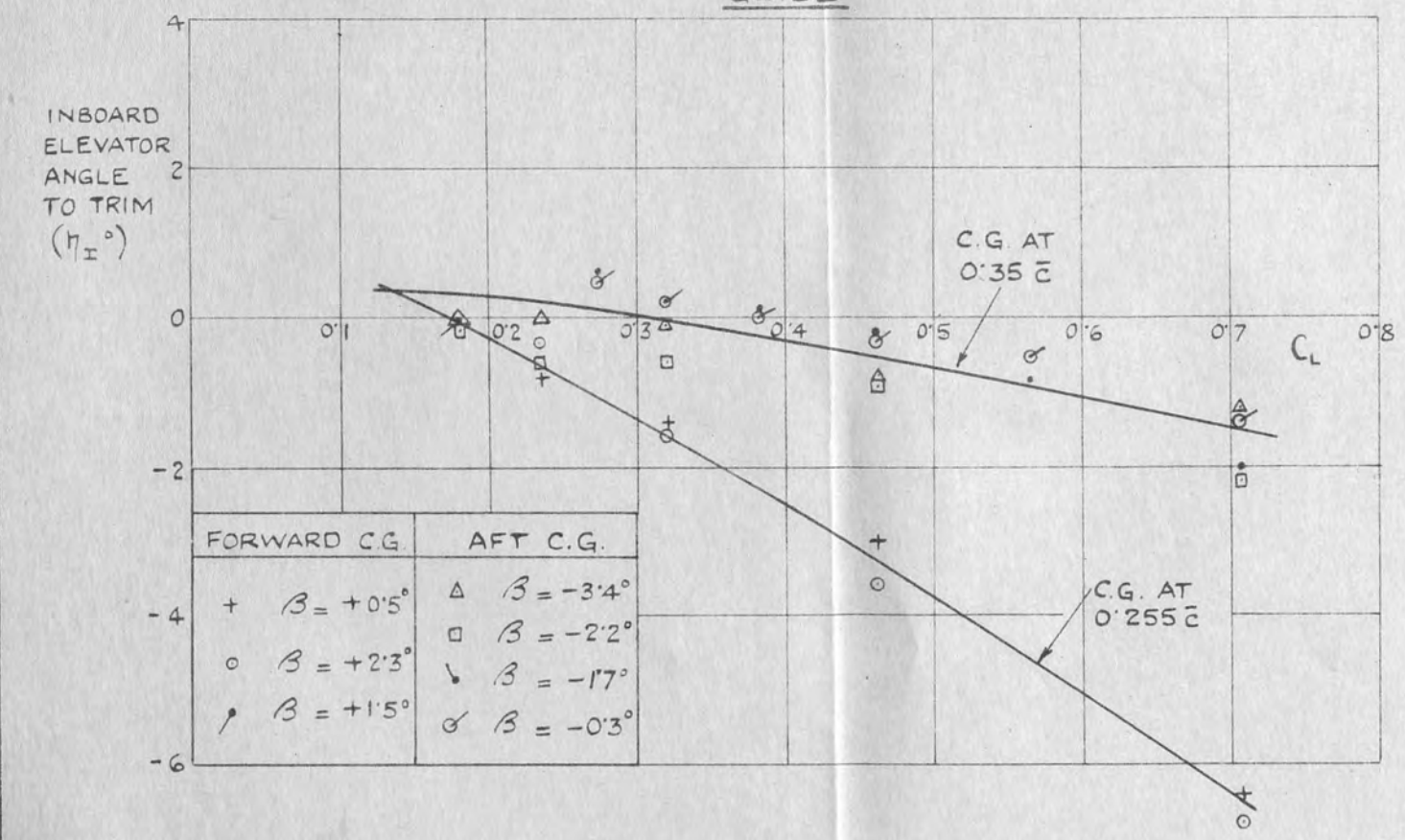

ELEVATOR ANGLE TO TRIM CURVES, CORRECTED FOR TAB LIFT.
(MEASURED AT THE CENTRE OF THE TORQUE TUBE.)

LANCASTER. R.5692.

FIG. 5.

12255.S

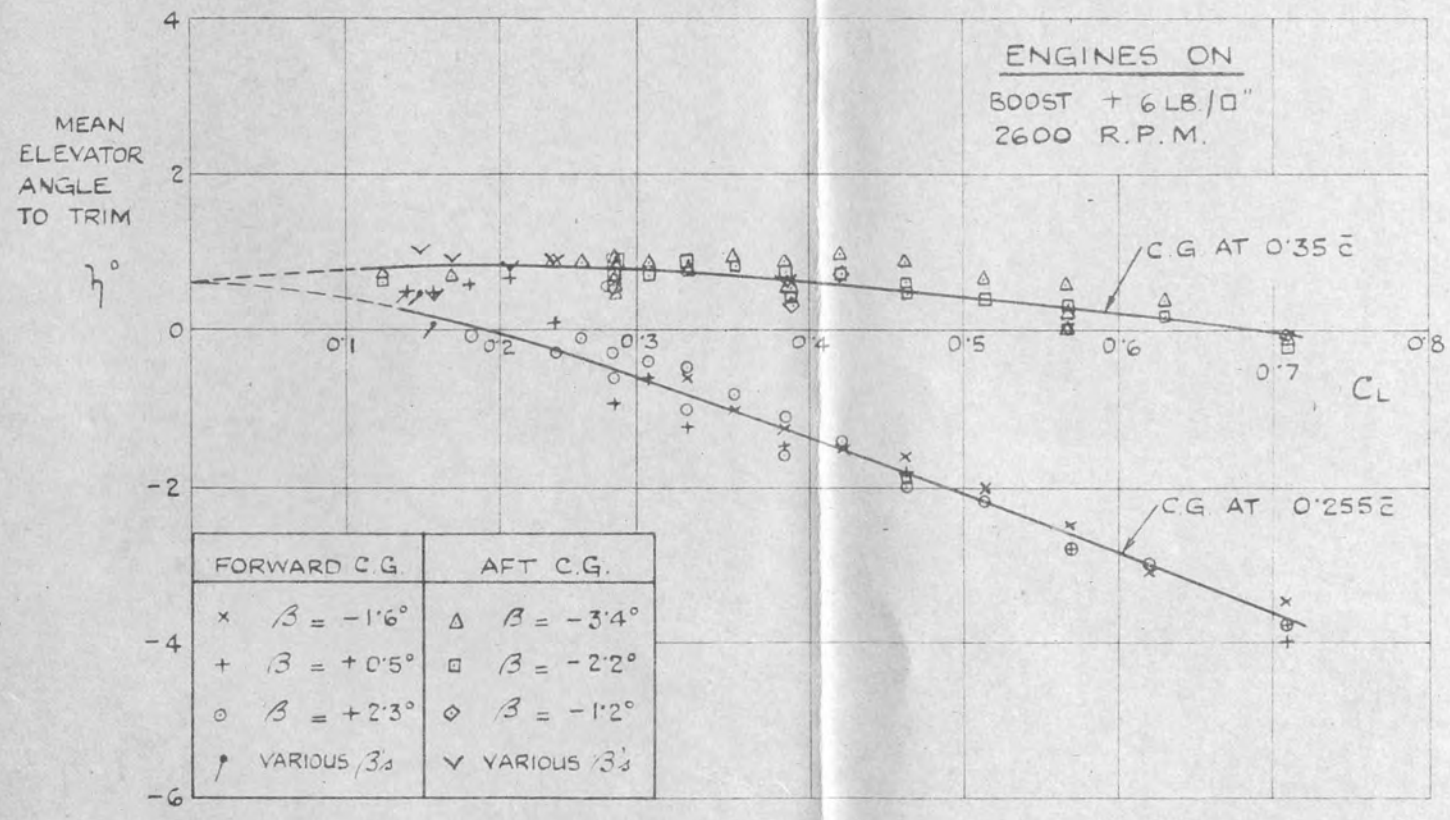

MEAN ELEVATOR ANGLE TO TRIM, CORRECTED FOR TAB LIFT AND ELEVATOR TWIST.

LANCASTER. R.5692.

FIG. 6

12256.S

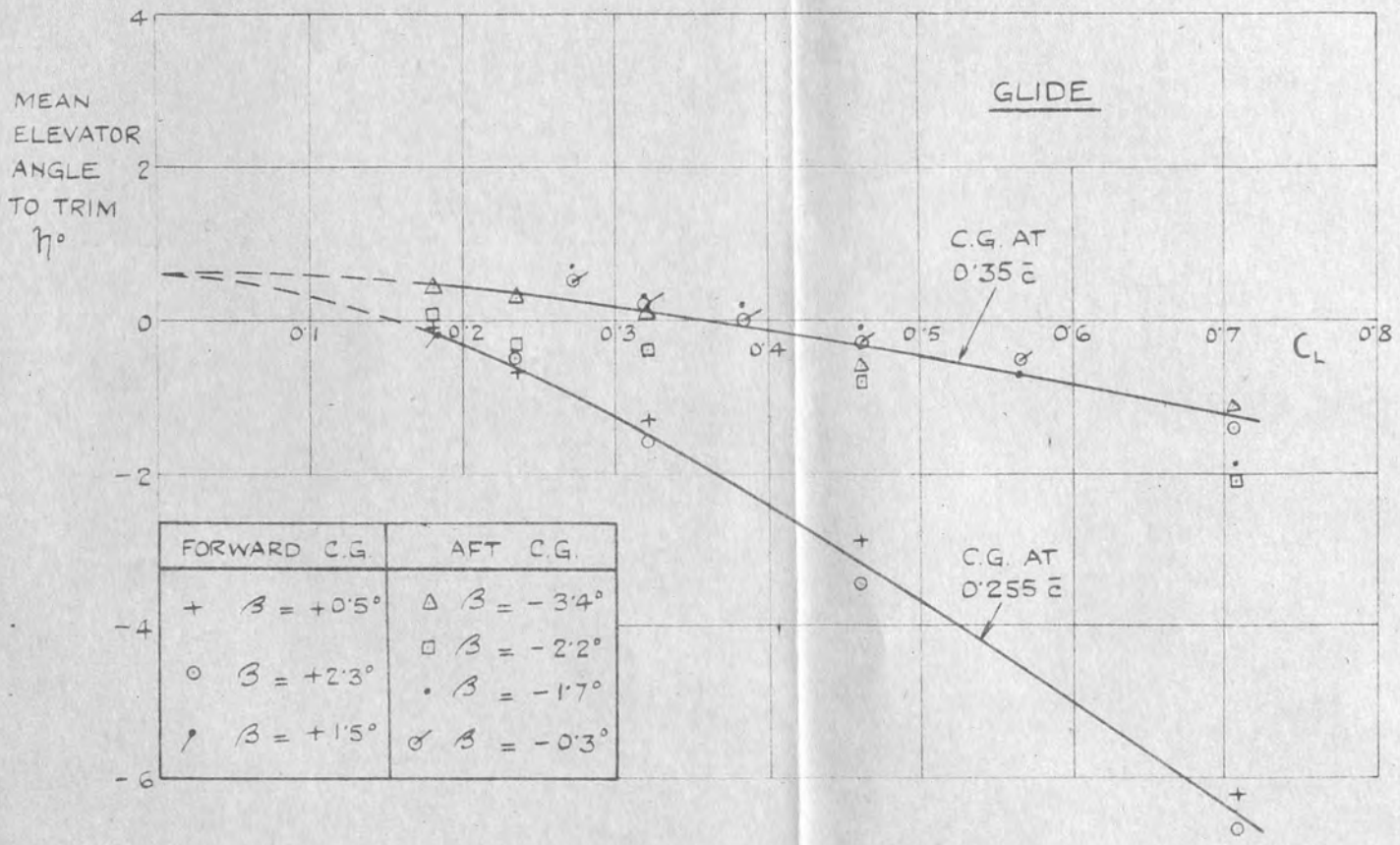

MEAN ELEVATOR ANGLE TO TRIM, CORRECTED FOR TAB LIFT & ELEVATOR TWIST.

LANCASTER. R.5692.

FIG. 7.

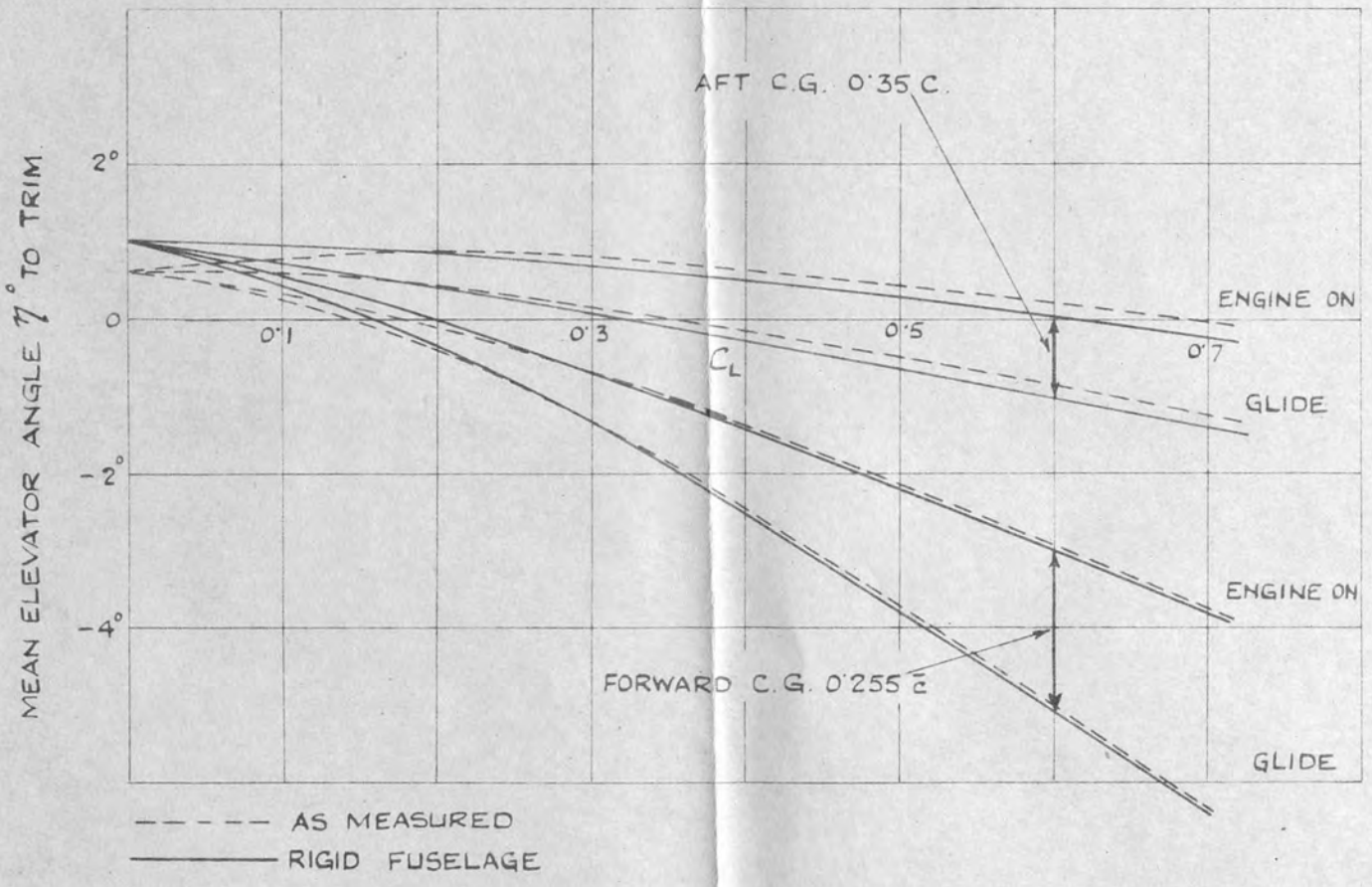

MEAN ELEVATOR ANGLE TO TRIM, SHEWING THE EFFECT OF FUSELAGE BENDING.

LANCASTER. R.5692.

FIG. 8

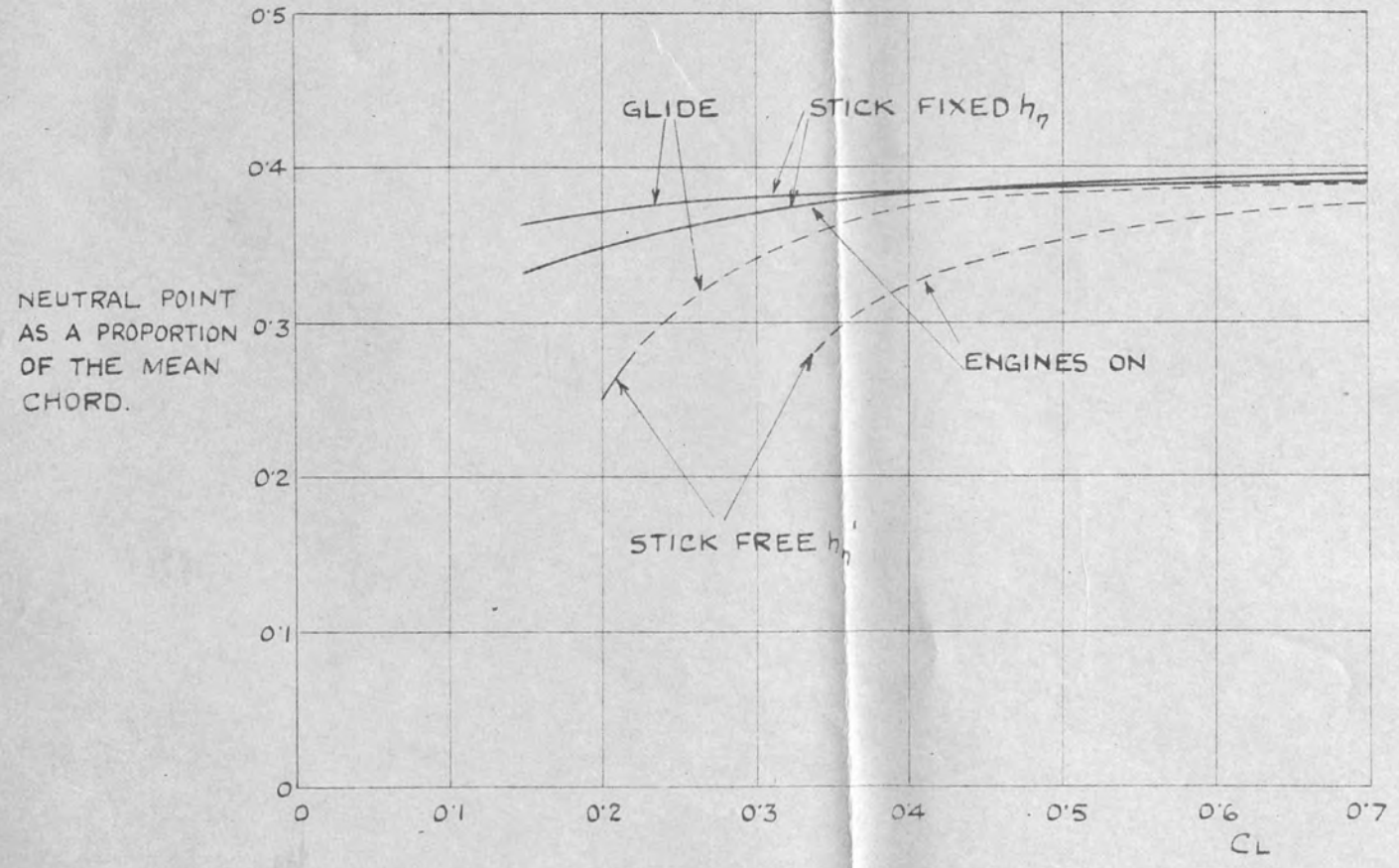

VARIATION OF NEUTRAL POINT WITH C_L, STICK FIXED & FREE.

LANCASTER. R.5692.

FIG. 9.

12259.S

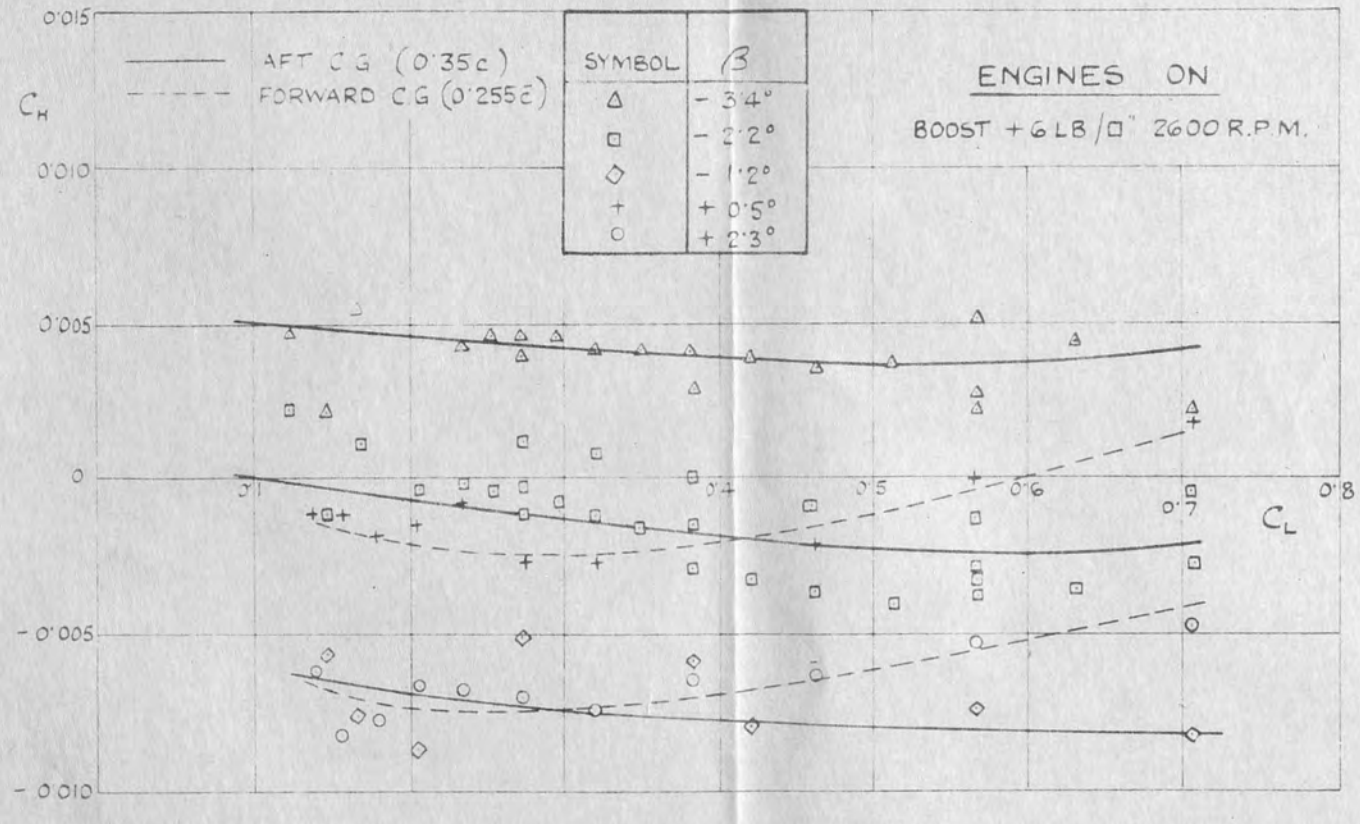

STICK FORCE CURVES TO TRIM WITH VARYING TAB ANGLE & C.G. POSITION.

LANCASTER. R.5692.

FIG. 10

12260.S

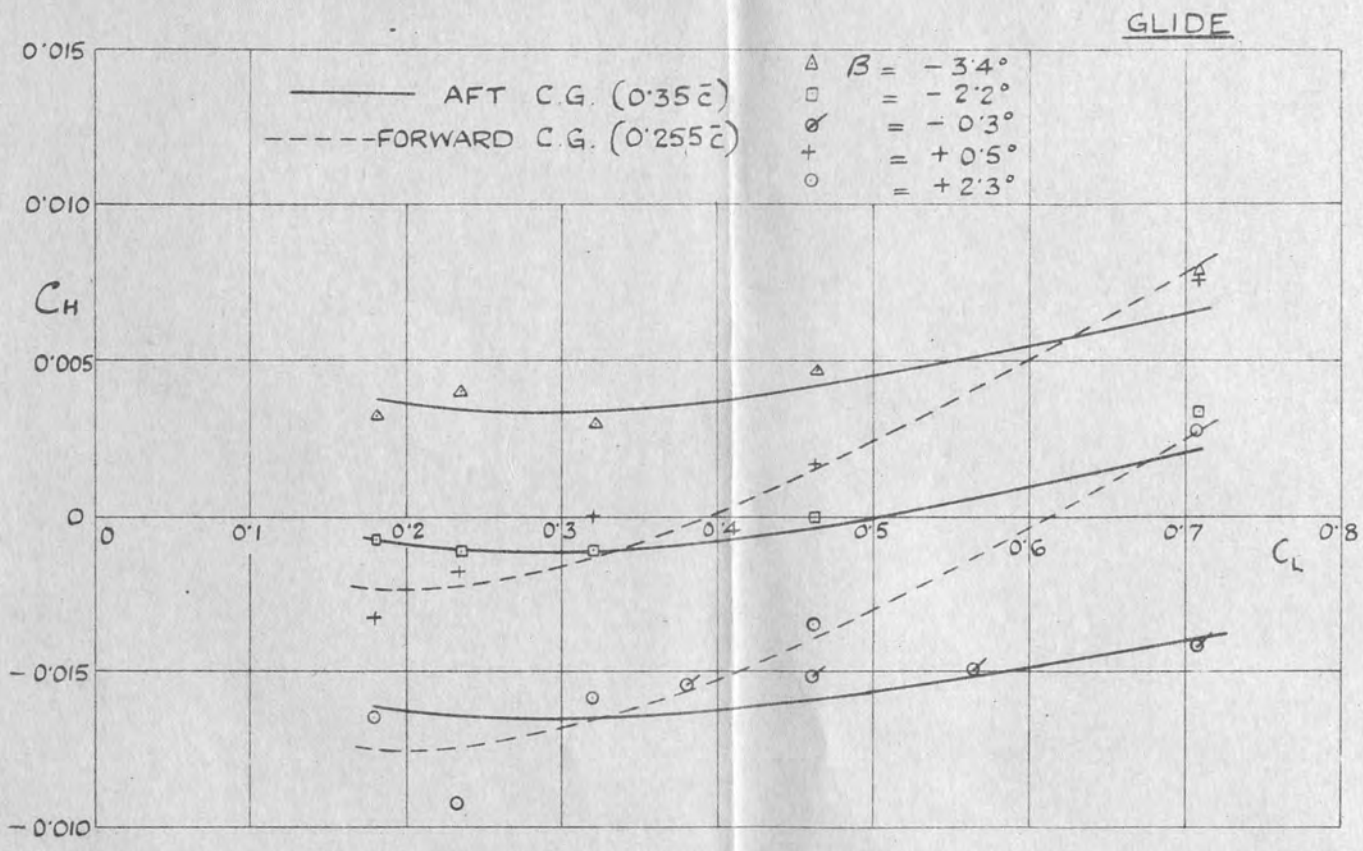

STICK FORCES TO TRIM WITH VARYING TAB ANGLE & C.G. POSITION.

LANCASTER. R.5692.

FIG. 11

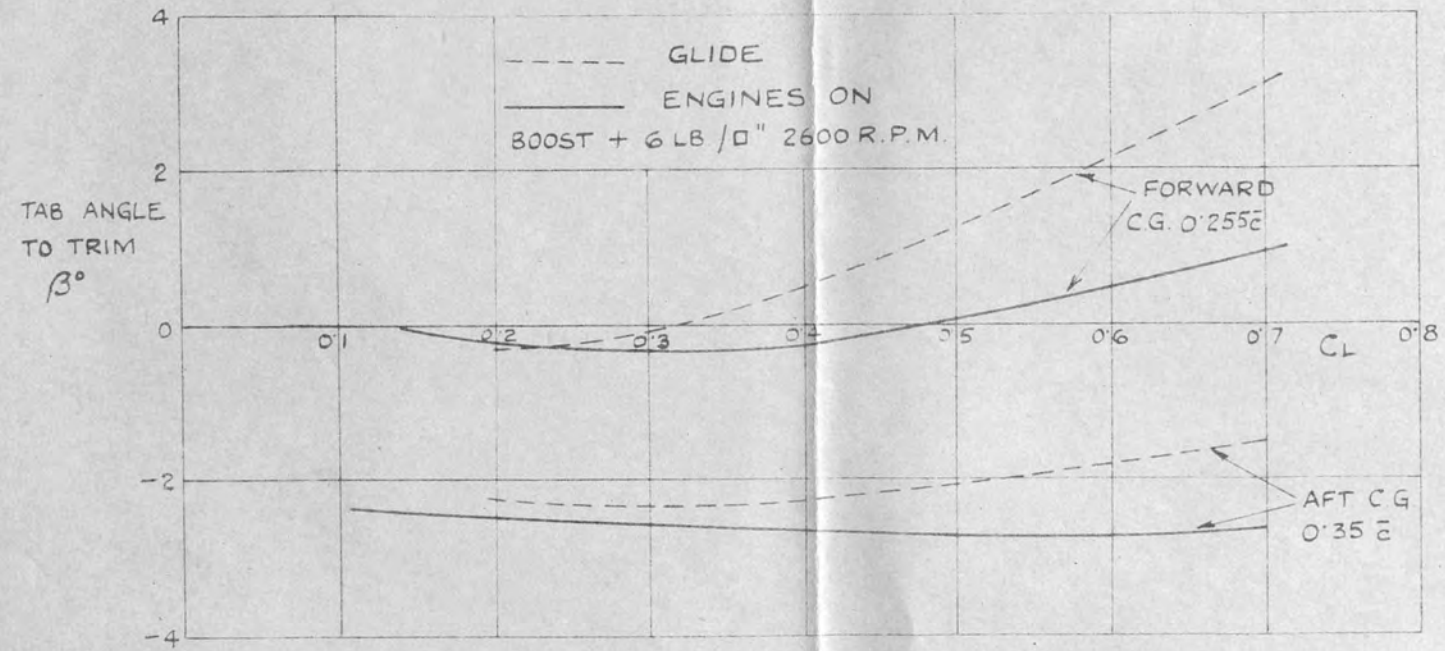

TAB ANGLES TO TRIM AGAINST C_L FOR TWO C.G. POSITIONS & WITH VARYING ENGINE CONDITIONS.

LANCASTER. R.5692.

FIG. 12

12262 S

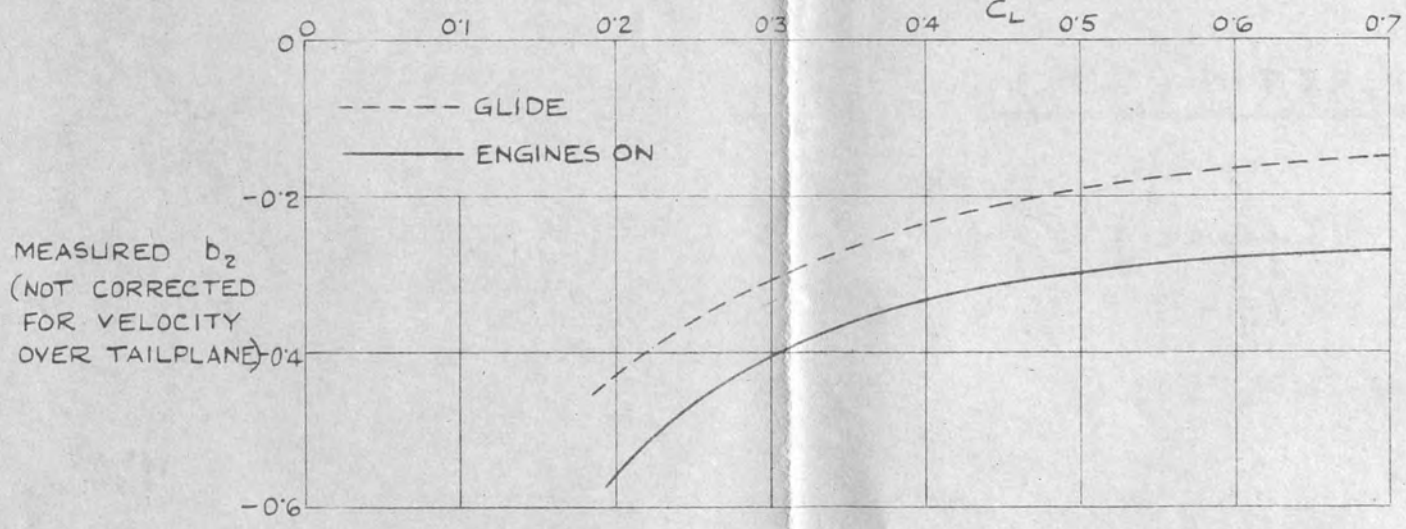

VARIATION OF b_2 FOR THE ELEVATOR (BALANCE TAB INCLUDED) WITH C_L

LANCASTER. R.5692.

FIG. 13